Fatigue behavior of carbon/epoxy AFP laminates containing gaps

Yasser Mahmoud Sami Abdelsamea Elsherbini

A Thesis

In the Department

of

Mechanical, Industrial and Aerospace Engineering

Presented in Partial Fulfillment of the Requirements
For the Degree of
Doctor of Philosophy (Mechanical Engineering) at
Concordia University
Montreal, Quebec, Canada

June 2017

Concordia University

School of Graduate Studies

This is to certify that the thesis prepared

By: **Mr. Yasser Mahmoud Sami Abdelsamea Elsherbini**

Entitled: **Fatigue behavior of carbon/epoxy AFP laminates containing gaps**

and submitted in partial fulfillment of the requirements for the degree of

Doctor of Philosophy (Mechanical Engineering)

Complies with the regulations of the University and meets the accepted standards with respect to originality and quality.

Signed by the final examining committee:

_____ Chair
Dr. D. Dysart-Gale

_____ External Examiner
Dr. Raghavan Jayaraman

_____ External to Program
Dr. Catharine C Marsden

_____ Examiner
Dr. Martin Pugh

_____ Examiner
Dr. Mehdi Hojjati

_____ Thesis Supervisor
Dr. Suong V. Hoa

Approved by: _____
Dr. Ali. Dolatabadi,
Graduate Program Director

June 28, 2017

_____
Dr. Amir Asif, Dean
Faculty of Engineering and Computer Science

Abstract

Fatigue behavior of carbon/epoxy AFP laminates containing gaps

Yasser Mahmoud Sami Abdelsamea Elsherbini, Ph.D.

Concordia University, 2017

Composite materials are widely used in many applications owing to their advantages over conventional ones. Among the different available manufacturing techniques of composites, automated fiber placement (AFP) attracted the attention of many industries due to its speed of material deposition and repeatability in manufacturing. Unfortunately, the occurrence of gaps between material strips during AFP manufacturing process is unavoidable. Even though there have been many studies that focused on the effect of these gaps on the static properties of the AFP laminates, to our knowledge, no work has been performed to test their effect on fatigue behavior.

In this dissertation, the effect of the induced gaps on fatigue performance of carbon/epoxy AFP laminates was investigated both experimentally and numerically. In the experimental part, fatigue tests were conducted on both reference, free from defects laminates, and defective laminates. Then, the fatigue performance of both types was compared and analyzed to obtain the effect of gaps. For better understanding the fatigue behavior of laminates containing gaps, many parameters were taken into consideration such as laminate stacking sequence, gap shape, gap orientation and number of gaps. Based on analyzing the results of fatigue testing of different stacking sequences, a few design recommendations are provided that can enhance the performance of the defective laminates and alleviate the effect of gaps.

In addition, infrared thermography was used as a non-destructive technique for in-situ detection of damage during fatigue loading. In order to examine the nature of the inherent damage within the laminate due to gaps, sectioning and inspection of specimens using scanning electron microscopy (SEM) were performed. The extensive fatigue experiments revealed the existence of a threshold stress value below which the effect of gaps on fatigue performance diminishes. The

main drawbacks in obtaining this threshold values using the traditional long fatigue testing method were the large number of specimens and long-time for the fatigue tests.

Consequently, infrared thermography and Risitano method were applied on AFP laminates containing gaps to provide a quick method for obtaining the threshold values. This method has a great potential in saving time and material required for performing traditional fatigue tests to develop stress/life curves. The obtained results of threshold values were in good agreement with the results obtained from the conventional method.

In the numerical part, a fatigue progressive damage model (FPDM) was developed using Ansys Parametric Design Language (APDL) and applied to the case of laminates containing gaps. The progressive damage model presented in this work is an integration of fatigue life model, failure criterion, sudden and gradual degradation of strength/stiffness. The predicted results from the model were compared to the experimental results for different stacking sequences. The model showed a good agreement with the experimental results for the case of unidirectional laminates. For the case of cross-ply laminates more work should be done for better prediction of results due to the complex nature of damage for off-axis laminates. Nevertheless, the model can be helpful in saving time and material in the preliminary design steps to have an idea about the damage behavior and the performance of the designed part.

Acknowledgment

First and foremost I would like to thank “ALLAH”. You have given me the power to believe in myself and pursue my dreams. I could never have done this without the faith I have in you, the Almighty.

I would like to express my deepest sense of gratitude to my thesis supervisor Professor Suong Van Hoa for giving me the opportunity to work under his supervision and for his continuous guidance and mental support during these years. I am heartily grateful to him, whose encouragement, guidance and support from the initial to the final level enabled me to develop an understanding of the subject. I am also grateful to him for careful reading and minute criticism of this thesis. I am really admiring him so much. I have been very lucky to have a supervisor like him.

I would also like to thank my committee members, Dr. Raghavan Jayaraman, Dr. Martin Pugh, Dr. Mehdi Hojjati and Dr. Catharine C Marsden for their helpful comments.

Special thanks to the Egyptian government that financially supported my program, giving me this golden opportunity to complete my graduate studies at Concordia University, one of the best universities here in Canada.

Also, many thanks for all the members of Concordia Center for Composites (CONCOM) for their help in completing my work. In addition I wish to thank all friends in particular Dr. Ali Naghashpour, Mr. Jeffery Simpson, Dr. Isoif Daniel Rosca and Mr. Heng Wang for their support and help to accomplish my work.

Most importantly, none of this would have been possible without the love and patience of my family. I would like to express my love and gratitude to my mother and father; although you

are thousands of miles away, you were always there whenever I needed you. I am thankful to you for your inspiration and encouragement.

Lastly, most of all for my loving, supportive, encouraging, and patient wife Amel and my daughters Haneen and Hala whose faithful support during all the stages of this research is so appreciated. Thank you so much.

Dedication

This thesis is dedicated to:

*my Creator "**ALLAH**", hope to be accepted,*

my mother and my father,

my wife, Amel,

and my kids, Haneen and Hala.

Contents

List of Figures ..... **xi**

List of Tables ..... **xix**

Nomenclature ..... **xx**

List of Abbreviations ..... **xxiii**

Chapter 1 Introduction **1**

1.1 Background 1

1.2 Effect of defects 7

1.3 Fatigue in composites 12

1.3.1 Factors affecting fatigue behavior 13

1.3.2 Fatigue damage mechanisms 16

1.4 Damage detection in composites 19

1.5 Motivation and objective 20

1.6 Thesis organization 22

Chapter 2 Material and experimental details **23**

2.1 Material 24

2.2 Specimen preparation and inspection 25

2.2.1 Specimen manufacturing and curing 25

2.2.2 Quality Inspection of laminates 27

2.2.3 End tabbing and specimen cutting 31

2.3 Defect configurations 31

2.3.1 Effect of gaps in 0^o layer for different stacking sequences 32

2.3.2 Effect of gap shape 34

2.3.3 Effect of gap orientation....35
2.3.4 Effect of number of gaps....37
2.4 Mechanical testing....39
2.4.1 Quasi-static tests....40
2.4.2 Fatigue test....46
2.5 Damage monitoring using IR thermography....49
2.6 Summary....52
Chapter 3 Experimental results and discussion....53
3.1 Quality inspection results....54
3.2 Characterization tests....55
3.3 Fatigue tests....58
3.3.1 Effect of gaps in 0^o layer for different stacking sequences....59
3.3.2 Effect of gap shape....99
3.3.3 Effect of gap orientation....102
3.3.4 Effect of number of gaps....107
3.4 Summary....115
Chapter 4 Fatigue threshold-stress evaluation using IR thermography....117
4.1 Overview....118
4.2 Material and IR thermography equipment....121
4.3 Methodology and results....122
4.4 Discussion and analysis....126
4.4.1 Damage mechanisms....127
4.4.2 Heat generation/dissipation....130
4.4.3 Thermal response of different stacking sequences....132

4.4.4 Behavior of defective laminates below threshold stress 136
4.4.5 Temperature plateau 140
4.4.6 Threshold stress 142
4.5 Using Risitano method for laminates with more gaps 142
4.6 Summary 145
Chapter 5 Finite element modeling 146
5.1 Model Development 147
5.1.1 Model generation and material definition 147
5.1.2 Fatigue life model 150
5.1.3 Gradual degradation of mechanical properties 152
5.1.4 Failure analysis 153
5.1.5 Sudden mechanical properties degradation 154
5.2 Model validation 157
5.2.1 Gaps in 0^o layers for different stacking sequences 157
5.2.2 Gaps with different orientations 166
5.2.3 Gap with different shapes 178
5.2.4 Defective laminates with more than one gap 180
5.3 Summary 185
Chapter 6 Conclusions, contributions and recommendations for future work 186
6.1 Conclusions 186
6.2 Contributions 189
6.3 Recommendations for future work 189
6.4 Publications 190
References 192

List of Figures

Figure 1-1: Automated tape lay-up machine [4].....3
Figure 1-2: Automated Fiber placement machine available in CONCOM.....4
Figure 1-3: Gaps occurrence at the boundaries of material strips during AFP manufacturing [10]. 6
Figure 1-4: Gaps occurrence at the boundaries of the manufactured component 6
Figure 1-5: Gaps occurrence at the end of tows during (a) fiber steering [11] and (b) complex part manufacturing [12].....7
Figure 1-6: Defects were created by manually removing material strips [17]. 9
Figure 1-7: Different defect configuration investigated by Croft et al. [18].....9
Figure 1-8: Comparison between tensile behavior of different unnotched laminates [24].....11
Figure 1-9: Stress-life curves at R=0.1 for different carbon fiber composites [36].....14
Figure 1-10: Fatigue strength for cross-ply and quasi-isotropic laminates at different temperatures [47] 16
Figure 1-11: Occurrence of matrix crack followed by fiber bridging or interface debonding [55]. 17
Figure 2-1: Cycom 977-2 material spools used in the study.....24
Figure 2-2: Autoclave used for panels curing 26
Figure 2-3 Curing conditions for the material (Cycom 977-2) [72] 27
Figure 2-4: Digital Scanning Calorimeter (DSC) used to check the degree of cure.....28
Figure 2-5: Vacuum mixer used to remove air bubbles.....29
Figure 2-6: Automatic polishing machines used to prepare the SEM samples.....30
Figure 2-7: Dimensions (in mm) of the specimen with gap at the middle.....33
Figure 2-8: Location of the gaps across thickness of (a) unidirectional, (b) cross-ply and (C) quasi-isotropic laminates. 34

Figure 2-9: Triangular gaps with sides of different aspect ratios: (a) 1, (b) 2 and (c) 3. 35
Figure 2-10: Schematic representation of the -45^{o} layer contacting gaps in the defective quasi-isotropic plate.....36
Figure 2-11: Schematic representation of the 90^{o} layer containing gaps in the defective cross-ply plate 37
Figure 2-12: In-plane gaps configurations: (a) x = 3 and (b) x = 10 mm. (x is the distance between gaps'centres).....39
Figure 2-13: Out-of-plane gaps configurations: (a) full tow and (b) half tow staggering 39
Figure 2-14: MTS testing machine used for quasi-static and fatigue tests. 40
Figure 2-15: Unidirectional (0^{o}) specimen with attached strain gages for quasi-static tensile tests (dimensions in mm).....42
Figure 2-16: Unidirectional (90^{o}) specimen with attached strain gages for quasi-static tensile tests (dimensions in mm) 42
Figure 2-17: Strain recording device Vishay 2160 43
Figure 2-18: Compression test fixture.....44
Figure 2-19: Specimens for compression tests (a) along fiber and (b) transverse to fibers. (dimensions in mm) 45
Figure 2-20: Specimens for the performed shear tests (dimensions in mm).....45
Figure 2-21: Applied stress in fatigue cycles in the form of sinusoidal waves 47
Figure 2-22: Infrared camera (FLIR 450SC) used to detect damage occurrence.....50
Figure 2-23: Schematic representation of the experimental test set up. 52
Figure 3-1 Thermal response during degree of curing inspection using DSC 54
Figure 3-2: Microscopic images for unidirectional specimen (a) across the width and (b) across the length.....55
Figure 3-3: Stress-strain relations for longitudinal tensile test.....56
Figure 3-4: Stress-strain relation for transverse tensile test 57
Figure 3-5 Shear stress-strain relation for ±45^{o} laminate under quasi-static tensile test. 58
Figure 3-6: Fatigue lives at each stress for unidirectional reference and defective specimens.....60
Figure 3-7: Stress/life curves for unidirectional reference and defective specimens with gaps in 0^{o} layer at 0.95 confidence level 61

Figure 3-8: Reversible and irreversible energy during each fatigue cycle. 63
Figure 3-9: Reduction in fatigue life of defective unidirectional specimens at different applied stresses 63
Figure 3-10 Statistical analysis of fatigue life data at applied stress of 1880 MPa for unidirectional defective specimen 66
Figure 3-11: S/N curves for reference and defective unidirectional specimens at different probabilities of failure 67
Figure 3-12: Microscopic image at X=6.5mm from the gap center showing delamination occurrence in a unidirectional laminate after 1000 cycles 68
Figure 3-13: Unidirectional 0^o specimen after final failure 69
Figure 3-14: Temperature increase for reference and defective specimens 69
Figure 3-15: (a) Detection of damage evolution using IR and (b) specimen at failure 70
Figure 3-16: Thermal behavior of unidirectional (a) defective and (b) reference specimens. 72
Figure 3-17: Fatigue lives at each stress for cross-ply reference and defective specimens 73
Figure 3-18: Stress/life curves for cross-ply reference and defective specimens with gaps in 0^o layer at 0.95 confidence level 74
Figure 3-19: Reduction in fatigue life for defective cross-ply laminate 76
Figure 3-20: S/N curves for reference and defective cross-ply specimens at different probabilities of failure 77
Figure 3-21: Cross-ply laminate after final failure 78
Figure 3-22: Microscopic image at X=6.5 mm from the gap center showing internal damage mechanisms in cross-ply laminate 79
Figure 3-23: Damage detection in cross-ply laminates using IR thermography 79
Figure 3-24: Shape of high temperature area in (a) unidirectional and (b) cross-ply laminates. 80
Figure 3-25: Thermal behavior at different stresses for defective cross-ply laminates 81
Figure 3-26: Fatigue lives at each stress for cross-ply reference and defective specimens 82
Figure 3-27: Stress/life curves for quasi-isotropic reference and defective laminates with gaps in 0^o layer 82
Figure 3-28: Fitted lines of S/N relation for different stacking sequences of reference laminates. 83

Figure 3-29: Reduction in fatigue life for defective quasi-isotropic laminate 84
Figure 3-30: S/N curves for reference and defective quasi-isotropic laminates at different probabilities of failure 85
Figure 3-31: Different damage mechanisms after failure of quasi-isotropic specimen. 86
Figure 3-32: Microscopic image at X=6.5mm from the gap center showing internal damage mechanisms in quasi-isotropic laminate 87
Figure 3-33: Damage detection using IR thermography for defective quasi-isotropic specimen .87
Figure 3-34: Temperature increase at different stresses for defective quasi-isotropic laminates..88
Figure 3-35: Different types of cross-ply laminates used to investigate the effect of the $0^o/90^o$ interface 90
Figure 3-36: Damage mechanisms for different types of cross-ply laminates after 100 000 cycles 91
Figure 3-37: Numbering code for different layers in the laminate 92
Figure 3-38: Volumes representing the 3D defect and the surrounding intact material representing the gap in the laminate 93
Figure 3-39: Microscopic images for (a) proposed and (b) original quasi-isotropic configurations at X=6.5 mm from gap center.....97
Figure 3-40: Effect of changing the shape of the gap on the fatigue performance.....101
Figure 3-41: Temperature increase for different gap configurations at 1850 MPa 101
Figure 3-42: Stress/life curves for cross-ply reference and defective laminates with gaps in 90^o layer.....103
Figure 3-43: Microscopic image at Y=7 mm from the gap center in cross-ply laminate with gap in 90^o layer.....104
Figure 3-44: Stress/life curves for quasi-isotropic reference and defective laminates. 105
Figure 3-45: Reduction in fatigue life of defective quasi-isotropic specimens with different gap orientation.....106
Figure 3-46: Microscopic image of a section cut parallel to 45^o layer in quasi-isotropic laminate with gap in -45^o layer. 107
Figure 3-47: Stress/life curves for unidirectional reference and defective laminates with two in-plane gaps at different distances 109

Figure 3-48: Reduction in fatigue life of defective unidirectional laminates with two in-plane gaps at different distances 110
Figure 3-49: Additional effect of one more gap in unidirectional laminate on threshold stress. 111
Figure 3-50: Stress/life curves for unidirectional reference and defective laminates with two out-of-plane gaps at different distances..... 113
Figure 3-51 Reduction in fatigue life of defective unidirectional laminates with two out-of-plane gaps with HTS and FTS techniques..... 113
Figure 3-52: Threshold stress values for different tested unidirectional laminates..... 114
Figure 4-1: Relation between temperature change and applied stress for carbon/epoxy laminates [64] 119
Figure 4-2: Schematic representation of (a) fifth layer (b) specimen cross section (dimensions in mm) 121
Figure 4-3: Temperature increase at different stresses for defective (a) unidirectional, (b) quasi-isotropic and (c) cross-ply laminates..... 124
Figure 4-4: Bilinear relation between the slope of temperature increase and the applied stress for (a) unidirectional (b) quasi-isotropic and (c) cross-ply defective laminates. 126
Figure 4-5: Damage detected after 10^5 cycles within unidirectional laminates 128
Figure 4-6: Damage detected after 10^5 cycles within cross-ply laminates across (a) width (at X=10mm, 1.5mm<Y<3.5mm) and (b) length (at Y=10mm, -1.1mm<X<1.1mm). 129
Figure 4-7: Damage detected after 10^5 cycles within quasi-isotropic laminates (at X=10mm, 1.8mm<Y<4mm). 129
Figure 4-8 Schematic representation of different damage mechanisms for (a) unidirectional, (b) cross-ply and (c) quasi-isotropic laminates. 130
Figure 4-9: Temperature change for different stacking sequence at the same stresses in 0^o layers, 1750 MPa..... 133
Figure 4-10: Thermal behavior at different maximum stress levels for defective: (a) unidirectional, (b) cross-ply and (c) quasi-isotropic laminates..... 137
Figure 4-11: Microscopic images at different distances from the gap centre for 300 000, 600 000 and 10^6 cycles for unidirectional laminates..... 138

Figure 4-12: Microscopic images at different distances from the gap centre for (a) quasi-isotropic and (b) cross-ply laminates.....140
Figure 4-13: Temperature change with cycles for unidirectional laminates with 2 gaps (a) in-plane and (b) out-of-plane 143
Figure 4-14: Bilinear relation between the slope of temperature increase and the applied stress for unidirectional laminates with 2 gaps (a) in-plane and (b) out-of-plane 144
Figure 5-1: 3D element Solid 185 from Ansys library used to develop FPDM [93].....147
Figure 5-2: Comparison between strain results obtained experimentally and from FEM 150
Figure 5-3 Sequence of different steps of the FPDM 156
Figure 5-4: Applied load and boundary conditions in the FEM for laminates containing gaps in middle 0^o layer 157
Figure 5-5 Normal in-plane stress distribution at the gap across the thickness of unidirectional laminate 158
Figure 5-6: Out-of-plane shear stress at the edge of the gap for a unidirectional laminates at applied stress of 1880 MPa.....159
Figure 5-7 Damage evolution in UD carbon/Epoxy laminate containing a gap in the middle 0^o layer under fatigue loading 161
Figure 5-8: Comparison between the predicted FPDM and experimental results for unidirectional laminates.....162
Figure 5-9: Schematic representation for cross-ply laminate of (a)FEM and the used coordinates, (b) matrix cracks in off-axis layers, (c) delamination propagation and (d) fiber failure propagation 163
Figure 5-10: Comparison between the predicted FPDM and experimental results for cross-ply laminates.....165
Figure 5-11: Comparison between the predicted FPDM and experimental results for quasi-isotropic laminates 165
Figure 5-12: 2-D scheme for the defective -45^o layer containing a gap in quasi-isotropic laminate 166
Figure 5-13: Variation of the longitudinal tensile strength in a small area in the model.....168

Figure 5-14: Damage evolution for cross-ply with gap in 90^o layer at 1200 MPa up to 140000 cycles 169
Figure 5-15: Damage evolution for cross-ply with gap in 90^o layer at 1200 MPa up to 43000 cycles 170
Figure 5-16: Damage evolution for cross-ply with gap in 90^o layer at 1200 MPa up to 140000 cycles 171
Figure 5-17: Effect of properties variation on fatigue life of cross-ply laminates with gaps in 90^o at 1200 and 1170 MPa. 172
Figure 5-18: Comparison between the predicted FPDM and experimental results for cross-ply laminate with gap in 90^o layer 172
Figure 5-19: Damage evolution for quasi-isotropic laminate with gap in -45^o layer at 750 MPa up to 17000 cycles 174
Figure 5-20: Damage evolution for quasi-isotropic laminate with gap in 45^o layer at 750 MPa up to 18000 cycles 175
Figure 5-21: Damage evolution for quasi-isotropic laminate with gap in 45^o layer at 750 MPa up to 28000 cycles 176
Figure 5-22: Effect of properties variation on fatigue life of quasi-isotropic laminates with gaps in 45^o at 750 and 800 MPa. 177
Figure 5-23: Comparison between the predicted FPDM and experimental results for cross-ply laminate with gap in 90^o layer 177
Figure 5-24 Interlaminar stress distribution at the boundaries of the triangular gap 179
Figure 5-25: Damage evolution for unidirectional laminate with triangular gap at 1850 MPa 179
Figure 5-26: Comparison between the predicted FPDM and experimental results for unidirectional laminate with triangular gaps with different aspect ratios at 1850 MPa. 180
Figure 5-27: Effect of separating distance between 2 gaps on fatigue life for unidirectional laminate at 1900 MPa. 181
Figure 5-28 Shear stress distribution for two gaps with separating distances of (a) (3,6) and (b) (10,6). 182
Figure 5-29: Damage evolution for unidirectional laminate with 2 gaps at separating distance of (3,6) 183

Figure 5-30: Comparison between the predicted FPDM and experimental results for unidirectional laminates with 2 in-plane gaps 184
Figure 5-31: Comparison between the predicted FPDM and experimental results for unidirectional laminates with 2 out-of-plane gaps 184

List of Tables

Table 2-1: Test program performed in the current study 48
Table 3-1: Number of cycles to failure obtained for unidirectional defective specimen at 1880 MPa 65
Table 4-1: Using of IR thermography for rapid determination of fatigue limit of several materials 120
Table 4-2 Different types of manufactured laminates 121
Table 4-3 Slopes of temperature increase at different stress and R^2 values from fitted regression lines 124
Table 4-4: Threshold stress values obtained from experiments and IR thermography 126
Table 4-5 Different Damage mechanisms and their contributions in heat generation/dissipation 132
Table 4-6: Different damage mechanisms and their extension within the laminates after 1000 cycles 135
Table 4-7: Threshold stress values obtained from experiments and IR thermography for laminates with 2 gaps 144
Table 5-1 Material properties of Carbon/Epoxy laminates used in the FEM 149
Table 5-2: Fitting parameters used in the fatigue life model [94] 151
Table 5-3: Fitting parameters used in strength and stiffness degradation models [94] 153
Table 5-4 Different failure modes and corresponding property degradation schemes 155

Nomenclature

A	Cross-section area of the specimen (mm^2)
a	Aspect ratio of triangular gap
D	Defective specimen
DL	Delamination size
E	Young modulus
G	Shear modulus of elasticity (GPa)
H	Heat loss coefficient
L_R	Probability of survival
N	Number of cycles to failure
n	Number of specimens
P	Force applied on the specimen (N)
Q_d	Dissipated amount of heat
$Q_{gen.}$	Heat generating from rubbing of delaminated surfaces
Q_s	Net heat stored in the material
R	Stress ratio during fatigue tests
S	Shear Strength
S_d	Standard deviation
T	Environmental temperature
T_s	Surface temperature of the specimen

t	Time
U	Uncertainty in the experimental results
u	Scale parameter of Weibull function
u_x	Relative displacement between delaminated surfaces during rubbing
X	Normal strength in fiber direction
Y	Normal strength in matrix direction

Greek Letters

γ	shear strain
ε	normal strain
σ	Normal stress
τ	Shear stress (MPa
υ	Poisson's ratio
$\propto$	Shape parameter of Weibull function
Δt	Increment of time

Subscripts

a	Amplitude
c	Compression
ext	Extreme values in results
m	Mean

max	Maximum
min	Minimum
R	Residual properties
ref	Reference specimen
t	Tensile
1	Fiber direction
2	Matrix direction across width
3	Thickness direction

List of Abbreviations

APDL	Ansys Parametric Design Language
CP	Cross-ply laminates
DSC	Digital scanning calorimeter
FEM	Finite element model
FPDM	Fatigue Progressive Damage Model
FTS	Full tow staggering
HTS	Half tow staggering
IR	Infrared
POF	Probability of failure
QI	Quasi-isotropic laminates
SEM	Scanning election microscopy
UD	Unidirectional laminates
UTS	Ultimate tensile strength

Chapter 1

Introduction

1.1 Background

Owing to their great advantages over traditional materials, composite materials are now widely used as primary structures in many applications such as aerospace, renewable energy, automotive and marine industries. Among these advantages are high strength/stiffness to weight ratios, fatigue resistance, low thermal expansion coefficient and corrosion resistance. Carbon fiber reinforced polymer composites are extensively used in aircraft and aerospace industries. Boeing 787 has almost 50 percent by weight of its airframe made of carbon fiber composites. This approach helps in a weight saving of 20 percent compared to conventional aluminum designs [1].

To get the most benefit of composites, they must be well designed and manufactured in such a way that saves cost and provides high repeatability and flexibility during manufacturing process. There are many techniques available for manufacturing of composites. The choice of the suitable manufacturing technique depends on the configuration of the manufactured part and the desired accuracy.

Hand lay-up is one of the commonly used manufacturing processes of composites. This process can be carried out in two different ways. In the first way, dry fibers are laid down manually on the mold surface then resin is poured to wet the fibers. This way is used for making low cost components in which glass fibers and polyester resins are widely used. In the other way, pre-impregnated fibers (pre-preg) are used for making components in aircraft industry in which carbon fibers and epoxy resins are widely used. Pre-pregs are cut manually into the required layers. The layers are laid down manually on the mold surface on top of each other to form the required orientation. Then, autoclave might be used to ensure full curing of the laminates. This process is mostly manual. So, it has many disadvantages such as: highly time consuming, high labor cost, high material waste and probable low efficiency as a result of human errors.

Filament winding is another manufacturing technique that is mainly used for making of cylindrical parts. In this process, dry fibers are passed through a resin bath then they are wrapped around a cylindrical mandrel to form the cylindrical component. After curing, the mandrel is extracted from the composite cylinder. The limitation in this process is that the curvature of the required shape should be positive. In case of concave surfaces, the tension in the fibers causes them to simply bridge the concave region [2].

As a high demand for more flexibility, repeatability and development of manufacturing techniques capable of overcoming the limitations of the traditional methods, hand lay-up and filament winding, the trend is toward robotic manufacturing of composites.

The first step toward the robotic manufacturing of composites was the automated tape laying (ATL) machines which allow the rapid deposition of composite pre-impregnated tapes to either a flat or curved tool. Pre-preg tape widths range from 3 inch (76.2 mm) to 12 inch (304.8 mm). ATL

was used heavily in 1980's in military aircrafts (B2 stealth bomber). It was also used in the commercial aircraft industry (A380 stabilizer skin panels) [3].

Figure 1-1: Automated tape lay-up machine [4]

ATL has great advantages in reducing the manufacturing time of large components because of the high deposition rate of material. The accuracy and the quality of the output product were also improved compared to traditional hand lay-up method. ATL is very convenient for manufacturing of large flat panels as shown in Figure 1-1. However, it might have a limitation in manufacturing of relatively small components due to material waste especially at the edges of the structure. Also, it has some limitations in manufacturing of complex shapes because of the large width of the used pre-preg tapes.

Automated fiber placement (AFP) machines became available to overcome the limitations of ATL. AFP is a fully automated process for production of composite laminates that combines the different capabilities of filament winding, because of the use of fiber tows, and automated tape laying, because of the automated process of manufacturing. Automated fiber placement technology applications to the fuselage resulted in a 53 percent cost saving since the V-22 aft fuselage skin

could be fabricated in one integral piece rather than assembly of 10 skin panels in the original design [5].

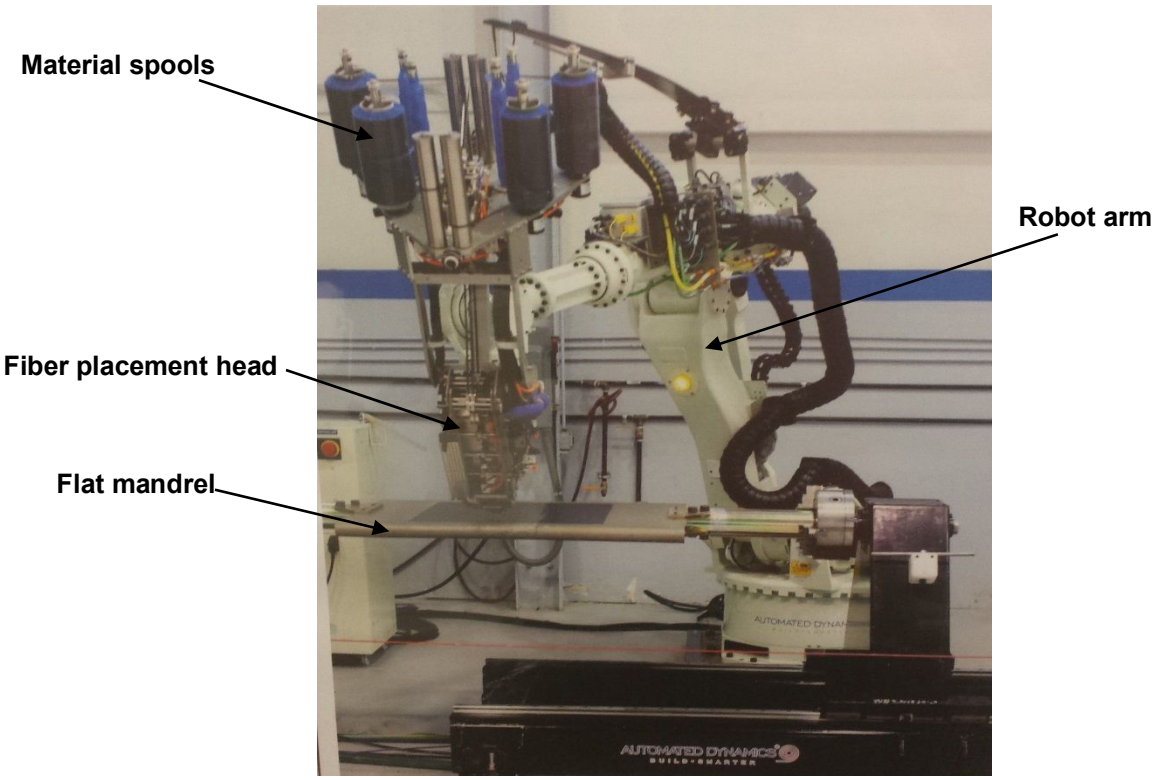

Figure 1-2: Automated Fiber placement machine available in CONCOM.

The AFP machine consists mainly of a fiber placement head attached to a robotic arm. Most fiber placement systems have seven axes of motion: three translation, three rotational and one rotational axis for the mandrel. This provides the machine with flexibility to position the fiber tows onto the complex surfaces enabling the production of complicated composite parts. Figure 1-2 shows the Automated Dynamics AFP machine available at Concordia Centre for Composites (CONCOM).

Each fiber tow is fed through its own guiding mechanism from individual spools attached to the placement head. Some heads have the ability to carry 32 spools which enables placing 32 fiber

tows simultaneously on the tool surface. The width of the tows can be reduced to 1/8 in (3.175 mm). A roller is used to compact the delivered tow against the tool surface which helps removing the trapped air and adhering the placed tow to the surface. The tow is also heated before reaching the surface using a hot gas torch to increase its tackiness to the surface. Using AFP machines allows not only the manufacturing of constant stiffness laminates, in which continuous straight fiber are used in each layer, but also variable stiffness ones in which the fiber orientation angles are continuously varied within the plane of the layers which helps enhancing the buckling performance [6-8].

One of the important options in fiber placement machines is the cut/restart capability. Each tow has its own cut/restart mechanism that enables individually controlling of tows. This option can be used to reduce the material waste close the surface edge and also enables variation of the course width, overall width of adjacent fiber tows, during manufacturing.

Automated fiber placement has some limitations such as minimum turning radius and minimum cut length. The minimum turning radius is the smallest turning radius the machine can perform without the fibers being wrinkled and it depends on the width of the tow. However, the minimum cutting length is the minimum distance which should be traveled by a tow before being cut-off by the machine cutter. It is dependent on the distance between the cutting mechanism and the compaction roller in the placement head [9].

For the ideal case, the material strips will be exactly adjacent to each other without any gaps among them. Practically, the generation of gaps during AFP manufacturing is due to machine inaccuracy, material tolerance and complexity of the manufactured component. The induced gaps can be divided into two types according to their occurrence locations:

1- Gaps parallel to fibers:

These gaps can generate at the boundaries between material strips as a result of inaccuracy of the placement head in following the pre-assigned fiber path due to the allowances of the machine movement (the tolerance is ±1 mm), vibration of the machine arm during operation and variation of strip width. This type of gaps is shown in Figure 1-3.

2- Gaps normal to fibers

These gaps generate at the end of material strips and normal to fibers as a result of tow cuts during manufacturing. This could happen at the boundaries of the manufactured parts as shown in Figure 1-4. Also, during steering of fibers, gaps can generate as a result of variation of course width, group of tows, at the boundaries of courses as shown in Figure 1-5(a). Finally, during manufacturing of complex parts, they are divided into sectors within which the orientation of the fibers is constant. Gaps normally generate at the boundaries between sectors as shown in Figure 1-5(b).

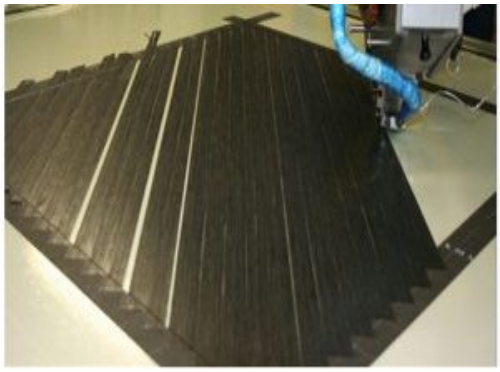

Figure 1-3: Gaps occurrence at the boundaries of material strips during AFP manufacturing [10].

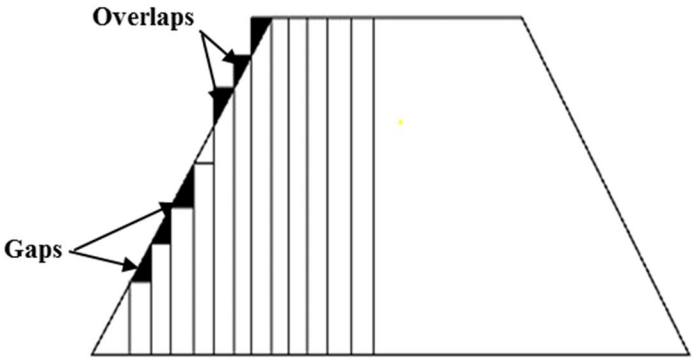

Figure 1-4: Gaps occurrence at the boundaries of the manufactured component

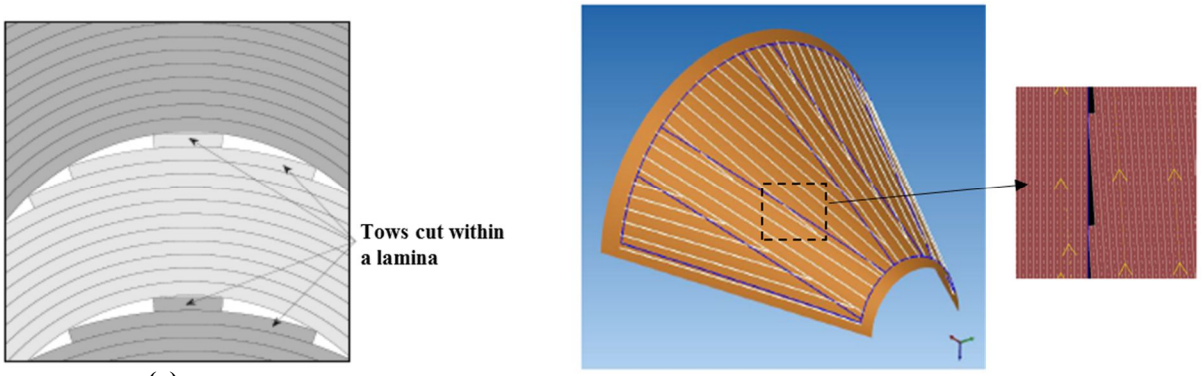

Figure 1-5: Gaps occurrence at the end of tows during (a) fiber steering [11] and (b) complex part manufacturing [12]

Consequently, it can be observed that the occurrence of gaps during composite manufacturing using AFP is unavoidable. In order to get the most benefit from the designed AFP laminates, it is important to understand their behavior while taking into account the effect of gaps that emerge during manufacturing process. In the literature, there is some work that focused on investigating the effect of defects on the behavior of composite materials. This will be discussed in the following. In many applications, the occurrence of overlaps is not recommended to avoid the increase in weight and local variations in thickness. So, most of the work focused in investigating the effect of gaps on mechanical behavior.

1.2 **Effect of defects**

In the early of 1990's, when AFP machines first became available, researches started to compare the laminates made by AFP to that made by conventional hand lay-up method. Walker et al. [13] observed some improvement of about 21% in the tensile strength of laminates manufactured by fiber placement machines compared to laminates manufactured by traditional lay-up method.

Later, Carins et al [14] used finite element model (FEM) to investigate the possible reasons for this observed improvement in tensile strength. They developed a FEM which modeled the laps

as double-stiffness elements and the gaps as resin-region elements. They found that incorporating the gaps in the model resulted in 3% reduction in the average strain (deformation) and 11% for the overlaps case. This improvement was small compared to the previously observed improvement by Walker [13] which was about 21%. They expected that the damage mechanisms that were developed as a result of these defects might have a significant effect on the improvement. They updated the model to detect the delamination and split. Delamination was simulated by releasing nodes through thickness while split was presented by releasing nodes in the plane of the layer. They found that a combination of split and delamination can reduce the average strain up to 36%. It was concluded that the occurrence of these damage mechanisms helped in redistributing and relieving stresses away from the notches and hence decreasing the local strain at notches.

The existence of gaps causes the occurrence of waviness especially at the layers adjacent to the gap locations. The resulting waviness affects severely the compression behavior of the laminate. So, in order to investigate the laminates under compression loading, waviness should be taken into account. It was found that both compression strength and stiffness degraded seriously by increasing the fiber waviness. The strength was found to be much more sensitive to waviness than stiffness [15]. Also, the effect of waviness depends on the anisotropy of the material. As the anisotropy of material increases, the sensitivity to waviness increases. So, carbon fiber composites are more affected by the existence of waviness than glass fiber composites because carbon fiber composites have higher stiffness in fiber direction compared to glass fiber composites. Consequently, the strength/stiffness will be greatly affected by the waviness introduced in fiber direction for carbon fiber composites. The waviness induced in the laminate can also affect the fatigue life of composites. Adam and his coworkers [16] found that samples without waviness showed a compressive fatigue strength of 75% of the static strength at 10^6 cycles. As a result of waviness, the compressive fatigue strength was reduced to about 45% of static strength.

Sawiki et al [17] studied the effect of gaps and overlaps on the compressive strength of composite materials (unnotched and with holes). They created the defects manually by removing or adding a strip of the material to form the required defect size as shown in Figure 1-6. The manufactured samples contained defects in the 90^o plies in order to give the chance for maximum waviness between the 0^o and 90^o layers because it mostly affects the compressive strength.

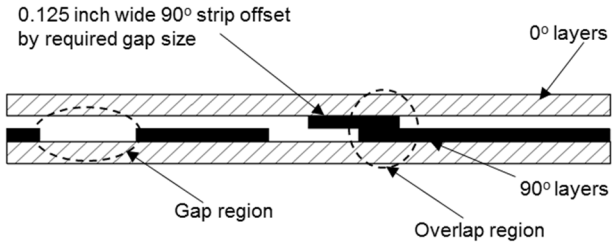

Figure 1-6: Defects were created by manually removing material strips [17].

Croft et al [18] studied experimentally the effect of gaps/laps and twisted tows on the compression and tension of unnotched and notched laminates. Each sample had one defect which was created manually during manufacturing of the tested panels by adding or removing two material strips along the whole length/width of the sample. The dimensions of the defects were one tow in width and two tows in thickness in order to create a significant effect so that the variability between different configurations can be captured. The investigated defects are shown in Figure 1-7.

They found a reduction in the tensile strength of about 3.4% and negligible reduction in case of compression by about 1% for both gaps and laps. In case of open hole tension (OHT), the defects has no obvious effect on the strength because the effect of stress concentration of the hole is more severe than the effect of defect. For open hole compression (OHC), defect along length, they found an increase in strength due to damage mechanisms which help relieving the stress away from the high stress region which was confirmed by Carins [14]. However, in the case of defects along the width, the strength decreased because it increased the stress concentration in a high stressed area and also because of the effect of induced waviness of 0° layers.

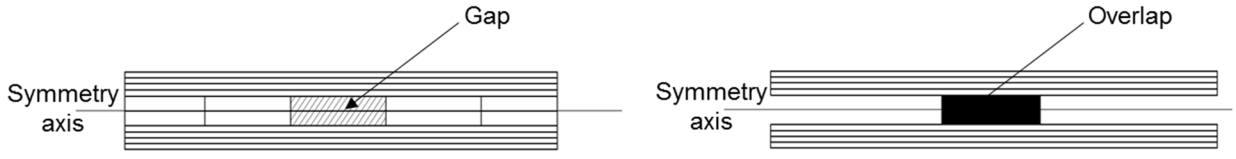

Figure 1-7: Different defect configuration investigated by Croft et al. [18]

Kimball [19] explored the effect of gaps in different orientations at tangency point of holes in quasi-isotropic laminates under open hole compression tests. He concluded that gaps tangent to holes in 0^o layers helped improving the strength by 7% as a result of stress redistribution in the high stress area around the hole.

The manufacturing parameters such as tow width and number of tows can contribute to the occurrence of gaps and laps in variable stiffness laminates. Increasing the number of tows and the width of a course reduced the gap area because of less occurrence of course boundaries. Also, as the tow width increases inside a course, the gap area increases because dropping a wider tow will cause larger defective area than of smaller one [20]. Blom et al. [21] found numerically that increasing the tow drop (gap) area causes a reduction in the buckling load of the laminate. In addition, using staggering technique, shifting the plies with same orientation with respect to each other across the thickness, improves the strength of the defective laminate.

Fayazbakhsh et al. [22, 23] used a finite element model platform (Ansys) incorporated with Matlab code to predict the effect of gaps/overlaps on the stiffness and buckling of variable stiffness laminates. They developed a method called defect element method to overcome the problem of using small size and large number of elements in the proposed approach of Blom [21]. The defect element can combine both regular composite material and embedded defect in the same element. The elastic properties of each element are changed based on the defect area percentage (gap/lap area in the element divided by total element area). This helps in reducing the required number of elements to capture the gaps/overlaps. The results of the FEM revealed that gaps caused a reduction in both buckling load and stiffness. On the other hand, the laps increased both of them.

It is worth mentioning that the experimental work of the aforementioned research focused on investigating the effect of defects at the boundaries of adjacent tows by manually adding or removing material strips at the required locations to formulate gaps/overlaps. Falco et al. [24] studied the effect of gaps between fiber courses, at the end of tows, for unnotched and open hole laminates under tension. They studied three different configurations: complete gap strategy (0% coverage), complete overlap strategy (100% coverage) and complete gap with staggering technique. For unnotched laminates, they found that the severe effect was for laminates containing gaps (0% coverage) and without applying staggering technique, as shown in Figure 1-8, due to the

coincidence of the defects across the thickness of the laminate. However, using staggering technique helped improving the tensile strength by 12%. They also observed the occurrence of delamination at the edge of the failed defective specimens which was attributed to the high interlaminar stresses due to the induced defects. For notched laminates, they found that the effect of stress concentration presented by the hole is higher than the effect of defects. Falco et al. [25] extended their experimental work on the defective laminates to investigate the effect of the defects on the compression after impact. They concluded that the reduction in the residual compression strength was very small between different configurations. They concluded that the effect of defects on compression after impact is negligible and the main reason for the reduction in the compression strength is the damage caused through the impact.

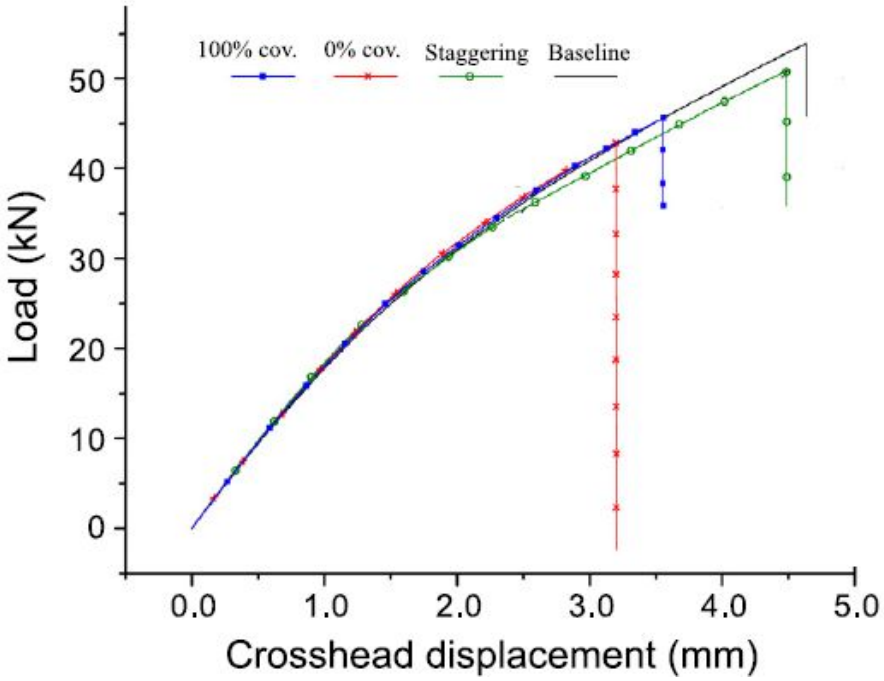

Figure 1-8: Comparison between tensile behavior of different unnotched laminates [24]

More recently, X. Li et al [26] developed a 3D progressive damage model to investigate the effect of the manufacturing defects in different layers on the tensile and compression behavior of AFP quasi-isotropic laminates. The model revealed that the gaps/overlaps caused a larger knock

down in compression strength than tensile strength and the defects in 45^{o} and -45^{o} layers have larger effect compared to defects in 90^{o} layers.

Lan et al [27] investigated the effect of using caul plate during curing of defective cross-ply laminates on the tensile properties of carbon reinforced laminates. They found that the existence of the caul plate helped reducing the thickness variation, enhancing the resin flow and alleviating the effect of gaps under tensile loading. The same authors extended their experiments to investigate the effect of gaps and overlaps on the in-plane shear and compression properties [28]. For the case of shear tests, it was found that the gaps caused a drop in both shear modulus and shear strength by 10-14% compared to the reference laminate. This reduction decreased by using caul plate during curing. For the overlap, there was a slight increase in the property by 2-4% due to the local increase in thickness when a caul plate was not used. However, using the caul plate eliminates the effect of overlaps. For compression tests, the defects had a severe influence on mechanical properties. Using the caul plate helped in limiting the effect of the induced gaps and overlaps.

Automated fiber placement is now widely used in automotive, aircraft and aerospace industries because of its ability to save material waste and to manufacture complex geometries. Although most of the critical loads in these applications are fatigue loadings, to our knowledge, there has been no research that studied the effect of AFP manufacturing induced defects on fatigue behavior of composites. In the following subsection, the main parameters affecting the fatigue behavior and the different damage mechanisms occurred during the fatigue life of composite laminates will be briefly described.

1.3 **Fatigue in composites**

Fatigue of materials refers to the degradation of the mechanical properties of the material when subjected to repeated or cyclic loading. This type of loading can cause failure of the material at low stress levels compared to the ultimate static strength.

In 1960's, many researchers believed that metals suffered from fatigue in many accidents such as the Comet, F-111, B707 at Lusaka, Aloha Airlines B737and C130A Firefighting Aircraft [29]. So, there was a trend for using composites but there was a belief then that composite materials

especially carbon fiber composites do not suffer from fatigue. This misconception was due to the very high stiffness of carbon fiber laminates in fiber direction. But as a result of the anisotropy of carbon fiber composites, there may be a high stresses transverse to fiber direction that might initiate damage and eventually cause failure [30].

Some of the earlier research in the field of fatigue in composite was by Baker who studied the behavior of metal matrix composites under reversed fatigue bending [31]. This was followed by work of Owen [32] where he observed the damage development in chopped glass/polyester laminate under fatigue loading.

1.3.1 **Factors affecting fatigue behavior**

There are many factors that affect the fatigue behavior of composite material and can be divided into internal and external. Internal factors are such as type of matrix/fiber, laminate configuration and type of reinforcement. External factors are environmental and loading conditions. The fibers are the main load carrying agents in composites so the fatigue behavior is affected by the type of fibers. Glass fibers are more sensitive to fatigue loading than carbon fibers [33]. The main reason is that glass fibers have less stiffness (70-80 GPa) than carbon fibers (220-700 GPa). This reduced stiffness gives decreases the overall stiffness of the laminates and gives the matrix the chance to elongate more which increases the risk of occurrence of matrix cracking.

On the other hand, carbon fibers have high stiffness so they restrict the matrix from large deformation and reduce the probability of crack initiation. Also, for a composite laminate, with glass or carbon fibers, in the first cycles of loading, some weak fibers can be broken as a result of scattering in the strength of fibers. This will be followed by crack initiation from these weak locations [34]. Since carbon fibers have higher strength than glass fibers, so the spread of these spots is less. Besides, in the same type of fibers, there are different grades. Glass fibers have many types such as E-glass, S-glass and C-glass. Each of them behaves differently under environmental conditions [35]. Carbon fiber has also many types such as T300, AS4 and IM6. Each of them has different static and fatigue behavior [36, 37] as shown in Figure 1-9.

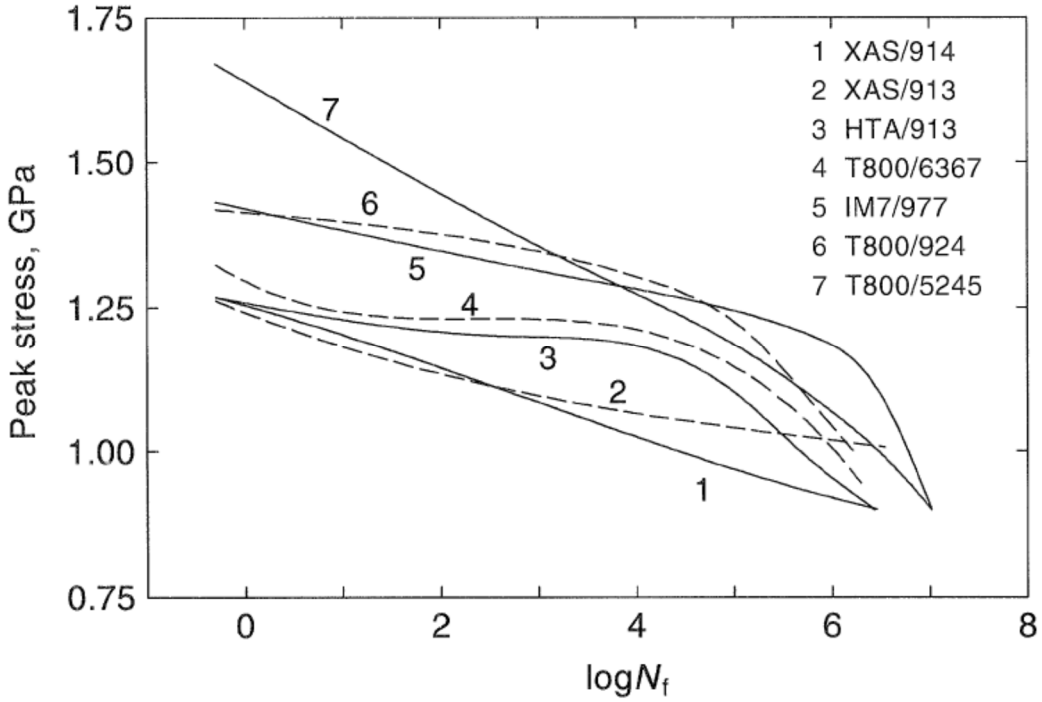

Figure 1-9: Stress-life curves at R=0.1 for different carbon fiber composites [36].

Also, changing the type of the used reinforcement, between woven and non-woven, affects the fatigue behavior. It was found that both the static and fatigue behaviors were degraded for composites reinforced by woven carbon fibers compared to non-woven fibers [38].

In addition, the type of matrix affects the fatigue life of composite laminate. Thermoplastic resins give the composites longer fatigue life than thermoset resins because they have higher ductility and fracture toughness which improves the resistance to crack propagation [39]. Bathias [40] also found that delamination damage mechanism was less in the case of thermoplastic composites because of the high interlaminar fracture toughness and strong fiber/matrix interface. Some additives to the resin can improve the fatigue performance. Nagaligam [41] added nano-powder to polyester resin with different weight ratios. He found that adding nano particles to the polymer matrix improved the ultimate tensile strength by about 24% and fatigue life by about 20%.

The strength of the interface has also a great role in controlling the damage behavior. As the interface strength increases, the probability of fiber/matrix debonding decreases [42]. Sometimes surface treatments to fiber surface are used in order to improve the wettability and compatibility between fiber and matrix such as coupling agents and fiber sizing [43]. Adding Silane coupling agent to the glass fibers was found to enhance the static and fatigue performance [44].

Moreover, the fatigue life depends on external factors such as loading conditions. Mandell et al [45] studied the effect of stress ratio and load frequency on the fatigue life. They found that fatigue life increased by increasing the frequency for the same stress value and also by increasing the stress ratio. Also, the fatigue response of composites is different under different types of loading. For instance, composites that contain Aramid fibers show a shorter fatigue life under compression loading than in tension loading. This is due to the chemical structure of Aramid in which the molecules are linked by a weak Hydrogen bond [30, 43]. Besides, the dominant damage mechanism under tensile loading of unidirectional laminates is fiber breakage while under compression loading is fiber buckling.

Environmental conditions, such as temperature and moisture, are also external factors. The increase in temperature degrades the resin properties, hence, makes it easier for crack initiation, so the fatigue behavior at high temperatures is different from matrix one type to another. Kawai [46] studied the fatigue behavior of different types of resin under 100 ^{o}C. He found that the laminate based on thermoplastic (PEEK) resin had the best off-axis fatigue behavior among the other tested laminates. Also, Jen et al [47] studied the effect of temperature increase for cross-ply and quasi-isotropic laminates. They found that the fatigue strength, defined as the stress value corresponding to 10^6 cycles, decreases by increasing the temperature for both stacking sequences as shown in Figure 1-10. Moisture also negatively affects the fatigue behavior of composites and weakens the fiber/matrix interface [48, 49].

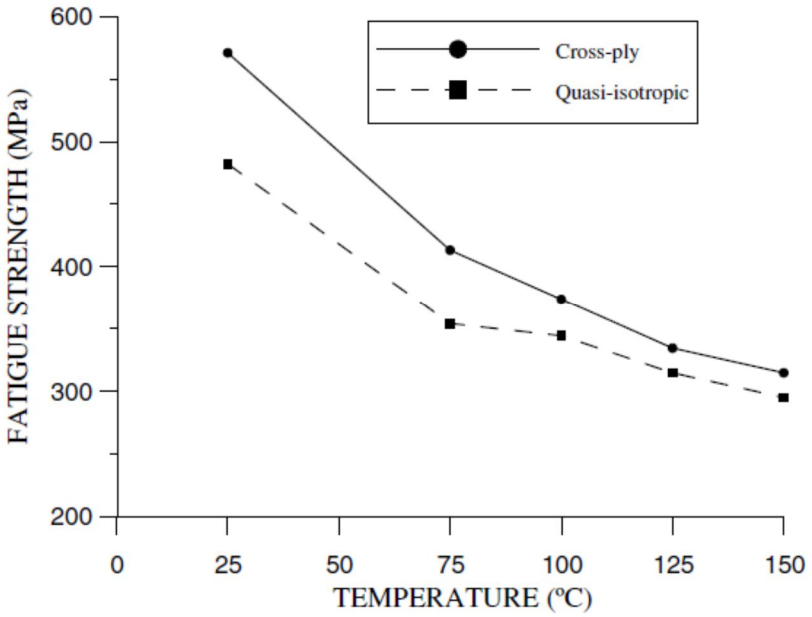

Figure 1-10: Fatigue strength for cross-ply and quasi-isotropic laminates at different temperatures [47]

1.3.2 **Fatigue damage mechanisms**

Fatigue damage in composites is different from that in metals. In the case of metals, there may be a dominant crack that initiates and propagates till final failure. The crack normally initiates at the surface due to the environmental effects on the metal surfaces and the propagation plane of the crack is normal to tensile direction. However, in composites the fatigue behavior is more complex because there are many damage mechanisms such as matrix cracking, fiber/matrix debonding, delamination and fiber breakage. Crack propagation may be parallel or normal to loading direction [50].

The previously mentioned damage mechanisms could happen successively or simultaneously. Matrix cracking has many forms. It could be transverse, through thickness or width, or longitudinal cracks parallel to fibers. It is the mostly common damage mechanism in angle-ply laminates. Matrix cracking behavior is different in fatigue compared to quasi-static loading. The density of matrix cracking in off-axis plies is much higher in fatigue than in static

loading [51]. Fiber/matrix debonding depends on the strength of the interface between fibers and matrix [52].

Delamination is caused as a consequence of matrix cracks or fiber/matrix debonding and due to high interlaminar stresses [53]. Delamination starts to initiate either at the edge due to free edge effect or within the layers as a result of the high density of matrix cracking. At the final stages of loading, the fibers are subjected to high stress or high strain levels and this causes fiber breakage to happen and consequently failure. So, matrix cracking is the dominant mechanism at early stage of loading, delamination and debonding are in intermediate stage and fiber breakage is at the last stage which causes failure [30].

The damage development process during fatigue loading can be divided into three stages. The initial stage occurs when cracks initiate at different locations in the laminate. In the second stage, slow damage propagation occurs and a saturation state is reached. The final stage takes place when fiber breakage happens rapidly and final failure occurs [54]. The saturation in the second stage may happen when the spacing between cracks form the opposite edges reaches a certain limit. Hence, the damage growth rate decreases and saturation occurred [51].

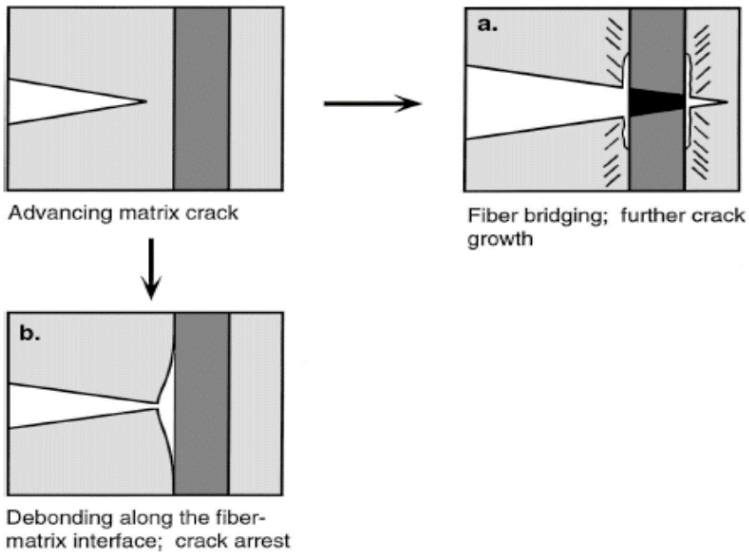

Figure 1-11: Occurrence of matrix crack followed by fiber bridging or interface debonding [55].

Many authors investigated the fatigue behavior and occurrence of damage mechanisms for composite laminates with different configurations. For unidirectional laminates, the damage mechanism started by some weak fiber breakage which is randomly distributed. The shear stress between fiber and matrix increases at the tip of the broken fibers which causes crack initiation from these high stressed regions. Cracks propagate transverse to fiber direction followed by fiber bridging or interface debonding till failure [34, 55] as shown in Figure 1-11.

For cross-ply laminates [56], damage initiated at the edge in the form of both transverse matrix cracking and delamination then they propagated from the edge across the width of the specimen. Finally fiber breakage and failure occurred. The cracks density increased by increasing the number of cycles till reaching saturation. These observed damage mechanisms agreed with the damage mechanisms observed by Talreja [34] for cross-ply laminates.

Hosoi and his coworkers [57, 58] focused their study on the quasi-isotropic laminates under high cyclic fatigue loading. The main damage mechanisms for all stress levels were the same, transverse cracks and delamination. The only difference was that the initiation and propagation of damage were retarded for low stress level compared to higher ones. The delamination was found to be more effective at high fatigue cycles and low stress levels. In another study by the same authors [59] they focused on the behavior of transverse cracking. It was found that transverse cracks initiated at the edges. Then, after saturation at the edges, these cracks started to propagate through the width of the samples. Edge delamination propagated also to the width when the transverse cracks density at the edges reached a saturation level.

Fatigue behavior of composites was found to be sensitive to pre-existing defect such as delamination. Colombo et al. [60] studied the effect of pre-existing delamination on the fatigue life of glass fiber reinforced composites. It was found that the existence of induced delaminated area did not affect the static strength of tested laminates. However, the fatigue life was greatly reduced by introducing the delamination inside the laminate. The delamination had a noticeable effect on the damage behavior during fatigue for stresses higher that the fatigue limit.

To sum up, based on reviewing some work focused on investigating the fatigue behavior of composites, it can be observed that fatigue damage in composite is a very complicated process due

to the variety of damage mechanisms and the anisotropy of the material. In addition, the fatigue performance is affected by the existence of defects in the composite laminates.

Defects in composites can be manufacturing induced defects or in-service defects. The former one is caused during manufacture process such as resin rich areas, fiber waviness, fiber misalignment and delamination caused by drilling or cutting of composite laminates. The later can be caused by impact damage and crack propagation due to loading [61]. For better understanding of the fatigue behavior of composite laminates and in order to ensure the integrity of a structure, it is of importance to provide practical information about the damage state within the material. One of the main goals for aerospace industry is the detection of damage caused by the existence of various defects during the whole fatigue life of a component.

1.4 **Damage detection in composites**

Recognition of damage in composites is more difficult compared to the case of metals since most of the damage occurs beneath the surface of the laminate. Damage in composites under fatigue loading conditions has been investigated by a variety of destructive and non-destructive techniques.

Destructive sectioning of coupons followed by inspection using scanning electron microscopy (SEM) is one of the commonly used destructive techniques for detection of inherent damage. This method can provide information on the location and type of damage. It also sometimes can be used for quantification of damage such as the density of cracks or the extension of delamination along the interface [56, 62, 63]. Since the inspected specimen cannot be tested again so investigating the damage evolution requires a large number of specimens to be inspected.

On the other hand, there are various non-destructive techniques that have been used for detection of damage due to fatigue loading such as ultrasound, X-ray radiography and acoustic emission [54, 63]. The use of these methods may not be appropriate for real time monitoring of damage. They require a well-controlled environment in addition to the need to remove the specimen from the testing set-up to be inspected. Infrared (IR) thermography has also been used

as a non-destructive method for in-situ detection of damage development during fatigue loading [64-67].

IR thermography is a non-destructive and non-contact technique that can be used to detect IR energy, emitted naturally from any object whose temperature is absolute zero or higher, and convert this energy to a temperature distribution using IR cameras. It can be divided into two types: active and passive. The first one needs an external source of stimulation such as heat source or mechanical loading to increase the temperature of the object. For example, detecting defects may need stimulating them to be distinguishable from surrounding material. The second one does not need any external source and can be used when the object has some temperature difference from the surrounding [68]. The main advantages of IR thermography are:

- Detection of large size components in short time.
- Can be used with one-side access of the specimen.
- Used to detect defects in components while being in-service.
- Easy interpretation of results.

IR thermography was used for defect detection in thick glass fiber composites [69] and carbon/carbon composites [68]. The depth of the defect represents one of the limitation with this technique. It was found that the maximum depth of detectable defect for composites using IR thermography was about 4 mm for one side inspection [61]. It was also found that the detectability of defects decreased linearly by increasing the depth of defect and it increased by increasing the damaged area. The thickness of the damage zone has also an effect on its detectability. This means that defective zone with large size but small thickness will be difficult to be detected [70, 71]. Upon reviewing the aforementioned research, it can be concluded that IR thermography can be efficiently used not only for detection of defects but also for damage monitoring during fatigue loading.

1.5 **Motivation and objective**

Referring to the aforementioned discussion, the following gaps in the literature were observed:

1- Most of the work presented in the field of the effect of gaps induced during AFP manufacturing focused on the gaps at the boundaries of the tows, parallel to fiber direction. There is a lack of investigating the gaps at the end of tows perpendicular to fibers.
2- The work presented in the literature focused on investigating the effect of defects on the static behavior of laminates manufactured using AFP technique and their impact on the mechanical properties such as tensile and compressive strength. To the best of our knowledge, no work has been performed to study the effect of the induced defects during AFP manufacturing on the fatigue behavior of laminates.
3- In the literature, it was mentioned that the AFP defects, such as gaps, are critical because of the probability of damage initiation from these locations. Nevertheless, the dominant damage mechanisms as a result of these manufacturing defects were not investigated.

Motivated by the desire to cover these aforementioned gaps in the literature, the objectives of this presented research are as follows:

1- Experimental investigation of the effect of induced gaps on the fatigue performance of laminates manufactured by AFP technique. For better understanding of the effect of these defects, some parameters were considered within the study such as laminate configuration, gap shape, number of gaps and orientation of gaps.
2- Using IR thermography as a non-destructive technique for real time detection of damage during fatigue loading of laminates containing gaps.
3- Using of sectioning and inspection using SEM as a destructive technique for investigating the occurrence of internal damage that arises at the location of the manufacturing defects.
4- IR thermography was also used in the study as a method for rapid evaluation of the stress values below which there is no effect of induced gaps on the fatigue life of AFP laminates.
5- A fatigue progressive damage model (FPDM) was developed and applied to the case of laminates containing gaps and subjected to fatigue loading. This model is helpful in saving time and material required for performing real fatigue tests especially in the initial design steps.

1.6 **Thesis organization**

A general overview is presented in chapter (1) focusing on the previous research in the field of the effect of AFP defects in the literature. In addition, a brief overview about fatigue behavior, damage and detection of damage in composites is discussed.

Details of experimental work performed to investigate the effect of gaps on fatigue behavior are illustrated in chapter (2). Procedures of manufacturing and testing of specimens are elaborated and the specifications of the used testing and detecting equipment are presented in this chapter. The results of the performed experiments are shown in chapter (3) accompanied by the analysis and explanations of the obtained results. Moreover, the results of using IR thermography as a real time method for damage detection during fatigue loading are discussed in this chapter.

At the end of chapter (3) it is found that the main drawbacks in determining the threshold stresses, value of stresses below which the effect of gaps on fatigue life diminishes, are the extensive time and material consumption. Consequently, in chapter (4), IR thermography is used as a rapid and accurate method for evaluation of the threshold stress values. This is found to overcome the drawbacks of the traditional fatigue testing method performed in chapters (2) and (3).

Chapter (5) is devoted for the developed fatigue progressive damage model (FPDM). This chapter is divided into two main parts. In the first part, the main steps of the FPDM are explained in details. In the second part, validation of the developed model is performed by comparing the predicted results from the FPDM with the results obtained from the conducted experiments, illustrated in chapter (3).

In Chapter (6), a comprehensive conclusion for all of the chapters and suggested future work are presented.

Chapter 2

Material and experimental details

The purpose of the experimental work is to have a good understanding of the effect of the unavoidable gaps during AFP manufacturing on the mechanical performance of composite laminates subjected to fatigue loading. In order to reach this goal, two sets of tests were performed. The first set is a group of static tests for material characterization. The static tests aim at obtaining the mechanical properties of the material required as inputs for the finite element model. The second set is the fatigue tests performed on both defective specimens and reference, free from defects, specimens to investigate the effect of gaps on the fatigue behavior of laminates made by AFP. Hereafter, detailed procedures for specimen fabrication will be presented followed by the methodology used for creating the defects in the manufactured laminates. Then, different procedures for static and fatigue testing will be elaborated.

2.1 **Material**

The material used in the study was carbon/epoxy prepreg (CYCOM 977-2-35-12K HTS-145) supplied by Cytec company. The material is supplied in spools of strips whose width is 0.25 inch (6.125 mm), shown in Figure 2-1. The material was formulated for autoclave curing with a curing temperature of 177 ^{o}C and it has many applications in aircraft and space fields. The material spools were stored in vacuum sealed bags and kept in freezer at -18 ^{o}C. The sealed bags were taken out from the freezer one day before using to thaw to room temperature. The used material did not exceed the out-life which was 30 days and the tackiness of the material was found to be good during manufacturing.

Figure 2-1: Cycom 977-2 material spools used in the study

2.2 Specimen preparation and inspection

2.2.1 Specimen manufacturing and curing

All the manufactured plates within the study were made using the AFP machine available at Concordia Center of Composites (CONCOM). The AFP machine supplied by Automated Dynamics is shown previously in Figure 1-2. These are some specifications for the machine:

1- Kawasaki robot arm with six degrees of freedom.
2- Fixture for cylindrical and flat mandrels with one degree of freedom (rotation around its axis) shown in Figure 1-2.
3- Head interface connection was designed to accept both thermoset and thermoplastic composites.
4- The system is supported by independent tow control capability which can cut/restart each tow individually
5- Head-mounted creel can carry up to four material spools with 0.25 inch (6.35 mm) wide tows.

The AFP machine laid down the material strips in any orientation on a flat mandrel. The dimensions of the manufactured panels were 12 inch (304.8 mm) length and 15 inch (381 mm) width. The parameters used during AFP manufacturing process were kept the same for all of the composite panels to avoid any effect of parameters change. The manufacturing parameters were:

- Torch temperature: 100 ºC
- Compaction force: 60 lbf.
- Layup speed: 3 in/sec

After manufacturing, the panels were vacuum bagged and prepared for autoclave curing. The vacuum bag assembly was then checked for any air leakage then it was placed inside the autoclave as shown in Figure 2-2. The autoclave is a cylindrical chamber that can apply pressure and temperature simultaneously during the curing process. The temperature is required for activating the curing (cross linking) reaction of the thermoset resin used and also for decreasing

the viscosity of the resin which consequently facilitates the resin flow among fibers to ensure full wetting and squeezing out any air voids in the layers. The pressure is also needed for compacting the layers together in order to remove the trapped air voids out of the laminate.

The recommended curing cycle from the manufacturer [72] was followed as shown in Figure 2-3. It consists of temperature ramp-up with 2.5 ^{o}C/min up to 177 ^{o}C, followed by holding at 177 ^{o}C for 3 hours then cooling down with 2.5 ^{o}C/min. Both pressure and vacuum were kept constant at 70 psi and 15 psi respectively during the whole curing cycle.

Figure 2-2: Autoclave used for panels curing

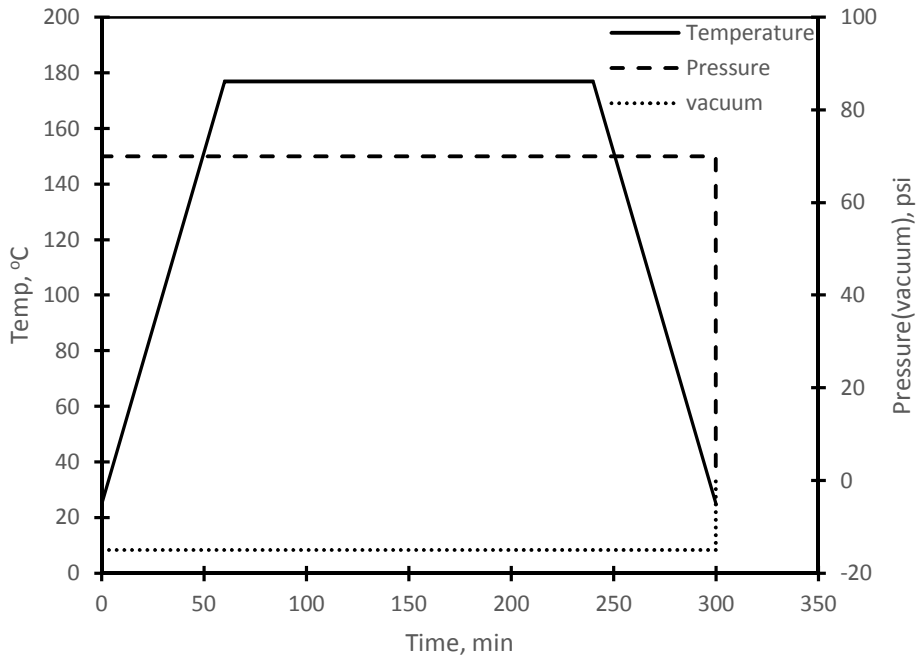

Figure 2-3 Curing conditions for the material (Cycom 977-2) [72]

The curing conditions were kept constant for all fabricated laminates to perform as accurate comparison as possible among different types of laminates. After curing, a distance of 1 inch (25.4mm) was trimmed from each side of the plate and all edges were cut parallel and perpendicular to the fiber direction. Cutting process was performed using a water-cooled diamond blade.

2.2.2 **Quality Inspection of laminates**

After manufacturing of the composite panels, some specimens were cut and inspected to check the quality of the manufactured laminates. This section represents the performed inspection procedures using Digital Scanning Calorimeter (DSC) and optical imaging.

2.2.2.1 **DSC characterization**

Mechanical properties of thermoset polymer composites are greatly affected by the degree of cure of the manufactured laminates. So, before starting of the mechanical tests, some samples

were inspected using DSC to check the degree of cure of the manufactured samples. The DSC used was Q-200 manufactured by TA instruments, shown in Figure 2-4.

Figure 2-4: Digital Scanning Calorimeter (DSC) used to check the degree of cure

Three samples of 10 mg each from a unidirectional plate were cut and put in an aluminum pan to be cured. The device subjects the specimen to 2 heating/cooling cycles. The curing reaction is an exothermic reaction. So, if any uncured resin existed in the laminate, it will cure during the heating portion of the cycle and exothermic heat will be detected. If no peaks of heat were detected during the tests, then this means that the tested specimen was fully cured.

2.2.2.2 **Microscopic inspection**

Mechanical properties, especially fatigue properties, can be severely affected by the void contents inside the laminate. So, some sections were cut from the cured laminates at different locations and inspected using Scanning Electron Microscopy (SEM). The purpose of this inspection was to check the quality of the manufactured samples in terms of void contents and the

volume fraction. The following steps summarize the procedures followed for samples preparation for SEM inspection:

1- Samples of 1 inch (25.4 mm) length and 0.5 inch (12.7 mm) width were sectioned from the cured plates from various locations, close to the edges and at the middle area of the plates.
2- In order to polish these sections, they should be immersed in epoxy resin and left to be cured. Then the polishing procedures are carried out. To do this, 15 gm of epoxy (Anamet-DER324) and 1.65 gm of hardener (DEH-24) were added together and mixed using a vacuum mixer (Thinky-ARV200) as shown in Figure 2-5 to get rid of any air bubbles in the mixture. The mixture was poured in cylindrical plastic molds containing the samples and left to be cured for 24 hours at room temperature.

Figure 2-5: Vacuum mixer used to remove air bubbles

3- After curing of epoxy containing the samples, the surface of samples was polished using automatic polishing machine (Persi Mecatech 234), shown in Figure 2-6. The following steps were performed to obtain a well-polished samples' surface:

- Grinding with 180 grade sanding paper for 60 seconds.
- Grinding with 320 grade sanding paper for 120 seconds.
- Grinding with 600 grade sanding paper for 120 seconds.
- Polishing with 9 µm pad for 200 seconds.
- Polishing with 3 µm pad for 200 seconds.

4- Then the samples were ready for being inspected using “FEIN Optic RX50 microscope”.

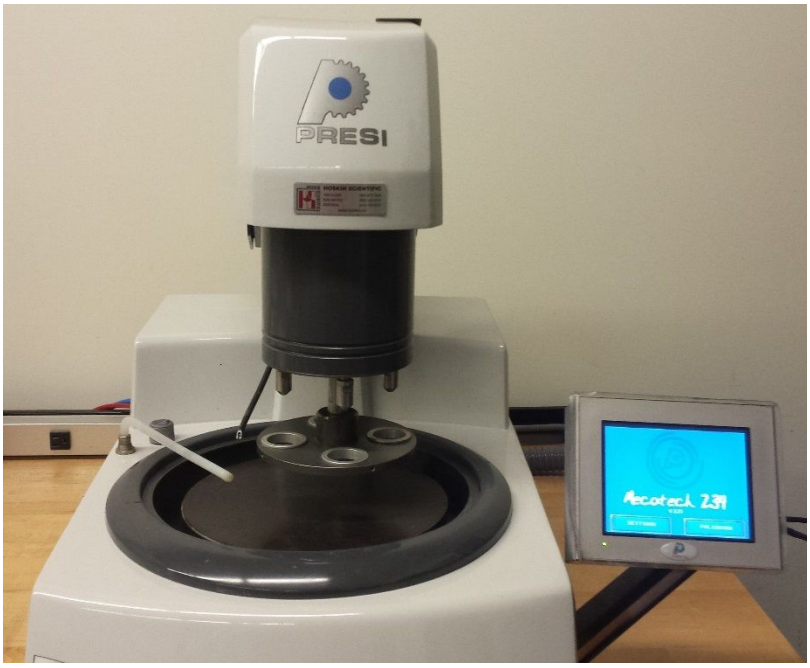

Figure 2-6: Automatic polishing machines used to prepare the SEM samples

Image analysis was performed on the captured microscopic images using ImageJ software which can be used for stitching of many magnified images together to obtain one continuous image for the entire width of the samples. Also, it can be used for measuring the fiber volume fraction and void contents in the samples based on the ratio between the areas of fibers/voids to the total area of the captured images.

2.2.3 **End tabbing and specimen cutting**

To avoid high stresses from the testing machine grips during testing, GFRP tabs were bonded to the edge of the cured plates according to ASTM standards [73]. 3M-162S scotch adhesive film was used to bond the tabs to the laminates. The adhesive film needs to be cured at 105 ^{o}C for 90 minutes with applied vacuum of 10 inches of mercury. Hence, the plates with the end tabs were vacuum bagged again and placed inside the oven (Heratherm oven) for 90 minutes.

Finally, the plates were cut into samples with the required testing dimensions, which will be illustrated later in "mechanical testing" sub-section, using a water-cooled diamond saw. The cutting procedures were performed with caution to avoid any misalignment or deviation of fibers from the required directions.

2.3 **Defect configurations**

As mentioned previously, gaps can generate during manufacturing using AFP either parallel or perpendicular to fiber direction. The second type of gaps, gaps normal to fibers, is more severe than the first one because as a result of cutting of fibers, high stresses generate at the edge of the gap that might cause damage initiation. So, the present work focused on studying the gaps created normal to fibers as a result of tow cuts.

In reality, the generated gaps have a triangular shapes. For the sake of simplicity, gaps were assumed to have a rectangular shape. However, within the study the effect of changing the gap shape to triangular gaps was investigated and compared to the rectangular ones. In the following subsections, in order to fully understand the effect of the gaps on the fatigue behavior of AFP laminates, a variety of parameters will be considered. The present work focused on the following parameters:

1- Effect of gaps in 0^{o} layers for different stacking sequences.
2- Effect of gap shape.
3- Effect of gap orientation.
4- Effect of number of gaps.

The methodology for creating the different defects for studying the aforementioned parameters will be presented in the following subsections.

2.3.1 **Effect of gaps in 0^o layer for different stacking sequences**

The purpose of this study is to investigate the effect of the gaps in the 0^o layers in laminates manufactured with AFP. The gaps will be created normal to fibers as mentioned previously. Fatigue tests were conducted on unidirectional, cross-ply and quasi-isotropic laminates in order to investigate the behavior of different stacking sequences and to check the repeatability of the behavior among the commonly used laminates in industrial applications. The lay-up sequences for the tested laminates are:

- Unidirectional: $(0)_9$.
- Cross-ply: (90/0/90/0/0/0/90/0/90).
- Quasi-isotropic: (90/45/-45/0/0/0/-45/45/90).

Initially, reference plates, free from gaps, with different stacking sequences were manufactured. These plates were designed for obtaining the fatigue behavior of the reference specimens.

In order to investigate the effect of the manufacturing gaps on the fatigue behavior, other defective plates containing gaps with the same stacking sequences were manufactured. Gaps were created in the middle 0^o layers for all different stacking sequences.

The AFP machine was used to create the gaps in the middle layers during laminates manufacturing. Gaps were created using cut/restart capability of the machine. The dimensions of the created gaps were 3 mm along the length of the sample and 1 tow width (6.35 mm) across the width. After laying down the middle layer on the tool plate and creating the gaps, the machine was stopped and the locations of the gaps were marked at the edge of the plates so that the gaps locations can be easily identified after curing of the laminates. Then, the machine continued to lay down the rest of the laminates.

After manufacturing, the plates were cured according to the previously illustrated curing cycle. Then, specimens were cut from the plates using a water cooled diamond blade so that each specimen contains only one gap at the middle of the thickness and the middle of the width.

Figure 2-7 shows the dimensions of the tested samples and Figure 2-8 shows the location of the gaps across the thickness for the different stacking sequences.

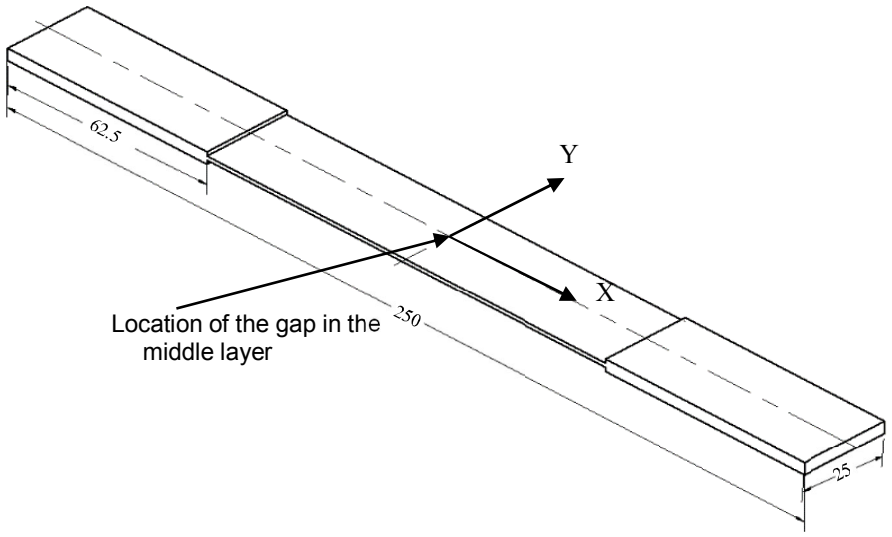

Figure 2-7: Dimensions (in mm) of the specimen with gap at the middle

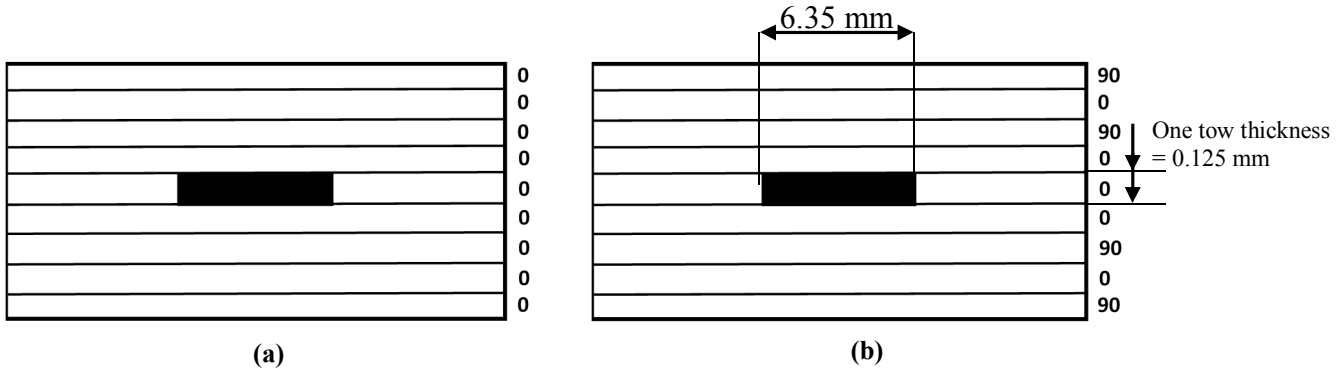

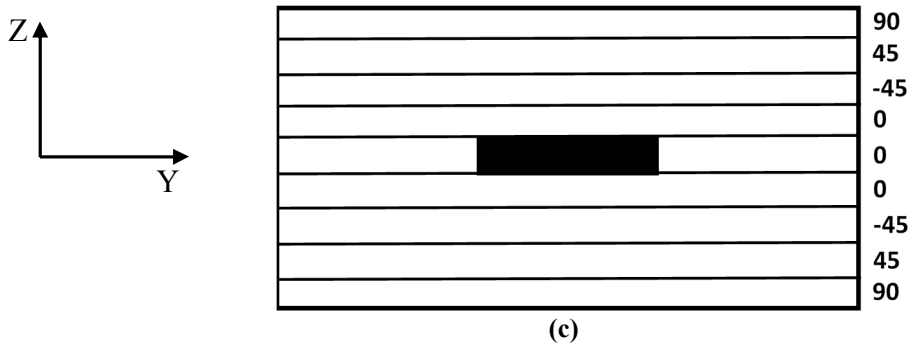

Figure 2-8: Location of the gaps across thickness of (a) unidirectional, (b) cross-ply and (C) quasi-isotropic laminates.

2.3.2 **Effect of gap shape**

In most practical cases due to width variation while steering of fibers, or at the cross boundaries between sectors while manufacturing complex parts, straight cutters in the AFP machine head are used to trim the fiber tows at the required location to avoid overlapping of fibers specially at boundaries between adjacent courses. Each fiber tow is cut by a different cutter which enables cutting of fibers individually during positioning of material strips upon the tool surface. In reality, this cutting process reveals gaps with triangular areas as shown previously in Figure 1-5.

The formulated gaps can have different sizes. Consequently, in the present study, the effect of changing the gap size and shape from the rectangular to the triangular shape was investigated. This was done by creating triangular gaps in the middle of the laminates with sides of different aspect ratios: 1, 2 and 3 as shown in Figure 2-9. The triangular gaps were created in 0 layers since this represents the worst case scenario. In order to create triangular gaps, some tows should be cut inclined to fiber direction. The cutting mechanism of the AFP machine can only create cuts normal to fibers. Consequently, the tows were cut manually to form the required triangular gaps.

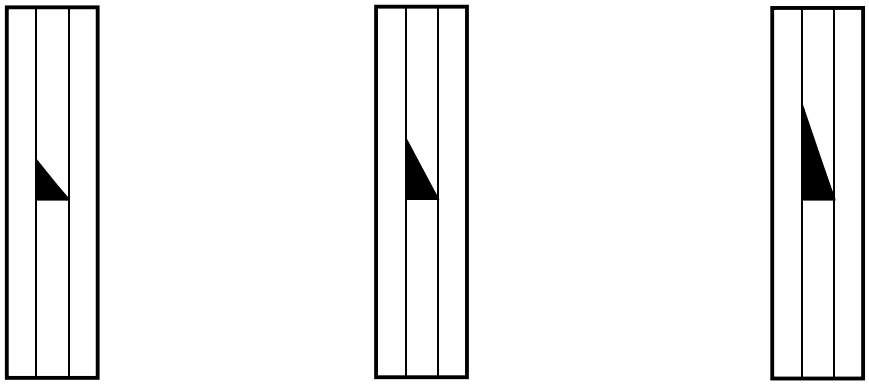

Figure 2-9: Triangular gaps with sides of different aspect ratios: (a) 1, (b) 2 and (c) 3.

Prior to manufacturing, individual tows were cut to form triangular gaps with three different aspect ratios. During manufacturing process, after laying down the fifth layer the AFP machine was stopped and the laid tows were replaced with the manually cut ones at the required location of the gaps then the machine continued to lay down the rest of the laminate.

2.3.3 **Effect of gap orientation**

Any structural component made of composite material consists of many layers with different orientations. The most commonly used orientations are 0^o, 90^o and 45^o. During AFP manufacturing process of laminates containing multiple layers with different orientations, gaps can emerge in any of those layers. The orientation of the induced gap is controlled by the orientation of the fibers in the layer since tows are cut normal to fiber direction.

In the present study, the effect of changing the orientation of the gaps was investigated by creating the gaps in 90^o and -45^o layers. Quasi-isotropic laminates (90/45/-45*/0/0/0/-45/45/90) were used to investigate the effect of gaps in 45^o layers while cross-ply laminates (90/0/90*/0/0/0/90/0/90) were used to investigate the effect of gaps in 90^o layers. The layer denoted by (*) symbol is the defective layer.

Figure 2-10 shows the distribution of the gaps in the -45^o defective layer and the dashed lines are the boundaries of the specimen to be cut from the plate. Each specimen contains only one gap. By comparing the fatigue behavior of the quasi-isotropic specimens containing one gap in the -45^o

layer with the quasi-isotropic specimens containing one gap in 0º layer, the effect of changing the orientation of the gap from 0º to 45º can be obtained.

Figure 2-11 shows the distribution of the gaps in the 90º layers. The dashed lines represents the boundaries of the specimen to be cut. The minimum cutting length of the machine is two inches (50.8 mm) which means that the machine should travel a distance of two inches (50.8 mm) before cutting the placed fibers. If the AFP machine was used to create the gaps in 90º layers during manufacturing, then the distance between the created gaps will be at least 2 inches (50.8 mm). Since the required width of the specimen was one inch (25.4 mm) with a gap at the middle of the width, then there will be a waste of material between the defective specimens. Consequently, in order to avoid the material waste during manufacturing, gaps were created manually at the required locations with a separating distance of one inch (25.4) as shown in Figure 2-11. By comparing the fatigue behavior of the cross-ply laminates with gaps in 0º layer with cross-ply laminates with gaps in 90º layer, the effect of changing the orientation of the gap from 0º to 90º can be obtained.

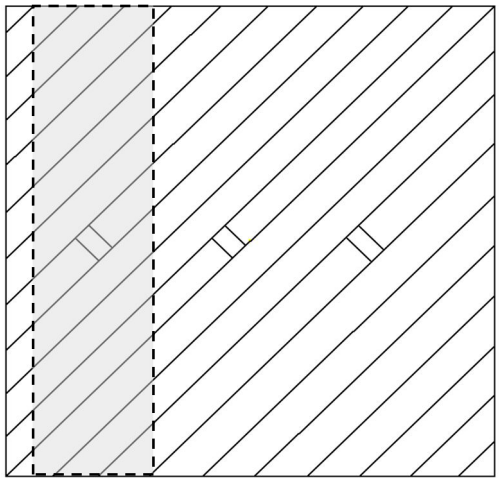

Figure 2-10: Schematic representation of the -45º layer contacting gaps in the defective quasi-isotropic plate

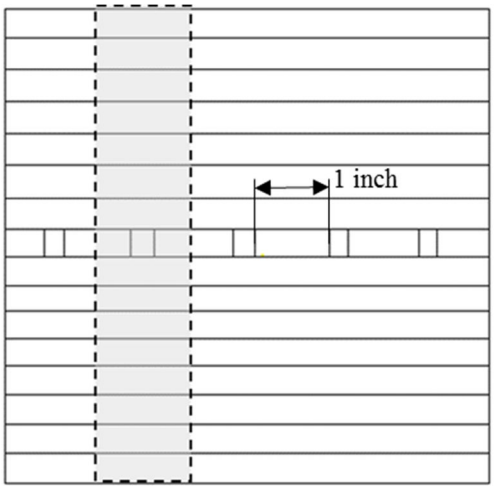

Figure 2-11: Schematic representation of the 90^{o} layer containing gaps in the defective cross-ply plate

2.3.4 **Effect of number of gaps**

Practically, during AFP manufacturing process many gaps can arise in the layer as a result of the intersection of many tows at the boundaries of courses as shown previously in Figure 1-4 and Figure 1-5. So far, in the previous subsections specimens with one gap were manufactured to investigate the effect of one gap. In order to have a step forward to approach the practical cases, the effect of increasing the number of gaps needs to be studied. Unidirectional specimens containing two gaps were manufactured and fatigue tested in order to investigate the interaction between gaps and to figure out the effect of increasing the number of gaps. By comparing the fatigue behavior of laminates containing one gap with that of two gaps, the behavior can be extrapolated for laminates containing many gaps.

The number of gaps was increased in two different directions: in-plane and out-of-plane. The in-plane increasing of number of gaps means adding more gaps in the same layer. However, out-of-plane increasing means adding more gaps in different layers.

For the in-plane case, two different gap configurations were manufactured and tested. In the first configuration the two gaps were located in two adjacent tows while the centers of the two gaps were shifted by X = 3 mm (gap length) along fiber direction as shown in Figure 2-12 (a). It can be observed that this gap configuration occurs in reality when the two gaps have a point in common as shown in Figure 1-5. In the second configuration, the gaps were located in two adjacent tows while the center of the two gaps are shifted by X = 10 mm along fiber direction as shown in Figure 2-12 (b). The dashed lines represent the boundaries of the specimen to be cut and tested. By comparing the fatigue behavior of the different configurations, the effect of increasing the number of gaps and the distance between gaps can be determined.

For the out-of-plane case, two gap configurations were selected. In the first configuration, the two gaps were located in two adjacent layers while being shifted across the width with respect to each other by a distance of full tow width. This configuration represents a full tow staggering (FTS) technique as shown in Figure 2-13 (a). In the second configuration the two gaps were shifted across the width with respect to each other by a distance of half tow width which represents a half tow staggering (HTS) technique as shown in Figure 2-13 (b). By comparing the fatigue behavior of the different configurations, the effect of out-of-plane increasing the number of gaps and the staggering distance can be determined.

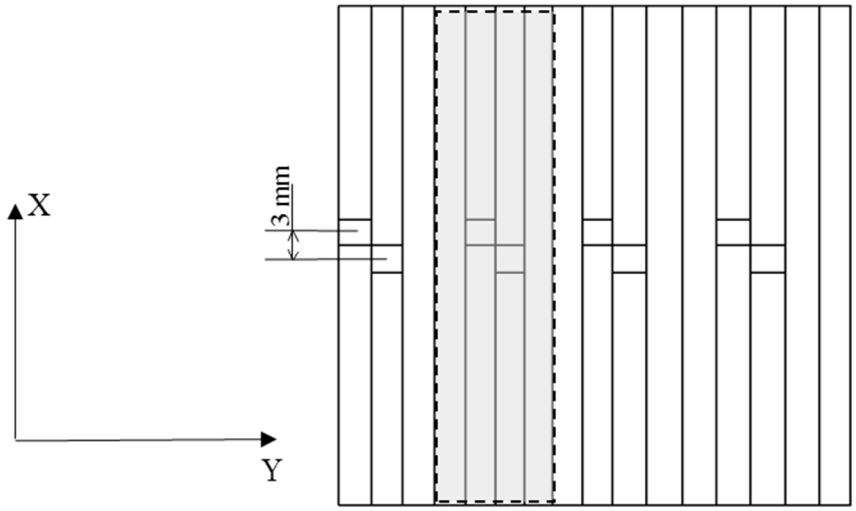

(a)

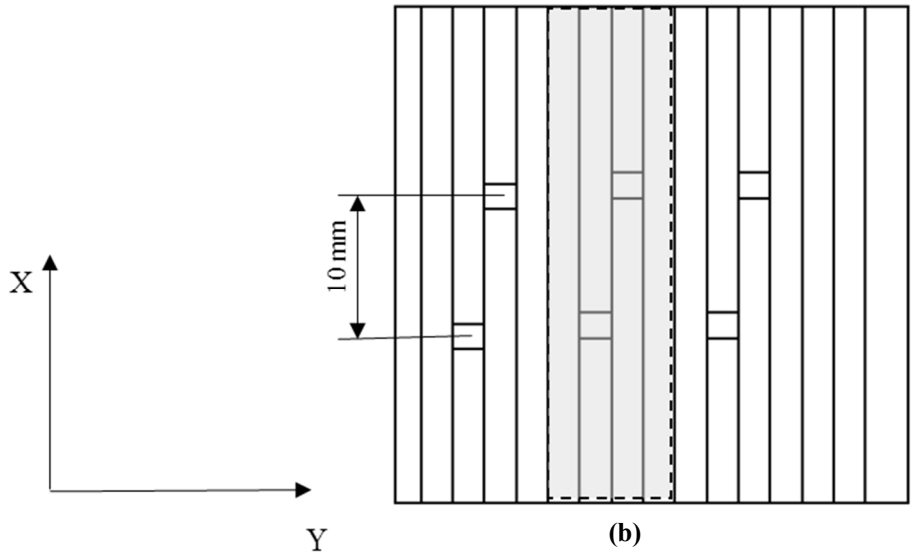

Figure 2-12: In-plane gaps configurations: (a) x = 3 and (b) x = 10 mm. (x is the distance between gaps'centres)

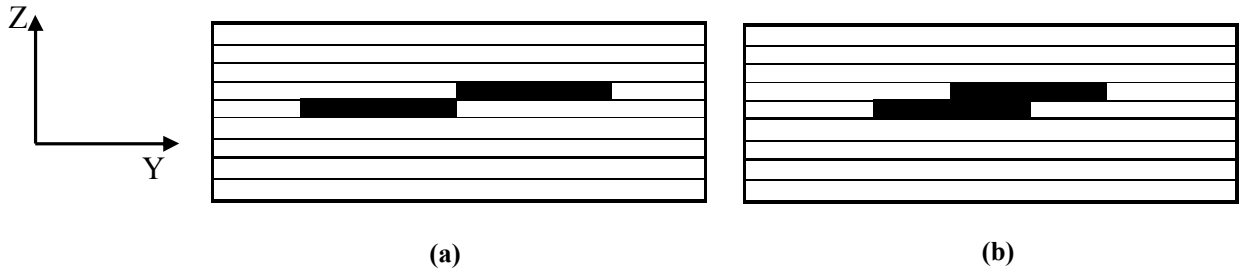

Figure 2-13: Out-of-plane gaps configurations: (a) full tow and (b) half tow staggering

2.4 **Mechanical testing**

The following subsections detail the testing conditions for both quasi-static and fatigue tests. All tests were conducted on a servo-hydraulic MTS testing machine with a maximum capacity of 250 kN available in CONCOM lab, shown in Figure 2-14.

The MTS loading unit is capable of performing quasi-static and dynamic mechanical tests. The system features an extremely stiff frame which provides stability during testing. The machine's digital servo-controllers provides high accuracy of head positioning. The machine can be controlled by MTS's Multipurpose Testware software through a computer connected to the control unit of the testing machine. The computer also controls the operation of the hydraulic power unit (HPU) which is responsible for supplying the system with the required hydraulic power.

Figure 2-14: MTS testing machine used for quasi-static and fatigue tests.

2.4.1 **Quasi-static tests**

Characterizing the material is very essential in understanding the behavior and the performance of the real structure. In order to characterize the material used in the study, various quasi-static tests were performed to obtain the basic material properties such as tension,

compression and shear properties. The resulting mechanical properties were used as inputs for the finite element modeling platform used in the present work (ANSYS). The characterization tests were performed according to the ASTM standards and the specimens were manufactured using AFP process. These experiments were designed based on the assumption that laminate is transversely isotropic which means that the properties transverse to fiber directions are the same.

2.4.1.1 **Tensile test**

The specimen preparation and testing were conducted according to ASTM D3039 [73]. Tensile tests were performed on rectangular specimens in a displacement control mode with 2 mm/min cross head displacement. Fiber glass end tabs were used to alleviate the effect of grips. For each of the following described tests, five specimens from the same plate were cut and tested and the results were averaged.

Two different stacking sequences were manufactured for these tests. Unidirectional (0^o) specimens with fibers oriented in the loading direction were tested to determine E_{11}, υ_{12} and X_t which are the Young modulus in fiber direction, major Poisson ratio in 1-2 plane and tensile strength in fiber direction, respectively. Two perpendicular strain gauges were bonded to the specimen's surface in the longitudinal and transverse directions in order to measure the axial and transverse strain to get the Poisson ratio. Figure 2-15 shows the dimensions of the used standard specimens. The strain gauges were Vishay 350 Ω resistance with a gage factor of 2. The modulus of elasticity was determined at 0.3 % strain level and the Poisson ratio was calculated based on the ratio between the normal and transverse strain according to ASTM D3039 [73] . The ultimate strength was obtained by dividing the maximum load at the point of complete failure and the cross sectional area of the specimen.

For all the tests, the cross sectional area was calculated using the thickness and width of the specimen. Both thickness and width were measured at three different locations along the length of the specimen and the average were obtained. A micrometer with a precision of 0.001 mm was used for taking the measurements. The average variation in thickness was 0.01 mm and width was 0.5 mm.

The other stacking sequence was unidirectional (90°) with fibers oriented perpendicular to loading direction. These specimens were tested to obtain E_{22} and Y_T which are Young modulus transverse to fiber direction and transverse tensile strength. For this type of specimen, only one strain gauge was attached in the loading direction as shown in Figure 2-16.

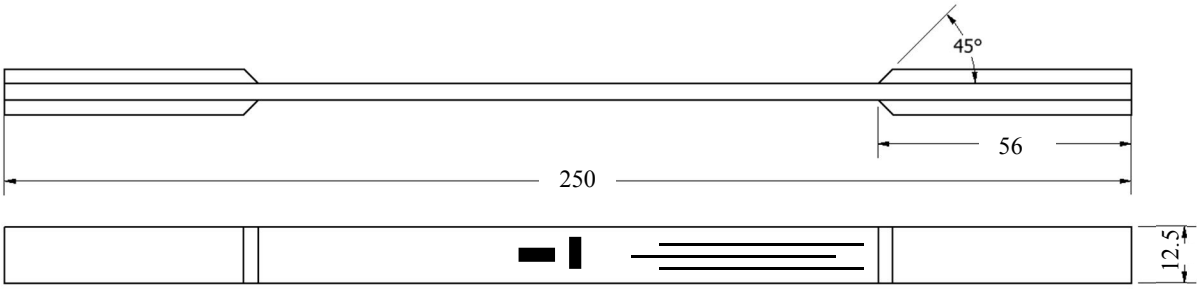

Figure 2-15: Unidirectional (0°) specimen with attached strain gages for quasi-static tensile tests (dimensions in mm).

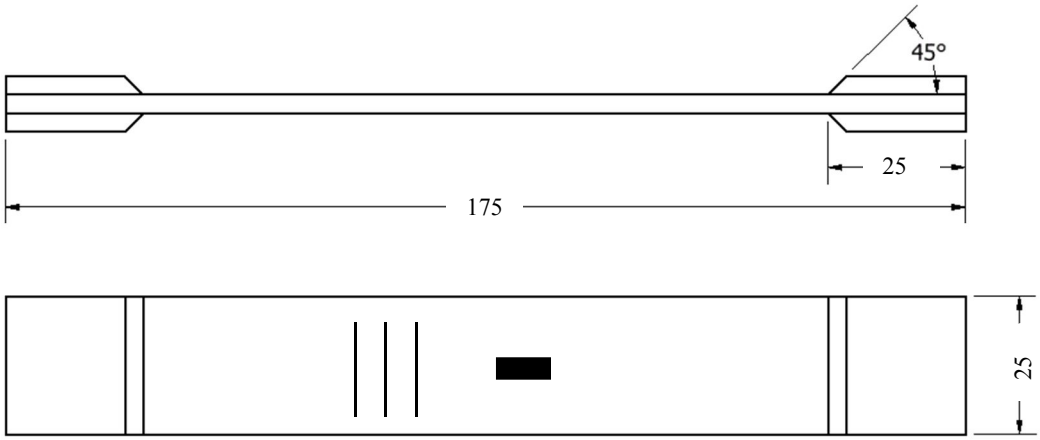

Figure 2-16: Unidirectional (90°) specimen with attached strain gages for quasi-static tensile tests (dimensions in mm)

In order to collect the recordings of the strain gauges attached to the specimens, a strain indicator Vishay 2160, shown in Figure 2-17, was used. This device has four channels that can be used simultaneously and it was connected to both the active strain gauges and the computer which

records the values of the force and displacement from the testing machine. Consequently, by synchronizing the machine with the strain indicator, the strain readings corresponding to the recorded force can be obtained.

Figure 2-17: Strain recording device Vishay 2160

2.4.1.2 **Compression test**

The specimen manufacturing and testing were conducted according to ASTM D3410 [74]. Compression tests were performed on rectangular specimens in a displacement control mode with 1.5 mm/min cross head displacement using a compression fixture shown in Figure 2-18. Such as the case of tensile tests, compression tests were conducted on parallel, Figure 2-19 (a), and transverse to fiber directions, Figure 2-19 (b), in order obtain the ultimate compression strength in fiber direction, X_c, and in transverse direction, Y_c. The ultimate strength was obtained by dividing the maximum load at the point of complete failure and the cross sectional area of the specimen.

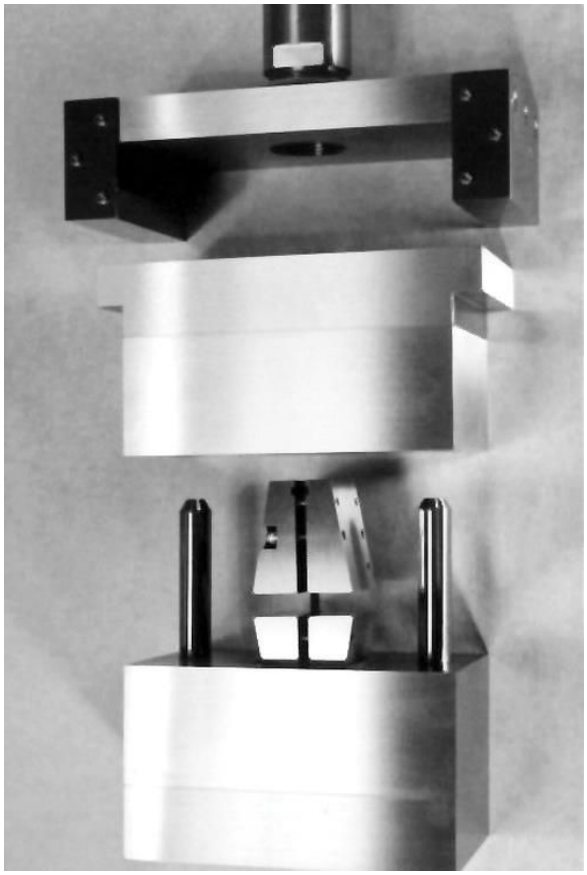

Figure 2-18: Compression test fixture

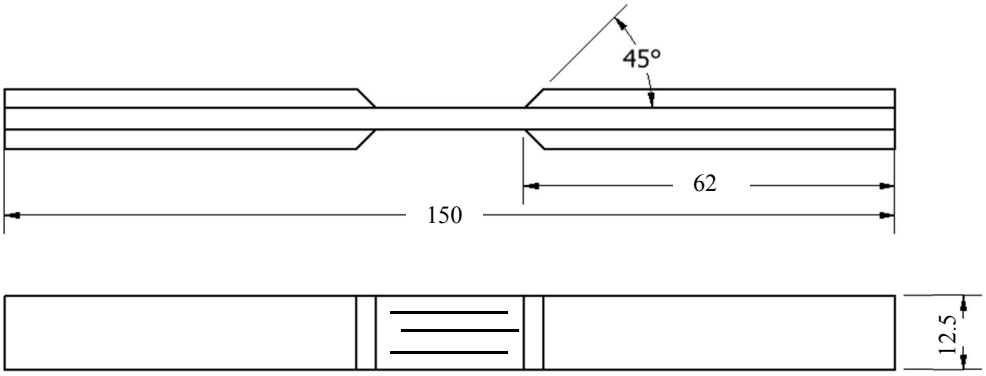

(a)

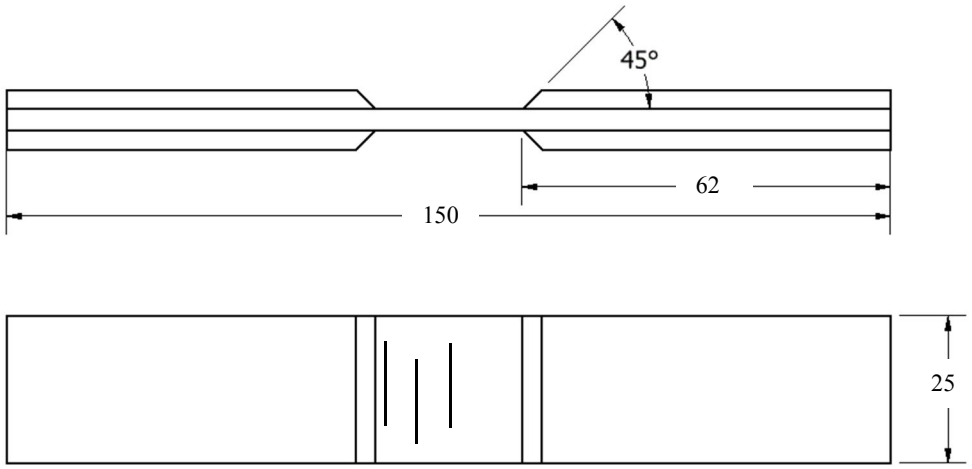

(b)

Figure 2-19: Specimens for compression tests (a) along fiber and (b) transverse to fibers. (dimensions in mm)

2.4.1.3 **Shear test**

The purpose of this group of tests is to determine τ_{12} and G_{12} which are the in-plane shear strength and in-plane shear modulus, respectively. This test was performed according to ASTM 3518 [75] in which tensile test is conducted on specimens with fibers oriented in ±45° to loading direction. Two strain gages are bonded parallel and transverse to loading directions as shown in Figure 2-20. The shear modulus of elasticity is determined at 0.4% shear strain. The ultimate shear strength is obtained from the ultimate or failure tensile loading according to [75].

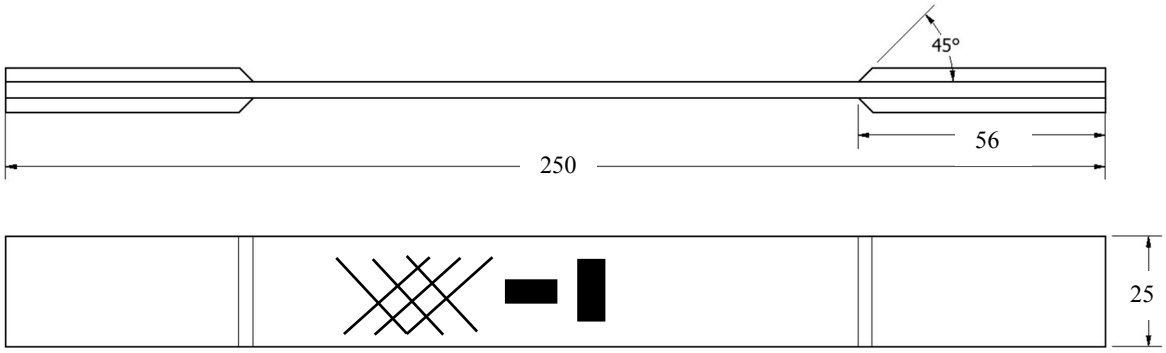

Figure 2-20: Specimens for the performed shear tests (dimensions in mm)

2.4.2 **Fatigue test**

The goal of performing the fatigue tests is to investigate the effect of the unavoidable gaps induced in laminates during AFP manufacturing process on the fatigue performance of the material. These tests were performed on the same MTS machine used for the quasi-static tests. During fatigue tests, the machine was set to load control mode in which the applied load is kept constant and the specimen becomes more compliant with cycles.

The applied load was in sinusoidal wave form as shown in Figure 2-21. The ratio between the maximum and the minimum stress (R) in each fatigue cycle was 0.1 which means that the specimens will be subjected to tension/tension fatigue tests. This loading condition was chosen as a simple start for investigating the effect of the gap on the fatigue performance. However the work should be extended for more complicated cases such as compression/compression. The used frequency in the test was 5 Hz. Higher frequencies were avoided to reduce the heat generated during fatigue at high frequencies which negatively affects the matrix properties. The dimensions of all specimens tested under fatigue loading were 10 inches (254 mm) in the loading direction and 1 inch (25.4 mm) in transverse direction.

In order to perform the fatigue experiments, the testing machine was programmed so that the applied load ramped-up from zero to the mean stress. Then, the cyclic loading started with the predefined frequency and stress ratio. During the first ramp up loading, the displacement rate (2 mm/min) was chosen to be the same as that performed in case of quasi-static tests to avoid any effect of changing the strain rate. The data acquisition stored the force and the displacement at two points in each cycle which correspond to the maximum and minimum applied stresses.

Fatigue tests were stopped at final failure of specimen when it was pulled apart into two portions or when the specimen reached 10^6 cycles without failure and considered as a run-out specimen.

Fatigue tests were performed for different stress levels of different ratios to the ultimate tensile strength of the tested laminate and five specimens were tested at each stress level. The maximum applied stresses were plotted against the obtained number of cycles to failure in a log scale to develop the stress/life (S/N) curves. By comparing the fatigue behavior represented by the

S/N curves for reference and defective laminates, the effect of the gaps on the fatigue life can be concluded.

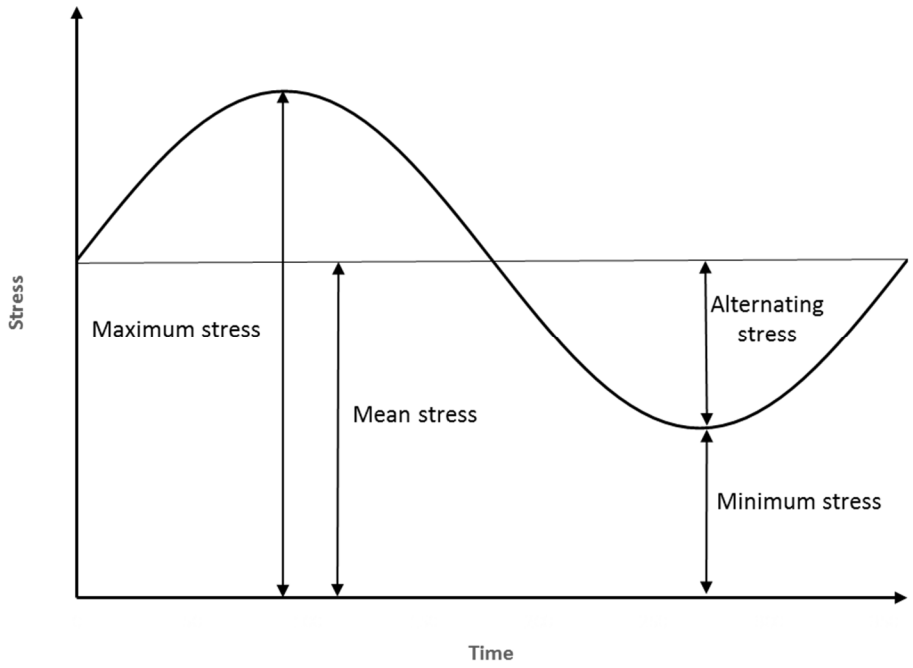

Figure 2-21: Applied stress in fatigue cycles in the form of sinusoidal waves

Sectioning of specimens was also performed in order to examine the different internal damage mechanisms that occurred within the laminate due to the existence of gaps. The procedures for preparing specimens for inspection using SEM were mentioned in detail in section (2.2.2.2).

Table 2-1 shows the test program designed for investigating the different parameters and the codes assigned to the fatigue tested specimens in addition to the number of specimens tested for each set of tests.

Table 2-1: Test program performed in the current study

Studied parameter	Specimen configuration	Type of specimen	# of sp.
Gap shape	UD-Rec UD-Tri	-Unidirectional with rectangular gaps [0/0/0/0/0*/0/0/0/0] -Unidirectional with triangular gaps [0/0/0/0/0*/0/0/0/0]	50
Stacking sequence	UD-Ref UD-D	-Unidirectional without gaps [0/0/0/0/0/0/0/0/0] -Unidirectional with gap in 0º layer [0/0/0/0/0*/0/0/0/0]	50
	CP-Ref CP-D	-Cross-ply without gaps [90/0/90/0/0/0/90/0/90] -Cross-ply with gaps in 0º layer [90/0/90/0/0*/0/90/0/90]	50
	QI-Ref QI-D	-Quasi-isotropic without gaps [90/45/-45/0/0/0/-45/45/90] -Quasi-isotropic with gaps in 0º layer [90/45/-45/0/0*/0/-45/45/90]	50
Gap orientation	CP-D-90	-Cross-ply with gap in 90º layer [90/0/90*/0/0/0/90/0/90]	20
	QI-D-45	-Quasi-isotropic with gap in 45º layer [90/45/-45*/0/0/0/-45/45/90]	20
Number of gaps	UD-2 gaps-3	-2 gaps in the same layer with 3 mm distance between centers	20

		[0/0/0/0/0**/0/0/0/0]	
	UD-2 gaps-10	-2 gaps in the same layer with 10 mm distance between centers [0/0/0/0/0**/0/0/0/0]	20
	UD-2 gaps-FTS	-2 gaps in 2 layers with full tow staggering [0/0/0/0*/0*/0/0/0/0]	20
	UD-2 gaps-HTS	-2 gaps in 2 layers with half tow staggering [0/0/0/0*/0*/0/0/0/0]	20

2.5 **Damage monitoring using IR thermography**

One of the major concerns in the aerospace industry is detecting the defects and the consequence of its existence such as the developed damage mechanisms. In the present study, the existence of these mechanisms was evaluated using both destructive and non-destructive techniques. Sectioning of specimens prior to failure represents the former technique and it was presented previously.

Infrared (IR) thermography was used as a non-destructive method for detecting the damage that emerged as a result of gaps. IR thermography provides the temperature distribution on the surface of the specimen based on the infrared radiation emitted from the surface. As a result of damage initiation and propagation from the gaps existed in the laminate during fatigue tests, energy is released from the defective locations. The heat transferred by conduction through the thickness of the laminate from the damage location to the surfaces causes the temperature of the specimen's surface to increase which can be detected using IR thermography. Figure 2-22 shows the IR system used to detect temperature change at the surface of the specimens.

Figure 2-22: Infrared camera (FLIR 450SC) used to detect damage occurrence

The IR camera was FLIR 450SC with the following specifications:

- Produces thermal images of 320 x 240 Pixels.
- Creating both images and radiometric real time recordings.
- Sensitivity NETD @ 30 C : 80mK.
- Frame Rate : 30 Hz
- Accuracy: ±1 ºC.
- Object temperature range : -40°C to +1500°C

Figure 2-23 shows a scheme for the test setup. The IR camera was fixed on a tripod at a distance of one meter facing one side of the sample while being fatigue tested. The camera displays the thermal map for the specimen's surface showing the temperature gradient as a result of any damage occurrence within the laminate providing a method for detection of defects and damage process. As a result of the gripping of the machine on the tabs at the end of the specimen, heat is

generated at the gripping locations. So, the camera was focused on the area at the middle of the specimen and centered on the gap location away from any temperature disturbance due to grips.

The IR camera can be used in two different modes. It can be used to capture images similar to the function of personal digital cameras but with providing the temperature distribution on the captured images. In addition, it can be used to record thermal videos. The advantage of the second mode is that the data is stored in the video and can be post processed after recording with the capability of modifying the display parameters such as the contour colors and the temperature scale. This advantage is not available in the picture mode in which the display of the image cannot be modified after capturing. The only drawback of the video mode is that it requires a large space for storing the data.

In the current work, the camera was set to video mode to provide the surface temperature during the whole period of testing to be able to capture minor changes in the temperature distribution during testing time. The camera was connected to a computer to collect and store the thermal data. The computer is supported by a Research IR software which acted as an interface between the IR camera and the computer and can be used for extracting and analyzing the thermal data after recording.

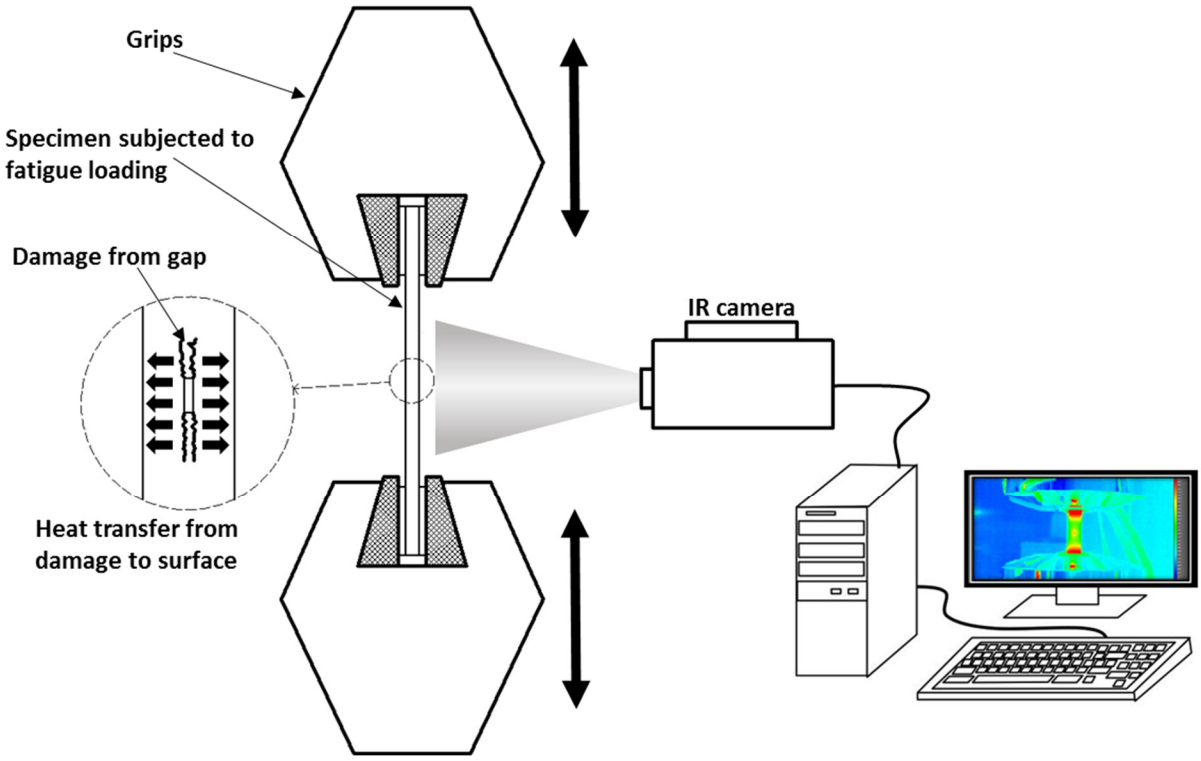

Figure 2-23: Schematic representation of the experimental test set up.

2.6 **Summary**

This chapter presents the detailed procedures for the experimental work performed and the specifications of the equipment in the current study. In addition, the objective of each set of experiments was illustrated and the methodology performed to satisfy these objectives was presented. In the following chapter the results of these conducted tests will be presented and discussed.

Chapter 3

Experimental results and discussion

The aim of this chapter is to present the experimental results which consist mainly of inspection and testing results, infrared thermography and optical imaging analysis. The first part of this chapter will focus on the results of the quasi-static tests performed to characterize the material. In the second part, the effect of the gaps on the fatigue performance will be presented and discussed accompanied by the thermographic analysis and the microscopic images.

3.1 **Quality inspection results**

Before starting the tests, DSC was used to check the degree of cure of the manufactured and cured plate. Figure 3-1 shows the result of the DSC test for one unidirectional sample. No temperature peaks were observed during the heating/cooling cycles. This indicates no exothermic reaction and fully cured tested specimen. From such a curve, the glass transition temperature can be obtained at the midpoint of slope shifting region during the heating phase. It was found to be 189 ^{o}C.

Figure 3-2 (a) shows a microscopic image of a cured sample across the width. No voids were found in the tested specimens. The average volume fraction was obtained using IMAGJ software at different sections to be 60.1% with a variation of 3%. Some sections were also cut exactly at the middle of the defective specimens in order to check that the gaps were created at the required locations. It was found that the gaps were in the proper positions and it was observed that the gaps appeared as resin pockets in the laminates, completely filled with resin as shown in Figure 3-2 (b).

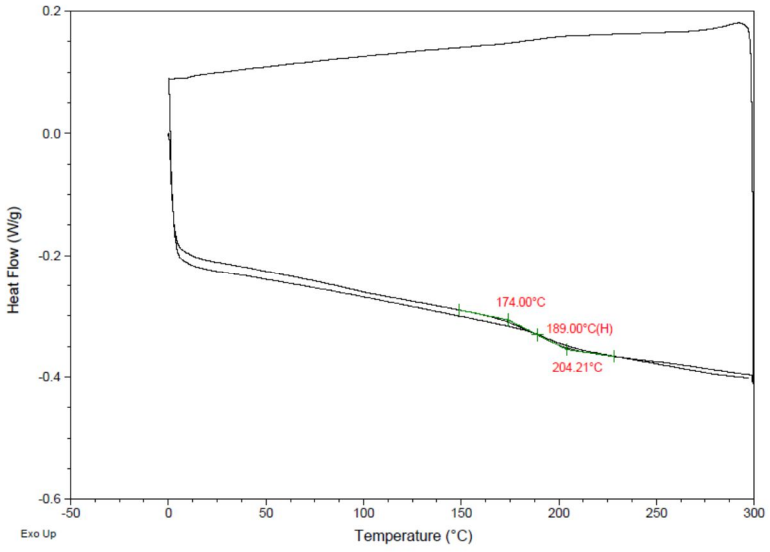

Figure 3-1 Thermal response during degree of curing inspection using DSC

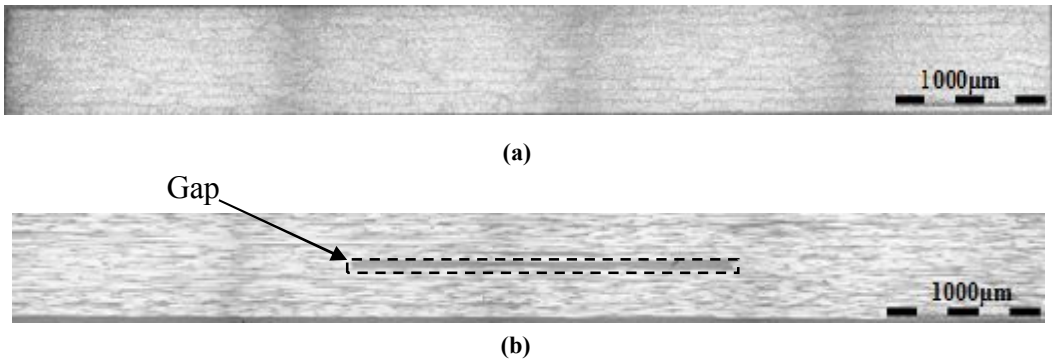

Figure 3-2: Microscopic images for unidirectional specimen (a) across the width and (b) across the length

3.2 **Characterization tests**

Quasi-static tensile tests were performed on unidirectional 0° laminates to determine E_{11}, υ_{12} and X_t which are the Young's modulus in fiber direction, major Poisson's ratio in 1-2 plane and tensile strength in fiber direction, respectively. Figure 3-3 shows the stress strain relations in axial and transverse directions for the case of reference specimens obtained from the two strain gauges mounted on the specimen's surface. The illustrated results are for one sample as an example. It can be observed that the behavior is linear in both directions up to final failure of the specimen. The ultimate strain to failure in the longitudinal and transverse directions were 0.0165 and -0.0044 με, respectively. The slope of the stress-strain relation in the axial direction was used to get the Young modulus in fiber direction, E_{11}. The average value of the 5 tested specimens was found to be 140 GPa.

The major Poisson's ratio, υ_{12}, is the ratio between the strain from the transverse strain gauge and the strain from the longitudinal one when the load is applied in the fiber direction. The average value was found to be 0.28. The ultimate tensile strength was calculated by dividing the maximum load at failure to the cross sectional area of the specimen. The average value was found to be 2500 MPa for the reference specimen. Figure 3-3 also shows the longitudinal stress-strain relation for a defective specimen. It can be observed that the slope of the linear curve is almost the same as the

case of reference specimen and there is a small reduction in the value of the maximum load to failure. The average tensile strength of defective specimen was 2350 MPa which means a reduction of only 6% between the defective and reference specimens.

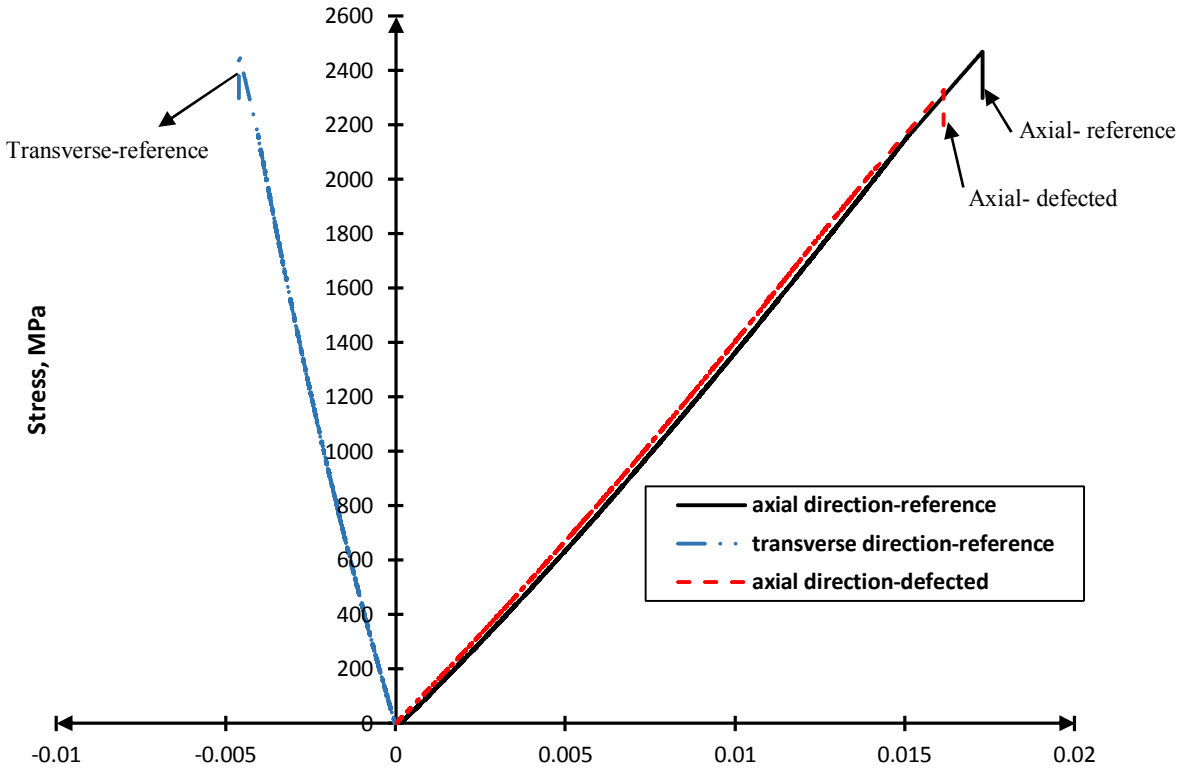

Figure 3-3: Stress-strain relations for longitudinal tensile test

The damage mechanisms for unidirectional specimen subjected to loading in fiber direction started with some weak fibers breakage as a result of the scattering in fiber strength and this was distinguished by hearing the breaking sound of these randomly distributed weak fibers. The shear stress at the end of these broken fibers increases and causes the initiation of some matrix cracks that might propagate transverse or parallel to fibers. When the applied stress reaches the strength of the fibers, failure occurred catastrophically by splitting and fiber breakage.

Specimens with 90^{o} layers were also tensile tested to obtain E_{22} and Y_T which are Young's modulus transverse to fiber direction and transverse tensile strength, respectively. Figure 3-4

shows the stress-strain behavior in the transverse direction obtained from the strain gauge mounted in the direction of loading. It can be observed that the behavior was also linear up to final failure which occurred at an average value of 60 MPa. The Young's modulus in the transverse directions was calculated from the slope of the linear curve and the average value of the five tested specimens was 11 GPa.

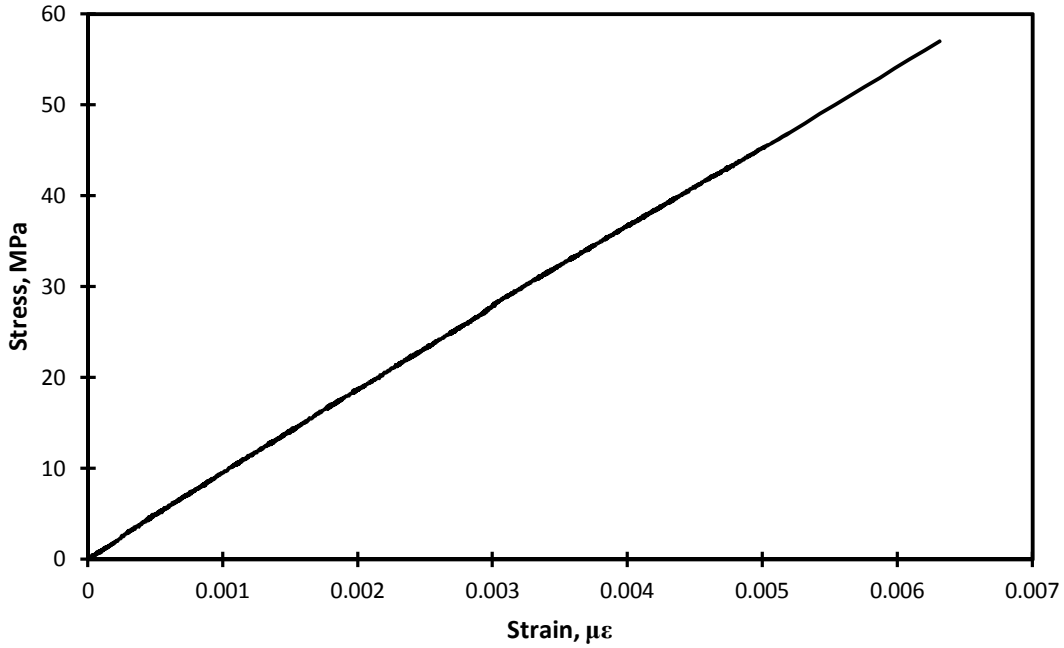

Figure 3-4: Stress-strain relation for transverse tensile test

The dominant damage mechanism in the case of 90º laminates is matrix cracking. It initiates from weak locations within the layers such as resin rich areas then these cracks grow parallel to fibers by increasing the load up to final failure that occurs by matrix failure.

Specimens with ±45 layers were tensile tested to obtain τ_{12} and G_{12} which are the in-plane shear strength and in-plane shear modulus, respectively. Figure 3-5 shows the shear stress strain relation which exhibits a non-linear behavior. The average shear strength was calculated using the maximum force reached at failure to be 100 MPa. The shear modulus was found to have an average

of 5 GPa. The dominant damage mechanisms for the case of ±45° laminates were matrix cracking in 45° and -45° layers and delamination.

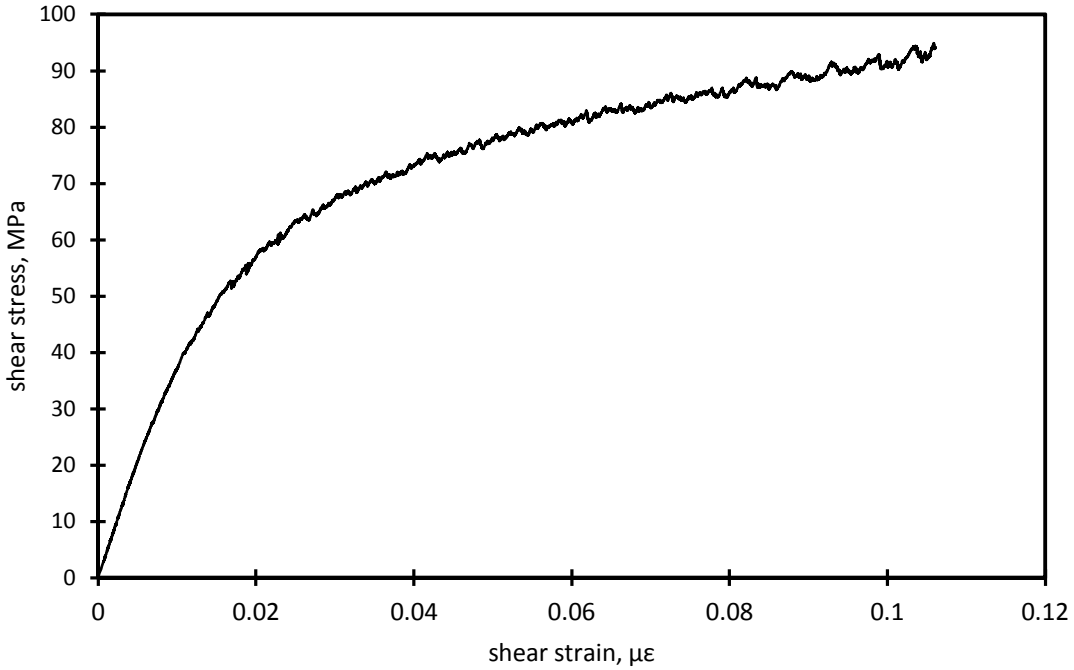

Figure 3-5 Shear stress-strain relation for ±45° laminate under quasi-static tensile test.

For the specimen of 0° and 90° laminates tested under compression, no strain gages were used with the tested specimens since the objective of the tests was to determine the compression strength. The average longitudinal and transverse compression strength values were found to be 1450 MPa with a standard deviation of 62 MPa and 200 MPa with a standard deviation of 36 MPa, respectively. The final failure occurred by brooming for the case of 0° laminates while it occurs in the form of matrix failure in the case of 90° laminates.

3.3 **Fatigue tests**

This section will present the results of the fatigue tests performed to investigate the effect of the gaps on the fatigue performance taking into account different parameters.

3.3.1 Effect of gaps in 0º layer for different stacking sequences

3.3.1.1 Unidirectional laminates

Unidirectional reference and defective 0^o laminates were subjected to tension-tension fatigue tests up to final failure or when the specimen runs out at 10^6 cycles. The specimens were tested at four stress levels, in addition to the run out stress level denoted by an arrow, that range between 70% and 80% of the ultimate tensile strength (UTS) of the reference laminates in an effort to make the specimens fail between 10^3 and 10^6 cycles. Although in real application the applied stress might be less than these tested values, but it is very important for the designer to have a full understanding of the behavior of the defective material at both high and low stresses to account for any sudden increase or severe loading conditions. Five specimens were tested at each stress level in order to develop the stress/life (S/N) curves for both reference and defective unidirectional specimens. Figure 3-6 shows the obtained number of cycles to failure at each stress level for both reference and defective unidirectional specimens.

Basically, the fatigue data can be represented in terms of stress/life curves or strain/life curves. In conducted tests in the study, the fatigue cycles were performed in load control mode so all the input parameters were used in terms of load (stress). In addition, in the finite element modeling work, a stress based failure criteria was used, Hashin failure criteria [76], since it can distinguish between different failure mode. Consequently, the fatigue data was presented in terms of stress/life curves for ease of interpretation and use of results.

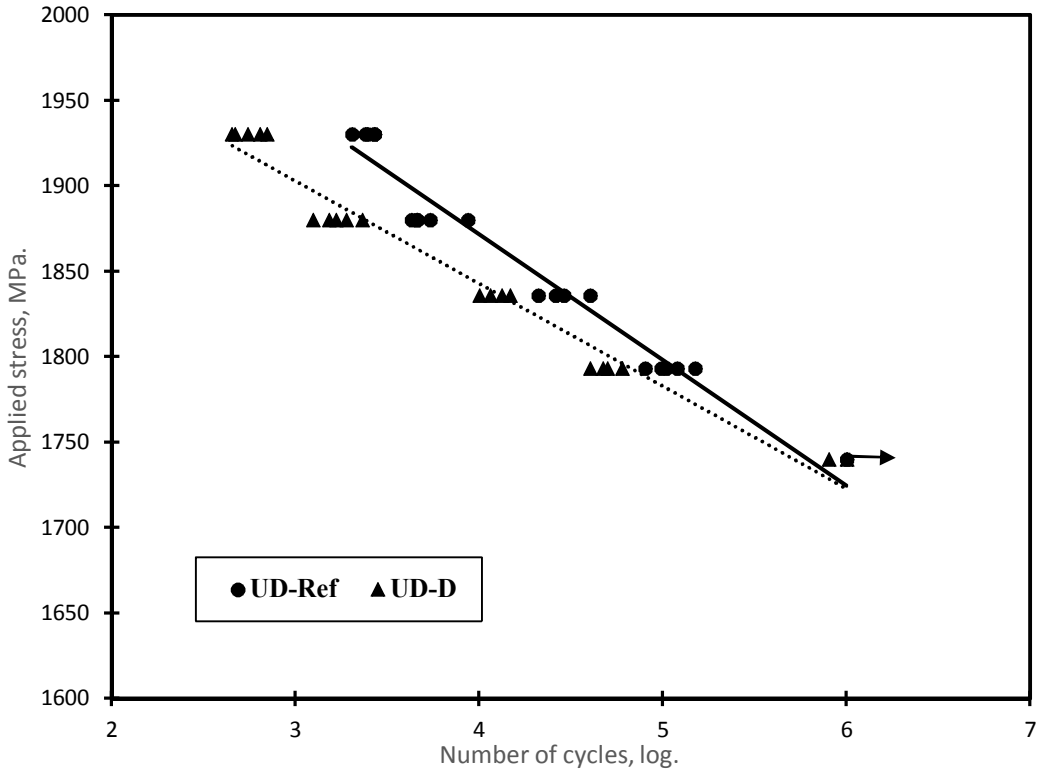

Figure 3-6: Fatigue lives at each stress for unidirectional reference and defective specimens

In order to assess the reliability of the fatigue results, two methods of statistical analysis were used. The first statistical method was based on a confidence level of 0.95. At each stress level, the average number of cycles and the uncertainty in the obtained results based on 0.95 confidence level were calculated [77].

$$N_{i.av} = \frac{\sum_{j=1}^{n_i} N_j}{n_i} \quad (3.1)$$

$$U_i = k \frac{S_{di}}{\sqrt{n_i}} \quad (3.2)$$

$$N_{i.ext.} = N_{i.av} \pm U_i \quad (3.3)$$

Where:

$N_{i.av}$ …. Average number of cycles to failure at stress σ_i.

n_i…. Number of specimens tested at σ_i.

N_j…. Number of cycles to failure for each tested specimen j.

U_i…. Uncertainty in the experimental results at σ_i.

k…. Factor equals 2 for a confidence level of 0.95.

S_{di}….Standard deviation at σ_i.

$N_{i.ext.}$…. Extreme values for number of cycles to failure at σ_i.

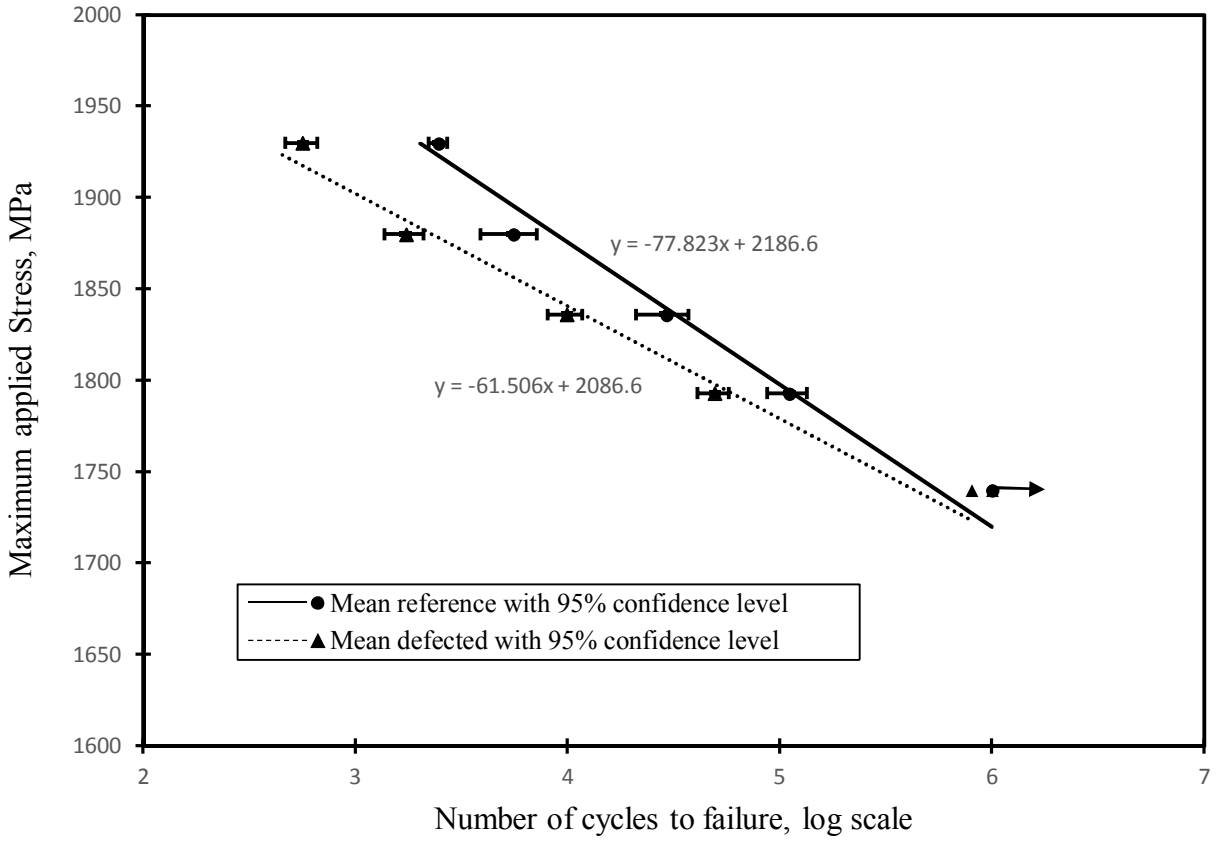

Figure 3-7: Stress/life curves for unidirectional reference and defective specimens with gaps in 0º layer at 0.95 confidence level

Figure 3-7 shows the fitting lines for the plots relating the maximum applied stress and the number of cycles to failure using least square method. It also shows the scattering range in the failure cycles at each stress level based on 0.95 confidence level. In spite of the existence of scattering, there is an obvious difference in the fatigue lives between the reference and the

defective specimens. It can be observed that there is a reduction in the life of defective specimens compared to the reference and this reduction varies by changing the applied stress. At high stresses, there is a severe reduction in fatigue life indicating a significant effect for the gap. For instance, at 1940 MPa the average number of cycles to failure for the defective laminates was 560 cycles which is 22% of the fatigue life of the reference laminate, 2450 cycles, with a fatigue life reduction of 78% at this stress level. However, by decreasing the applied stress, the behavior of the defective specimens approaches that of the reference ones showing an alleviated effect for the gap. For instance, at 1790 MPa the average number of cycles to failure for the defective laminates was 49500 cycles which is 45% of the fatigue life of reference laminate, 110250 cycles, with a life reduction of 55% at this stress level. Hence, at lower stresses, although there is a difference between the absolute values of the fatigue lives of reference and defective specimens, but normalizing this difference to the reference fatigue life can show the alleviated effect of the gap by decreasing the applied stress.

Each fatigue cycle consists of loading and unloading parts. During each cycle, some mechanical energy is stored in the material which represents the irreversible part of energy and can be identified by the hysteresis in the fatigue cycle. The other part is released back during the unloading portion of the cycles and represents the reversible energy as shown in the schematic illustration of Figure 3-8. The energy stored in the material is the driving force for initiating the cracks from any pre-existing flaws in the material and also for propagating the existing cracks. At high stresses, the stored energy is high and the ability of the material to create damage from the gap is high. However, by decreasing the applied stress, this ability decreases and the effect of the gap on the fatigue life diminishes gradually.

By decreasing the maximum applied stress, the two S/N curves for the reference and defective specimens converged to each other and intersected at applied stress value of 1725 MPa. So, at this stress value the fatigue lives of both reference and defective specimens are the same. Figure 3-9 shows a quantification of the reduction in fatigue life of unidirectional defective specimens at different applied stresses. The reduction curve was obtained from the regression fitting lines of the S/N curves for the reference and defective specimens. The reduction in life was represented as follow:

$$RD = \frac{N_{Ref} - N_D}{N_{Ref}} \qquad (3.4)$$

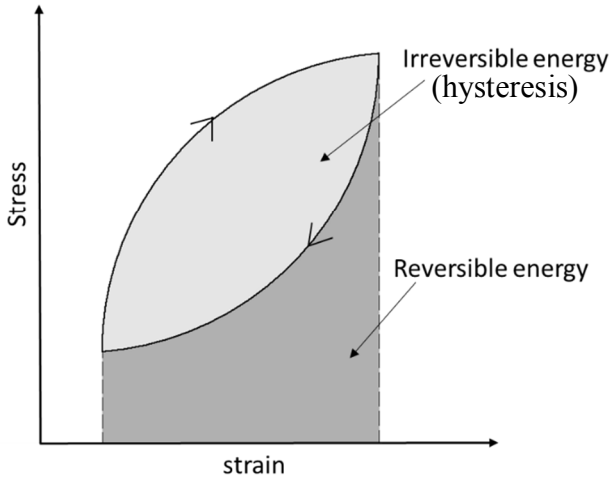

Figure 3-8: Reversible and irreversible energy during each fatigue cycle.

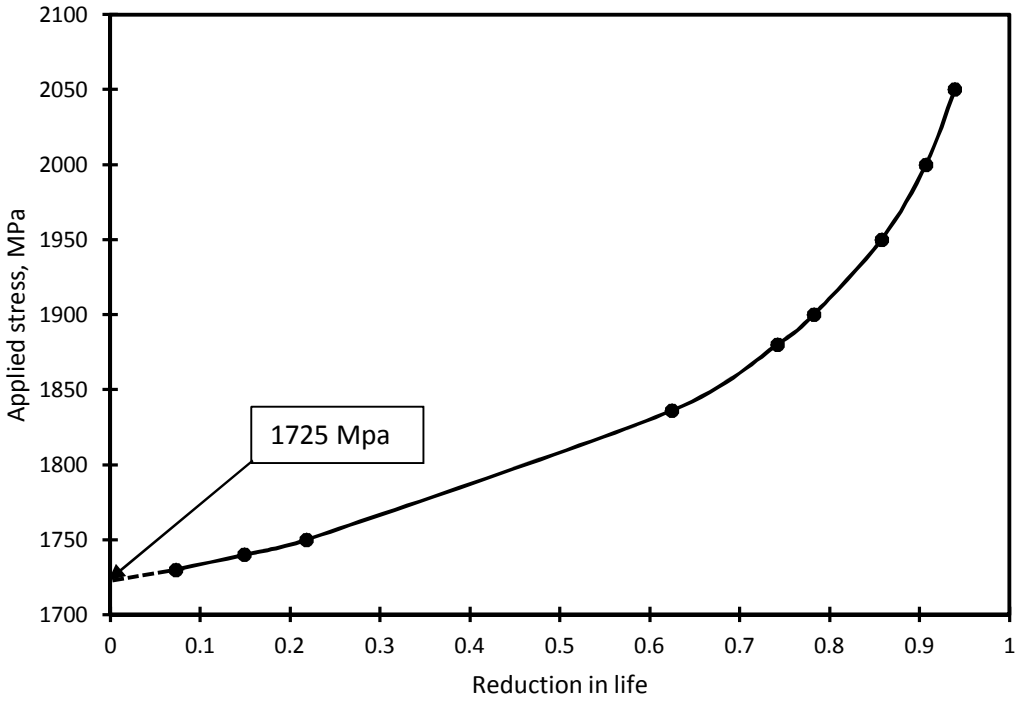

Figure 3-9: Reduction in fatigue life of defective unidirectional specimens at different applied stresses

N_{Ref} and N_D are the number of cycles to failure for the reference and defective specimen at the same applied stress, respectively. From Figure 3-9, it can be observed that by decreasing the maximum applied stress during the fatigue cycles, the effect of the gaps is alleviated and the reduction in the fatigue life decreases. The point of the intersection of the two S/N curves was found by extrapolating the two regression lines to be 1725 MPa. At this point, both types, reference and defective laminates, have the same life and hence no reduction at this point occurs. This value of stress corresponding to the intersection of the two S/N curves is called in the present study: threshold stress. It represents the value of the applied stress below which there is no effect for the gap on the fatigue life of laminates and it can be determined as the intersection of the reduction in life curve with the vertical axis, applied stress axis, in Figure 3-9. The threshold stress for the case of unidirectional specimens was 1725 MPa.

The second statistical method was based on the Weibull distribution function. Based on Weibull function, the obtained data at any stress level can be used to get the life (N_f) at different probabilities of failure (POF).

The distribution function (F) of two parameters Weibull distribution for random variable (N_f) is [78]:

$$F(x, u, \propto) = 1 - \exp\left(-\left(\frac{N_f}{u}\right)^{\propto}\right) \tag{3.5}$$

Where $\propto$ is shape parameter and u is the scale parameter. The reliability function or the probability of survival L_R can be defined as:

$$L_R = 1 - F \tag{3.6}$$

$$L_R = \exp\left(-\left(\frac{N_f}{u}\right)^{\propto}\right) \tag{3.7}$$

By taking the Logarithms twice for the both sides:

$$ln\left(ln\left(\frac{1}{L_R}\right)\right) = \propto ln(N_f) - \propto ln(u) \tag{3.8}$$

This represents a linear relation between $ln\left(ln\left(\frac{1}{L_R}\right)\right)$ and $\ln(N_f)$ which can be used to get the values for $\propto$ and u. The reliability function L_R can be estimated by the following relation [79]:

$$L_R = 1 - \frac{i-0.3}{n+0.4} \qquad (3.9)$$

in which n is the total number of specimens and i is the specimen number.

As an example, the case of applied stress of 1880 MPa for the defective specimens will be presented. The obtained fatigue lives at this applied stress are arranged in an ascending order as shown Table 3-1.

Table 3-1: Number of cycles to failure obtained for unidirectional defective specimen at 1880 MPa

Specimen no. (i)	N_f
1	1246 cycles
2	1520 cycles
3	1660 cycles
4	1885 cycles
5	2310 cycles

Eqn. (3.9) with n =5 was used to obtain L_R then $\ln\left(\ln\left(\frac{1}{L_R}\right)\right)$ is plotted against $\ln(N_f)$. Then, the data was fitted to linear curve using least square method as shown in Figure 3-10. The slope of the line represents the shape parameter, $\propto = 4.425$, and the intersection of the line with the vertical axis can be used to obtain the scale parameter, $u = 1885.874$.

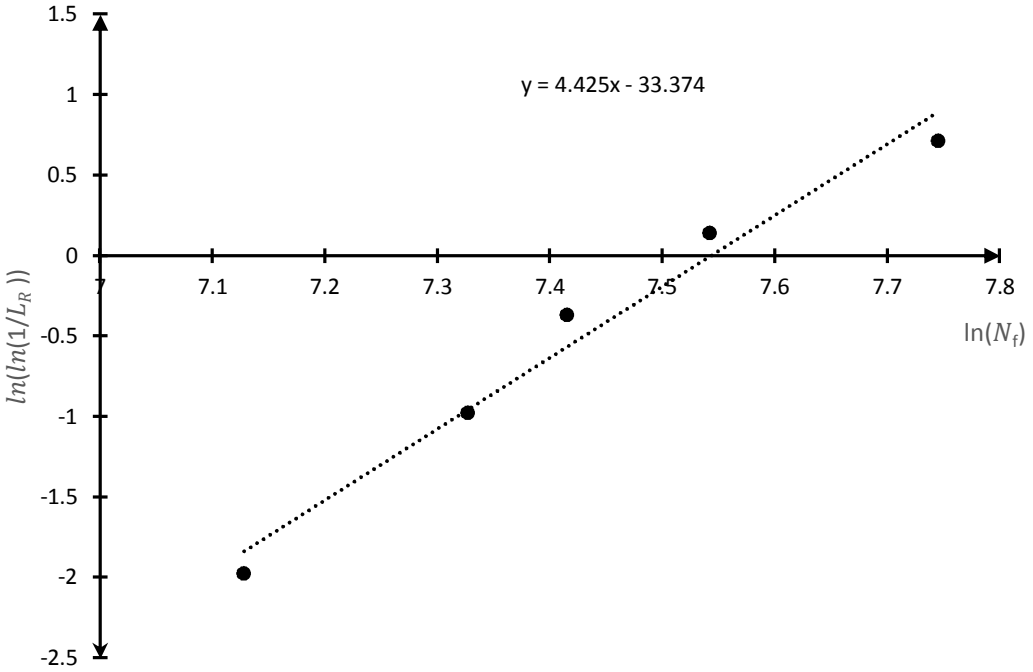

Figure 3-10 Statistical analysis of fatigue life data at applied stress of 1880 MPa for unidirectional defective specimen

By inserting the probability of failure P_f in Eqn. (3.8) such that:

$$L_R = 1 - P_f \tag{3.10}$$

Then: $$ln\left(ln\left(\frac{1}{1-P_f}\right)\right) = \propto \ln(N_f) - \propto \ln(u) \tag{3.11}$$

By arranging Eqn. (3.11):

$$N_f = \exp\left[\frac{ln\left(ln\left(\frac{1}{1-P_f}\right)\right) + \propto \ln(u)}{\propto}\right] \tag{3.12}$$

Using Eqn. (3.12) with the obtained shape and scale parameter at applied stress of 1880 MPa, the fatigue life N_f can be calculated at different probabilities of failure. Three probabilities of failure were used during this statistical analysis: 0.95, 0.5 and 0.05. The same procedures were followed for different stresses and fatigue lives shown in Figure 3-6.

Figure 3-11 shows the S/N curves for reference and defective samples at three different probabilities of failure. The same fatigue behavior can be observed at any probability of failure. For instance, at 0.95 POF the effect of gap is more evident at high stresses. By decreasing the applied stress, the S/N curves for reference and defective specimens converge to each other which indicates alleviation of gap effect.

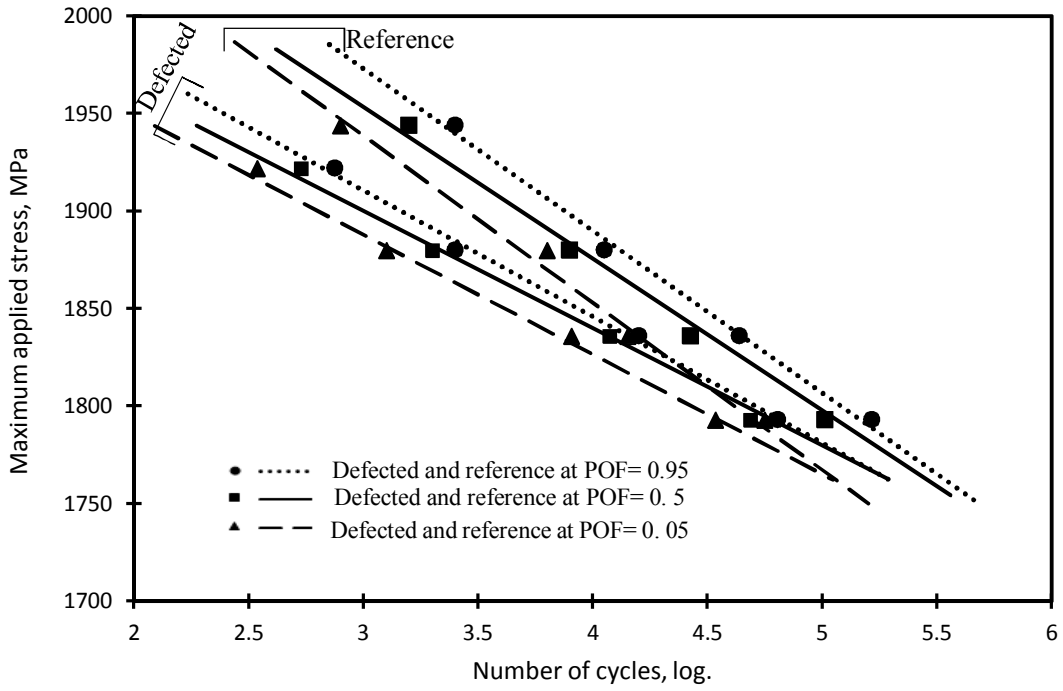

Figure 3-11: S/N curves for reference and defective unidirectional specimens at different probabilities of failure

Damage mechanisms and IR thermography

In order to figure out the main damage mechanism that occurs as a result of gap, some tested specimens were sectioned parallel and normal to fiber direction after 1000 cycles prior to complete failure. As a result of tow cut during manufacturing, the normal stress in the defective tow decays to a very low value at the edge of the gap. Consequently, the amount of stress carried by that defective tow is transferred to the adjacent tows in the upper and lower layers. As a result of shear transfer of load, high interlaminar stresses generate at the edge of the gap. These out-of-plane stresses help in initiating delamination, between the defective layer and the surrounding layers, from gap location which propagates in loading direction toward the grips. The occurrence of delamination reduces the ability of the material to transfer the load between layers and hence individual fibers will not sustain the applied stress. Then drastic failure happens by fiber breakage. Figure 3-12 represents a section cut normal to fiber direction at a distance of X=6.5 mm from the center of the gap (the edge of the gap is at 1.5 mm), referring to the schematic illustration shown in Figure 2-7, showing the delamination that occurred between the middle defective 0^o layer and the adjacent 0^o layers. It was also observed that the damage propagated only along the length (X-) direction without any transverse propagation along the thickness (Z-) or the width (Y-) directions. The width of the detected delamination was the same as the width of the gap, 0.25 inch (6.35 mm). Figure 3-13 shows a unidirectional 0^o specimen after failure. Final failure took place in the form of longitudinal matrix cracks (split) and fiber breakage.

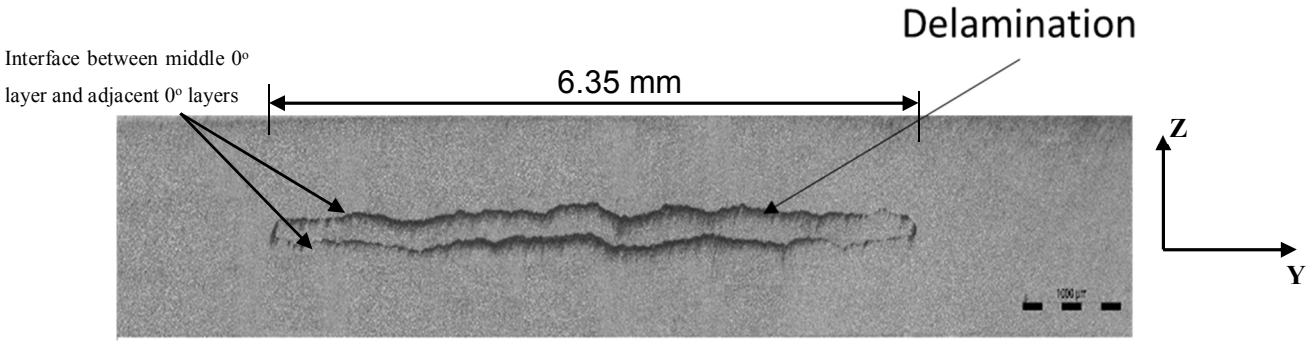

Figure 3-12: Microscopic image at X=6.5mm from the gap center showing delamination occurrence in a unidirectional laminate after 1000 cycles

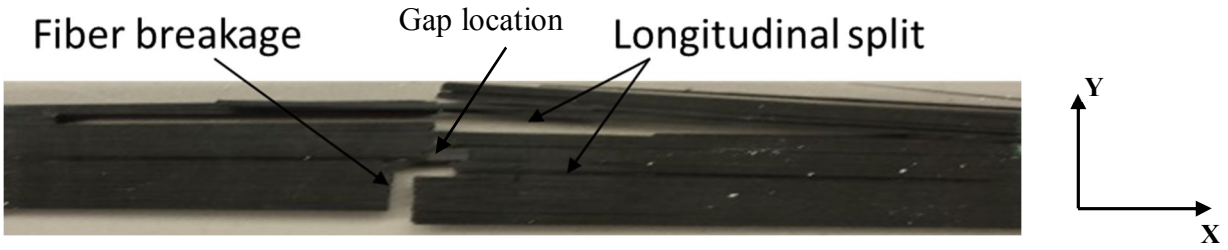

Figure 3-13: Unidirectional 0º specimen after final failure

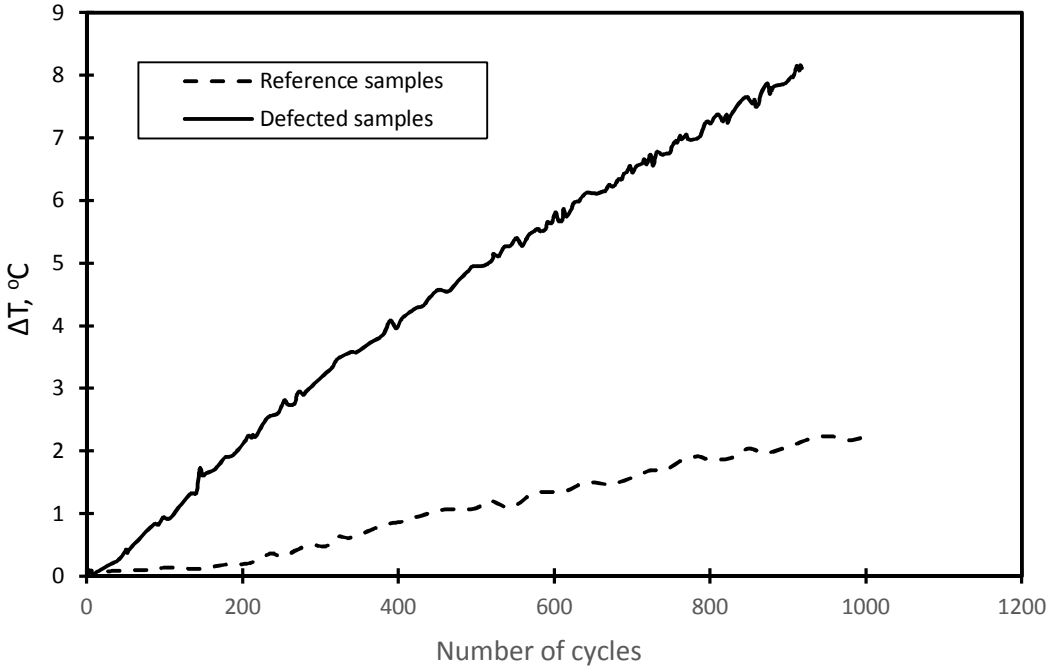

Figure 3-14: Temperature increase for reference and defective specimens

To investigate the effect of gap on thermal behavior of laminates, two specimens, reference and defective, were tested at the same applied maximum stress (1880 MPa) and the temperature of the same location (at the center of the specimen on the surface) was monitored using IR camera. Figure 3-14 shows the temperature increase as a function of the number of cycles for 1000 cycles of specimens' life. It was observed that as a result of the heat released from damage initiation and

propagation from the gap location in the middle of the defective specimen, there was a high temperature increase at the surface.

Based on this observation, it can be concluded that IR thermography can be efficiently used to monitor the propagation of damage as a result of gap. Figure 3-15 (a) shows thermal images captured at different ratios of number of cycles to failure at maximum applied stress of 1880 MPa. At the start of the fatigue test, the surface temperature of the specimen was uniform. Then, the temperature started to increase at the middle of the specimen as an indication of occurrence of damage and it continued to increase longitudinally toward the machine grips due to damage propagation along the length up to final failure of the specimen. Figure 3-15 (b) shows the same sample at failure. There is good correspondence between the temperature distribution and the location of final failure since failure occurred at the area of the highest temperature detected by the IR camera.

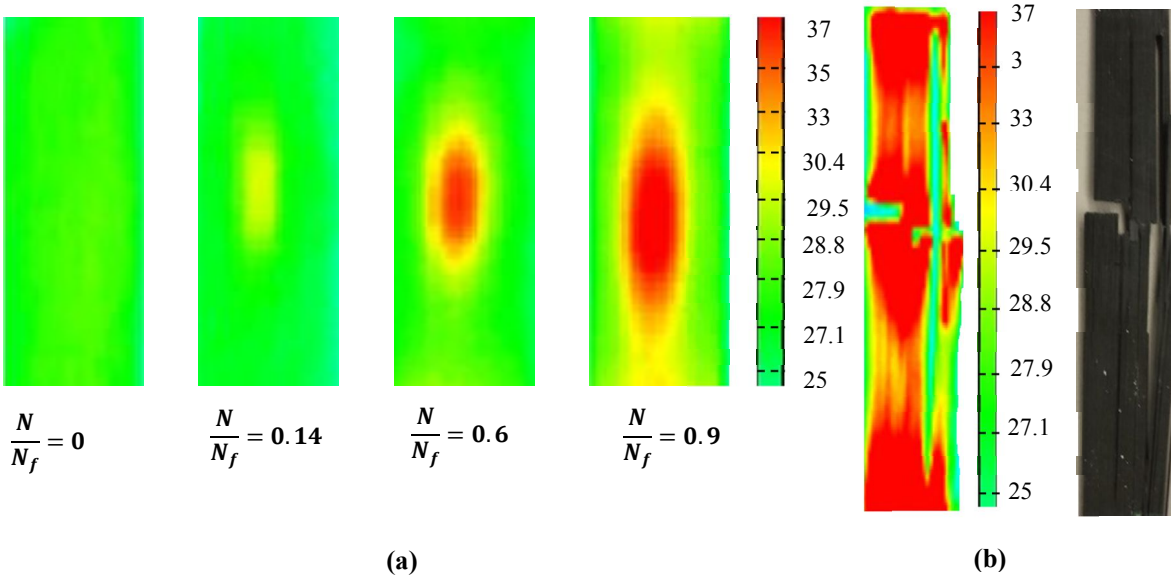

Figure 3-15: (a) Detection of damage evolution using IR and (b) specimen at failure

Figure 3-16 (a) shows the thermal behavior of unidirectional defective samples at different applied maximum stresses. At high stresses the temperature continues to increase till final failure

of specimens. However at lower stresses, initially, the rate of temperature increase was high followed by lower rate as illustrated for stress level of 1840 and 1790 MPa. Figure 3-16 (b) demonstrates the thermal behavior of the reference samples. Initially, there is a temperature increase as a result of damage growth from pre-existing manufacturing defects followed by constant temperature due to damage saturation in the specimen and finally a sudden increase at failure. In addition, in Figure 3-16 (b), the behavior of the defective specimen at the same applied stress, 1840 MPa, was shown for the purpose of comparing the thermal behavior of the two types.

There are two main sources responsible for temperature increase during fatigue loading. The first one is due to the viscoelastic nature of matrix material. The second one is due to the damage mechanisms. It was found in reference [64] that the heat generation by damage has the main contribution to the temperature increase. In addition, the viscoelastic effect can be assumed to be small due to the small size of the created gaps. The heat generated from damage mechanisms can be generated instantaneously as a result of damage occurrence. When damage occurs, energy is released from the damage location and causes the temperature of the material to increase. It can also be generated continuously as a result of rubbing of the created surfaces from delamination. The continuous rubbing of the surfaces created by the delamination can be considered as the major source of temperature increase during the fatigue life of the specimen.

This can also be confirmed by comparing the thermal behavior of both reference and defective specimens in Figure 3-16 at applied stress of 1840 MPa. It can be observed that the maximum temperature increase for the case of reference specimen which is mainly due to the viscoelasticity of matrix was 4 ^{o}C. However, for the case of defective specimen, the temperature increase which is mainly due to damage from the gap was about 12 ^{o}C. This might indicate that the damage due to the gap has the main contribution in the observed temperature increase in the defective specimens.

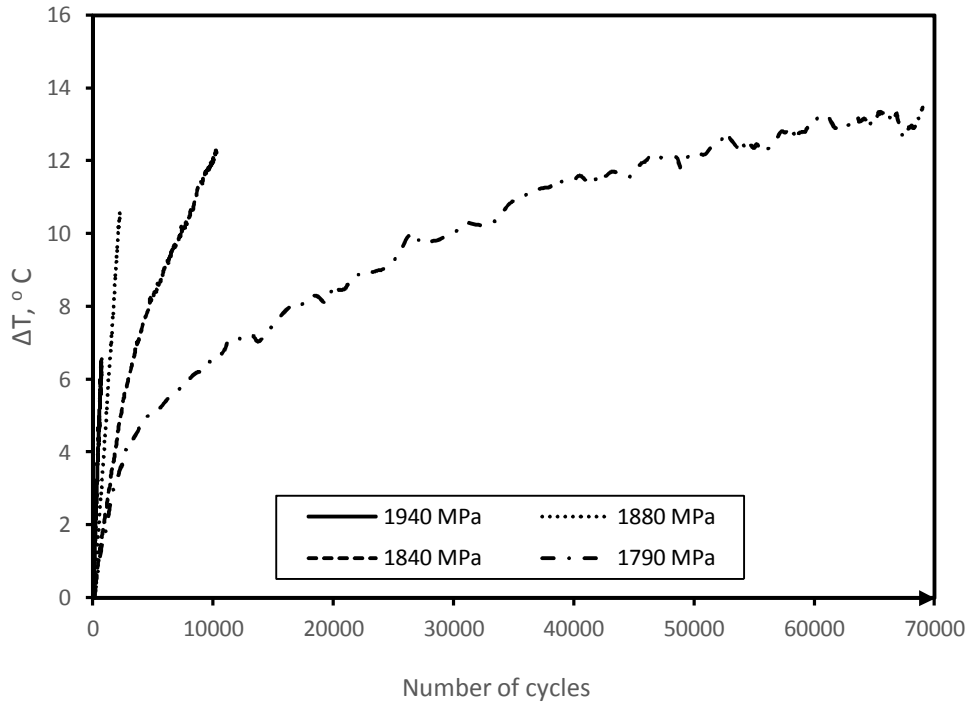

(a)

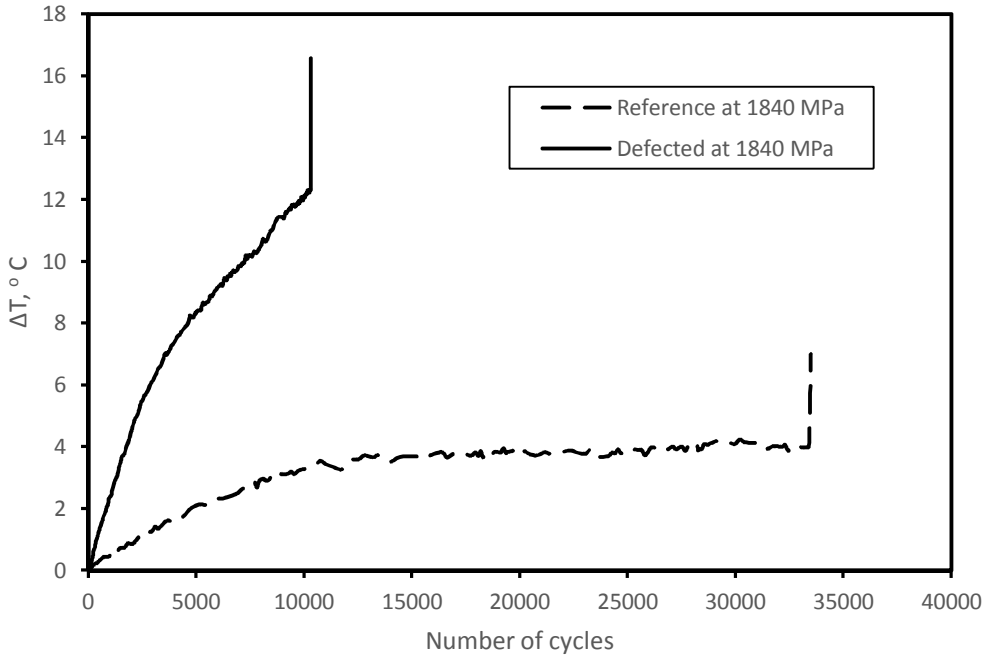

(b)

Figure 3-16: Thermal behavior of unidirectional (a) defective and (b) reference specimens.

3.3.1.2 **Cross-ply laminates**

Reference and defective cross-ply laminates were initially tested quasi-statically to determine the ultimate tensile strength. It was found that the average tensile strength for the reference cross-ply specimens was 1310 MPa. For the case of defective specimen containing gap in the middle 0^o layer the static strength was 1150 MPa. So, the reduction in the static strength in this case is 12%.

Following the quasi-static tests, both types of specimens, reference and defective, were fatigue tested at four selected stress levels with five replicates at each stress. The obtained data in terms of the fatigue life was plotted against the maximum applied stress and then it was fitted to regression lines using least square method. Figure 3-17 shows the fatigue lives obtained at different stresses for cross-ply laminates. Figure 3-18 shows the developed S/N curves for the reference and the defective cross-ply laminates based on 0.95 confidence level.

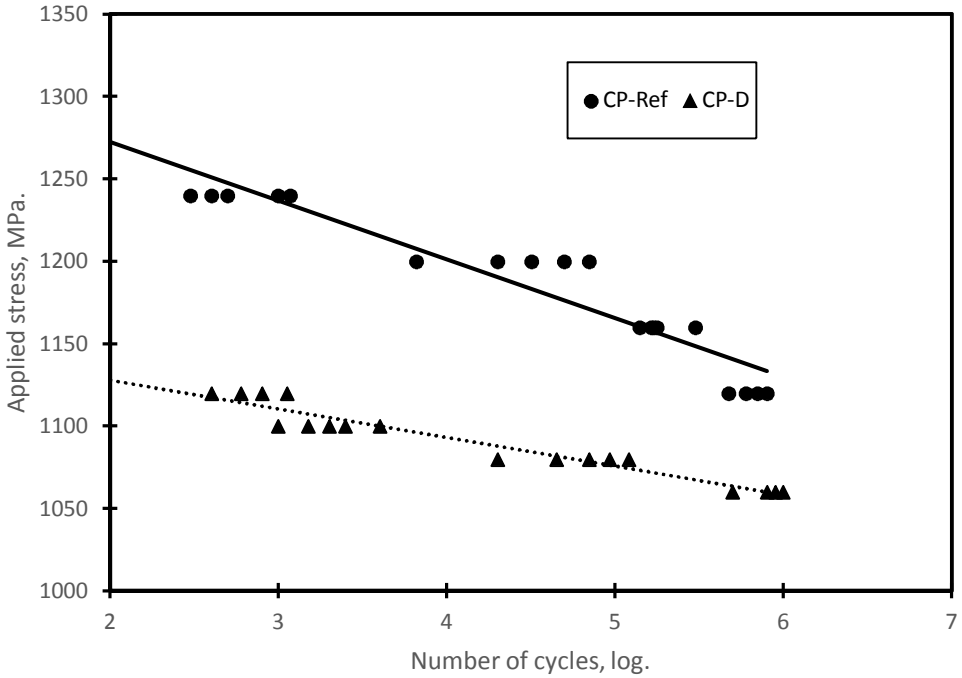

Figure 3-17: Fatigue lives at each stress for cross-ply reference and defective specimens

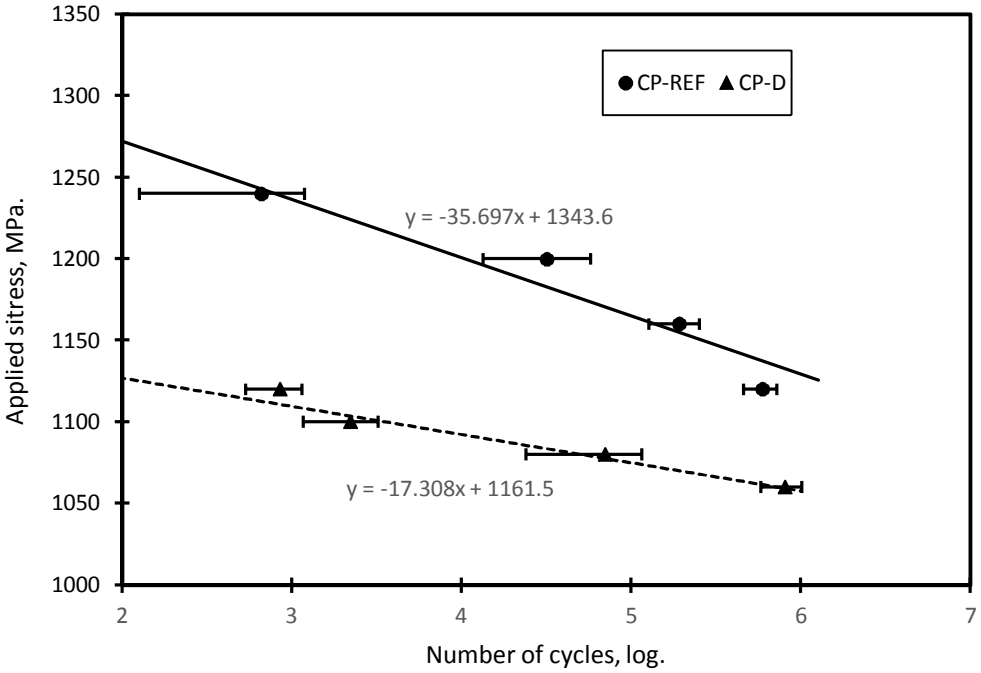

Figure 3-18: Stress/life curves for cross-ply reference and defective specimens with gaps in 0^o layer at 0.95 confidence level

Figure 3-18 shows the same behavior as in the case for unidirectional laminates. As a result of gap, there is a reduction in the fatigue life and this reduction depends on the applied stress. At high applied stress the reduction is high and as a result of the convergence of the two S/N curves the reduction decreases with decreasing the applied stress.

Moreover, there were two observations regarding the behavior of the cross-ply laminates under fatigue loading from Figure 3-18. The first observation is about data scattering. Compared to the case of unidirectional laminates shown in Figure 3-7, the scattering in the fatigue life obtained at each stress is high in case of cross-ply laminates and this can be indicated by the wide range of the fatigue life intervals between the extreme values at each stress level. The main reason for the scattering difference is the damage mechanisms [80]. For cross-ply laminates, one of the dominant damage mechanisms is matrix cracking especially in the off-axis layers (90^o layers for the case of cross-ply) which can help initiating delamination or fiber/matrix debonding that can accelerate final failure process. These matrix cracks are greatly affected by the existence of resin rich areas and manufacturing flaws in the laminates. Since the distribution and intensity of those

flaws are random for each specimen then the scattering range will be larger for this type of laminates.

The second observation is the decrease in the fatigue sensitivity for the case of cross-ply laminates which can be indicated by the decrease in the slope of the S/N curves for these laminates. The decrease in the slope of the cross-ply laminates was 55-70% compared to the unidirectional laminates. This means that the existence of the 90^o layers in the laminates improves the fatigue behavior and helps the laminate to perform better although they do not help in carrying the load. A possible explanation is that in case of unidirectional laminates one of the mechanisms that occurs during loading is the splits (longitudinal cracks between fibers in 0^o layers) which reduces the ability of transferring the load between fibers. The existence of 90^o layers in between the 0^o layers helps in holding the fibers in 0^o layers together in the transverse direction and reduces the probability of splitting occurrence. Also, the existence of more damage mechanisms in case of cross-ply laminates such as matrix cracks and delamination between 0^o and 90^o layers might help in relieving the stress and improving the behavior [81]. In addition, it was also found in reference [82] that the fatigue sensitivity decreases by increasing the number of 90^o layers in the laminates.

As mentioned previously, the fatigue tests were terminated at 10^6 cycles which for instance correspond to 1120 MPa for the reference cross-ply specimens and 1060 MPa for the defective cross-ply specimens. However, it was required to get the reduction in fatigue life at lower stresses in order to get the stress value at which the S/N curves for reference and defective specimens intersect with each other. This represents the value of stress at which the gap has no effect on the fatigue life of the specimens, threshold stress. So, the number of cycles to failure at lower stresses for all types of laminates were determined by extrapolating the data based on the linear fitting curves obtained from the performed experimental data.

Figure 3-19 shows the reduction in fatigue life for cross-ply defective specimens at different applied stress levels. The reduction curve was obtained from the regression fitting lines of the S/N curves for the reference and defective cross-ply specimens shown in Figure 3-18. It can be observed that at high stresses (1020 MPa), the reduction in the fatigue life is high (0.93) and it decays by decreasing the applied stress during fatigue cycles because of the convergence of the two S/N curves, as shown in Figure 3-18. At the point of the intersection of the S/N curves both

types have the same life and hence no reduction in fatigue life at this point occurs. The value of the stress corresponding to the intersection of the two S/N curves for the cross-ply laminates, threshold stress, was 983 MPa.

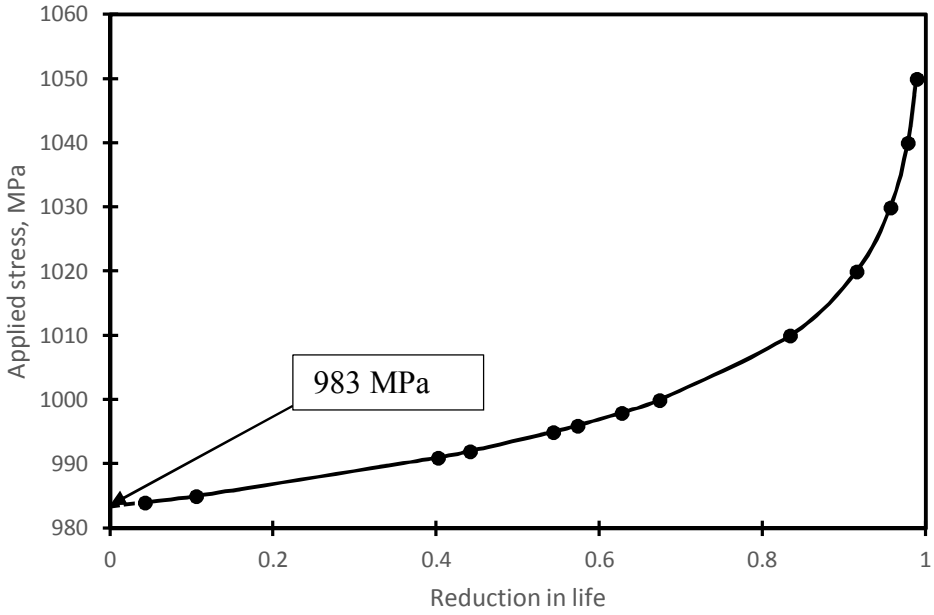

Figure 3-19: Reduction in fatigue life for defective cross-ply laminate

Figure 3-20 shows the developed S/N curves for cross-ply laminates, reference and defective, at three different probabilities of failure (POF): 0.95, 0.5 and 0.05. The same behavior can be observed at all POF. There is a great difference between the two S/N curves at high stresses and this difference decreases by reducing the stress since the two curves converge slowly to each other.

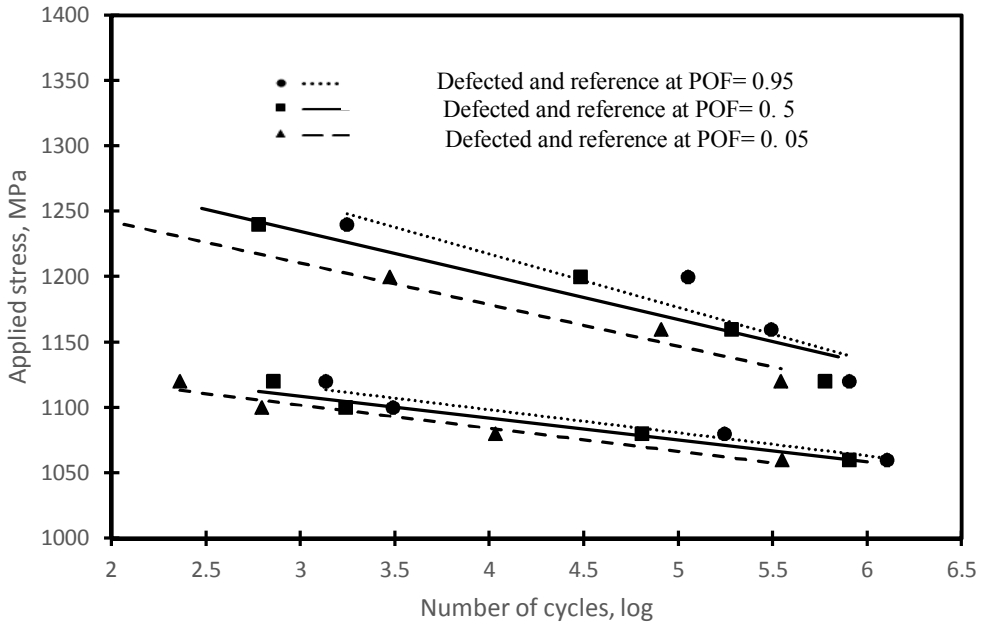

Figure 3-20: S/N curves for reference and defective cross-ply specimens at different probabilities of failure

Damage mechanisms and IR thermography

The damage sequence in the case of cross-ply laminates started with some failure of weak fibers in the laminates in the 0^o layers. Matrix cracks occurred at the early beginning of the fatigue life and these cracks increased in density upon increasing the fatigue cycles. Splits also occur in 0^o layers which might initiate from resin rich areas in the laminates or from the gap location in the defective specimen. Final failure occurred when the strength of the fibers in the 0^o layers degrades to a critical value and could not withstand more fatigue cycles. Delamination was also observed at the interface of the $0^o/90^o$ layers. Figure 3-21 shows a cross-ply laminate after failure indicating different damage mechanisms occurrence: delamination, transverse matrix cracks in 90^o layers and longitudinal splits in 0^o layers and fiber breakage.

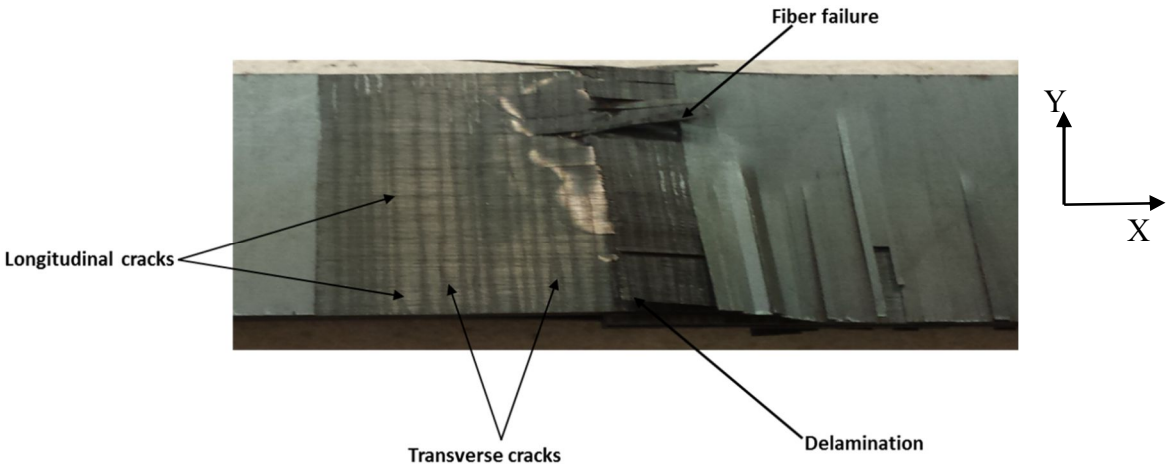

Figure 3-21: Cross-ply laminate after final failure

A few cross-ply laminates were cut prior to failure to inspect the occurrence of internal damage mechanisms as shown in Figure 3-22. Delamination was observed at the interface of the defective 0^o layer and upper/lower 0^o layers which is similar to the case of the unidirectional laminates. The major difference between the unidirectional and the cross-ply laminates is the occurrence of some transverse cracks growing from the delamination from the gap to the interface of the $0^o/90^o$ layers. The propagation of these cracks in the 0^o layers negatively affects their performance and reduces their capability of carrying load which consequently might accelerate the fiber failure process.

Figure 3-23 shows few thermal images captured at different ratios of number of cycles to failure at maximum applied stress of 1100 MPa during fatigue loading of cross-ply laminates. Initially, the surface temperature was uniform then by increasing the number of cycles the temperature started to increase at the middle of the specimen due to damage initiation and continued to increase toward the grips as a result of increase in the damage size.

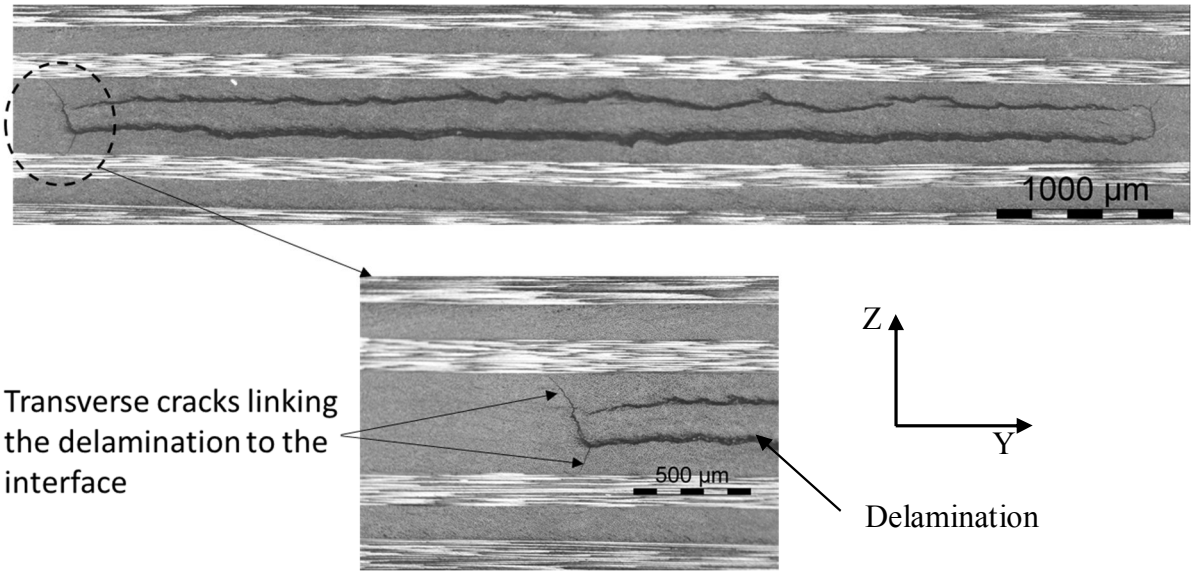

Figure 3-22: Microscopic image at X=6.5 mm from the gap center showing internal damage mechanisms in cross-ply laminate

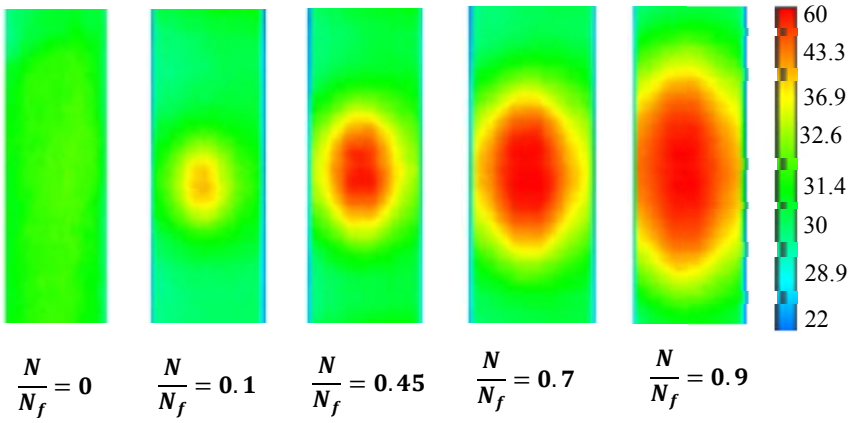

Figure 3-23: Damage detection in cross-ply laminates using IR thermography

An interesting observation could be made by comparing the shape of the high temperature area due to damage in both unidirectional and cross-ply laminates. As shown in Figure 3-24, for unidirectional laminates, the profile of the high temperature area is close to an elliptical shape. However for cross-ply laminates, it is close to a circular shape. Carbon fibers have high thermal conductivity along fiber direction compared to transverse direction which facilitates the

propagation of heat in the longitudinal direction for unidirectional specimens. For cross-ply laminates as a result of the existence of fiber in both longitudinal and transverse directions, the heat can easily propagate in both directions which creates almost circular-shaped high temperature area. Also, this might be attributed to more distributed damage in case of cross ply laminates compared to unidirectional ones.

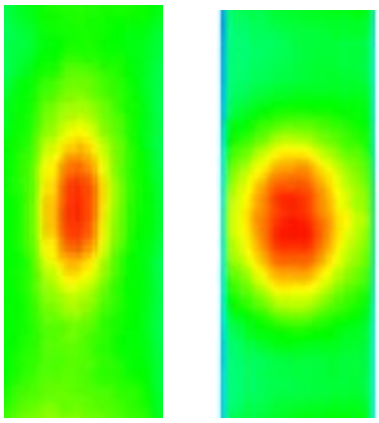

Figure 3-24: Shape of high temperature area in (a) unidirectional and (b) cross-ply laminates.

Figure 3-25 represents the temperature increase with number of cycles for defective cross-ply laminates. At high stresses, 1120 MPa, the temperature continued to increase up to complete failure of the specimen. It can be observed that at lower stresses, 1080 MPa, the temperature started to increase by high rate as a result of damage process and the rubbing of surfaces created by delamination. By increasing the number of cycles, more energy is dissipated to the surrounding. Then, when the damage reaches saturation, the amount of heat generated from the material becomes constant and the specimen reaches equilibrium between the generated heat and the dissipated heat to the environment and consequently reaches temperature plateau up to final failure.

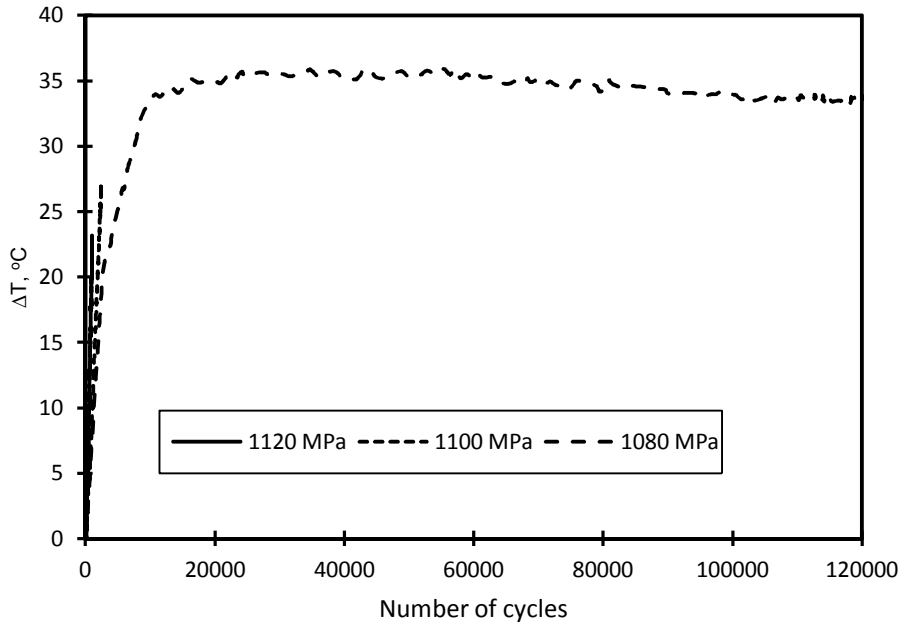

Figure 3-25: Thermal behavior at different stresses for defective cross-ply laminates

3.3.1.3 **Quasi-isotropic laminates**

Reference and defective quasi-isotropic laminates were initially tested quasi-statically to determine the ultimate tensile strength. It was found that the average static strength for the reference quasi-isotropic specimens was 1070 MPa while for the case of defective specimen containing gap in the middle 0^o layer the average static strength was 880 MPa. The reduction in the static strength in this case was 18%.

Reference and defective specimens were fatigue tested up to final failure or reaching 10^6 cycles. The specimens were subjected to different stress levels and five specimens were tested at each stress level. The obtained fatigue lives at each stress level were plotted against the maximum applied stress in the fatigue cycle. Figure 3-26 shows the fatigue lives obtained at different stresses for quasi-isotropic laminates. Figure 3-27 shows the developed S/N curves for the reference and the defective cross-ply laminates based on 0.95 confidence level.

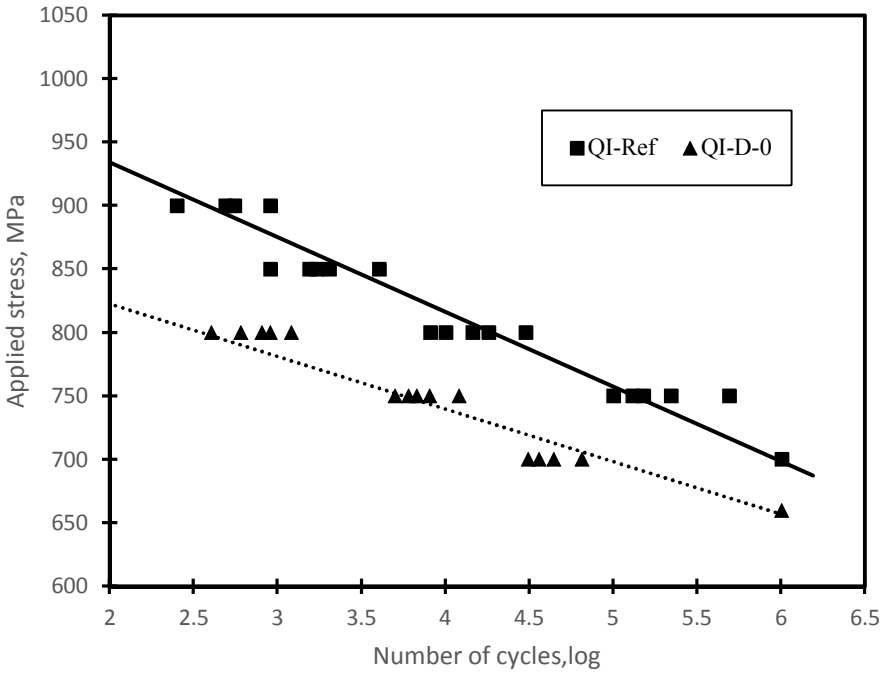

Figure 3-26: Fatigue lives at each stress for cross-ply reference and defective specimens

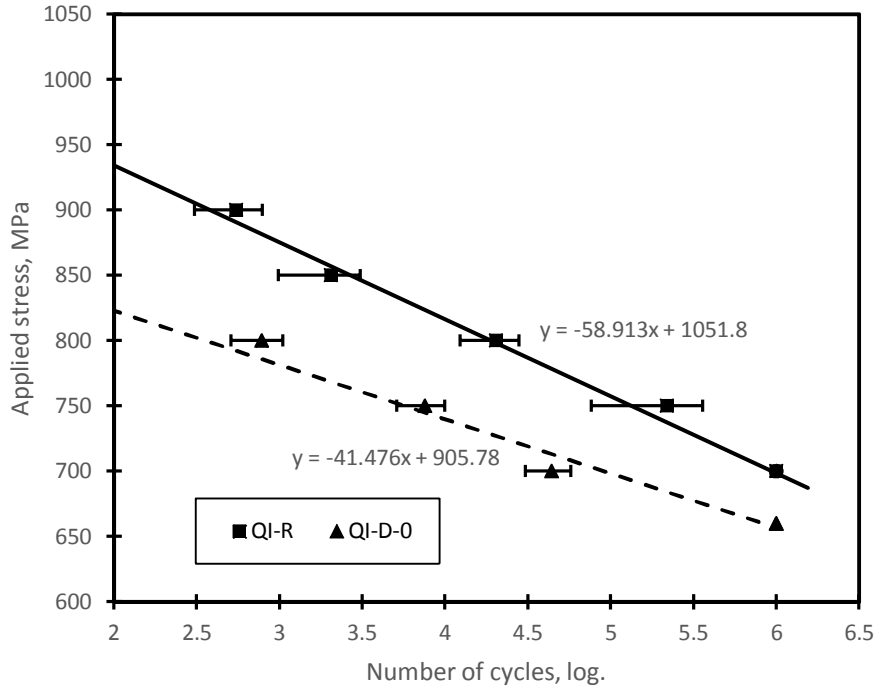

Figure 3-27: Stress/life curves for quasi-isotropic reference and defective laminates with gaps in 0º layer

In the case of quasi-isotropic laminates, the decrease in the fatigue sensitivity which can be indicated by the decrease in the slope of the S/N curve was 25-33% compared to the case of unidirectional laminates. This improvement can be attributed to the existence of 90^{o} layers in the laminates that positively affects the fatigue performance as explained in the cross-ply case. Also, this improvement was less than the case of cross-ply. A possible explanation is the variation of the number of 90^{o} layers since in case of cross-ply laminates, four 90^{o} layers were used while in the case of quasi-isotropic laminates only two 90^{o} layers were used. Figure 3-28 shows the fitted S/N curves for reference laminate with different stacking sequences in order to show the variation in the slope.

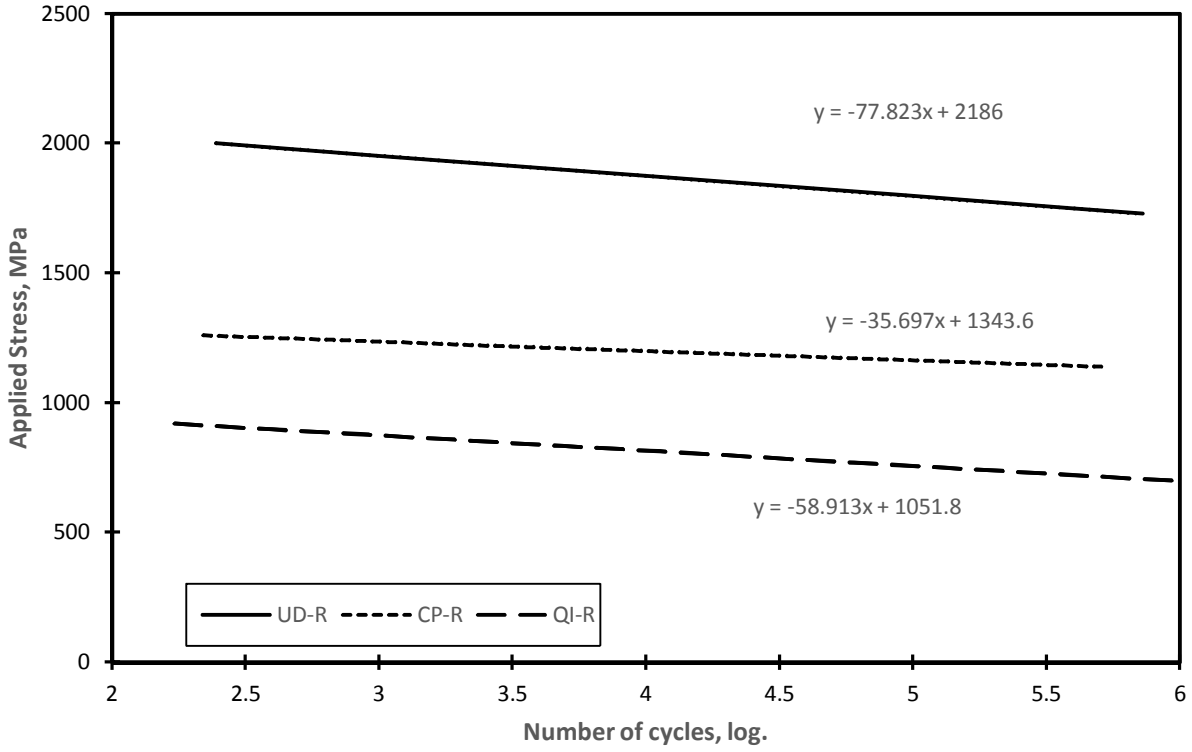

Figure 3-28: Fitted lines of S/N relation for different stacking sequences of reference laminates.

The previously observed behavior of the defective unidirectional and cross-ply laminates was also observed for the quasi-isotropic case. At high applied stresses the reduction in the fatigue life is high and it decreases by decreasing the applied stress. The run-out stresses that correspond to 10^6 cycles during fatigue tests were 700 MPa for the reference laminates and 650 MPa for the defective specimens. By extrapolating the S/N curves based on linear fitting curves, the reduction in fatigue life for quasi-isotropic defective laminates at lower stresses can be determined.

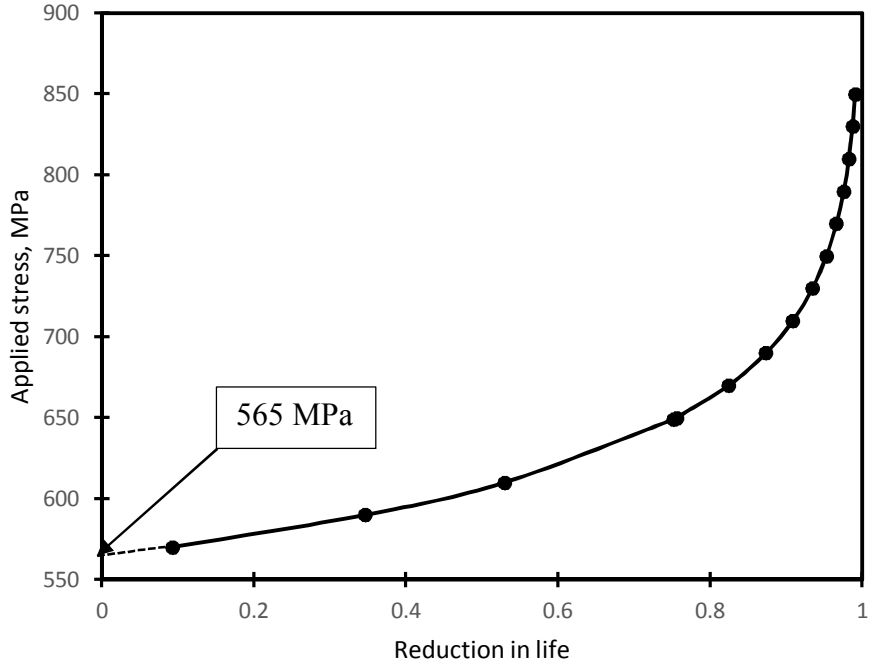

Figure 3-29: Reduction in fatigue life for defective quasi-isotropic laminate

Figure 3-29 shows the reduction in fatigue life at different applied stress for quasi-isotropic laminates. From the reduction curve of quasi-isotropic laminates in this figure, at 700 MPa the reduction in the fatigue life is 0.9 while at 580 MPa the reduction is 0.2. At the point of the intersection of the two S/N curves both types have the same life and hence no reduction at this point occurs. The value of the stress corresponds to the intersection of the two S/N curve, threshold stress, was 565 MPa.

Figure 3-30 shows the developed S/N curves for quasi-isotropic laminates, reference and defective, at three different probabilities of failure: 0.95, 0.5 and 0.05. The same behavior can be

observed at all POF. There is a great difference between the two S/N curves at high stresses and this difference relatively decreases by reducing the stress since the two S/N curves converge to each other.

The damage mechanisms in case of quasi-isotropic laminates consist of: matrix cracks in the off axis layers (45°, -45° and 90° layers) which occur early in the fatigue life, delamination at the interfaces between layers with different orientations (90°/45° and 45°/-45°) and fiber breakage at the end of the fatigue life which is followed by catastrophic failure. Figure 3-31 shows a quasi-isotropic laminate after failure indicating different damage occurrence: delamination, matrix cracks in 90° and 45° layers and fiber breakage.

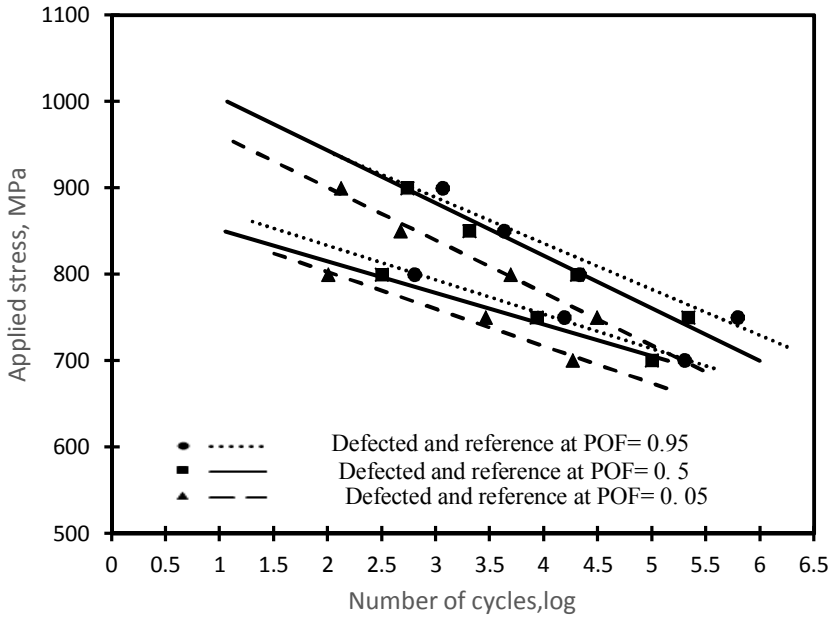

Figure 3-30: S/N curves for reference and defective quasi-isotropic laminates at different probabilities of failure

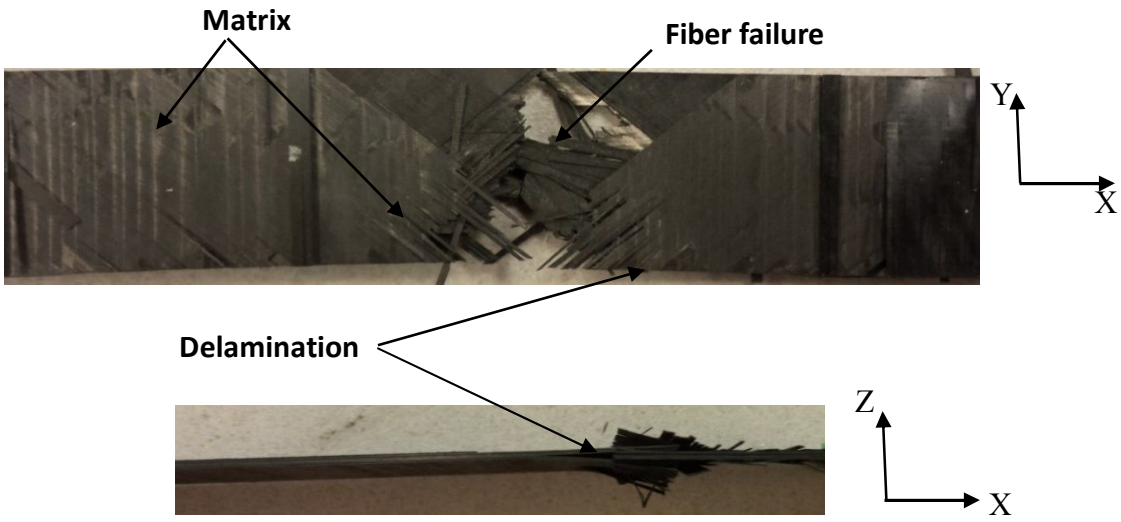

Figure 3-31: Different damage mechanisms after failure of quasi-isotropic specimen.

A few quasi-isotropic laminates were cut prior to failure to inspect the occurrence of internal damage mechanisms as shown in Figure 3-32. Delamination was observed at the interface of the defective 0^o layer and upper/lower 0^o layers which is similar to the case of the unidirectional and cross-ply laminates due to the transfer of load from the defective tow to the adjacent tows. Transverse cracks that grow from the delamination due to gap to the interface of 0^o/-45^o layers can be observed. The propagation of these cracks through the 0^o layers affects its ability for carrying the load and accelerates the fiber failure.

Figure 3-33 shows thermal images captured at different ratios of number of cycles to failure at maximum applied stress of 700 MPa during fatigue loading of quasi-isotropic laminates. Initially, the surface temperature was uniform then by increasing the number of cycles the temperature started to increase at the middle of the specimen due to damage initiation and continued to increase toward the grips as a result of increase in the damage size.

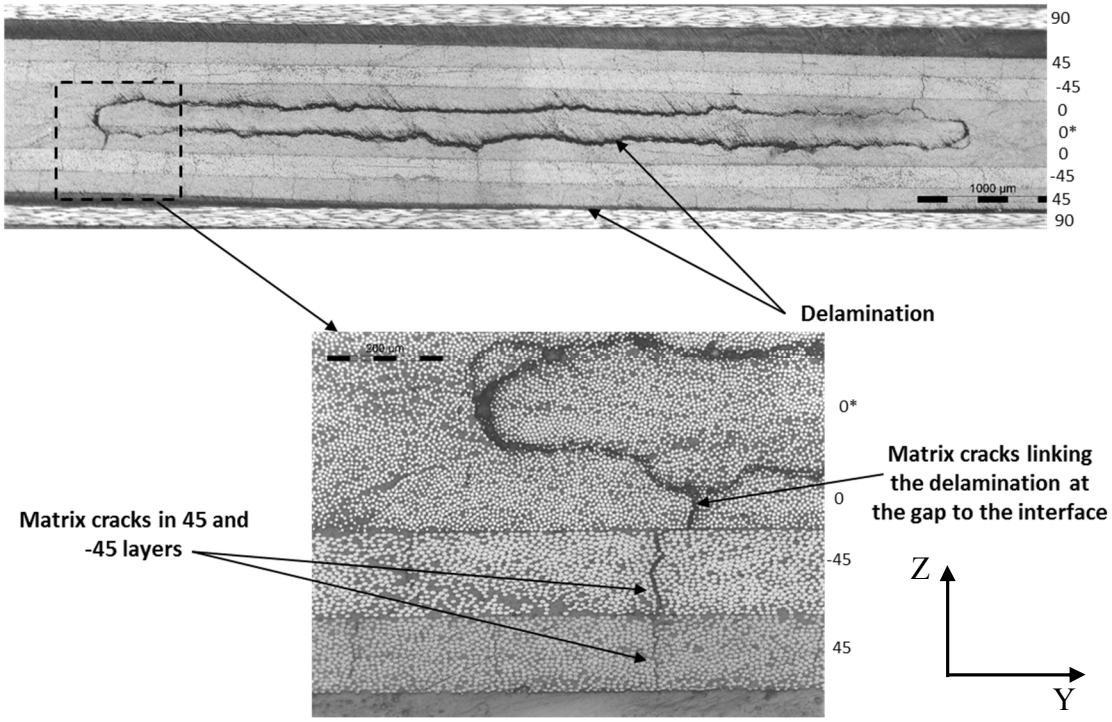

Figure 3-32: Microscopic image at X=6.5mm from the gap center showing internal damage mechanisms in quasi-isotropic laminate

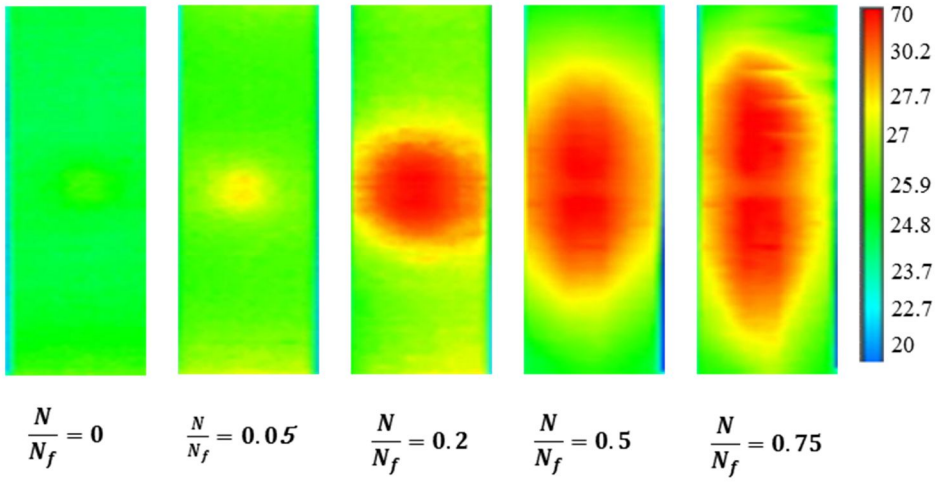

Figure 3-33: Damage detection using IR thermography for defective quasi-isotropic specimen

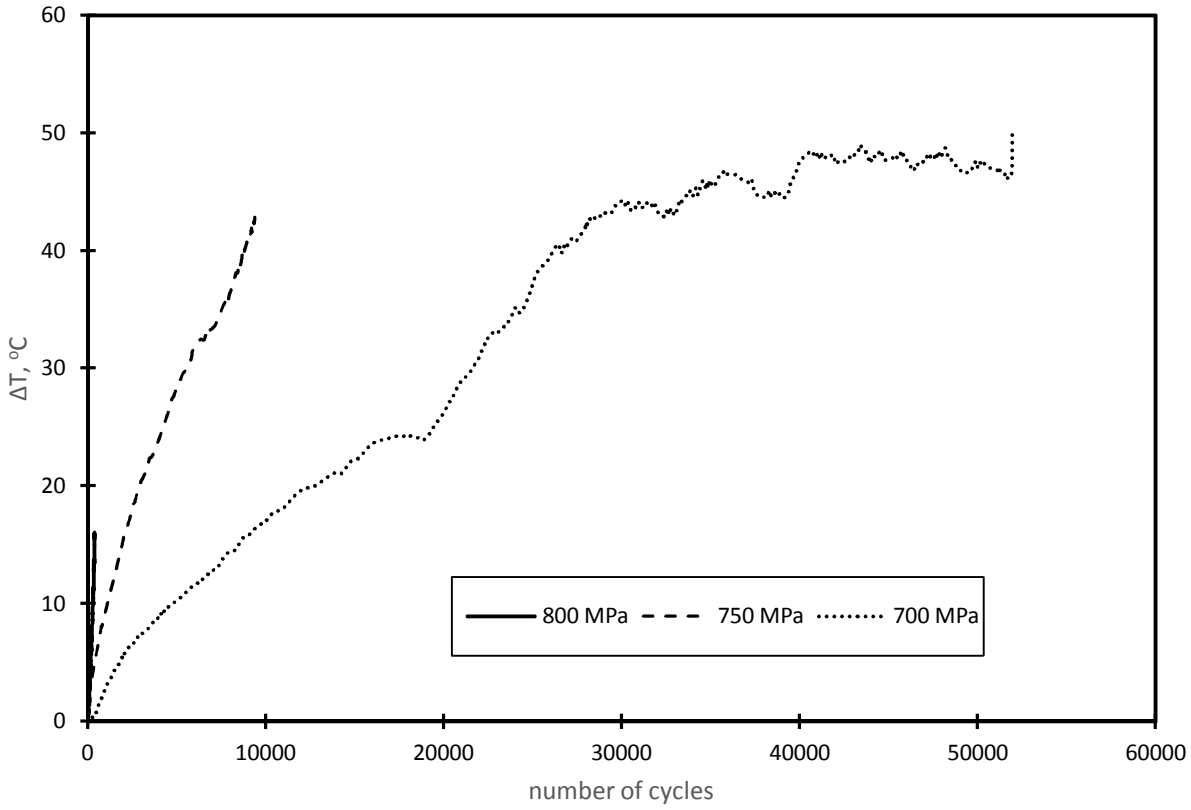

Figure 3-34: Temperature increase at different stresses for defective quasi-isotropic laminates

Figure 3-34 shows the temperature increase with number of cycles for defective quasi-isotropic laminates. At high stresses, 800 MPa, the temperature continued to increase up to complete failure of the specimen. It can be observed that at lower stresses, 700 MPa, the temperature started to increase by high rate as a result of damage process and the rubbing of surfaces created by delamination. By increasing the number of cycles it reaches the temperature plateau up to final failure due to the equilibrium between heat generation and heat dissipation similar to the case of cross-ply laminates.

3.3.1.4 **Damage mechanisms due to gaps in 0^o layer**

This sub-section aims at investigating and understanding the damage behavior of different stacking sequences containing a gap in 0^o layers. This could help proposing some recommendations that could be helpful in designing laminates manufactured by AFP.

Cross-ply laminates

It was mentioned previously that for the case of cross-ply laminates, in addition to the delamination that occurs at the gap location, there exist some transverse cracks that propagate from the delamination to the nearest interface of $0^o/90^o$ layers. It was believed that these cracks affect the performance of the laminate.

In order to investigate the effect of these transverse cracks on the cross-ply laminates, three different types of cross-ply laminates were manufactured and tested. For the three laminates, it was required to keep the same number of 0^o and 90^o layers to avoid any effect of changing thickness. Three stacking sequences were selected using five 0^o layers and four 90^o layers in order to create the first interface, which is closest to the gap, at different distances from the gap. In all of these configurations, the gap was located in the middle 0^o layer as shown in Figure 3-35. The three stacking sequences were:

1- (90/90/0/0/0*/0/0/90/90) with two 0^o layers separating the gap from the $0^o/90^o$ interface.
2- (90/0/90/0/0*/0/90/0/90) with one 0^o layer separating the gap from the $0^o/90^o$ interface.
3- (90/0/0/90/0*/90/0/0/90) in which the interface is directly adjacent to the gap.

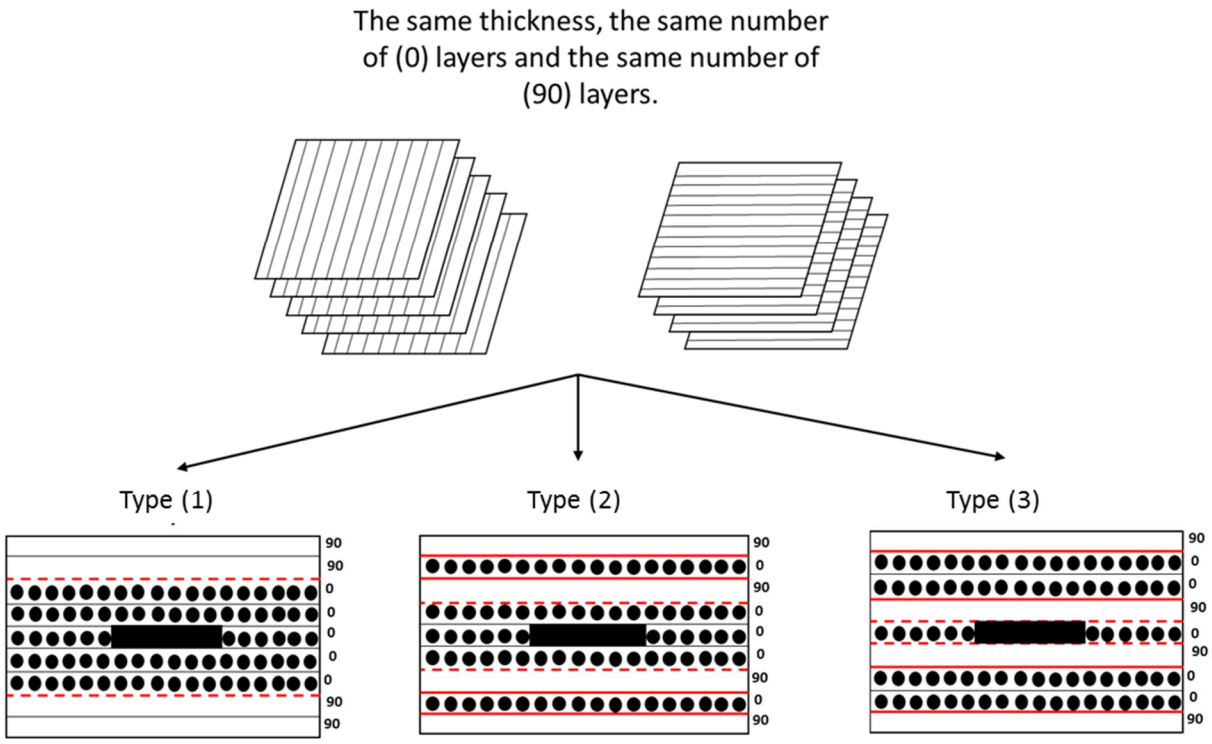

Figure 3-35: Different types of cross-ply laminates used to investigate the effect of the 0º/90º interface

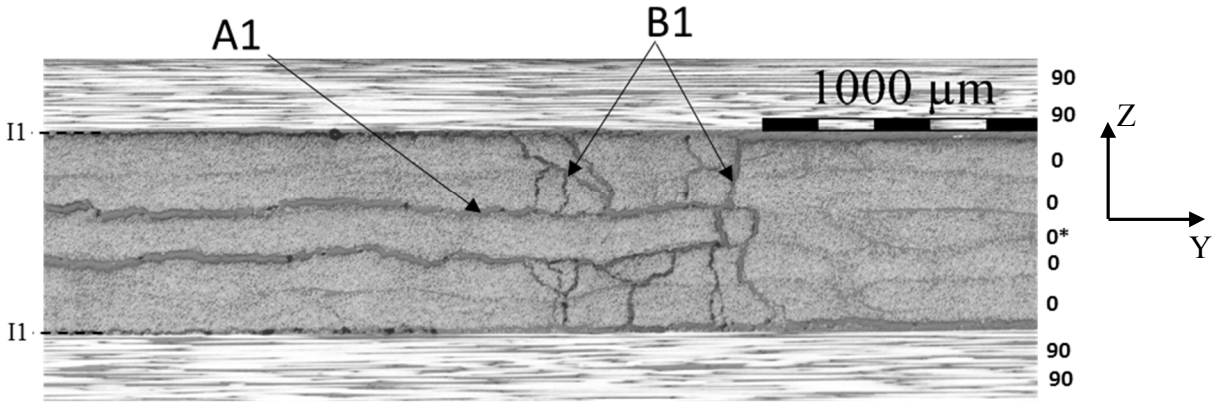

(a) Type (1)

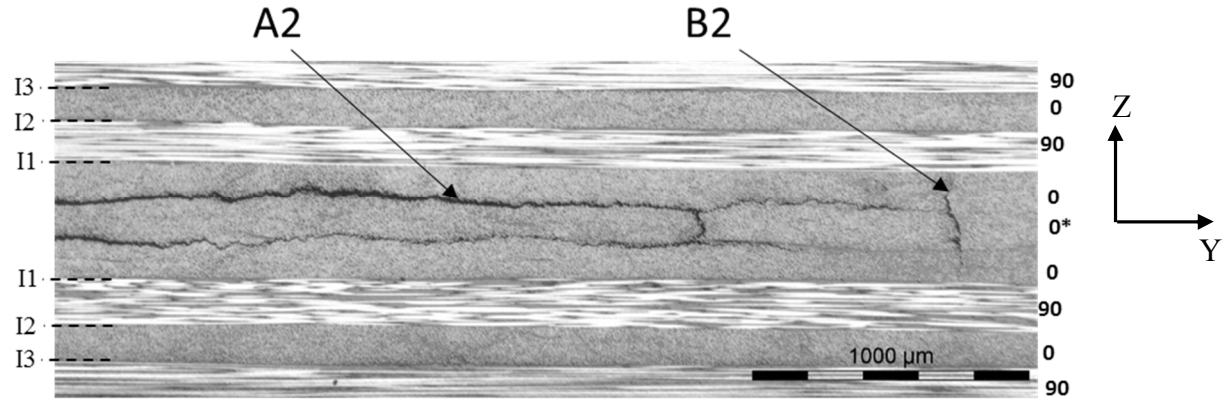

(b) Type (2)

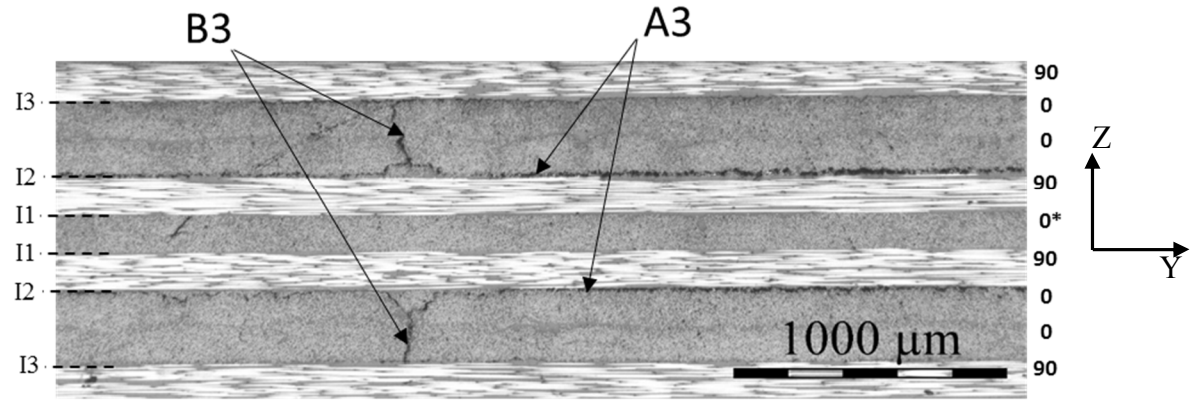

(c) Type (3)

Figure 3-36: Damage mechanisms for different types of cross-ply laminates after 100 000 cycles

Figure 3-36 shows microscopic images for the three tested stacking sequences illustrating the different damage mechanisms occurred within the laminates at a distance X = 5 mm from the gap. In the figure, the middle defective 0^o layer is denoted by (*). Also, the interfaces of $0^o/90^o$ layers are denoted by a letter (I) associated with a number indicating the order of the interface based on the distance between the defective layer and the interface. For instance, the symbol (I1) refers to the first interface of $0^o/90^o$ across the thickness from the defective (middle) layer, (I2) refers to the second interface of $0^o/90^o$ from the defective layer and (I3) refers to the third interface of $0^o/90^o$ from the defective layer. Also, for ease of identifying the layers in the laminates, layers numbering from 0 to 5 was used as shown in Figure 3-37.

Layer 4
Layer 3
Layer 2
Layer 1
Layer 0 (defected layer)
Layer 1
Layer 2
Layer 3
Layer 4

Figure 3-37: Numbering code for different layers in the laminate

In order to understand the behavior of different stacking sequences, Figure 3-38 is presented. We considered a 3D defect in the material represented by volume 1 in Figure 3-38. In addition volume 2' and volume 2'' represent volumes of intact material adjacent to the 3D defect (volume 1). If it was assumed that the defective material (volume 1) has a very low strength, since it represents a gap, then the generated stress on the faces of volume 1, when the material is under stress, will be very small. For instance, the generated stress σ_x on the face BGHC is low. As a result of stress distribution in the material between defective and intact regions, high stress σ_x will be generated on the faces B'G'H'C' and B"G"H"C" which are adjacent to the face BGHC. The same scenario can be applied to the faces normal to Y-direction. High stresses σ_y will be generated on the faces A'B'C'D' and A"B"C"D" which are adjacent to the face ABCD of the defective volume. This can reveal that as a result of the existence of a 3D defect in the material, high state of stresses in X- and Y- directions (σ_x and σ_y) will generate in the layers adjacent to the 3D defect.

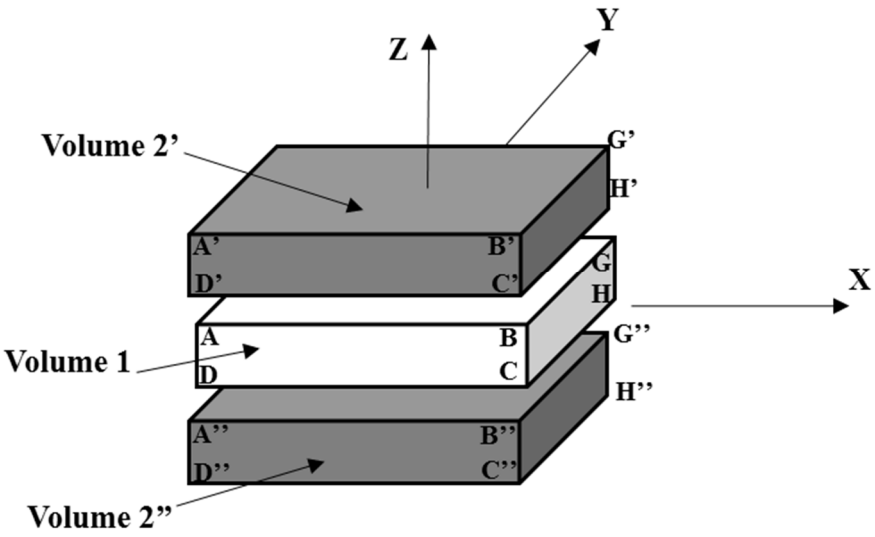

Figure 3-38: Volumes representing the 3D defect and the surrounding intact material

For type (1) in Figure 3-36 (a): it was found that delamination **(A1)** occurred at the interface of the middle (fifth) defective 0° layer (layer 0) and the adjacent 0° layers (layer 1). As a result of the gap (3D defect), the stresses (σ_x and σ_y) in layer 1 are high. Since layer 1 is a 0° layer and has weak properties along y-direction, so as a result of the high σ_y, transverse cracks **(B1)** occurred in layer 1. These occurred cracks (**B1)** keep propagating till reaching layer 2. Since layer 2 is also of the same orientation as layer 1, the same cracks continue through layer 2 till reaching the interface **(I1)** between layers 2 and 3. This means that in addition to the defective 0° layer, four extra 0° layers (layers 1 and layers 2) were affected by the occurrence of these transverse cracks. As such, in total five 0° layers became no more intact as a result of the gap.

For type (2) in Figure 3-36 (b): delamination **(A2)** occurred at the interface of the middle (fifth) defective 0° layer (layer 0) and the adjacent 0° layers (layer 1). As a result of the gap (3D defect), the stresses (σ_x and σ_y) in layer 1 are high. Since layer 1 is a 0° layer and has weak properties along y-direction, as a result of the high σ_y, transverse cracks **(B2)** occurred in layer 1. These cracks **(B2)** keep propagating till reaching the interface **(I1)** between layer 1 and layer 2. Since layer 2 is at a direction normal to the crack, layer 2 will constrain this crack without further propagation to the outer 0° layers (layers 3). This means that in addition to the defective 0° layer,

only two extra 0° layers (layers 1) were affected by the occurrence of these transverse cracks. As such, in total three 0° layers became no more intact as a result of the gap.

For type (3) in Figure 3-36 (c): As a result of the gap (3D defect), the stresses (σ_x and σ_y) in layer 1 are high. Since layer 1 is 90° layer and has weak properties along x-direction, so as a result of the high σ_x, transverse matrix cracks occurred in layer 1. The matrix cracks cause the occurrence of delamination **(A3)**. As a result of this delamination, layer 2 becomes no longer supported by the adjacent layers (layer 0 and layer 1) which weakens that layer (layer 2) and causes the occurrence of some transverse cracks **(B3)** propagated through the layer. Since layer 3 is also of the same orientation as layer 2, the same cracks continue through layer 3 till reaching the other interfaces **(I3)**. This means that in addition to the defective 0° layer in the middle of the laminate (layer 0), four extra 0° layers (layers 2 and layers 3) were affected by the occurrence of these transverse cracks which negatively affects the performance of the whole laminate. Also, some small delaminations were observed at the interfaces **(I1)** and **(I3)** but they were not as severe as the delamination **(A3)** at the interface **(I2)**. As such, in total five 0° layers became no more intact as a result of the gap.

So it can be concluded that due to the gap, the stresses are always high in the adjacent layers which helps in creating damage at those adjacent layers. For cross-ply laminates, the effect of the gap is not localized at the location of the gap, however, cracks propagate transversely across the thickness through the 0° layers. The subsequent results are that more 0° layers are affected. Although, initially there are some intact 0° layers in the laminate, but as result of the transverse cracks they no longer remian intact.

In order to investigate the effect of these transverse cracks on the tensile strength of the laminate, the different types of cross-ply laminates were subjected to quasi-static tensile testing. It was found that the average tensile strength for type (1) was 1060 MPa, type (2) was 1150 MPa and for type (3) was 1070 MPa. These obtained results were in good agreement with the observations found in the microscopic images shown in Figure 3-36. Although the shown microscopic images were obtained from fatigue tested specimen but they have good correspondence with the static

testing results. This might indicate that the observed damage mechanisms are also dominant in case of static loading and affect the failure stress.

Type (2) was less affected by the gap and the consequent occurred damage mechanisms compared to the other types. The existence of the 90^o layers at a distance of one layer away from the gap blocked the propagation of the transverse cracks (B2) which protected the outer 0^o layers. Hence these outer 0^o layers were not affected by the gap which consequently helped the laminate to carry more load. Both types (1) and (3) are severely affected by the gap because all the 0^o layers were affected by the transverse cracks (B1 and B3). This makes the static tensile strengths for the types (1) and (3) are almost the same which is 8% lower than the strength of type (2). This approach helped in reducing the negative influence of the cracks arising from the delamination.

By comparing the damage behavior in the case of defective unidirectional, shown previously in Figure 3-12, and cross-ply laminates shown in Figure 3-36, it can be concluded that for the case of unidirectional laminates, the damage is localized at the interface of the defective layer and the adjacent layers. However, for cross-ply laminates, the damage is no more confined at the interface because of the occurrence of transverse cracks propagating for the delamination at the interface.

The transverse cracks occur when two conditions are satisfied (a) delamination at the interface of 0^o layer due to gap and (b) interface of 0^o/90^o or 0^o/45^o close to the delamination due to the gap which creates high stresses at that location. Consequently, transverse cracks occur to link the two damage areas together.

To sum, it can be concluded that the occurrence of delamination at the interface of the intact (undefective) 0^o layers is critical. This is not only because of the lack of load transfer between the delaminated layers but also because of the transverse cracks that propagate through the thickness of 0^o layers between the delaminations created by the gap and the 0^o/90^o interface, as illustrated in Figure 3-36. As mentioned previously, these transverse cracks have a severe effect on the integrity of the 0^o layers and their ability in carrying the load. So, another approach to avoid the negative effect of these transverse cracks is to prevent the occurrence of delamination due to gap at the interface of 0^o layers which is the source of the transverse cracks as will be shown in the following.

Quasi-isotropic laminates

In the previous paragraphs, it was shown that putting 0^o layers at the location of layer 1 adjacent to the defective layer causes the delamination to occur at the interface of the defective and the adjacent 0^o layers, between layer 0 and layer 1, as shown in all cases of unidirectional, cross-ply (types (1) and (2)) and quasi-isotropic laminates as shown in Figure 3-12, Figure 3-22, Figure 3-32 and Figure 3-36.

In addition, putting 90^o layers at the location of layer 1 adjacent to the defective layer causes the delamination to occur at the interface of the 90^o layer and the next 0^o layer, between layer 1 and layer 2, as shown in cross-ply laminates of type (3), Figure 3-36.

As a result, it was expected that putting $\pm 45^o$ layers at layers 1 and 2 adjacent to the defective layer might help controlling the delamination. Hence, a quasi-isotropic laminate with $\pm 45^o$ layers adjacent to the middle defective layer was tested and the laminate was inspected using microscopic imaging to check the interior damage mechanisms. Figure 3-39 (a) shows the images for quasi-isotropic laminate of type (1) with $\pm 45^o$ layers adjacent to the middle defective 0^o layer in addition to the original quasi-isotropic laminate of type (2), Figure 3-39 (b), that was tested previously in the study with 0^o layers surrounding the middle defective 0^o layer.

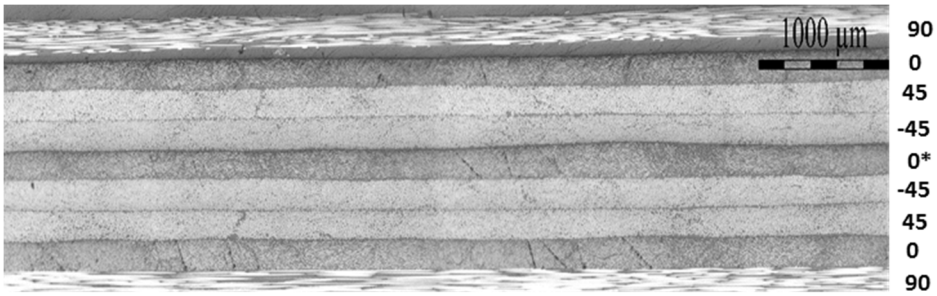

(a) Type 1

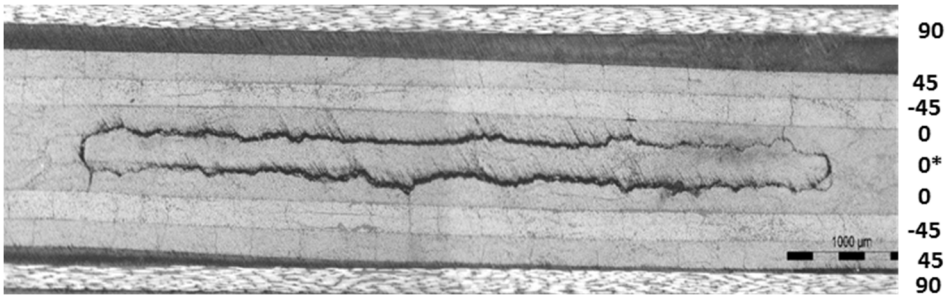

(b) Type 2

Figure 3-39: Microscopic images for (a) proposed and (b) original quasi-isotropic configurations at X=6.5 mm from gap center.

It can be observed that although both types of quasi-isotropic laminates consist of the same number of 0^o, 90^o and $\pm45^o$ layers but it is clear that no delamination occurred at the interface of the intact 0^o layers, layer 3, in the case of type (1) in which $\pm45^o$ layers were put adjacent to the middle defective layer as shown in Figure 3-39 (a). Although some small delaminations were observed in few specimens at the interface of 45^o and -45^o layers, but these delaminations do not have a severe effect because:

(1) They did not occur at the interface of the intact 0^o layers and hence they did not affect the integrity of those main load-carrying layers.
(2) The severe effect of the delamination at the interface of a 0^o layer comes from the transverse cracks that propagate from that delamination through the thickness of the layer. However, the occurrence of the delamination at the interface of 90^o or $\pm45^o$ layers does not have a severe effect because these layers already contain transverse matrix cracks because of their orientation with respect to loading direction.

However, in the case of quasi-isotropic laminates of type (2), a severe delamination occurred at the interface of the defective layer and the intact adjacent 0^o layer, layer 1, as shown in Figure 3-39 (b).

The explanation of this observed behavior is that the main reason of the delamination occurrence is the transferring of load from the defective layer to the adjacent layers. The transfer

of high amount of load generates high interlaminar stresses that initiate delamination at the interface.

In the case of quasi-isotropic laminate of type (2) shown in Figure 3-39 (b), as a result of tow cut in the middle 0^o layer, high amount of load was transferred to the adjacent 0^o tows which has a high strength in loading direction. As a result of transferring this high load, high interlaminar stress was generated at the interface causing delamination occurrence.

However, for the case of quasi-isotropic laminate of type (1) shown in Figure 3-39 (a), the $\pm 45^o$ layers have some strength in loading direction. When they were put adjacent to the defective 0^o layer, they can carry some of the transferred load relative to their stiffness and passed the remaining part of load to the following intact 0^o layers. The interlaminar stresses generated in this case at the interface of this intact 0^o layer, layer 3, were not enough to generate delamination at interface of this layer. This provides a method that can be used to control the occurrence of the delamination at the interface of the intact 0^o layers.

In addition, both types of quasi-isotropic laminates were subjected to quasi-static tensile test to determine the static strength. The average tensile strength of three tested specimens of type 1 and three of type 2 was 940 MPa and 880 MPa, respectively. This indicates an increase in the tensile strength of 8% of quasi-isotropic laminate of type 1 compared to that of type 2.

It can be concluded that adding $\pm 45^o$ layers in contact with the defective 0^o layers helps in gradual transition of load from the defective to the adjacent layers as a result of the contribution of the $\pm 45^o$ layers in carrying the load from the defective layer. This reduces the generated interlaminar stresses and controls the occurrence of the delamination especially at the interface of 0^o layers which eventually improved the performance of the laminate.

The conclusions of the aforementioned discussion can be summarized as follows:

1- The static strength of the laminate depends on the number of the intact 0^o layers.
2- Existence of 90^o layers at one layer away of the defective layers blocks the propagation of the transvers cracks and helps protecting the outer 0^o layers which alleviate the effect of the transverse cracks.

3- For quasi-isotropic laminates, the existence of ±45° layers adjacent to the defective layers helps in gradual transition of load from the defective 0° layers to the adjacent layers and prevents the occurrence of delamination at the interface of 0° layers. This will keep the 0° layers intact which improves the performance of the laminate.

3.3.2 **Effect of gap shape**

In this section, the results of the fatigue tests of unidirectional laminates with triangular gaps will be presented and compared to the results of the previously tested rectangular gaps. The purpose of these tests is to check the validity of assuming the shape of the gap to be rectangular instead of triangular which happens during real manufacturing.

Defective specimens containing triangular gaps with different aspect ratio (a), the ratio between the two sides of the triangular gap, were fatigue tested. Three aspect ratios were selected:

(1) a = 1. The two sides of the triangular gap equal to 6 mm and this case represents the same area of the gap as in the case of the rectangular gap (6 mm x 3 mm).
(2) a = 2. The lengths of the sides are 6 and 12 mm.
(3) a = 3. The lengths of the sides are 6 and 18 mm.

Two stress levels, 1850 and 1800 MPa, were selected and 5 specimens were fatigue tested at each one up to final failure. These two stress levels were selected because they are high stress levels and the effect of the gap is more evident at high stresses compared to lower ones. The columns in Figure 3-40 show the number of cycle to failure for the different gap configurations normalized to the number of cycles to failure of the reference laminates at the same stress level. This normalizing gives an indication on the effect of gap shape on the reduction in life. It can be observed that the scattering in the failure cycles is larger in case of 1800 MPa compared to the case of 1850 MPa. A possible reason for this is that the two sets of samples were cut from two different plates.

By comparing the results of the rectangular gaps and the triangular ones with a =1, both have the same area, it can be observed that the difference in the normalized fatigue life between the two cases is very small, 4% in case of 1850 MPa and less than 1% in case of 1800 MPa. On the other hand the average difference in the normalized fatigue life between the reference and defective specimens is 70% for 1850 MPa and 58% for1800 MPa. This means that the difference in the fatigue life between a specimen containing a rectangular gap and another specimen containing a triangular gap with the same area is very small with respect to the difference between the reference and defective specimen. As a result, it can be concluded that the effect of changing the shape of the gap on the fatigue behavior can be neglected compared to the effect of the gap itself.

Also, by comparing the triangular gaps of different aspect ratios with each other, it can be observed that the difference in fatigue life is very small compared to the difference between the reference and defective ones. For instance, in case of 1850 MPa, the maximum difference in the fatigue life in case of triangular gaps with different aspect ratios was 8% which can be neglected compared to the average 70% reduction in life of defective specimen compared to the reference. So, it can be concluded that the effect of changing the size of the gap can be neglected compared to the effect of the gap itself. A possible explanation for this is that as a result of tow cuts, delamination occurred at the edge of the gap regardless of the shape or the size of the formulated gap. The occurrence of the delamination causes a lack of load transfer between layers which in turn increases the stresses carried by fiber and consequently accelerates the fiber failure process.

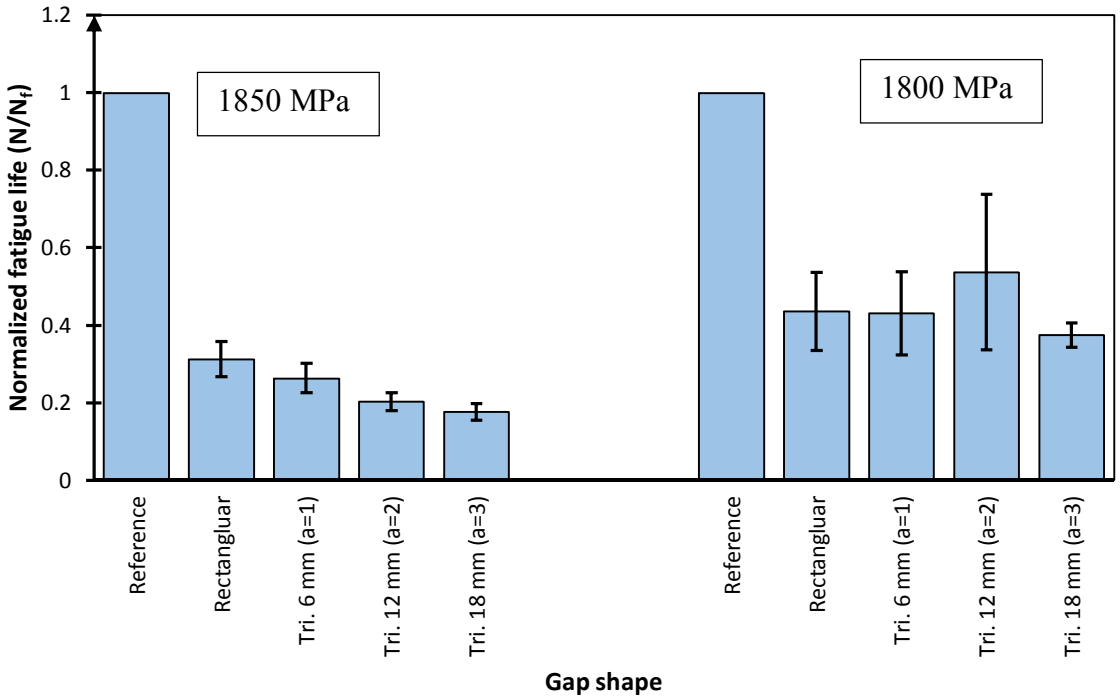

Figure 3-40: Effect of changing the shape of the gap on the fatigue performance

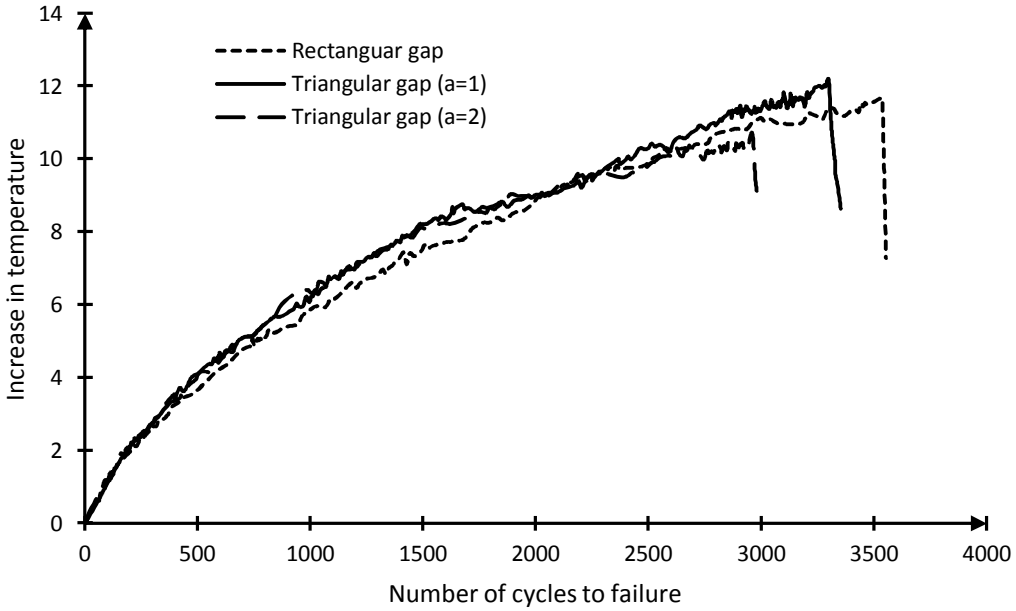

Figure 3-41: Temperature increase for different gap configurations at 1850 MPa

Figure 3-41 shows the surface temperature increase in the middle of the specimen as a result of damage development process for three gap configurations. It can be observed that the thermal plots are almost the same which indicates that the damage behavior is also the same.

In light of the previously discussed results, it can be concluded that the effect of changing the shape or the size of the gap is less important, and can be neglected, compared to the effect of inserting the gap itself. Hence, using the rectangular gaps instead of the triangular ones is valid with the advantage of more simplicity and automation in manufacturing process.

3.3.3 **Effect of gap orientation**

In this section, the effect of creating the gaps in layers other than 0^o layers will be discussed. First, the results of inserting the gaps in 90^o layer for cross-ply laminate will be presented followed by the results of creating the gap in -45^o layer for quasi-isotropic laminate. For each gap orientation, the fatigue results will be compared to the reference specimens to figure out the effect of changing the gap orientation.

Cross-ply laminates (90/0/90*/0/0/0/90/0/90) with a gap in 90^o layer were first subjected to quasi-static tensile test to get the tensile strength. The average tensile strength was found to be 1308 MPa, with a standard deviation of 32 MPa, which was almost the same as the reference laminates without any gaps, 1310 MPa, with a standard deviation of 40 MPa. So, the gaps in 90^o layers have no effect on the tensile static properties of the defective AFP laminates.

Following the static tests, fatigue tests were performed on the cross-ply specimens with gaps in 90^o layers up to final failure. Three stress levels were selected and five specimens were tested at each level. The obtained fatigue data was fitted to linear curve to get the S/N curve. Figure 3-42 shows the mean value and the variation in the fatigue life at the selected three stress levels for both reference and defective specimens. The S/N curves for the defective specimens were plotted for different POF: 0.05, 0.5 and 0.95. It is clear that the gap in 90^o layer does not have an effect also

on the fatigue performance since the scattering intervals of the number of cycles to failure for both reference and defective specimens are overlapping and the S/N curve for the reference specimens falls in between the boundaries of the fatigue lives of defective specimens which are at POF of 0.05 and 0.95.

In cross-ply laminates, most of the load is carried by 0° layers and very small amount is carried by 90° layers as a result of the low stiffness of 90° layers transverse to fiber direction. So, creating a defect in a layer that is not subjected to high stress will not have much effect neither on the tensile strength nor the fatigue behavior.

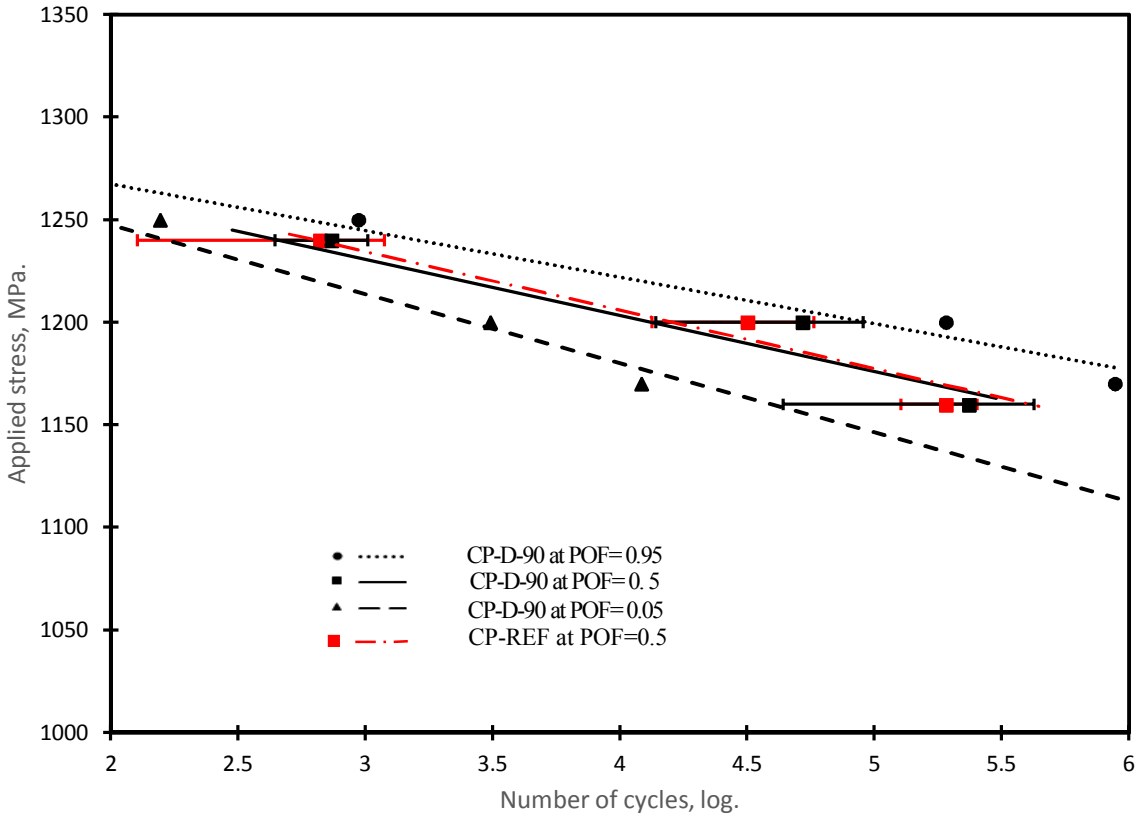

Figure 3-42: Stress/life curves for cross-ply reference and defective laminates with gaps in 90° layer

Some specimens were fatigue tested and the tests were terminated prior to failure to be used for inspecting the occurrence of different damage mechanisms within the laminate. Figure 3-43 shows a microscopic image for a section cut at distance of 7 mm along the width from the gap center. Only some matrix cracks can be observed in the 90^o layers without any delamination occurrence ahead of the gap contrary to the case of gaps in 0^o for different stacking sequences. The reason of delamination occurrence is the out-of-plane stresses that are generated due to stress transfer from the defective layer to the adjacent layers. In this case, since the defective 90^o layer is subjected to low stresses then transferring these low stresses will not generate enough interlaminar stresses to initiate delamination at the interface.

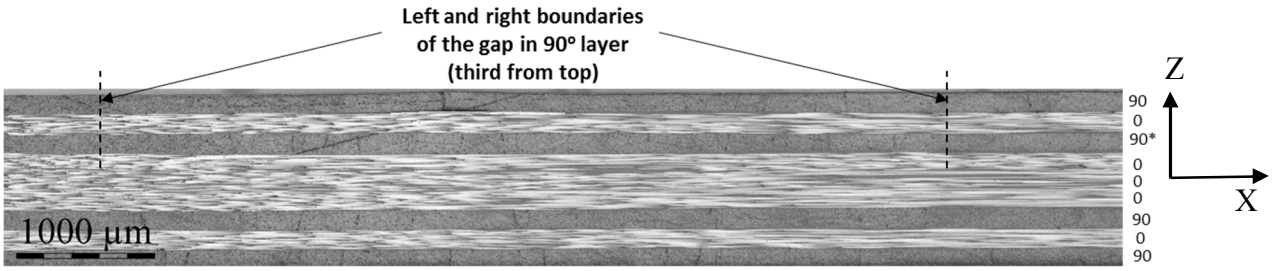

Figure 3-43: Microscopic image at Y=7 mm from the gap center in cross-ply laminate with gap in 90^o layer

Based on the previously discussed result, it can be concluded that the created gaps in 90^o layers do not affect the behavior of the laminate during static or fatigue tests.

Quasi-isotropic laminates (90/45/-45*/0/0/0/-45/45/90) with gap in -45^o layer were initially subjected to tensile tests to get the tensile strength. It was found that the average tensile strength was 960 MPa with a deviation of 20 MPa. The reduction in the tensile strength was 10% compared to the reference laminates. This value is in between the strength of the reference laminates, 1170 MPa with a standard deviation of 24 MPa, and that of the laminate containing a gap in 0^o layers, 880 MPa with a standard deviation of 30 MPa.

Fatigue tests were performed on the laminates at three stress levels and five specimens were tested at each one. Figure 3-44 shows the average number of cycles to failure at each stress level and the variation at 0.95 confidence level. The data was fitted to develop the S/N curve and in addition the S/N curves for the reference (90/45/-45/0/0/0/-45/45/90) and quasi-isotropic laminates with gap in 0° layer (90/45/-45/0/0*/0/-45/45/90) were presented for the purpose of comparison between different gap orientations of quasi-isotropic laminates.

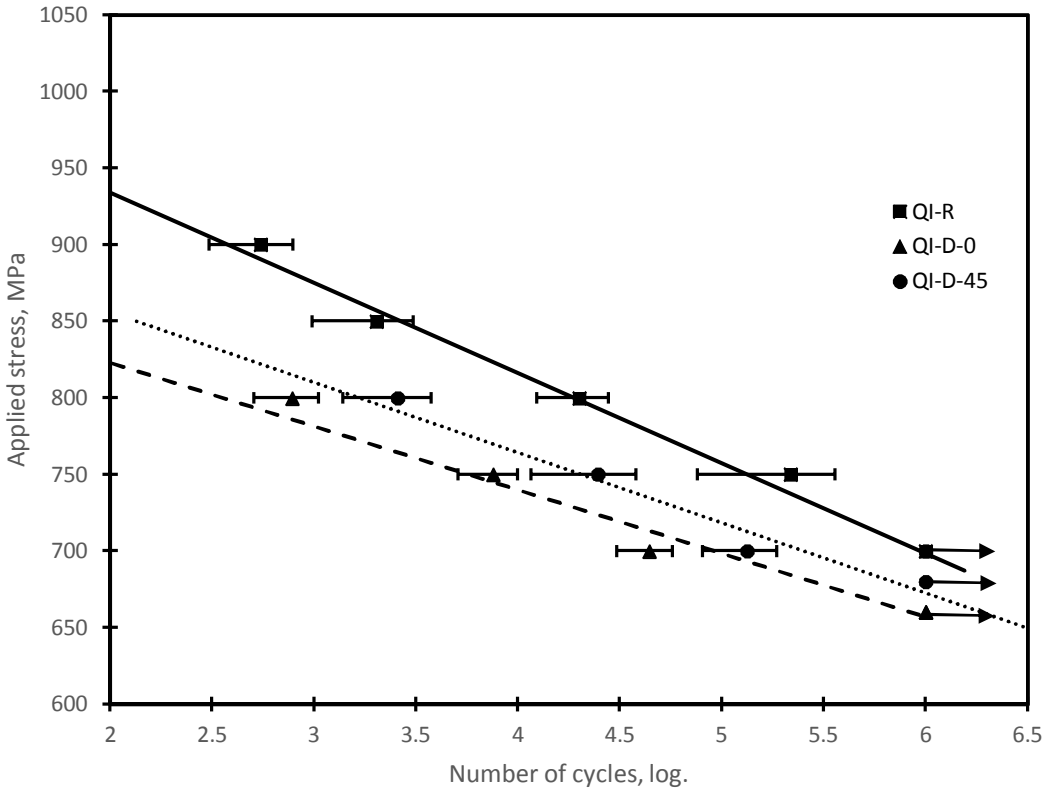

Figure 3-44: Stress/life curves for quasi-isotropic reference and defective laminates.

Similar to the case of static tensile testing, the average fatigue lives of specimens with gap in -45° layer fall in between that of the specimens without gaps and specimens with gaps in 0° layers. In quasi-isotropic laminates, the 45° layers carry less load compared to the load carried by the 0° layers. When a tow is cut in a layer, the load carried by this tow is transferred to the adjacent

intact tows. This load transfer process will cause the stresses in the intact tows to increase which will eventually help in failure initiation. When the layer is inclined to loading direction, it carries less load than if it was oriented in loading direction. Consequently, the effect of redistribution of small amount of stress from an inclined layer such as the case of tow cut in 45^o layer will be less than the effect of redistributing larger amount in case of cutting the tows in 0^o layer.

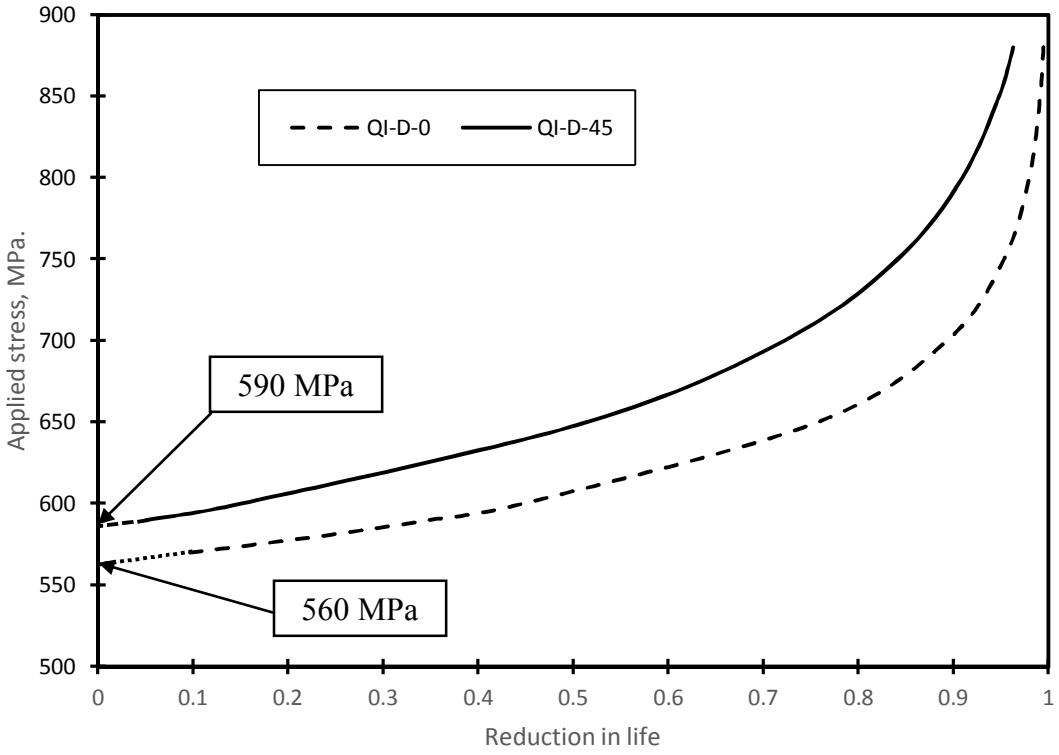

Figure 3-45: Reduction in fatigue life of defective quasi-isotropic specimens with different gap orientation

Figure 3-45 shows the reduction in fatigue life curves for quasi-isotropic laminates with cuts in 0^o layer (90/45/-45/0/0*/0/-45/45/90) and quasi-isotropic with cuts in -45^o layer (90/45/-

45*/0/0/0/-45/45/90). It shows also that at the same applied stress level the reduction in fatigue life is less in case of gaps in -45° layers with respect to gaps in 0° layers. The value of the stress corresponds to the intersection of the two S/N curve of the one with gap in -45 layers, threshold stress, was 590 MPa compared to 560 MPa for laminates with gap in 0° layers.

Figure 3-46 shows a microscopic image for a section cut parallel to fibers in 45° layer. The section was cut at a distance of 10 mm from the gap center along 45° direction. The right and left boundaries of the gap are shown in the figure by dashed lines. It can be observed that no delamination occurred at the interface of the -45° layer, defective layer, and the adjacent 0° layer.

As mentioned previously, delamination occurred as a result of high interlaminar stresses generated due to the transfer of high amount of load from a defective layer and the adjacent one. Since in this case, the tow was cut in an inclined layer, -45° layer, then the amount of load to be transferred to the adjacent 0° layer was not high enough to generate high interlaminar stresses that could initiate delamination at the interface of the defective -45° layer and the 0° layer.

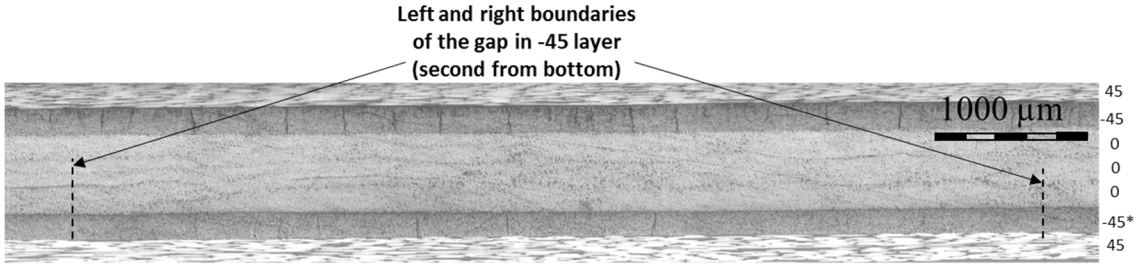

Figure 3-46: Microscopic image of a section cut parallel to 45° layer in quasi-isotropic laminate with gap in -45° layer.

3.3.4 **Effect of number of gaps**

So far, the fatigue behavior of manufactured laminates with one gap was discussed. Hereafter, the results of fatigue testing of unidirectional laminates containing 2 gaps will be presented in order to investigate the effect of increasing the number of gaps in the laminate. The case of unidirectional laminate was selected to avoid any complexity in the damage behavior that could result from the interaction between the damage due to gaps and the interface between

different layers. As mentioned previously, the number of gaps was increased in two directions: in-plane direction and out-of- plane direction.

3.3.4.1 **In-plane adding of gaps**

Two gaps were inserted in the same layer of a unidirectional laminate (0/0/0/0/0**/0/0/0/0) to represent increasing the number of gap in the in-plane direction. The gaps were created with 3 and 10 mm separating distances between centers along the length of the specimens while being in two adjacent tows in the same layer as shown previously in Figure 2-12. The two types of laminates were fatigue tested at 3 stress levels and 5 specimens were tested at each in addition to the run out stress level. Those selected stress level were common between the defective laminates, with one or two gaps, and the reference laminates. Figure 3-47 shows the average fatigue lives and the corresponding scattering intervals at each stress level for a confidence level of 0.95. The data was fitted to linear curves to develop the S/N curves based on least square method. It can be observed that there was a little improvement in the fatigue life for the specimens with 10 mm separating distance between gaps' centers compared to the ones with 3 mm separating distance.

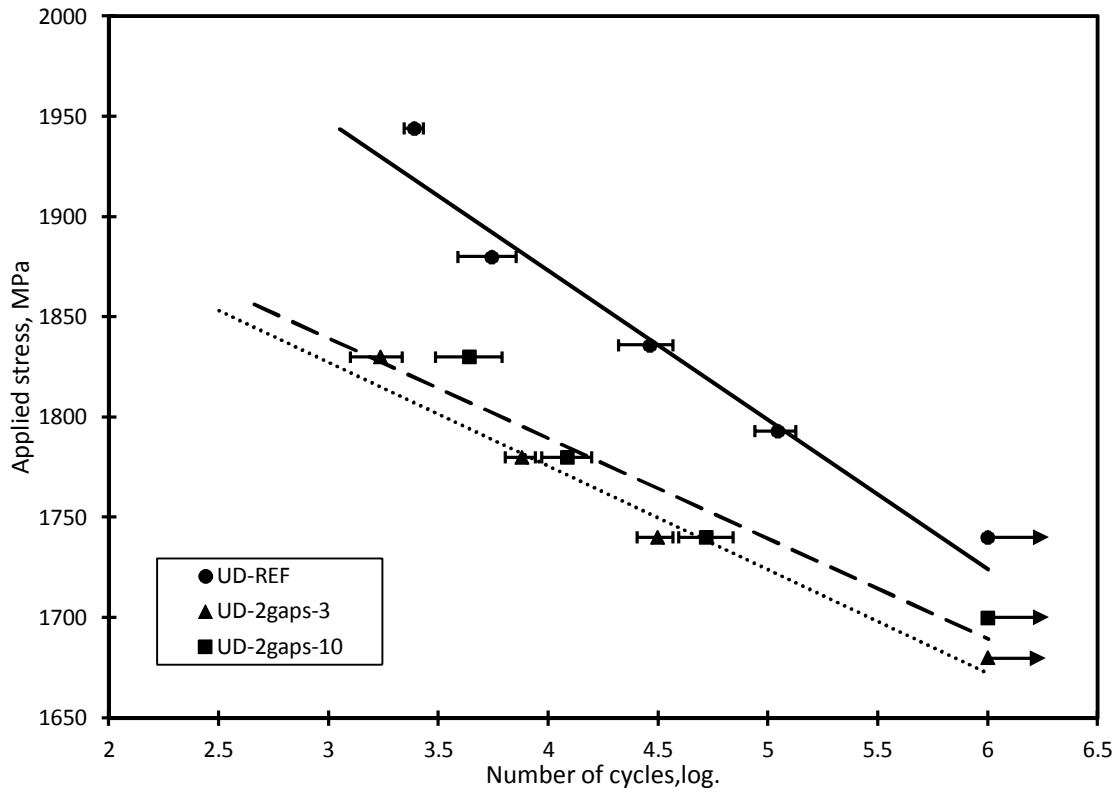

Figure 3-47: Stress/life curves for unidirectional reference and defective laminates with two in-plane gaps at different distances

For a specimen with two gaps separated with any distance, at each gap, delamination initiates at the interface between the defective 0^o layer and the adjacent layers. By increasing the number of cycles, the two occurred delaminations propagate along the specimen length. During damage evolution process, the two delaminations propagate toward each other in the area between the two gaps till reaching the tip of each other and combine together which creates a critical cross section across the specimen's width with large delamination size. The occurrence of this interaction or linking between the two damage areas helps accelerating the final failure process.

Hence, by increasing the distance between the two gaps, the process of linking the two delaminations takes longer time and hence the final failure will be retarded. So, the worst case

scenario will occur when the two gaps are located at the edge of each other with a 3 mm separating distance between centers.

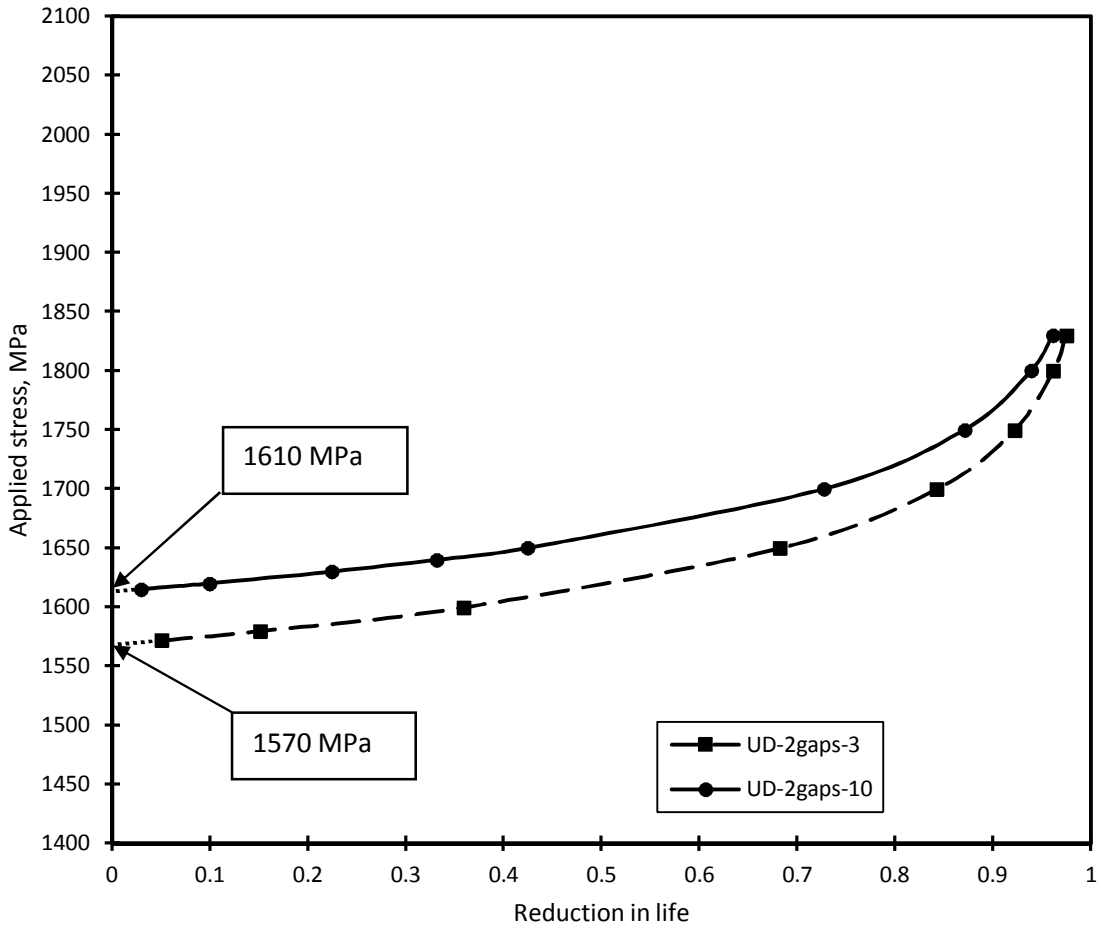

Figure 3-48: Reduction in fatigue life of defective unidirectional laminates with two in-plane gaps at different distances

Figure 3-48 shows the reduction of life curves at different applied stresses for the unidirectional defective laminates with two different separating distances. The stress value at which the fatigue lives of the laminate with 2 gaps at 10 mm distance and the reference are the

same, threshold stress, was 1610 MPa while for the case of laminate with 3 mm distance between 2 gaps' centers was 1570 MPa.

In order to figure out the effect of the additional gap at 3 mm distance from center of the first gap, worst case, on reducing the threshold stress and compare it to the case of only one gap in the laminates, Figure 3-49 was presented. The vertical axis is the ratio between the threshold stress and the static strength of the reference laminate and the horizontal axis is the different laminate types. Since the reference laminate is free from gaps then the ratio equals to 1.

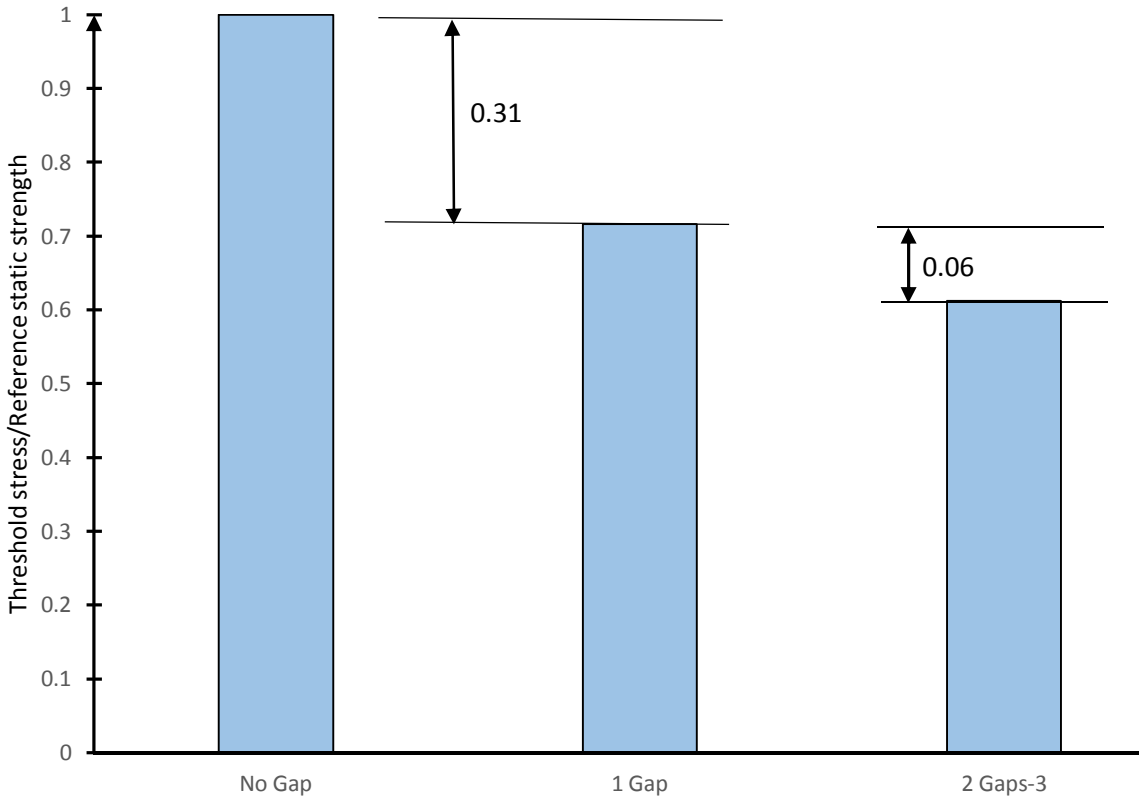

Figure 3-49: Additional effect of one more gap in unidirectional laminate on threshold stress

It can be observed that creating the first gap in the laminate causes a reduction in the threshold stress value by 31%. However, adding one more gap in the laminate causes an additional

reduction of only 6 %. This means that for a unidirectional laminate, adding more gaps has a small effect on the threshold stress compared to the initial severe effect of creating the first gap.

3.3.4.2 **Out-of-plane adding of gaps**

Two gaps were created in two adjacent layers in a unidirectional laminate (0/0/0/0*/0*/0/0/0/0) to represent increasing the number of gaps in out-of-plane direction. The laminates were manufactured using half tow staggering and full tow staggering techniques in order to investigate the effect of out-of-plane gaps while considering the effect of staggering as shown previously in Figure 2-13. The two types of laminates were fatigue tested at 3 stress levels and 5 specimens were tested at each in addition to the run out stress level. Figure 3-50 shows the average obtained fatigue lives and the scattering intervals with a confidence level of 0.95. The data was fitted to linear curves to develop the S/N curves based on least square method.

An improvement in the fatigue life of the laminates containing 2 out-of-plane gaps was observed by increasing the staggering distance since the number of cycles to failure of the specimens manufactured by full tow staggering technique was higher than that manufactured by half tow staggering technique at the same applied stress level. A possible explanation for this is that in case of half tow staggering, there is an overlap between the gaps in the two adjacent layers which creates a critical weak spot at the overlap region compared to the case of no gaps overlapping. The stress redistribution process from these weak spots to the intact adjacent tows results in an increase in the stresses in the intact tows to values higher than the case of full tow staggering in which no overlapping of gaps occurs.

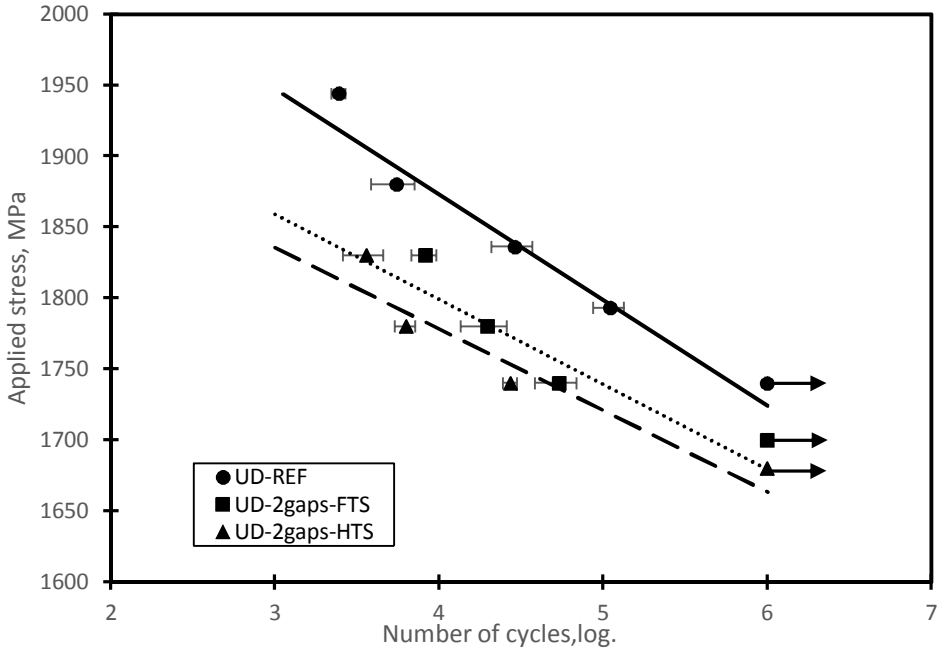

Figure 3-50: Stress/life curves for unidirectional reference and defective laminates with two out-of-plane gaps at different distances

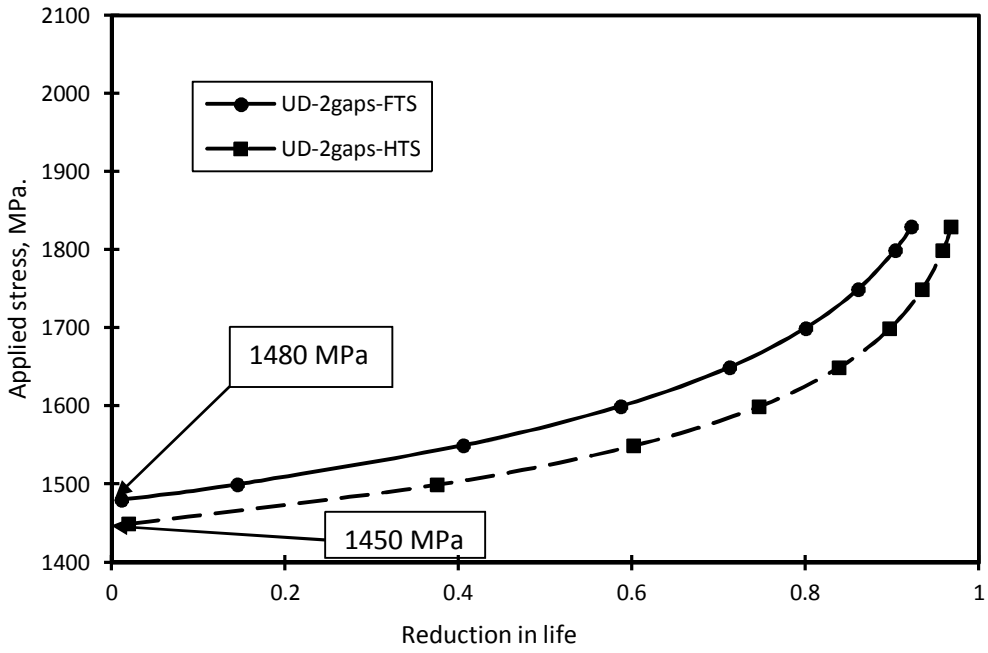

Figure 3-51 Reduction in fatigue life of defective unidirectional laminates with two out-of-plane gaps with HTS and FTS techniques

From the reduction in fatigue life curves in Figure 3-51, the threshold stress for laminates with full tow staggering technique was 1480 MPa while for the laminates with half tow staggering was 1450 MPa. By comparing the threshold stress value for the laminate with one gap to that of two out-of-plane gaps with half tow staggering, worst case, it can be concluded that the additional reduction in the threshold stress due to the second out-of-plane gap was 10% which is small compared to the initial reduction of one gap, 31%.

Based upon the results in the last two subsections, it can be concluded that the additional effect on the threshold stress values of adding more gaps is small compared to the severe effect of creating the first gap regardless the location, the same layer or different layers, or the configuration, half or full tow staggering, of the created gaps as shown in Figure 3-52. In this figure, for the case of reference laminate, since there are no gaps created in the laminate, then the threshold value was considered as the static strength value.

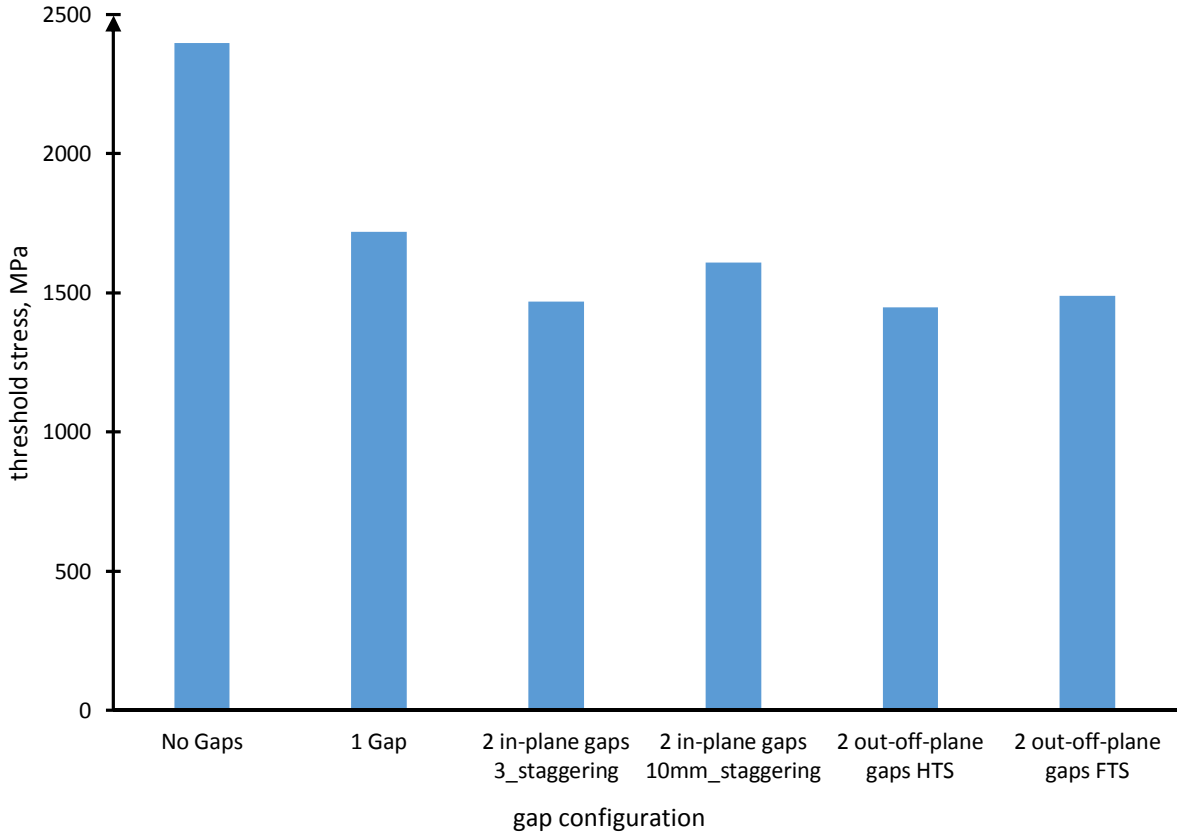

Figure 3-52: Threshold stress values for different tested unidirectional laminates

3.4 **Summary**

In light of the performed experiments in the current study it can be concluded that the existence of the induced gaps during AFP manufacturing affects the fatigue performance of the laminates. The effect of the gaps is more severe at high stresses and it decreases by decreasing the applied stress till reaching a threshold stress which can be defined as the stress value at which the fatigue life of both reference specimens, free from gaps, and the defective specimens are the same.

Existence of 90^o layers in cross-ply laminates causes the occurrence of transverse cracks that propagate through 0^o layers from the delamination due to the gap to the interface of the $0^o/90^o$ layers. This severely affects the integrity of the main load carrying 0^o layers. It was found from the performed experiments on different cross-ply laminates that the existence of 90^o layer at one layer away from the gap location helps in blocking the transverse propagation of these cracks and protecting the outer 0^o layers in the laminate which alleviates the effect of these cracks in the cross-ply laminates.

The existence of $\pm 45^o$ layers in contact with the defective 0^o layers helps in gradual transition of load from the defective to the adjacent layers which reduces the generated interlaminar stresses and controls the occurrence of the delamination especially at the interface of 0^o layers.

The existence of gaps in 0^o layers has the most severe effect compared to its presence in 90^o or 45^o layers. Also, the effect of changing the shape and the size of the gap was found to be small compared to the effect of inducing the gap in the laminate.

The additional reduction in the threshold stress due to adding more gaps in the same layer or in different layers was small compared to the initial severe reduction due to creating the first gap in the laminate

IR thermography was found to be a highly qualified method for detecting the non-uniformity in the laminates such as the existence of gaps generated during AFP manufacturing. Using the heat generation from the damage process inside the material, IR thermography provides a means for in-situ detection of damage occurrence for AFP laminates containing gaps and subjected to fatigue loading.

Using microscopic inspection of specimens with different stacking sequences revealed that the main damage mechanism due to gap was delamination at the interface of the defective layer and the adjacent layers as a result of the load transfer from the cut tow to the adjacent tows. This generates interlaminar stresses that might initiate delamination at the interface.

Finally, the threshold stress values determined for the different stacking sequences is very crucial for any designer. This value represents a limiting value since the maximum applied stress during fatigue loading should not exceed this value to avoid any effect of gaps on the fatigue life of the laminate. In order to determine these values for the laminates, large amount of specimens were tested for very long time. This process is very time and material consuming. This arises a question: is there any other method that can be used to determine the threshold values with saving in time and material? This will be answered in the next chapter.

Chapter 4

Fatigue threshold-stress evaluation using IR thermography

It was found from the previous chapter that there exists a threshold stress value below which the effect of gaps diminishes. The traditional method to evaluate this value is by conducting extensive fatigue tests which are very material and time consuming. The aim of this chapter is to use infrared thermography and apply Risitano method [83] on AFP laminates containing gaps to provide a quick method for obtaining the threshold value. This method has a great potential in saving time and material required for performing traditional fatigue tests to develop stress/life curves and obtain threshold stresses. To investigate the applicability of this technique to different stacking sequences, tests were conducted on unidirectional, quasi-isotropic and cross-ply defective

laminates. The results of threshold stress evaluation using IR thermography were also compared to the results obtained using the traditional way.

4.1 Overview

Some metals exhibit an endurance (fatigue) limit. It is useful for the designer to determine the stress value below which the structure is expected to have infinite life. The traditional way to determine this threshold is by conducting extensive fatigue tests using a large number of specimens. This method requires extensive testing time.

Risitano [83, 84] proposed a method that can be used to determine the threshold stress, or fatigue limit, of metal using thermographic methodology. The basis of this method depends on the increase in the surface temperature of the material when subjected to fatigue stress higher than the threshold value. During the fatigue loading, when the number of cycles is increased, the temperature first increases till it reaches a stabilization temperature. This stabilization temperature depends on the applied load and it corresponds to the damage saturation in the laminate. It is higher for higher applied stress level. Then, the temperature remains constant till before final failure where there is another temperature increase. So, by running fatigue tests at different increasing stress levels and getting the temperature gradient till the stabilization temperature, a relation between temperature change and stresses values would be obtained from which the threshold value can be determined. The main advantage of this technique is to overcome the drawbacks of the traditional method in terms of long fatigue testing time and large number of specimens.

In another method [85], the dissipation of energy from material when subjected to fatigue damage is used. According to Luong, the threshold stress of metals can be determined by measuring the energy dissipation from the material during cyclic loading. There is a bilinear curve representing the change in the dissipated energy with the stress levels. The intersection of the two linear portions gives the threshold stress.

The aforementioned thermographic methods were initially developed for conventional materials and later used with different composite materials. Colombo et al. [86] characterized the

mechanical behavior of basalt fiber reinforced composites under static and fatigue loading conditions. In addition, they used infrared thermography integrated with the two aforementioned methods to determine the fatigue limit of the used composite material. Also, Montesano et al. [64] used thermography with another composite material system, triaxially braided carbon/epoxy laminates, to obtain the fatigue limit of the material corresponding to 10^7 cycles, as shown in Figure 4-1, and validated the results with that obtained from the extended fatigue tests. Kordatos et al. [87] used the dissipation energy method with lock-in thermography to get the fatigue limit of both conventional, Aluminum grade 1050, and composite, ceramic matrix composite, materials.

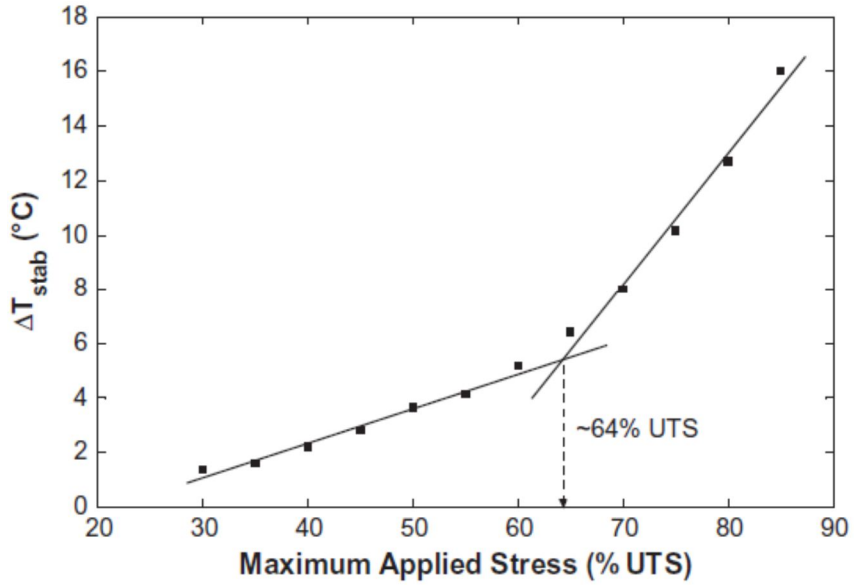

Figure 4-1: Relation between temperature change and applied stress for carbon/epoxy laminates [64]

The obtained fatigue limits from the thermographic approaches were validated by performing long fatigue tests to develop the S/N curves for the tested materials and the fatigue limit was defined as the value of stress at which the specimen did not fail up to a predefined number of cycles (run-out cycles) which ranges between 10^6 and 10^7 cycles. Table 4-1 shows some studies that used IR thermography to get the fatigue limit for different materials and the number of cycles corresponding to the fatigue limit in the performed long fatigue tests.

Table 4-1: Using of IR thermography for rapid determination of fatigue limit of several materials

Authors	Used Material	number of cycles corresponds to fatigue limit from experiments
Risitano [83, 84]	Steel	10^7
Luong [85]	Steel	10^7
Cura [88]	Steel	$2x10^6$
Crupi [89]	Welded steel joint	$5x10^6$
Colombo [90]	Glass/epoxy	$5x10^6$
Colombo [86]	Basalt fiber reinforced composites	$5x10^6$
Guagliano et al. [91]	Glass/epoxy	$5x10^6$
Li [92]	Aluminum	$2x10^6$
Kordatos et al. [87]	Aluminum 1050 SiC/BMAS glass–ceramic matrix composites.	10^6 cycles
Montesano et al.[64]	Braided carbon/polyimide resin	10^7 cycles
Colombo et al. [60]	Glass/epoxy	10^7 cycles

One of the major concerns for the designer focusing on fatigue performance of AFP laminates is obtaining this threshold value, stress below which the effect of defects on fatigue life diminishes. As shown in the experimental results in chapter 3, the traditional way to obtain the threshold value is by using Wohler method in which the S/N curves are developed by conducting long fatigue tests at several stress levels. It was found that the S/N curves for the reference and gapped specimens intersect with each other at this threshold point. The main drawback of this method is that it is highly time and material consuming.

Motivated by the desire to overcome the drawbacks of the traditional method, a thermographic approach similar to [64, 83, 84, 86] will be used during fatigue loading of unidirectional, quasi-isotropic and cross-ply gapped laminates to provide a method for quick determination of the value of the threshold stress. This is a novel application of Risitano method

for the case of AFP laminates containing gaps that commonly occur during AFP manufacturing process. This has a very high potential for saving time and material.

4.2 **Material and IR thermography equipment**

The same material was used, CYCOM 977-2-35-12K HTS-145) [72], to manufacture laminates with different stacking sequences: unidirectional, cross-ply and quasi-isotropic. The manufactured specimens contained one gap at the middle 0^o layer. Table 4-2 shows the details of the manufactured specimens. Figure 4-2 shows the location of the gap in the fifth layer and across the thickness (for quasi-isotropic specimen as an example).

Table 4-2 Different types of manufactured laminates

(0/0/0/0/0*/0/0/0/0)	Unidirectional Defective with one gap	UD-D
(90/0/90/0/0*/0/90/0/90)	Cross-ply Defective with one gap	CP-D
(90/45/-45/0/0*/0/-45/45/90)	Quasi-isotropic Defective with one gap	QI-D
* refers to the layer containing the gap		

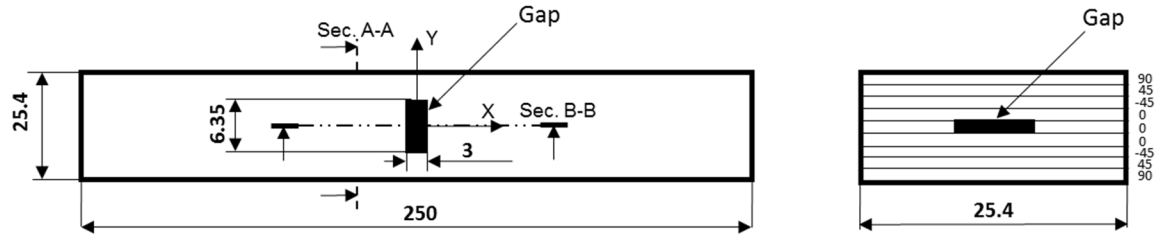

(a) (b)

Figure 4-2: Schematic representation of (a) fifth layer (b) specimen cross section (dimensions in mm)

4.3 **Methodology and results**

In the previous chapter, long-time fatigue tests were conducted on different laminates to determine the threshold stress using the conventional method. It was found that the threshold stress values obtained from the reduction in life curves shown in Figure 3-9, Figure 3-19 and Figure 3-29 are 1725, 983 and 565 MPa for unidirectional, cross-ply and quasi-isotropic laminate with gaps in 0^o layers, respectively. In the current chapter, short-time fatigue tests were devoted for determining the threshold stress using IR thermography.

In the method used in [64, 83, 84, 86], the specimens were tested till reaching a constant temperature (stabilization temperature) which depends on the applied stress. For the defective specimens containing gaps in the current study, it was noticed that at some stresses the temperature did not have this plateau and kept increasing as a result of the continuous heat generation from the rubbing of the delaminated surfaces as shown previously in Figure 3-16 for defective unidirectional laminates. It was required to test all the specimens up to the same number of cycles to avoid extensive testing time. For specimens subjected to the highest fatigue stress level, the number of cycles to failure was around 1000 cycles.

Hence, in the present study, the defective specimens with different stacking sequences were fatigue tested at different stress levels (high and low) to the first 1000 cycles and IR thermography was used to obtain the surface temperature change during this period. During the tests, the IR camera (FLIR T450 SC) was set to focus on the area at the middle of the specimen to avoid any heat disturbance from the machine grips. The camera was connected to a computer supported with a Research IR software for extracting and analyzing the thermal data.

Unidirectional defective specimens were fatigue tested at maximum stress ranges between 1940 MPa (83% of ultimate static strength (UTS) of defective laminates) and 1300 MPa (56% of UTS) to investigate the effect of changing the applied stress on the thermal behavior. The maximum applied stress in the case of quasi-isotropic laminates ranges between 800 MPa (90% of UTS) to 200 MPa (20% of UTS) while for cross-ply laminates it ranges between 1120 MPa (97% of UTS) to 500 MPa (43% of UTS).

Figure 4-3 shows the increase in the surface temperature at the middle of the specimens with number of cycles up to 1000 cycles at different applied stresses and using a frequency of 5 Hz. It can be observed that the thermal behavior has the same trend for all different stacking sequences. During the first period of the fatigue life the trend of the temperature increase is almost linear. By increasing the applied stress, the rate of temperature change increases and at any specific number of cycles the temperature increase is higher for higher applied stresses compared to the lower ones.

It can be assumed that the main source of temperature increase is the damage process and the effect of viscoelasticity is small due to the small size of the gap as mentioned previously. Then, a possible explanation for the observed thermal trends is that higher stresses means higher damage propagation rate. At the same number of cycles, the damage size is probably larger for higher stresses. In addition, the heat generated from rubbing of the damage surfaces is higher. So, at any time, the temperature increase is higher for higher stresses. Another interesting observation was that the maximum temperature increase was higher for the case of cross-ply laminates (23°C) followed by quasi-isotropic (17°C) and unidirectional laminates (11°C). This will be discussed later.

The thermal trends shown in Figure 4-3 were fitted to regression lines using least square method. Then the slopes of these lines were determined. High R-squared values for the fitted regression lines were observed indicating that the obtained data is close to the linear trend. The obtained average slopes and the R-squared values at each stress are shown in Table 4-3.

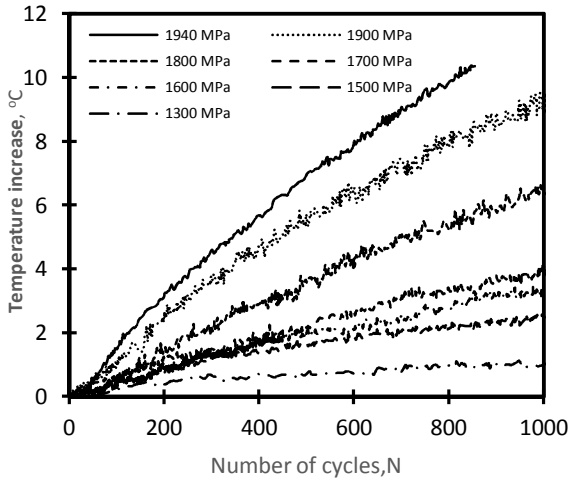

(a)

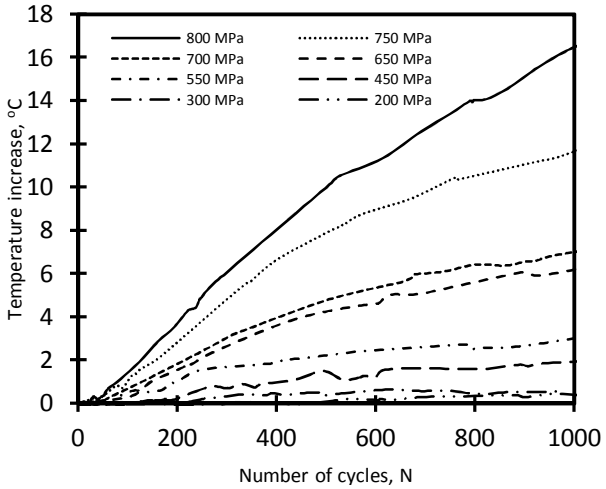

(b)

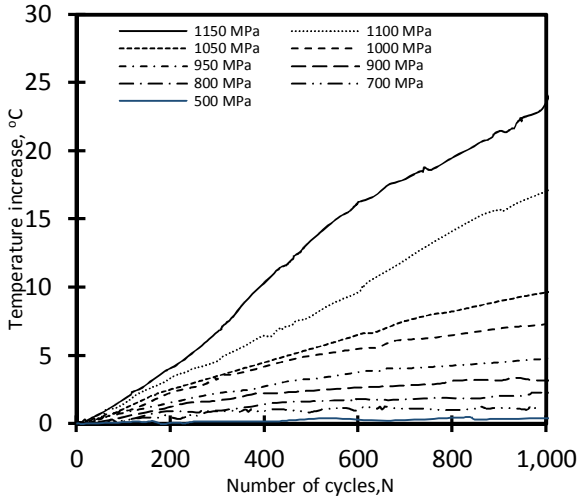

(c)

Figure 4-3: Temperature increase at different stresses for defective (a) unidirectional, (b) quasi-isotropic and (c) cross-ply laminates

Table 4-3 Slopes of temperature increase at different stress and R^2 values from fitted regression lines

Unidirectional			Quasi-isotropic			Cross-ply		
Stress (MPa)	Slope	R-squared	Stress (MPa)	Slope	R-squared	Stress (MPa)	Slope	R-squared
1940	0.00801	0.9908	800	0.01887	0.9919	1150	0.02455	0.9895
1900	0.00642	0.9844	750	0.01372	0.9643	1100	0.01681	0.9972
1800	0.00362	0.9887	700	0.00997	0.9641	1050	0.01232	0.9901
1700	0.00227	0.9809	650	0.00787	0.9677	1000	0.00962	0.9601
1600	0.00211	0.9755	550	0.00421	0.9061	950	0.00642	0.9393
1500	0.00167	0.9841	450	0.00227	0.9287	900	0.00477	0.8967
1300	0.00121	0.8506	300	0.00085	0.8851	800	0.00312	0.9164
			200	0.00028	0.8466	700	0.00192	0.8515

By plotting the slopes of the fitted regression lines against the maximum applied stress for each fatigue test, Figure 4-4 was obtained. The obtained slopes can be fitted to two linear curves. The intersection of these two lines corresponds to a threshold stress value. Above this threshold point, there is a significant increase in the slope of the temperature change curves compared to the slopes for stresses below that point.

The observed threshold values obtained from the bilinear curves are illustrated in Figure 4-4 for unidirectional, quasi-isotropic and cross-ply laminates.

Table 4-4 shows a comparison between the threshold stresses obtained from long fatigue tests, Wohler method, and IR thermography techniques. In addition, it shows a comparison between the required time for testing using the traditional and IR methods. Thanks to IR thermography, the threshold stresses can be obtained with very good agreement with the experimental results and with a high potential of saving material and time.

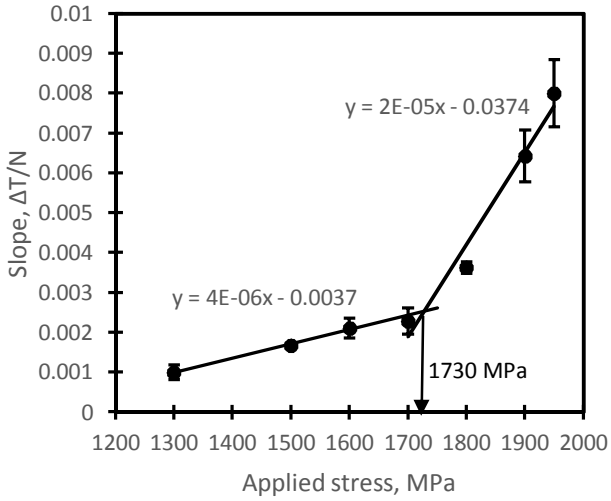

(a)

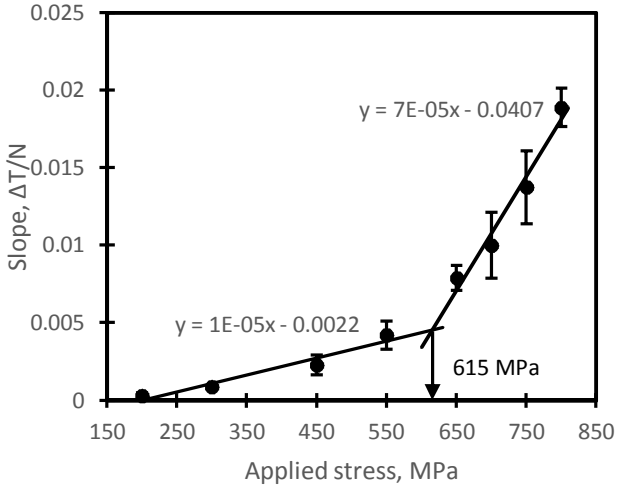

(b)

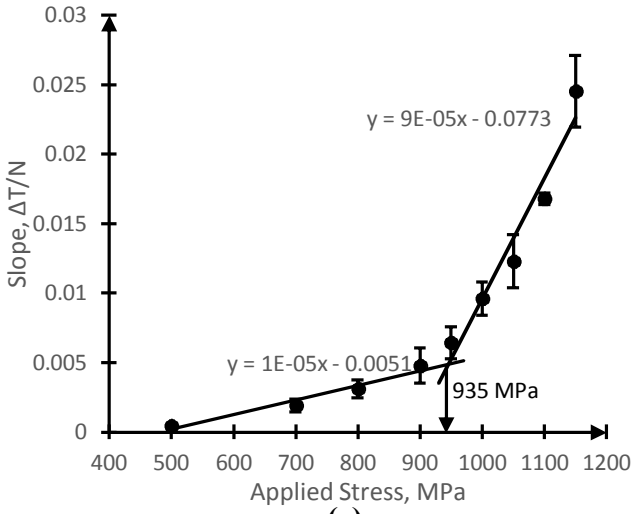

(c)

Figure 4-4: Bilinear relation between the slope of temperature increase and the applied stress for (a) unidirectional (b) quasi-isotropic and (c) cross-ply defective laminates.

Table 4-4: Threshold stress values obtained from experiments and IR thermography

Laminate configuration	Wohler (MPa)	IR (MPa)	Error (%)	Testing time (Wohler) (hrs)	Testing time (IR)(hrs)
Unidirectional	1725	1730	0.3	219.7	0.39
Quasi-isotropic	565	615	8.8	334.4	0.44
Cross-ply	983	935	-4.89	189.2	0.5

4.4 **Discussion and analysis**

Prior to discussing the possible explanations for the observed phenomena, it was required to investigate the damage mechanisms and the thermal response of different stacking sequences during fatigue loading that will help better understanding of the thermal behavior.

4.4.1 **Damage mechanisms**

The damage process in composite is very complicated because of the variety of mechanisms that can occur during loading. The existing damage mechanisms differ from one stacking sequence to the other. Some specimens of different stacking sequences were fatigue tested and the tests were interrupted after 100 000 cycles then the specimens were cut and inspected using scanning electron microscopy (SEM) to detect the interior damage mechanisms.

Figure 4-5, Figure 4-6 and Figure 4-7 show microscopic images for sections cut at different distances from gap center for unidirectional, cross-ply and quasi-isotropic laminates, respectively. Figure 4-8 shows a schematic representations of sections A-A and B-B (refer to Figure 4-2) that illustrate all the damage mechanisms for the investigated stacking sequences. For each laminate configuration there are different damage mechanisms that can be identified.

For the case of unidirectional laminates, it can be observed that the only damage mechanism is (Type A) in Figure 4-8 (a) which is the delamination due to gap that occurred at the interface of the defective 0^o layer and the adjacent 0^o layers. It initiates at the gaps boundaries and propagate along the length of the specimen without any propagation along width direction.

For the case of cross-ply laminate, as shown in Figure 4-8 (b), it can be observed that the damage mechanisms are:

(1) **Type A**: Delamination at the gap location between the defective 0^o layer and the adjacent 0^o layers similar to the unidirectional case.
(2) **Types B**: Delamination at interfaces of layers with different orientations (0^o/90^o). It can be divided into two types: (a) Type B' which is the delamination at 0^o/90^o interfaces that can propagate across the width till reaching the edge of the laminate and (b) Type B" which is the internal delamination that could not reach the edge.
(3) **Type C**: transverse cracks that propagate through 0^o layers from the delamination at the gap to the closest interface of 0^o/90^o layers.

(4) **Types D**: Matrix cracks in 90^o layers. It can also be divided into two types according to their location: (a) Type D' which are the matrix cracks in the outer 90^o layers and (b) Type D" which are the matrix cracks in the inner 90^o layers.

For quasi-isotropic laminates, as shown in Figure 4-8 (c), the observed damage mechanisms are:

(1) Type A: Delamination at the gap location between the defective 0^o layer and the adjacent 0^o layers as that observed for unidirectional and cross-ply laminates.

(2) **Types B:** Delamination at interfaces of layers with different orientations (90^o/45^o, 45^o /-45^o and -45^o /0^o). It can be divided into B' and B" types as shown in the case of cross-ply laminates.

(3) **Type C:** transverse cracks that propagate through 0^o layers from the delamination at the gap to the closest interface of 0^o /-45^o layers.

(4) **Types D:** Matrix cracks in 90^o, 45^o and -45^o layers. In this case, we have only outer 90^o layers. So, the 90^o cracks are of Type D'. However, the other matrix cracks in the 45^o and -45^o layers are inner cracks of Type D".

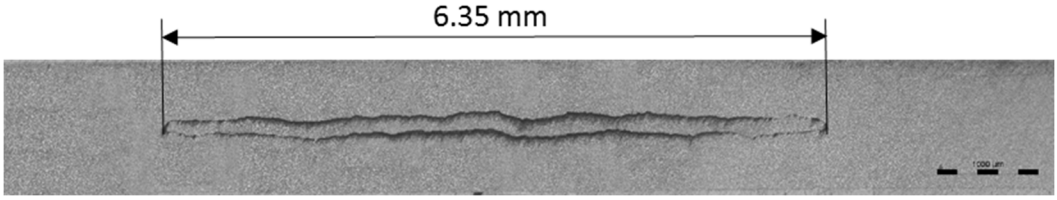

Figure 4-5: Damage detected after 10^5 cycles within unidirectional laminates (at X=10mm, -5mm<Y<5mm).

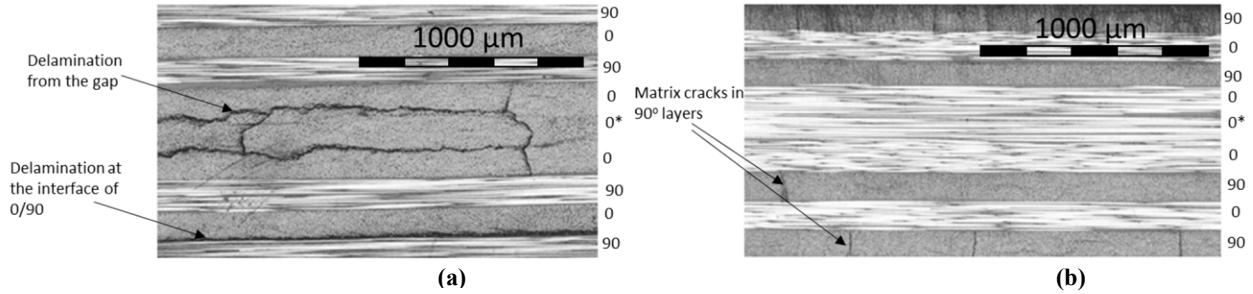

Figure 4-6: Damage detected after 10^5 cycles within cross-ply laminates across (a) width (at X=10mm, 1.5mm<Y<3.5mm) and (b) length (at Y=10mm, -1.1mm<X<1.1mm).

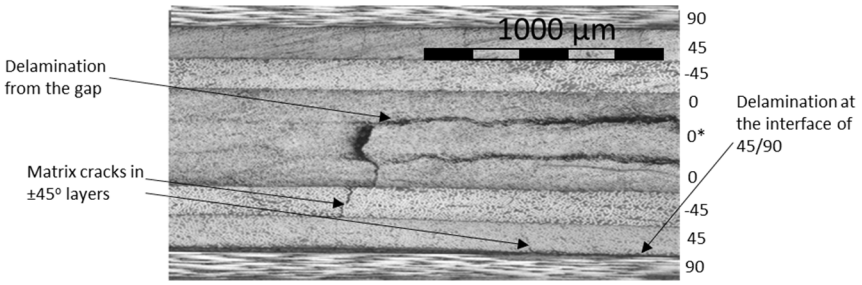

Figure 4-7: Damage detected after 10^5 cycles within quasi-isotropic laminates (at X=10mm, 1.8mm<Y<4mm).

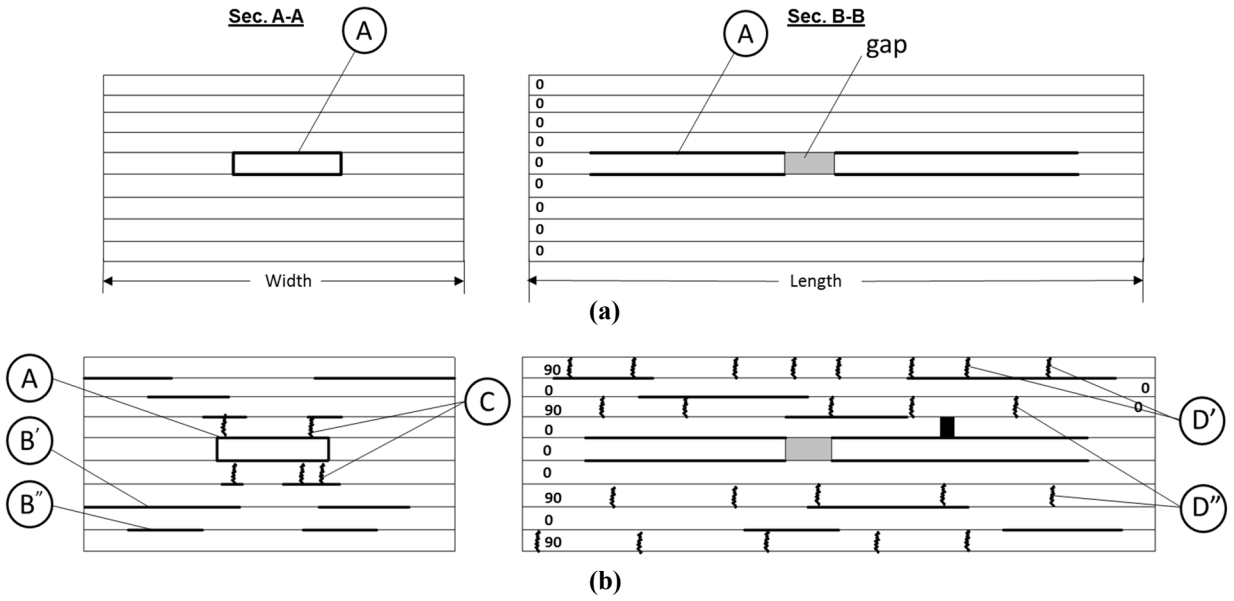

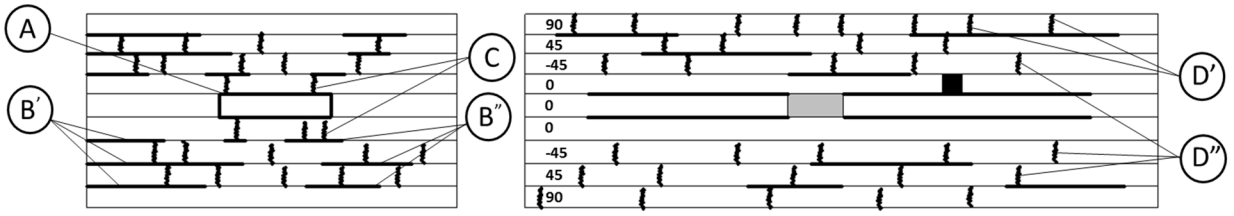

(c)

Figure 4-8 Schematic representation of different damage mechanisms for (a) unidirectional, (b) cross-ply and (c) quasi-isotropic laminates.

Some of the aforementioned damage mechanisms can generate heat and others can dissipate heat. Also, some of them might contribute to both heat generation and dissipation. In the following subsection, a detailed analysis about the contribution of each mechanism to heat generation/dissipation will be illustrated.

4.4.2 **Heat generation/dissipation**

The existence of damage mechanisms in the laminates can help in generation of heat during fatigue loading. One of the major sources of heat generation is the rubbing between the surfaces created by the damage initiation and propagation process. For instance, if we consider the occurrence of delamination of size DL at the interface between two 0^o layers (such as the case of Type A) during fatigue loading which generates a shear stress τ_{xz} at the interface and the relative velocity between the surfaces during rubbing is u_x, then the amount of heat generated due to the rubbing of those created surfaces during time t will be:

$$Q_{gen.} = \tau_{xz} \, . DL \, . u_x \, . t \qquad (4.1)$$

On the other hand, direct exposure of material volume to the environment due to some of the damage mechanisms could help in heat dissipation from the specimen to the surrounding. Each of the previous mechanisms can help in generation and/or dissipation of heat as follow:

(1) Type (A): this internal delamination due to gap can contribute only to heat generation as a result of continuous rubbing of the surfaces created at the delamination locations during loading/unloading portions of each fatigue cycles.

(2) Type (B'): this delamination contributes not only to heat generation but also to dissipation of heat as it can reach the edge of the laminate and hence can dissipate heat to the environment.

(3) Type (B"): this delamination is an internal delamination and can contribute to heat generation.

(4) Type (C): these are internal transverse cracks in the 0^o layers and can contribute to heat generation.

(5) Type (D'): these external cracks can efficiently help in heat dissipation because they are in direct contact with environment. Regarding heat generation, if these cracks occurred in 90^o layers, they will not be responsible for heat generation since there is no relative motion between the surfaces of the cracks in 90^o layers during loading/unloading because the main loading direction is normal to the formed cracks. However, if they occurred in $\pm 45^o$ layers, they can contribute to generating heat since the main applied load can be resolved to a force component parallel to the formed $\pm 45^o$ cracks and hence it can cause a relative displacement and rubbing of the cracks' surfaces which in turn generates heat.

(6) Type (D"): these internal matrix cracks might generate heat if they occurred in layers other than 90^o layers (as mentioned in Type (D'). Also, these cracks might help in heat dissipation using channels connecting the cracks to the surrounding. For instance, in the scheme of the quasi-isotropic laminate shown in Figure 4-8 (c), the type D" cracks formed in the inner 45^o layer (second layer), although they are not in direct contact with the surrounding but the occurrence of type B delamination at $45^o/90^o$ interface (first and second layers) and type D' cracks in the outer 90^o layer can secure a channel (D"/B/D'/surrounding) that can be used for heat dissipation from the inner 45^o cracks to the surrounding. Table 4-5 summarizes the different damage mechanisms and their role in heat generation/dissipation.

Table 4-5 Different Damage mechanisms and their contributions in heat generation/dissipation

Damage mechanism	Heat generation	Heat dissipation
Delamination at gap (A)	√	---
Delamination at interfaces • Within the laminate (B") • Extended to the edge (B')	√ √	√ (if it can find path to surrounding) √
Transverse cracks in 0^o layer (C)	√	---
Matrix cracks in 90 layers • Inner layers (D") • Outer layers (D')	--- ---	√ (if it can find path to surrounding) √
Matrix cracks in $\pm 45^o$ layers • Inner layers (D") • Outer layers (D')	√ √	√ (if it can find path to surrounding) √

Understanding the aforementioned different mechanisms and their contribution in heat generation and dissipation will help to understand the difference in the thermal response observed previously in Figure 4-3.

4.4.3 **Thermal response of different stacking sequences**

As mentioned in the observations on Figure 4-3, the maximum temperature increase for the case of cross-ply laminate was the highest and followed by quasi-isotropic and unidirectional ones. Having a deeper look reveals that this is not a fair comparison since the stresses generated in the 0^o layers, the main carriers of load in the laminate, in each laminate is different. One way to compare fairly between different types of laminates is by subjecting them to different applied stresses that will generate the same amount of stresses in the 0^o layers.

Figure 4-9 shows the temperature change of the three different stacking sequences, unidirectional, cross-ply and quasi-isotropic laminates, at maximum applied stress of 1750, 1020 and 770 MPa during the first 1000 cycles. Using classical lamination theory, these applied stress levels were selected so that the initially induced stresses in the 0^o layers for all of the three types of laminates will be the same, 1750 MPa. This approach enabled us to compare between different stacking sequences based on the same generated stresses in the main carriers of load in the laminates, 0^o layers.

It was found that the order of the maximum temperature increase changes. The highest temperature increase was observed for the case of quasi-isotropic laminates followed by cross-ply and unidirectional laminates. In order to investigate the possible reasons for this, the fatigue tests were interrupted and the specimens were sectioned at different X-distances from the gap and polished to be inspected using SEM to check the various damage mechanisms occurred within the laminate during this 1000 cycles. Once the damage was detected, the polishing process was repeated several times to get the approximate extension of the damage along X-direction.

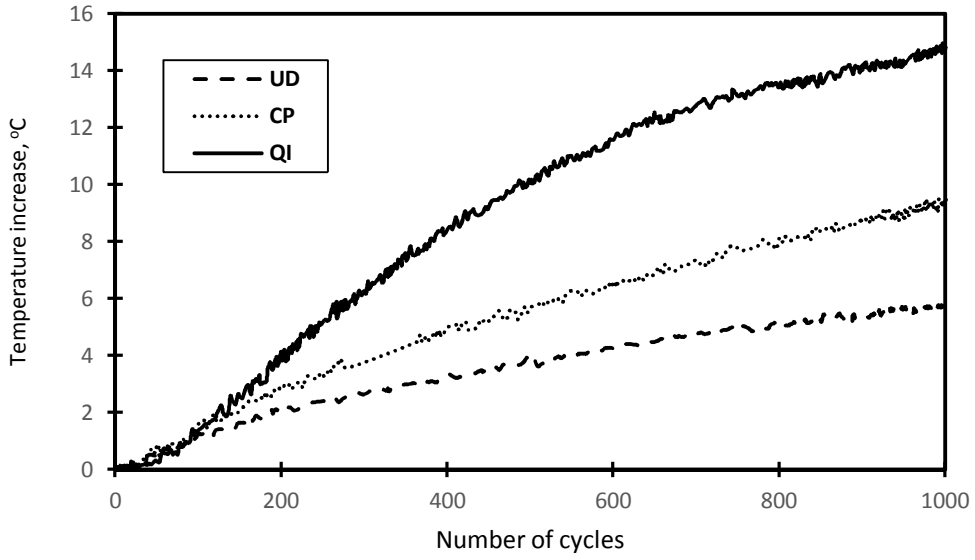

Figure 4-9: Temperature change for different stacking sequence at the same stresses in 0^o layers, 1750 MPa

Table 4-6 illustrates the observed damage mechanisms after 1000 cycles and their extension measured using SEM. For each detected damage mechanism, there is a corresponding letter and

sign. The letter refers to the type of the damage mechanism while the sign refers to whether this mechanism generates heat (+), dissipates heat (-) or none of them (nil). The net area was calculated while taking into account the sign of the individual areas. For instance, the net area for cross ply laminate is: 108-140+207 = 175 mm^2. This is more representative to the behavior in Figure 4-9 since this figure expresses the temperature increase due to the net heat, generated and dissipated, in the material.

It was found that the net damage area was highest in case of quasi-isotropic laminates followed by cross-ply and unidirectional ones. Consequently, the net heat stored in the case of quasi-isotropic laminates is the highest one which explains the observed ordering in the temperature change of different stacking sequences in Figure 4-9.

For the case of unidirectional laminates, the existence of 0^o layers constrains the laminate and confines the propagation of damage. However, for laminates containing off-axis layer, the existence of matrix cracks in the off-axis plies after loading reduces the stiffness of the laminate and causes an increase in the stress in 0^o layers that helps propagating the damage. In the investigated laminates, the quasi-isotropic laminates had more off-axis layers (6 layers) compared to the cross-ply ones (4 layers) which might be responsible for the increase in the damage area for quasi-isotropic laminate compared to the cross-ply one.

Also it can be observed that the ratio between the maximum temperature increases is different from the ratio of the net damage area. For instance, the maximum temperature increase for unidirectional and cross-ply laminates, from Figure 4-9, were 5.8 and 9.4ºC, respectively, with a ratio of $\left(\frac{5.8}{9.4} = 0.6\right)$. However the ratio between the net damage areas of the two types, from Table 4-6, was $\left(\frac{60}{175} = 0.34\right)$. The interesting observation is that the ratio of maximum temperature increase (0.6) is almost equal to the ratio between the delamination areas due to gap (type A) for the two stacking sequences which was $\left(\frac{5}{9} = 0.56\right)$. This can also be confirmed by comparing the unidirectional to quasi-isotropic laminates. The ratio of maximum temperature increase, between unidirectional and quasi-isotropic from Figure 4-9, was $\left(\frac{5.8}{14.8} = 0.39\right)$ and the ratio between the

delamination areas due to gap (type A), from Table 4-6, was $\left(\frac{5}{12} = 0.42\right)$. These observations can reveal that the delaminations that occurred at the gap (type A) have the highest contribution to the heat generation and net thermal behavior. A possible explanation for this is that the relative displacement between the two surfaces created by the damage is highest in case of type A damage compared to the other types (B, C and D) which helps to generate more heat according to Eqn. (4.1).

Table 4-6: Different damage mechanisms and their extension within the laminates after 1000 cycles

Damage mechanism	**UD**	**CP**	**QI**
Delamination at gap	-Length: 5 mm **(A+)** -Width: 6.35 mm -# of interfaces: 2 -Area=5x6.35x2=60mm^2	-Length: 9 mm **(A+)** -Width: 6.35 mm -#of interfaces: 2 -Area=9x6.35x2=108mm^2	-Length: 12 mm **(A+)** -Width: 6.35 mm -#of surfaces: 2 -Area=12x6.35x2=144mm^2
Matrix cracks in 45	----	----	Average 20 cracks extended for 20 mm **(D" +)** - Total length of cracks/layer= 600 mm - Area= 600x 4layers x 0.14 thick = 336mm^2
Matrix cracks in 90	----	- Assumed 20/layer extended over the width of the specimen* - Outer layers **(D'-)** A=20x 2layers x 0.14 x 25 width=140mm^2 - Inner layers **(D" nil)** A=20 x 2layers x 0.14 x 25 width=140mm^2	- Assumed 20 extended over the width of the specimen - Outer layer **(D'-)** A=20x2layersx0.14x25 width =140mm^2 - No inner 90^o layers.
Delamination at interfaces	----	- Average width = 9mm extended for 23 mm along length **(B"+)** - Area=9x23=207 mm^2	No delamination was observed after 1000 cycles
Net area	60 mm^2	175 mm^2	340 mm^2

* The sections were cut parallel to 90^o layers so it was not possible to detect 90^o cracks. They were assumed to be equal to the number of 45^o cracks.

4.4.4 **Behavior of defective laminates below threshold stress**

Since it is not practical to test both reference and defective specimens at stresses lower than the threshold values till the final failure occurrence, so the tests were conducted to the first million cycles and the thermal behavior was observed. This might help giving an explanation to what happens below the threshold values.

In order to investigate the behavior of the defective samples below the threshold point, some fatigue tests were conducted on defective samples with maximum applied stress of 1600 MPa, 550 MPa and 800 MPa for unidirectional, quasi-isotropic and cross-ply laminates, respectively, and IR thermography was used to monitor the temperature change during the tests. The results of the fatigue tests showed that final fiber failure did not occur up to 10^6 cycles for all the samples tested below the threshold stress. The increase of the surface temperature with number of cycles for the whole period of testing showed that there was an initial temperature increase then it was followed by a constant temperature period which represents most of the fatigue life of the tested samples. The same behavior was observed for all different stacking sequences.

This observed thermal behavior was similar to the behavior of the reference specimens which consists of initial temperature increase followed by temperature plateau for the majority of the fatigue life. This might indicate that the behavior of both reference and defective specimens is the same below threshold stress values.

Figure 4-10 shows the temperature change for different stacking sequences subjected to maximum stress with different ratios to the threshold stress ($Ratio = \frac{\sigma_{max}}{\sigma_{threshold}}$). It should be noticed that all specimens subjected to stresses lower than the threshold stress were fatigue tested up to 10^6 cycles. However, the horizontal axes in Figure 4-10 show only the first 500 000 cycles so that the behavior at higher stresses and lower cycles can be clearly seen in the same figure.

It can be observed that for all stacking sequences below the threshold stress there was a temperature increase at the middle of the specimen at the beginning of the fatigue test due to damage initiation at the gap location. The temperature continued to increase in the loading

direction then it reached a plateau. The temperature was almost constant up to the end of the test at 10^6 cycles.

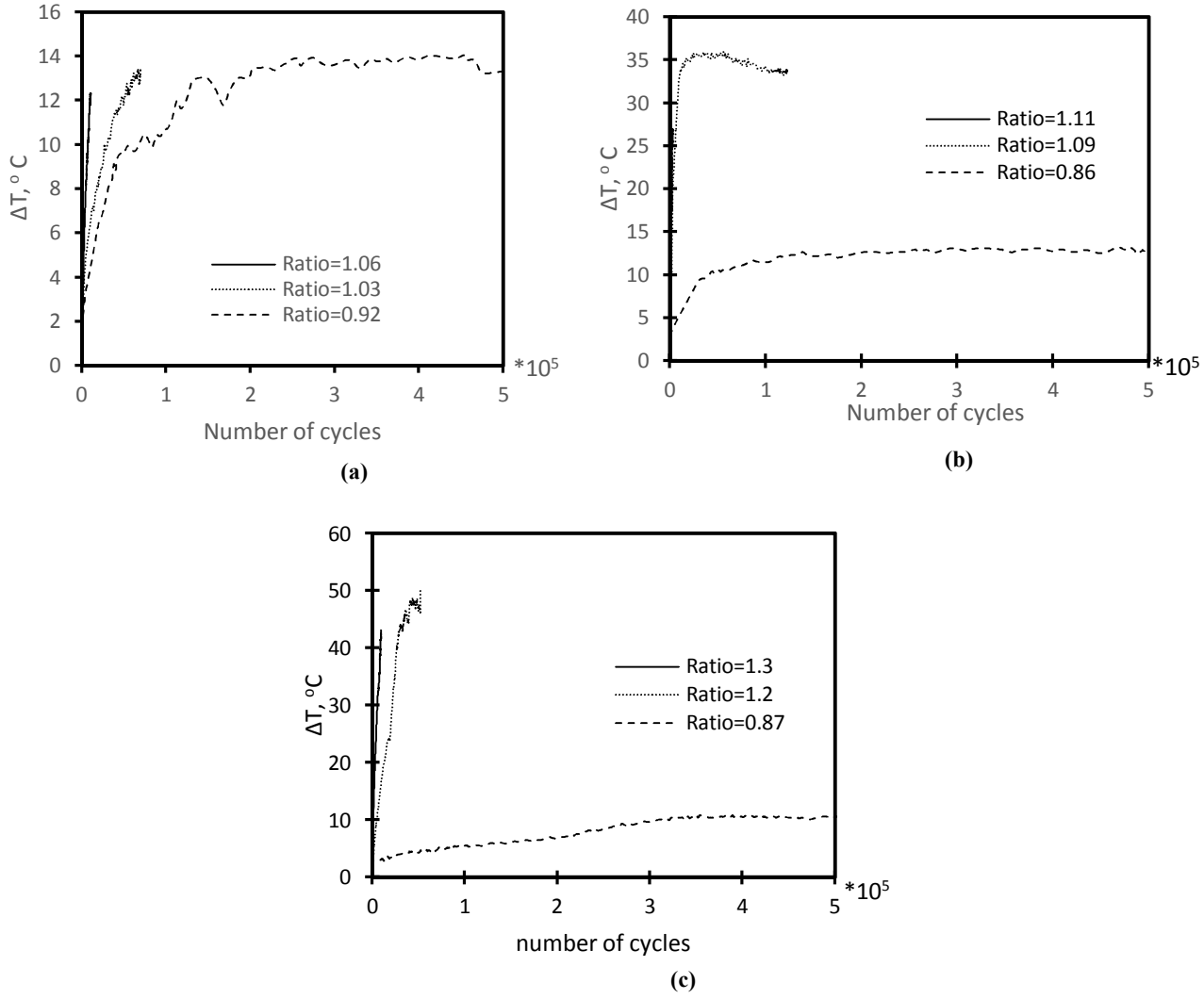

Figure 4-10: Thermal behavior at different maximum stress levels for defective: (a) unidirectional, (b) cross-ply and (c) quasi-isotropic laminates

Based on the observation of the thermal behavior it might be assumed that damage initiated and propagated during the first part of the life then there was only minor, or no, additional damage progression for the rest of the specimen's life, during which the temperature was constant, as there

was no additional heat being generated to increase the surface temperature of the specimen. In order to validate this assumption, more specimens of different stacking sequences were tested at the same fatigue loading, below the threshold values, and the tests were interrupted at different cycles and the specimens were sectioned and inspected using SEM.

The attention was focused on the part of life during which no temperature increase occurred. So one specimen, of each stacking sequence, was tested till reaching the beginning of that period (300,000 cycles). The second specimen was tested up to 600,000 cycles which almost corresponds to the middle of the no-temperature increase period. The last sample was tested up to 10^6 cycles. Each specimen was cut at different sections located at different distances from the gap in order to approximately detect the extension of the damage after certain number of cycles. Figure 4-11 shows the different sections cut at different distances from the gap center at the middle of the specimens and the corresponding number of cycles for the case of unidirectional laminates as an example.

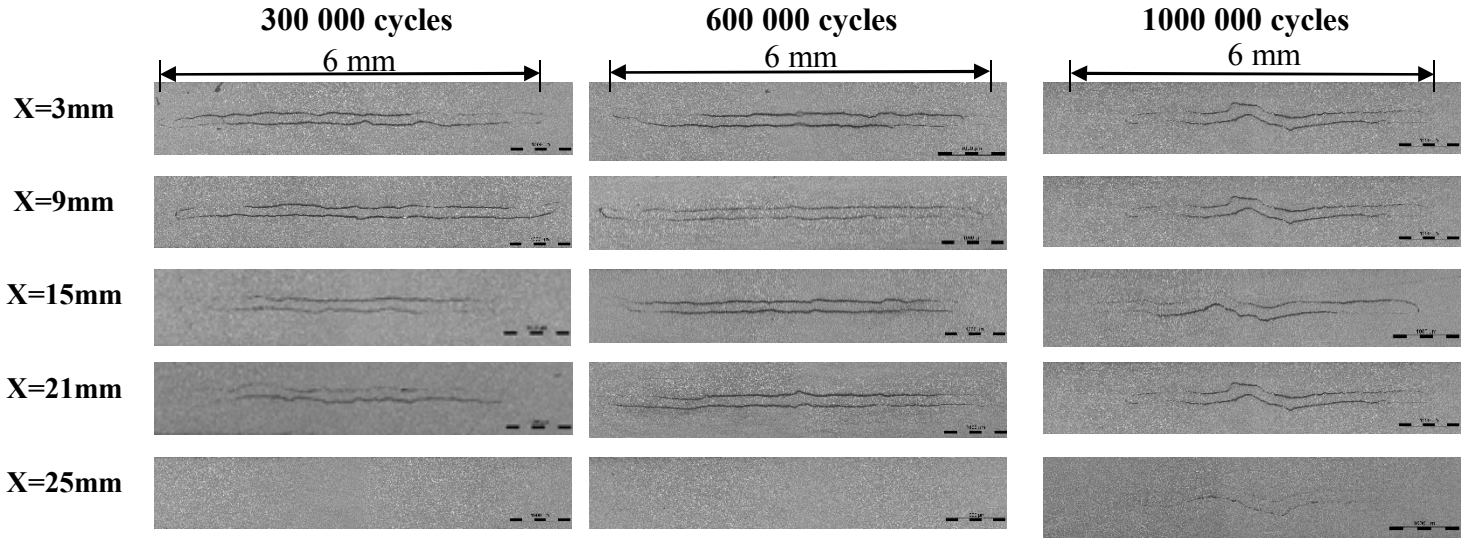

Figure 4-11: Microscopic images at different distances from the gap centre for 300 000, 600 000 and 10^6 cycles for unidirectional laminates

For the case of the specimen tested up to 300 000 cycles, it was observed that damage extended from the gap edge and terminated at 21 mm. For the specimen tested up to 600 000 cycles, the same damage extension was observed, no damage was observed at a distance of 25

mm. For the sample tested till 1000 000 cycles, the damage propagated up to 25 mm from the gap edge and the detected damage was not as clear as in the previous section, 21 mm, which reveals that the damage extension is close to its end. Another section was cut at 27 mm for this sample and no damage was found.

In light of these observations, it can be concluded that damage occurred in the first part of the life which caused the temperature of the sample to increase. As a result of the low applied stress, the damage almost stopped propagating for the rest of the sample's life and the temperature stopped increasing. The arresting of damage during the majority of the fatigue life retarded the occurrence of final failure up to 1000 000 cycles. The same observations were found for the case of quasi-isotropic and cross-ply laminates as shown in Figure 4-12 for quasi-isotropic and cross-ply laminates. The damage initiated and propagated in the first part of the fatigue life then there was no more damage occurrence in the rest of the life up to 10^6 cycles.

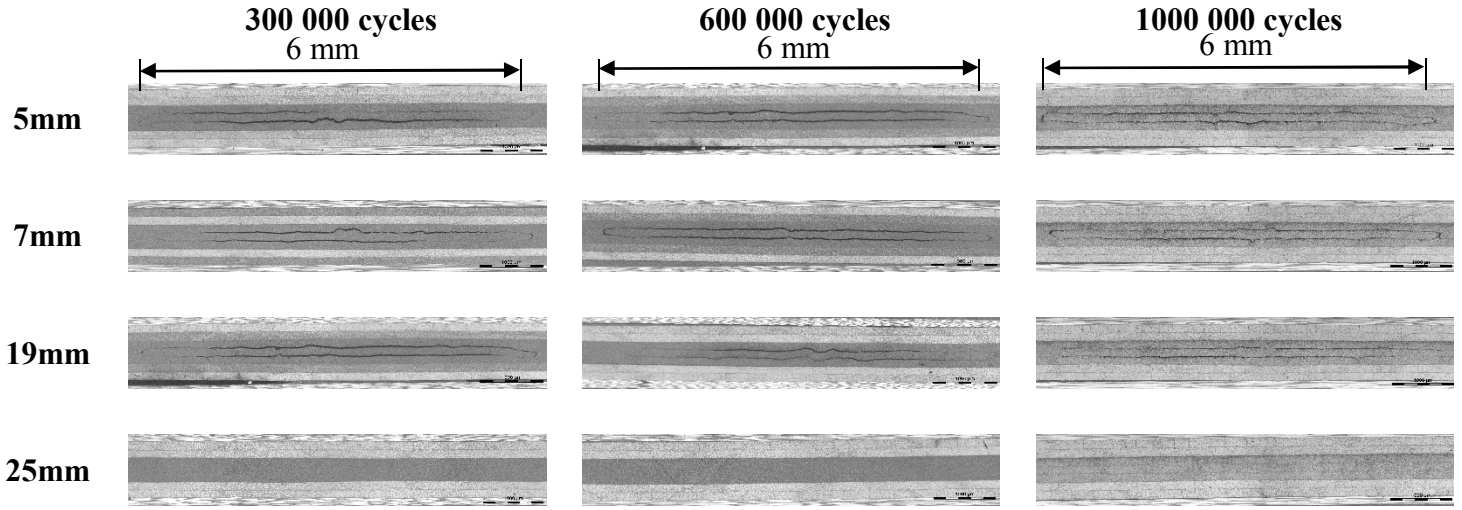

(a)

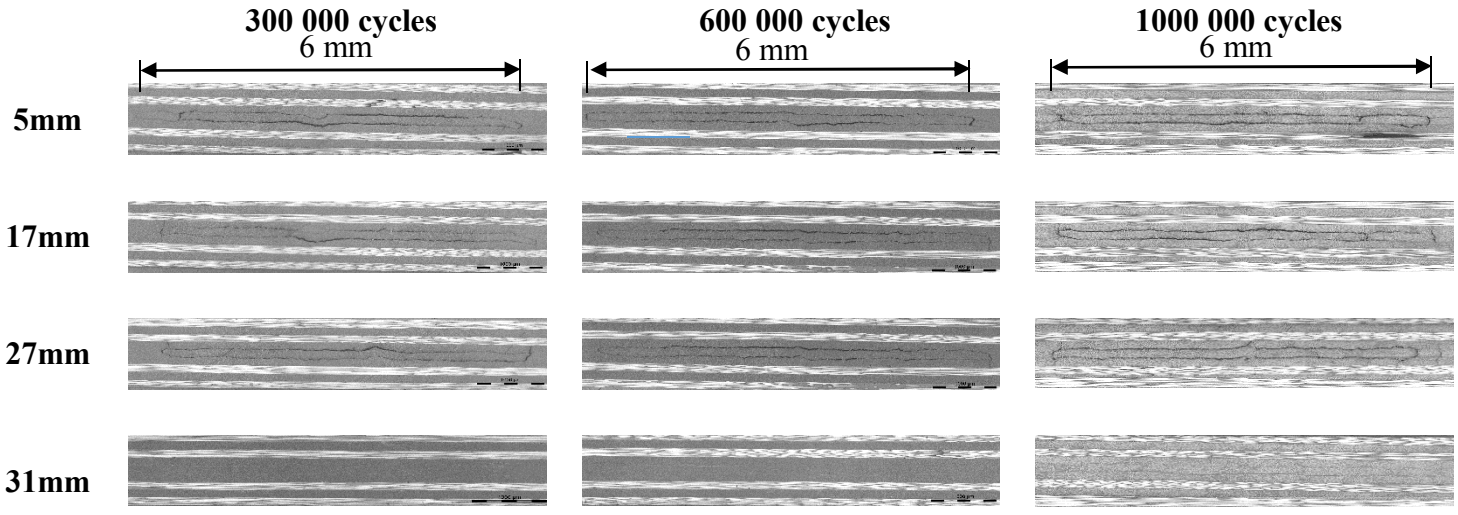

(b)

Figure 4-12: Microscopic images at different distances from the gap centre for (a) quasi-isotropic and (b) cross-ply laminates

4.4.5 **Temperature plateau**

One of the characteristics observed for the specimens subjected to stresses lower than the threshold values is that the temperature change has a plateau. As explained previously, there are two opposing components responsible for the thermal state of the specimen which are the heat generation and dissipation components. The net amount of heat stored in the material up to time ($t + \Delta t$) is:

$$Q_S^{t+\Delta t} = Q_S^t + Q_g^{\Delta t} - Q_d^{\Delta t} \qquad (4.2)$$

While the amount of dissipated heat from the specimen to the surrounding is:

$$Q_d^{\Delta t} = H\left(T_{s,av}^{\Delta t} - T\right).\Delta t \qquad (4.3)$$

Q_S^t, $Q_g^{\Delta t}$ and $Q_d^{\Delta t}$ are the stored heat in the material up to time (t), the generated heat during time (Δt) and the dissipated heat during time (Δt), respectively. H is the heat loss coefficient. $T_{S,av}^{\Delta t}$ is the average surface temperature of the specimen during Δt. T is the environmental temperature. If at any time the amount of generated heat is more than the dissipated one then some amount of heat will be accumulated to the heat stored in the material causing the net stored energy

to increase which will lead eventually to increase the temperature of the specimen. On the other hand, if the amount of heat generated was equal to the dissipated heat then the stored energy in the material will be the same which consequently results in constant temperature (temperature plateau) with time/cycles.

At the beginning of the fatigue life, cracks started to occur and increase in density due to damage accumulation with cycles causing high heat generation (Q_g). Initially the amount of heat dissipation (Q_d) is small which results in continuous increase of the net stored energy in the material that causes the temperature to keep increasing with time.

Then, the rate of damage growth decreases till it reaches a saturation state with no more cracks occurrence. This will make the amount of heat generation (Q_g) constant. On the other hand, the amount of heat dissipation component (Q_d) increases continuously because of the increase in the surface temperature of the specimen, according to Eqn. (4.3), till it becomes equal to the heat generation component (Q_g) which leads to a constant amount of net heat stored in the material and the material reaches a temperature plateau.

In the present study, for the case of unidirectional laminates, it was observed that the material has the temperature plateau when the applied stress is less than the threshold as shown in Figure 4-10 (a) for R=0.92. However, for the case of cross-ply and quasi-isotropic laminates, it was observed that the material might have the temperature plateau even for stresses higher than the threshold point as shown in Figure 4-10 (b) at R=1.09 for cross-ply laminates and Figure 4-10 (c) at R=1.2 for quasi-isotropic laminates. A possible explanation for this is the existence of some damage mechanisms that could help in dissipating heat such as types B' and D' in Figure 4-8. These mechanisms do not exist for the case of unidirectional laminates. The occurrence of these mechanisms helps in creating more surfaces that enhance and accelerate the dissipation of heat to the surrounding and reaching a constant temperature.

4.4.6 **Threshold stress**

For reference specimens without gaps, the damage initiates from the non-uniformities existing in the material such as manufacturing flaws and resin rich areas which lead eventually to final failure. For the defective specimens containing gaps, at high applied stresses, the elastic energy stored in the material is high. This high energy helps in propagating the damage from the gap which consequently accelerates the final failure and reduces the fatigue life of the defective specimen compared to the reference one. So, in this case the effect of the gap is more severe than the effect of the heterogeneity in the material.

However, for the case of defective specimens subjected to stress lower than the threshold stress, the elastic energy stored in the material is too low to keep the damage propagating from the gap and damage arresting occurs during the majority of the fatigue life as shown in Figure 4-11 and Figure 4-12. So, in the case of low stresses and very long fatigue life, there is enough time for the damage from small defects or heterogeneity localized in the reference material to aggregate and give rise to similar effect of the arrested damage due to gaps created in the defective specimens.

4.5 **Using Risitano method for laminates with more gaps**

It was required to investigate the applicability of IR thermography for rapid evaluation of threshold stresses of laminates containing more gaps. Two types of unidirectional specimens were manufactured: specimens with 2 in-plane gaps and specimens with 2 out-of-plane gaps. Then, the same procedures explained previously were followed in order to determine the threshold stress. The specimens were fatigue tested for the 1000 cycles and the surface temperature was monitored and recorded using IR camera. Figure 4-13 shows the temperature change with number of cycles during the first 1000 cycles of the fatigue life. The observed behavior was similar to that of the case of one gap which was almost linear temperature increase with cycles.

The obtained thermal trends were fitted to regression lines and the slopes were obtained. Then they were plotted against the applied stress as shown in Figure 4-14. The plotted slopes can be fitted to two linear portions whose intersections correspond to the threshold stresses. Table 4-7

shows a comparison between the threshold stresses obtained from long fatigue tests, Wohler method, and IR thermography techniques. In addition, it shows a comparison between the required time for testing using the traditional and IR methods. It can be concluded that IR thermography can be efficiently used for rapid evaluation of the threshold stresses for the case of laminates containing more than one gap.

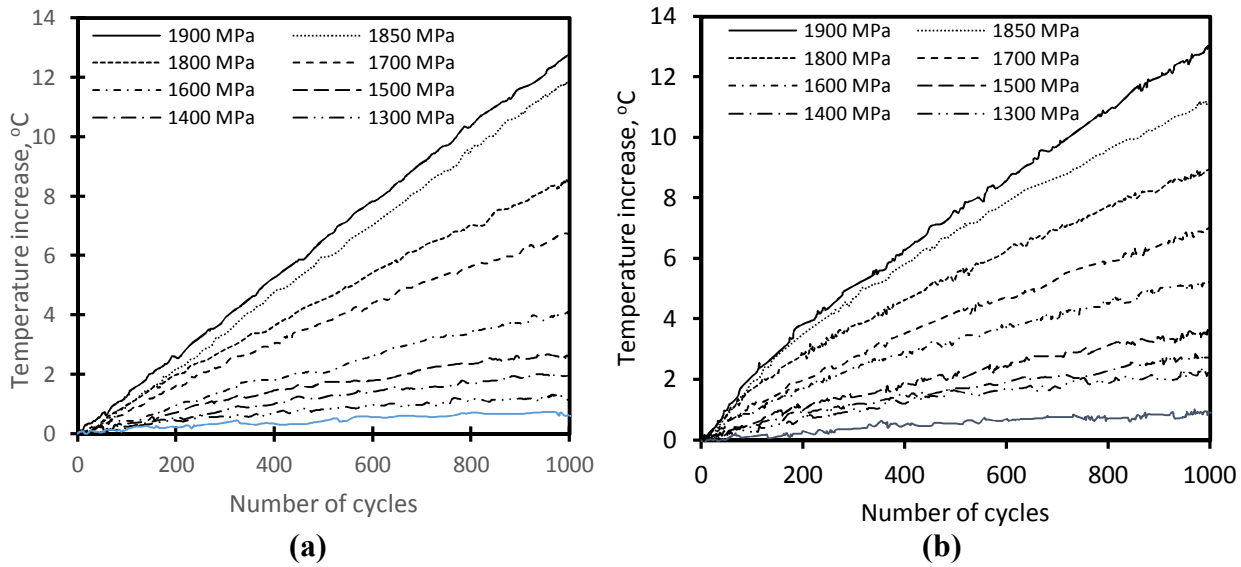

Figure 4-13: Temperature change with cycles for unidirectional laminates with 2 gaps (a) in-plane and (b) out-of-plane

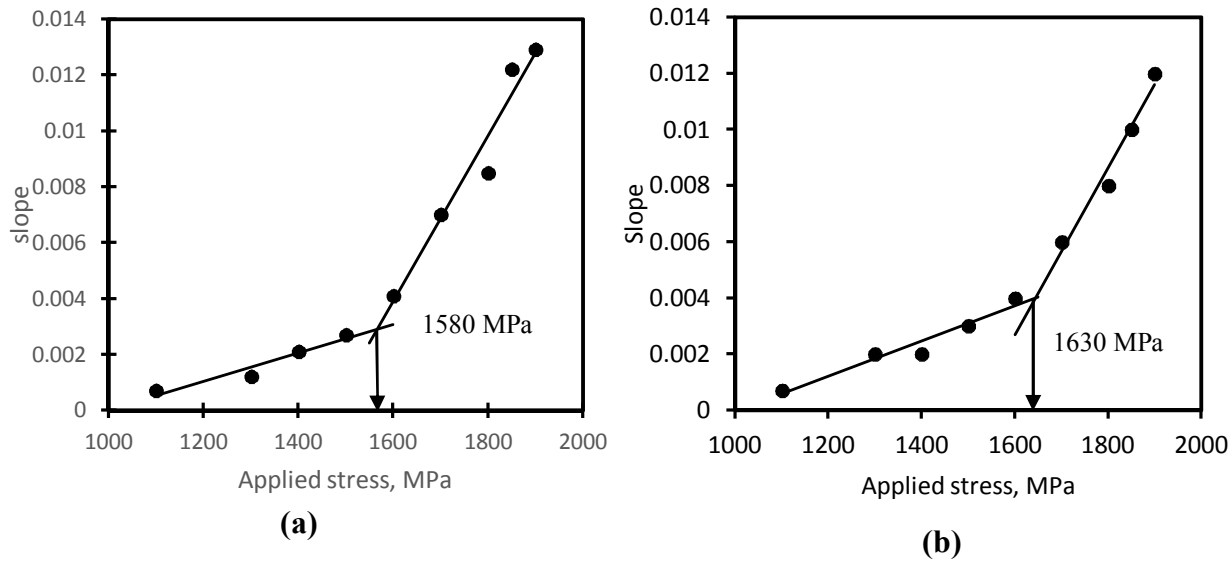

Figure 4-14: Bilinear relation between the slope of temperature increase and the applied stress for unidirectional laminates with 2 gaps (a) in-plane and (b) out-of-plane

Table 4-7: Threshold stress values obtained from experiments and IR thermography for laminates with 2 gaps

Laminate configuration	Wohler (MPa)	IR (MPa)	Error (%)	Testing time (Wohler) (hrs)	Testing time (IR)(hrs)
2 in-plane gaps	1570	1580	0.51	180	0.5
2 out-of-plane gaps	1480	1630	9.2	190	0.5

4.6 **Summary**

Subjected to fatigue loading, AFP laminates containing gaps showed a threshold stress below which the effect of the manufacturing gaps diminishes. IR thermography was used to provide a method for quickly determining the threshold stress in an effort to overcome the obstacle of the long time and high material consumption in the traditional Wohler (S/N curves) method.

Thermal observations of gapped specimens with different stacking sequences containing one or two gaps showed a bilinear relation between the rate of the temperature increase and the applied stress from which a threshold stress could be obtained. At applied fatigue stresses lower than the threshold values, as a result of the low applied stress and long-time of testing, the effect of the gaps in defective specimens becomes equivalent to the effect of the heterogeneities in the reference specimens. This eliminates the effect of the gap on the fatigue life.

The results of the threshold stress values for different stacking sequences obtained using IR thermography were in very good agreement with that obtained using Wohler method. IR thermography was found to be a powerful alternate to the traditional method and capable of determining the threshold fatigue stress for AFP laminates containing gaps while retaining the great advantage of saving time and material.

Chapter 5

Finite element modeling

Development of finite element models helps engineers in all different fields. First, they contribute to saving time and material required for conducting experimental tests by performing virtual tests using many platforms such as Ansys, Abaqus…etc. Second, it can help the designer understanding different phenomena observed during the performed experiments. This chapter focuses on illustrating the fatigue progressive damage model (FPDM) developed in the study. This model helps in understanding and predicting the behavior of laminates manufactured by AFP and containing gaps. The chapter is divided into two main parts. In the first part, the components of the FPDM will be described in details. Then in the second part, validation of the model will be performed by comparing the results of the fatigue tests performed and illustrated in chapter 3 to the predicted results of the FPDM.

5.1 Model Development

A fatigue progressive damage model (FPDM) was developed in order to predict fatigue damage growth and final failure of laminates containing gaps as a representation of induced defect during manufacturing using AFP. The model was developed for different stacking sequences using Ansys Parametric Design Language (APDL) v15.0. The progressive damage model presented in this work is an integration of fatigue life model, failure criterion, sudden and gradual degradation of strength/stiffness. In the following subsections, the main procedures to develop the FPDM will be described.

5.1.1 Model generation and material definition

Ansys v15.0 was used to develop a 3D model. In the developed model, each layer was represented by one volume then the volumes were bonded to each other. Before meshing the volumes, different local coordinate systems were defined according to the orientation of the different layers in the laminate to be modeled. For instance, if the laminate is quasi-isotropic, then four local coordinate systems are defined: 0, 90, 45 and -45. These coordinate systems are assigned to the generated volume according to the configuration of the laminate. Then the volumes are meshed.

Element type Solid185 brick element was used to mesh the model, shown in Figure 5-1. It is defined by eight nodes having three degrees of freedom at each node: translations in the nodal x, y, and z directions.

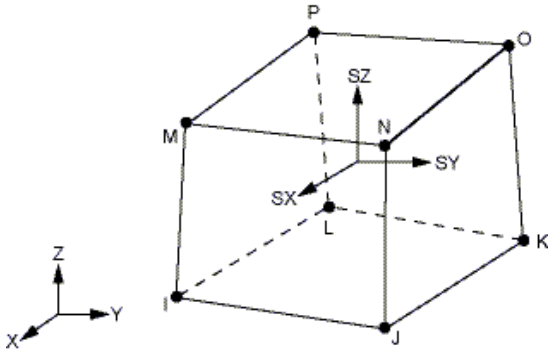

Figure 5-1: 3D element Solid 185 from Ansys library used to develop FPDM [93].

The reasons for selecting a 3D element for the model are that:

1- It was found from experimental observations that the main damage mechanism due to gaps was delamination which is mainly caused by out-of-plane stresses. Consequently, a 3D element was used to accurately capture the out-of-plane stresses within the laminate especially at the location of the gap.
2- Using 3D model enables to represent each layer by one element across the thickness of the laminates. Hence, mechanical properties degradation can be applied to the required element in the required layer without affecting the mechanical properties of the other layers.

For Solid185, structure solid option was chosen and orthotropic material properties were assigned to the elements. So, initially two material types were defined:

1- Isotropic material properties were assigned for the elements representing the gap with properties of epoxy resin. The gap was assumed to be filled with resin based on the microscopic images for the section containing the gap.
2- Orthotropic material properties were assigned for all other elements.

Table 5-1 (second column) shows the results of static tests for material characterization performed in the study. These values were used as inputs in the finite element modeling software (ANSYS). Also, by comparing both the second and third columns in Table 5-1, it can be observed that the mechanical properties of the used material in the current study are close to those of the one used in reference [94]. Consequently, it was assumed that the fatigue response of both materials are similar and hence the required constants for the finite element modeling obtained from this previous work [94] will be used as will be shown later.

Table 5-1 Material properties of Carbon/Epoxy laminates used in the FEM.

Material Property	977-2 carbon/epoxy	AS4/3501-6 carbon/epoxy [94]
E_{11} (Young modulus in fiber direction)	140 GPa	147 GPa
$E_{22} = E_{33}$ (Young modulus in 2- and 3- direction)	11 GPa	9 GPa
$G_{12} = G_{13}$ (Shear modulus in 1-2 and 1-3 planes)	5 GPa	5 GPa
G_{23} (Shear modulus in 2-3 planes)	4 GPa	3 GPa
$\upsilon_{12} = \upsilon_{13}$ (Major Poisson's ratio in 1-2 and 1-3 planes)	0.28	0.3
υ_{23}* (Major Poisson ratio in 2-3 plane)	0.28	0.42
X_t (Tensile strength in fiber direction)	2500 MPa	2000 MPa
X_c (Compressive strength in fiber direction)	1450 MPa	1200 MPa
$Y_t = Z_t$(Tensile strength in transverse direction)	60 MPa	53 MPa
$Y_c = Z_c$(Compressive strength in transverse direction)	200 MPa	205 MPa
$S_{xy} = S_{xz}$ (shear strength)	100 MPa	137 MPa
S_{yz} (assumed equal to that of [94])	42 MPa	42 MPa
* Poisson's ratio was assumed to be the same in all planes		

It was required to assess the accuracy of the mesh and the applied boundary and loading conditions of the model, so a simple case from the experiments, which is the quasi-static tensile testing of unidirectional laminates, was chosen and the output strains of the model at different values of load were compared to the results recorded from strain gages during the test. Figure 5-2 shows a comparison between the strain gages results and strains from the finite element model at the same location.

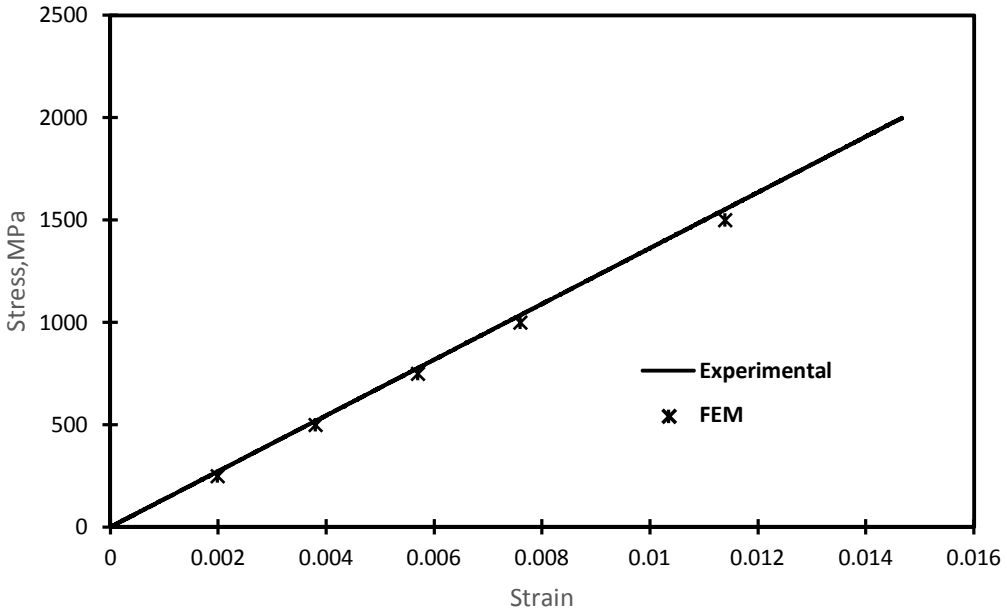

Figure 5-2: Comparison between strain results obtained experimentally and from FEM

For modelling of tensile-tensile fatigue loading, it was assumed that the damage occurs at the maximum stress in the cycle. Therefore, the stress analysis was performed based on the maximum applied stress during the fatigue tests. Then, the on-axis stresses were obtained for each element in the model. Eventually, each element has six on-axis components of stresses: three normal stresses (σ_{11}, σ_{22} and σ_{33}) and three shear stresses (τ_{12}, τ_{23} and τ_{13}).

5.1.2 **Fatigue life model**

The purpose of using the fatigue life model is to determine the number of cycles to failure in each direction by using the on-axis stresses/strength on those directions for each element and stress ratio ($R=\frac{\sigma_{min}}{\sigma_{max}} = 0.1$). The power law fatigue life model was developed by Gathercole et al. [95]:

$$a = f\,[(1-m)(c+m)]^{u} \qquad (3.1)$$

Where u is a curve fitting parameter linearly related to number of cycles to failure N_f.

$$\mathbf{u = A + BlogN_f} \quad (3.2)$$

f = 1.06 [95].

$a = \frac{\sigma_a}{S_t}$, $\sigma_a = \frac{\sigma_{max} - \sigma_{min}}{2}$

$m = \frac{\sigma_m}{S_t}$, $\sigma_m = \frac{\sigma_{max} + \sigma_{min}}{2}$

$c = \frac{S_c}{S_t}$

σ_{max} and σ_{min} are the maximum and minimum on-axis stresses in each element. In case of normal stresses in longitudinal and transverse directions, S_t and S_c are the tensile and compressive on-axis strength in those directions. For shear case, c = 1 and S_t refers to shear strength. A and B are curve fitting parameters determined experimentally from fatigue characterization of the material by running longitudinal, transverse and shear fatigue tests at different maximum stress levels. They were obtained from [94] due to similarity of both materials as shown in Table 5-1. The constants used in the study for the fatigue life model are listed in Table 5-2.

Table 5-2: Fitting parameters used in the fatigue life model [94]

Fatigue Loading condition	Constants for Eqn. (3.2)	
	A	B
Longitudinal tension	1.06	0.07
Longitudinal compression	1.06	0.07
Transverse tension	0.99	0.096
Transverse compression	0.99	0.096
In-plane shear	0.1	0.2
Out-of-plane shear	0.3	0.1

During fatigue loading, mechanical properties can change due to gradual or sudden degradation. Gradual degradation occurs continuously as a result of change of mechanical properties with cycles. However, sudden degradation occurs only when any failure mode is detected and hence the ability of the material to carry load is drastically decreased as illustrated in the following subsections.

5.1.3 **Gradual degradation of mechanical properties**

At the beginning of the fatigue test, the residual strength and stiffness of the laminate are equal to the static values. By increasing the number of cycles, the residual properties decrease. When the number of cycles reaches a critical value which is the number of cycles to failure (N_f), these residual properties reach critical values at which failure occurs. The evolution of damage and degradation of mechanical properties pass by three phases during the fatigue life of a composite part: initial change, almost constant level and finally a drastic change prior to failure [65]. The model in the study, developed by Adam et al. [96] and modified by Shokrieh [94], simulates this behavior of residual properties:

$$S_R(n) = \left[1 - \left(\frac{\log(n)-\log(0.25)}{\log(N_f)-\log(0.25)}\right)^{\beta}\right]^{\frac{1}{\propto}} (\mathrm{S} - \sigma) + \sigma \tag{3.3}$$

$$E_R(n) = \left[1 - \left(\frac{\log(n)-\log(0.25)}{\log(N_f)-\log(0.25)}\right)^{\lambda}\right]^{\frac{1}{\gamma}} \left(\mathrm{E} - \frac{\sigma}{\varepsilon_f}\right) + \frac{\sigma}{\varepsilon_f} \tag{3.4}$$

$S_R(n)$ and $E_R(n)$ are the residual strength and stiffness, respectively, in different directions (longitudinal, transverse and shear) at any number of cycles (n). S and E are the static strength and stiffness in the corresponding directions as shown in Table 5-1. σ is the on-axis stress in the corresponding directions obtained from the stress analysis. $\beta, \propto, \lambda$ and γ are curve fitting parameters determined experimentally by performing interrupted longitudinal, transverse and shear fatigue tests followed by static tests at different cycle ratios $\left(\frac{N}{N_f}\right)$ to determine the residual properties. ε_f is the average strain to failure during fatigue loading. These required constants are shown in Table 5-3.

Table 5-3: Fitting parameters used in strength and stiffness degradation models [94]

Fatigue Loading condition	Constants for Eqn. (3.3)		Constants for Eqn.(3.4)		
	β	α	λ	γ	ε_f
Longitudinal tension	0.47	10.03	14.6	0.3	0.019
Longitudinal compression	0.03	49.06	14.6	0.3	0.019
Transverse tension	0.13	9.63	14.8	0.12	0.006
Transverse compression	0.001	67.4	14.8	0.12	0.006
In-plane shear	9.11	0.16	0.7	11	0.1
Out-of-plane shear	12	0.2			

5.1.4 **Failure analysis**

In static failure criteria, the state of stresses is compared to the static strength in each material direction. However, in case of fatigue as a result of continuous degradation of material properties with cycles, the state of stresses is compared to the residual material properties. Based on the on-axis stresses obtained from stress analysis and the residual properties of each element obtained from equation (3.3), failure was checked against a fatigue failure criterion. Initially, Hashin failure criterion [76] was used to check different modes of failure since it can distinguish between different modes:

Fiber Failure in Tension: $\left(\frac{\sigma_{11}}{X_{tR}}\right)^2 + \left(\frac{\tau_{12}}{S_{12R}}\right)^2 + \left(\frac{\tau_{13}}{S_{13R}}\right)^2 = 1\,, \quad \sigma_{11} > 0$ (3.5)

Fiber failure in compression: $\frac{\sigma_{11}}{X_{cR}} = 1\,, \quad \sigma_{11} < 0$ (3.6)

Matrix tensile failure: $\left(\frac{\sigma_{22}}{Y_{tR}}\right)^2 + \left(\frac{\tau_{12}}{S_{12R}}\right)^2 + \left(\frac{\tau_{23}}{S_{23R}}\right)^2 = 1\,, \quad \sigma_{22} > 0$ (3.7)

Matrix compression failure: $\left(\frac{\sigma_{22}}{Y_{cR}}\right)^2 + \left(\frac{\tau_{12}}{S_{12R}}\right)^2 + \left(\frac{\tau_{23}}{S_{23R}}\right)^2 = 1\,, \quad \sigma_{22} < 0$ (3.8)

Fiber-matrix shearing: $\left(\frac{\sigma_{11}}{X_{cR}}\right)^2 + \left(\frac{\tau_{12}}{S_{12R}}\right)^2 + \left(\frac{\tau_{13}}{S_{13R}}\right)^2 = 1\,, \quad \sigma_{11} < 0$ (3.9)

Delamination in tension: $\left(\frac{\sigma_{33}}{Z_{tR}}\right)^2 + \left(\frac{\tau_{13}}{S_{13R}}\right)^2 + \left(\frac{\tau_{23}}{S_{23R}}\right)^2 = 1 \quad \sigma_{33} > 0$ (3.10)

Delamination in compression: $\left(\frac{\sigma_{33}}{Z_{cR}}\right)^2 + \left(\frac{\tau_{13}}{S_{13R}}\right)^2 + \left(\frac{\tau_{23}}{S_{23R}}\right)^2 = 1 \quad \sigma_{33} < 0$ (3.11)

In this criterion, σ_{ii} and τ_{ij} denote the normal and shear stresses in material directions, respectively (both i and j represent 1- , 2- and 3-directions). In the denominators, X, Y and Z denote normal strength in 1-, 2- and 3-direction, respectively, and S is for shear strength. Subscripts t and c refer to tensile and compression properties, respectively. Subscript R indicates residual strength values obtained from equation (3.3). It was found [97, 98] that using Hashin failure criterion alone led to a very conservative prediction of fiber tensile failure mode as a result of the interaction between the shear and tensile stresses in fiber failure mode as shown in equation (3.5). In the case of the laminate with gap, high shear stresses generate at the edge of the gap as a result of cutting of fibers. The contribution of shear stress component in fiber failure mode, equation (3.5), might cause early prediction of fiber tensile failure. As a result, Hashin failure criterion was used to check only fiber compressive failure, matrix tensile and compressive failure, fiber matrix shearing under compression and delamination in both tension and compression. In its place, maximum stress criterion [2] was used to check fiber tensile failure instead of equation (3.5):

$$\frac{\sigma_{11}}{X_{tR}} = 1 \ , \qquad \sigma_{11} > 1 \qquad (3.12)$$

5.1.5 **Sudden mechanical properties degradation**

Once any failure mode is detected in an element, the material properties of this element are degraded by implementing a sudden degradation rule. The scope of using sudden degradation rules is to disable elements from carrying a load in a certain direction. Thus, for each mode of failure there exists a corresponding degradation rule. The stiffness degradation takes place according to Table 5-4 [99]. To avoid numerical problems due to assigning zero to some material properties in stress analysis step, the properties are degraded to small values.

Table 5-4 Different failure modes and corresponding property degradation schemes

Fiber failure	$E_{11}= E_{22}= E_{33}= \upsilon_{12} = \upsilon_{23} = \upsilon_{13} =G_{12}=G_{23}= G_{13}= 0$
Matrix failure	$E_{22}= \upsilon_{12}= 0$
Fiber/matrix shearing	$\upsilon_{12}= G_{12}=0$
Delamination failure	$E_{33} =G_{23} =G_{13} = \upsilon_{23} = \upsilon_{13} = 0$

To integrate all the previously mentioned components in FPDM, a user macro-routine was developed using Ansys Parametric Design Language (APDL). Figure 5-3 shows the sequence of the different procedures of the FPDM. After performing the stress analysis and obtaining the on-axis stresses in each element, fatigue life model is performed to obtain the failure cycles in each direction for each element using equations (3.1-3.2).

Then, gradual degradation of strength/stiffness is conducted to account for the degradation of properties with increasing the number of cycles using equations (3.3-3.4). Failure in each element is checked using the fatigue failure criteria according to equations (3.6-3.12).

If no failure was detected in the elements then the number of cycles will be increased with an increment ΔN. If any failure mode is detected, then sudden degradation rules are applied according to Table 5-4. Stress redistribution is performed and failure is rechecked again. The number of cycles will not increase unless no more failure was detected in the model. This loop is

repeated continuously till the final failure of the model which was defined as the propagation of fiber failure mode across the whole width of the model.

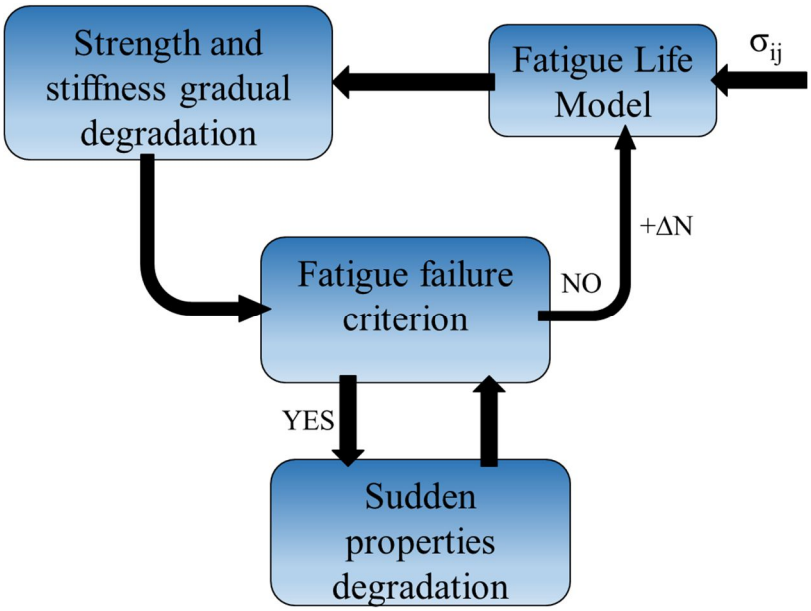

Figure 5-3 Sequence of different steps of the FPDM

5.2 Model validation

It is of importance for any developed finite element model to be validated. The best way to validate the model is by comparing its predicted results with the results of the conducted experiments. The main privilege of using the FPDM is to be able to capture the damage growth from stress concentrations in the material (such as notches and defects). In the present work, the model was applied for the different scenarios of defective samples investigated experimentally. In the following subsections the results of the model will be illustrated and compared with that of the fatigue experiments.

5.2.1 Gaps in 0º layers for different stacking sequences

For the case of different laminates containing gaps in the middle 0º layers, due to symmetry of the laminate, only one quarter of the laminates was modeled and symmetry boundary conditions were applied to the areas located at X=0 and Y=0. The load was applied to the area located at the right end of the sample as illustrated in Figure 5-4.

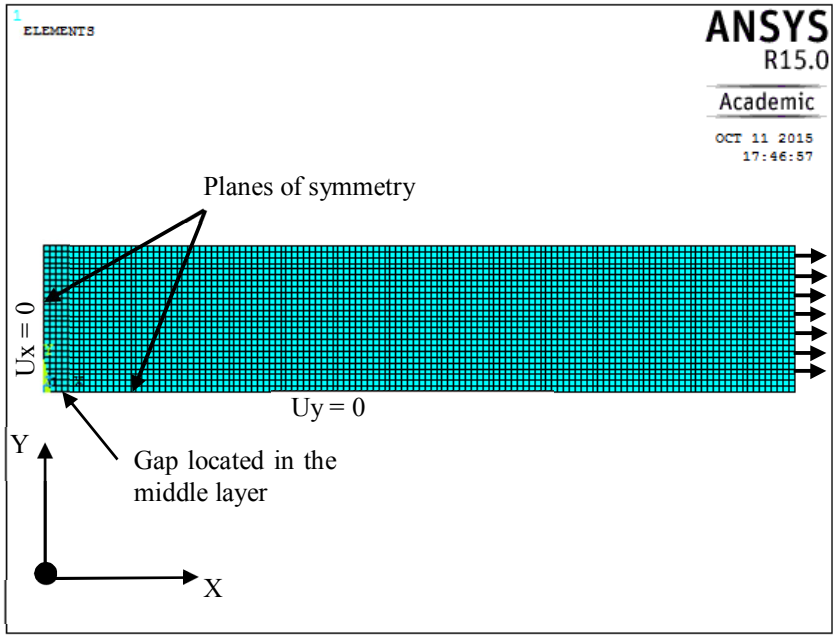

Figure 5-4: Applied load and boundary conditions in the FEM for laminates containing gaps in middle 0º layer

It was mentioned that the reason of the delamination occurrence between the defective layer and the adjacent layers is the high interlaminar stresses generated as a result of the transfer of high amount of normal in-plane stresses between those two layers. Figure 5-5 shows the normal in-plane stress distribution across the thickness of the laminate at the gap location when the laminate is subjected to 1850 MPa. It can be observed that the stress at the middle layer is small due to gap existence (180 MPa). Due to stress redistribution, the differential stress (1670 MPa) is transferred to the adjacent 0^o layers causing stress increase as shown in the 4^{th} and 6^{th} layers.

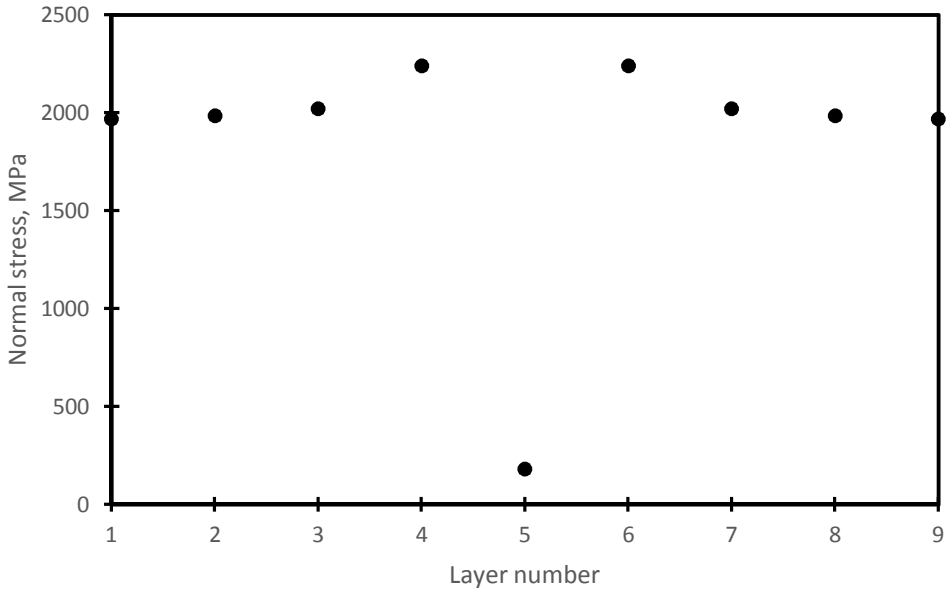

Figure 5-5 Normal in-plane stress distribution at the gap across the thickness of unidirectional laminate

It should be mentioned that the stresses that need to be transferred from the defective layer are not equally distributed among the other layers of the laminate. However, the layers which are severely affected by the stress distribution are those directly adjacent to the defective layer. Then the effect of the gap is alleviated through the thickness by moving further from the gap. The adjacent layers (4^{th} and 6^{th} layers) carry together 47% of the differential stresses transferred from the defective area while the remaining 53% is carried by the other layers.

As a result of transferring high amount of load to the adjacent intact layer, interlaminar stresses are generated at the interface between the layers. A stress path was defined at the edge of

the gap along fiber direction, line AB, as shown in Figure 5-6. It can be observed that there is a high out-of-plane stress, τ_{xz}, at gap edge as a result of load transfer between the two layers and these induced stresses cause initiation of delamination in the laminate which was observed from the microscopic images of a section cut ahead of the gaps locations.

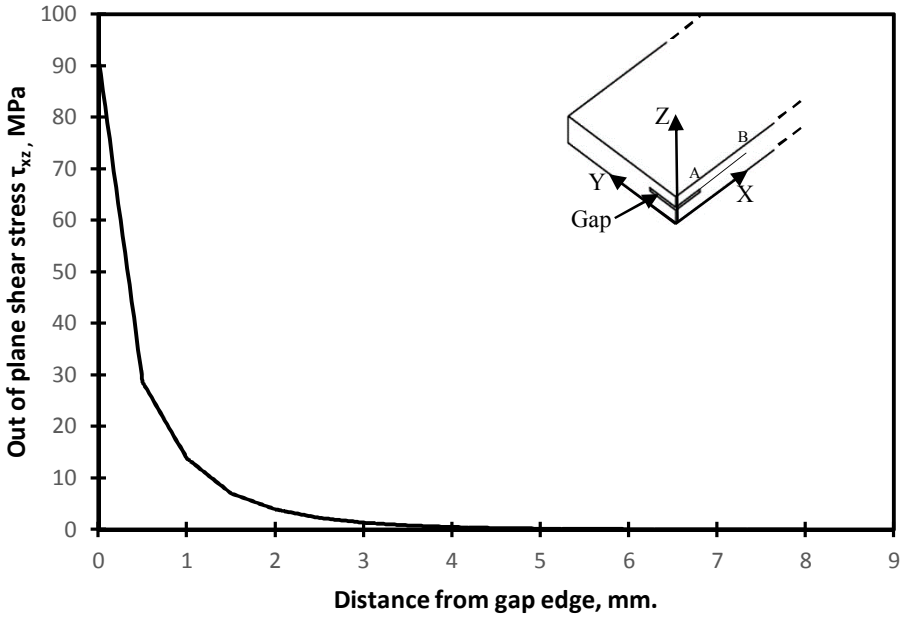

Figure 5-6: Out-of-plane shear stress at the edge of the gap for a unidirectional laminates at applied stress of 1880 MPa

Figure 5-7 shows the damage progression of a unidirectional laminate containing a gap at different cycle ratios for stress level of 1880 MPa. Initially, there was high interlaminar shear stress at the gap edge as shown in Figure 5-6. These induced stresses did not cause static failure because they were less than static strength of the elements. By increasing the number of cycles, gradual mechanical properties degradation occurred till reaching a point at which the developed interlaminar shear stresses became higher than the residual shear strength of some elements and consequently failure started to occur. Delamination initiated at the edge of the gap at early stages of fatigue life, Figure 5-7(b), and it was followed by sudden degradation of failed elements and stresses were redistributed to the intact elements. Stress redistribution process caused delamination to propagate to the intact elements, Figure 5-7(c). At the end of fatigue life, fiber tensile failure

mode started to occur and propagated across the length and the width of the model till reaching the edge which indicated final failure, Figure 5-7(d) and (e).

Delamination is a progressive failure mode and the model can reach stability after stress redistribution process and hence going forward to the next increment of cycles. However, fiber failure is a catastrophic mode of failure and once it occurs, Figure 5-7(d), the model could not reach stability and it continues propagating across the width of the specimen at the same last step up to final failure detection, Figure 5-7(e). That is why the damage shown in Figure 5-7(d) and Figure 5-7 (e) occurred at the same number of cycle at the end of the fatigue life.

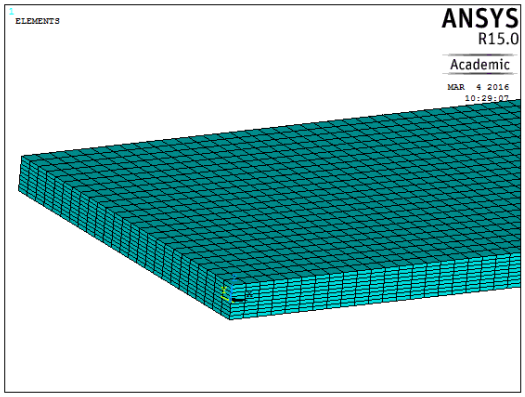

(a) $\frac{N}{N_f} = 0$

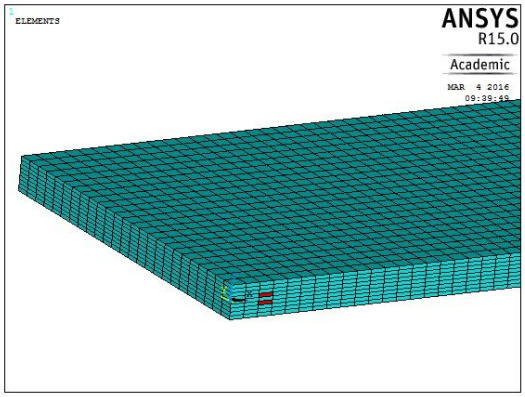

(b) $\frac{N}{N_f} = 0.1$

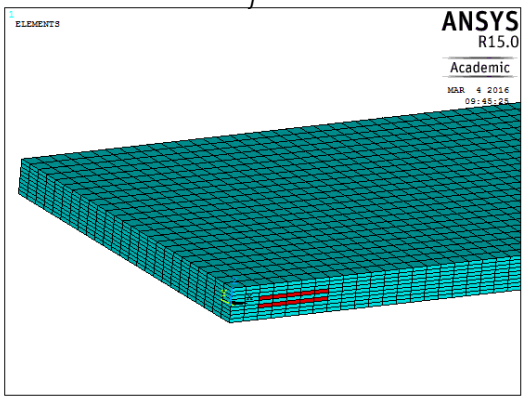

$(c)\frac{N}{N_f} = 0.28$

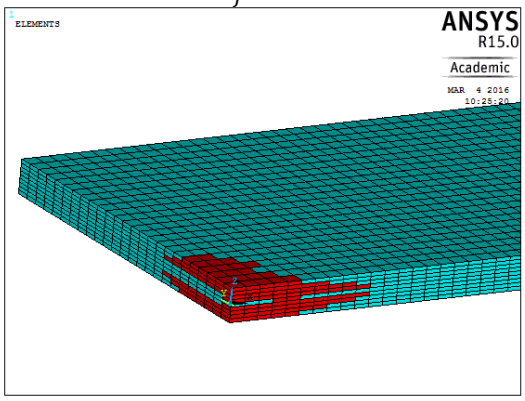

(d) $\frac{N}{N_f} = 1$

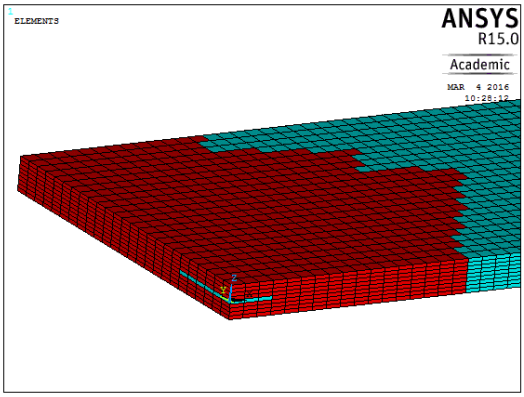

$$(e)\ \frac{N}{N_f} = 1$$

Figure 5-7 Damage evolution in UD carbon/Epoxy laminate containing a gap in the middle 0° layer under fatigue loading

Figure 5-8 shows a comparison between the experimental and the predicted life of FPDM for carbon/epoxy unidirectional laminate at different applied stress levels. It can be observed that the FPDM over predicts the fatigue life of the defective laminates. In reality, there are some issues that can negatively affect the performance of the tested specimens such as: manufacturing flaws (resin rich areas, voids, fiber misalignment, and waviness), cutting process flaws (delamination at the edges and inaccuracy of cutting) and testing flaws (gripping pressure at the grips of the specimen and misalignment of the specimen with the grips of the machine). These issues were not taken into account in the model.

In addition, the used curve fitting parameters in the fatigue life model and the stiffness/strength degradation models were taken from a previous study [94]. Although these parameters were taken from another material whose mechanical properties are close to that used in the current study, however, characterizing the used material in the current study and using its own fitting parameters might lead to better predicted results. The resulting inaccuracy due to using these parameters might positively affect the longitudinal behavior, which is the dominant behavior in the unidirectional laminates, and eventually causes overestimation of predicted results.

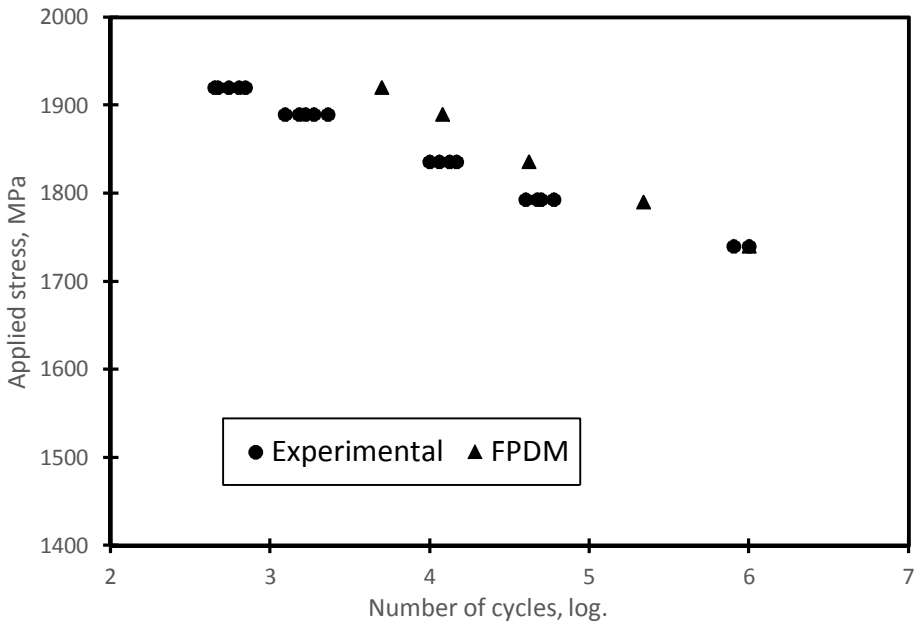

Figure 5-8: Comparison between the predicted FPDM and experimental results for unidirectional laminates

The model was also applied for the case of cross-ply (90/0/90/0/0*/0/90/0/90) and quasi-isotropic laminates (90/45/-45/0/0*/0/-45/45/90) with a gap created in the middle 0° layer indicated by (*) symbol in each stacking sequence. Figure 5-9 shows a schematic illustration for the damage mechanisms observed from FPDM of the cross-ply laminate, as an example, during the fatigue life. Figure 5-9 (a) shows a scheme for the model and the used coordinate system. For both cases, there are three observed damage mechanisms:

1- Referring to Figure 5-9 (b), damage starts by matrix cracks that occur at the beginning of the life in the off-axis layers such as 90° layers. This also happens for the case of ±45° layers in quasi-isotropic laminates. This mechanism took place for all elements representing the off-axis layers because the on-axis stresses in the matrix direction were higher than the strength of the matrix material for those elements.
2- Delamination occurs as a result of the high interlaminar stress at the gap edge similar to that observed in Figure 5-6 for case of unidirectional laminate. By increasing the number

of cycles, delamination propagates along the length of the specimen (X-direction) as shown in Figure 5-9 (c).

3- At the end of fatigue life, fiber failure initiates at the location of the delamination at the 0° layers and propagates aggressively across both width and length direction of the specimen (X- and Y- directions) up to final failure as shown in Figure 5-9 (d).

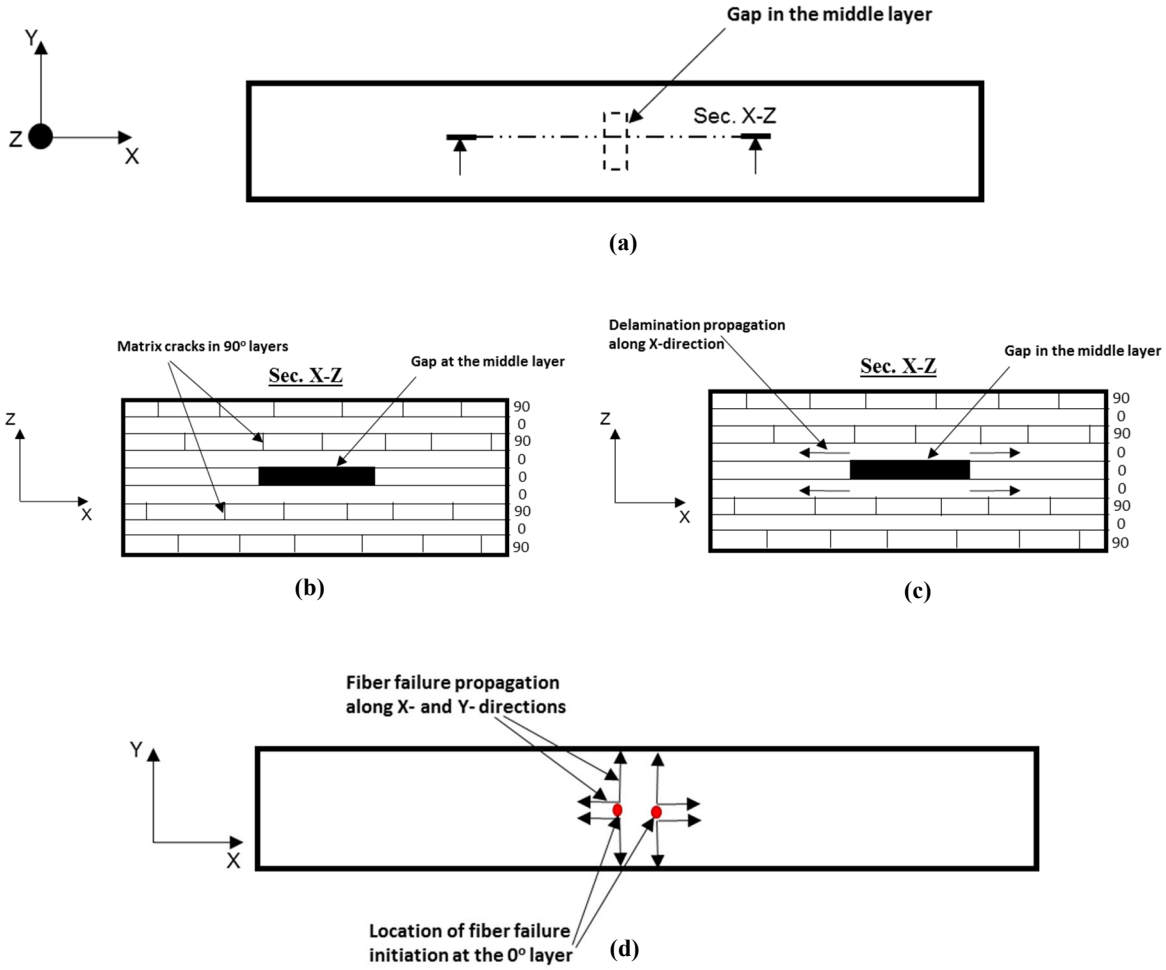

Figure 5-9: Schematic representation for cross-ply laminate of (a)FEM and the used coordinates, (b) matrix cracks in off-axis layers, (c) delamination propagation and (d) fiber failure propagation

However, the model did not predict the occurrence of the transverse cracks, which were observed in the experimentally tested specimens, propagating through 0^o layers from delamination due to the gap to the interface of $0^o/90^o$ layers. The occurrence of such cracks is greatly affected by the stresses at the interfaces between different layers. A possible reason is that the predicted stresses from the developed FPDM between layers were not accurate. Using interface elements at the interface between layers might help in more accurate prediction of stresses at the interface which improves the simulation of damage mechanisms. Using interface element approach will increase the complexity of the model and was not considered in the current study.

Figure 5-10 and Figure 5-11 show a comparison between the experimental and the predicted results for FPDM for cross-ply and quasi-isotropic laminates. It can be observed that the FPDM underestimates the fatigue lives for cross-ply laminates. For quasi-isotropic laminates, at some stresses it overestimates but to a less extent compared to the unidirectional laminates.

It was found from the fatigue experiments that adding 90^o layers improves the performance of the laminate and increases the fatigue life. Consequently, a possible reason for the observed deviation is the set of parameters used in the fatigue life models and stiffness/strength degradation models. The inaccuracy resulting from the use of these parameters might negatively affect the performance of 90^o layers and might eventually reduce the predicted fatigue life. The tested cross-ply laminate has more 90^o layers than the quasi-isotropic ones. Hence, the effect of the inaccuracy in the parameters is more severe on the cross-ply compared to the quasi-isotropic laminates.

Moreover, in the previous study [94], the fitting parameters were calibrated using stress levels of 60% and 80% of the ultimate strength of the material. However, in the case of cross-ply laminates the ratios of the applied stress to the static strength were higher than 80%. This might also attribute to the deviation of the predicted results.

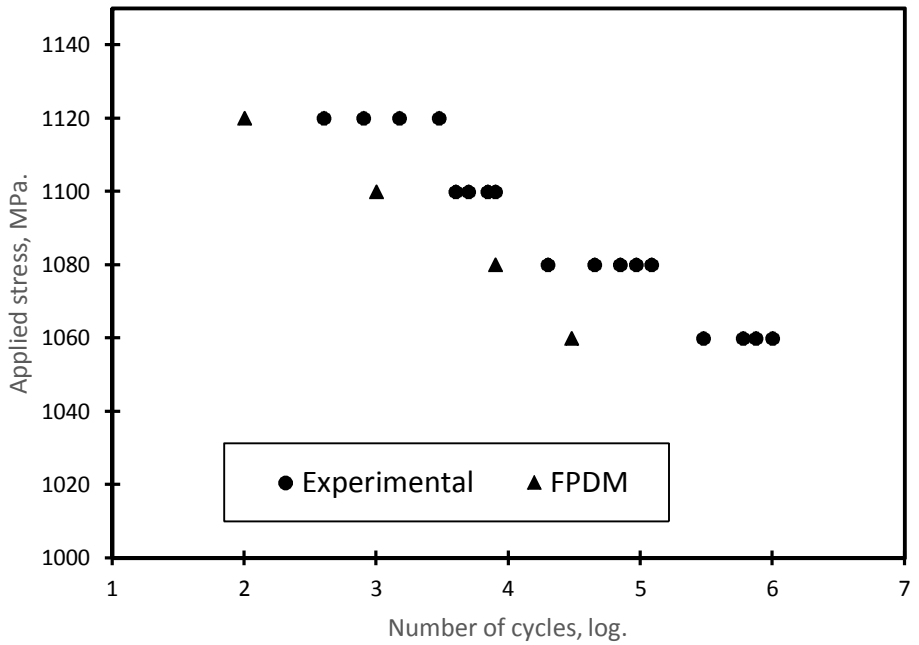

Figure 5-10: Comparison between the predicted FPDM and experimental results for cross-ply laminates

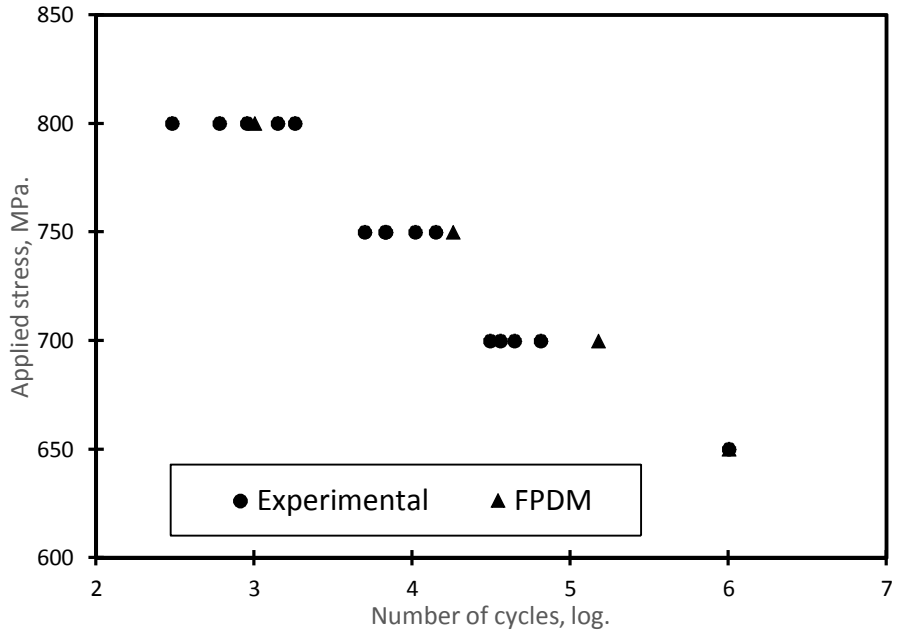

Figure 5-11: Comparison between the predicted FPDM and experimental results for quasi-isotropic laminates

5.2.2 **Gaps with different orientations**

In this part, the FPDM was developed for the case of cross-ply laminate (90/0/90*/0/0/0/90/0/90) containing a gap in 90º layer, indicated by (*) symbol, and quasi-isotropic laminate (90/45/-45*/0/0/0/-45/45/90) containing a gap in -45º layer, indicated by (*) symbol. In order to build up the model for the case of cross-ply laminate with gap in 90º, the volume representing the gap was created within the volume representing the 90º layer. Resin properties were assigned to the gap volume. For the case of quasi-isotropic laminate with a gap in -45º layer, the volume of the gap was created in the volume representing the -45º layer. The gap volume was oriented with -45º with respect to loading direction to represent the real specimen in which the gap is created by cutting fibers oriented with -45º with respect to loading direction. Then the material of the gap volume was defined using resin properties as shown in Figure 5-12.

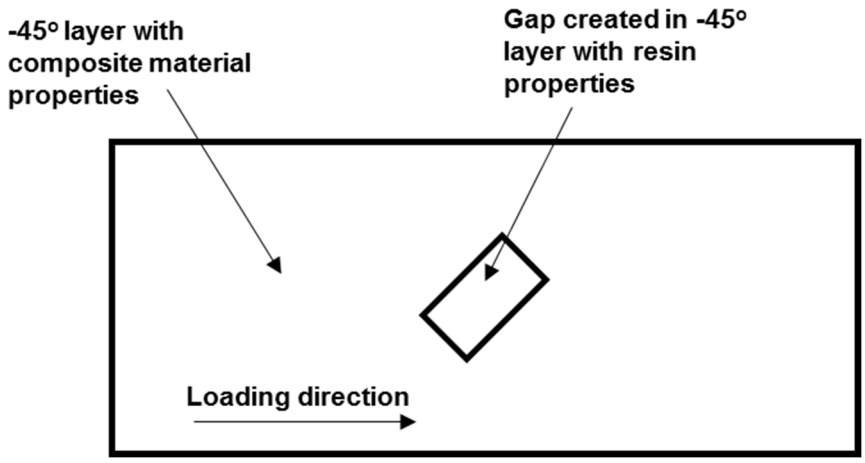

Figure 5-12: 2-D scheme for the defective -45º layer containing a gap in quasi-isotropic laminate

Initially, the same procedures for model development described for the case of the laminates containing gaps in 0º layers were followed within the present case with gaps created in 90º and -45º layers. It was found that the predicted number of cycles to failure from FPDM was too high

compared to those obtained from experiments for both laminates, cross-ply and quasi-isotropic. For instance, in the FPDM for a cross-ply laminate with a gap in 90^o layer and subjected to 1240 MPa, the specimen failed at 240000 cycles. However the average fatigue life from experiment was 3000 cycles. This might be attributed to the following:

1- In the case of different laminates with gaps in 0^o layers, a defect is created in the main load carrier in the laminate. Hence, the consequent damage mechanism from this defect affects severely the final failure of the laminate because it affects the integrity of the 0^o layers. So, in this case, the effect of these defects was assumed to be higher than the effect of non-uniformity in the material. As a result, all the elements in the model, except for the gap elements, were assumed to have the same mechanical properties.
2- For the case of laminates with gaps in layers rather than 0^o layers, cutting is performed in fibers not oriented in loading direction which makes the effect of this cut to be small compared to cuts in 0^o layers. In addition, it was found from the model that after stress distribution from the defective to intact layers, the stress increase in the intact 0^o layers was so small that it did not even initiate delamination or failure in the 0^o layers. Consequently, it was expected that considering the non-uniformity in the model will create weak spot from which damage can initiate and also it will be more representative to reality. Hence, for the laminates containing gaps in 90^o or 45^o layers, it was expected that the non-uniformity in the mechanical properties plays an important role in initiation of damage and occurrence of final failure.

In order to incorporate the effect of non-uniformities in the FPDM, different mechanical properties should be assigned to different elements. It was found from the literature that the material properties follow a normal distribution function [100]. So, random numbers were generated for material property using normal distribution function based on the mean value and the standard deviation obtained from the performed experiments during characterization of the material. After generation of different mechanical properties, they were assigned to the elements in the model. Consequently, each element in the FPDM had its own set of mechanical properties which was different from other elements. Figure 5-13 shows the variation of the tensile strength in fiber direction in an area of 25 mm x 4 mm in the model as an example. It can be observed that

each element has a longitudinal tensile strength that is different from the surrounding elements. This technique enables us to simulate the effect of the non-uniformities existed in the material.

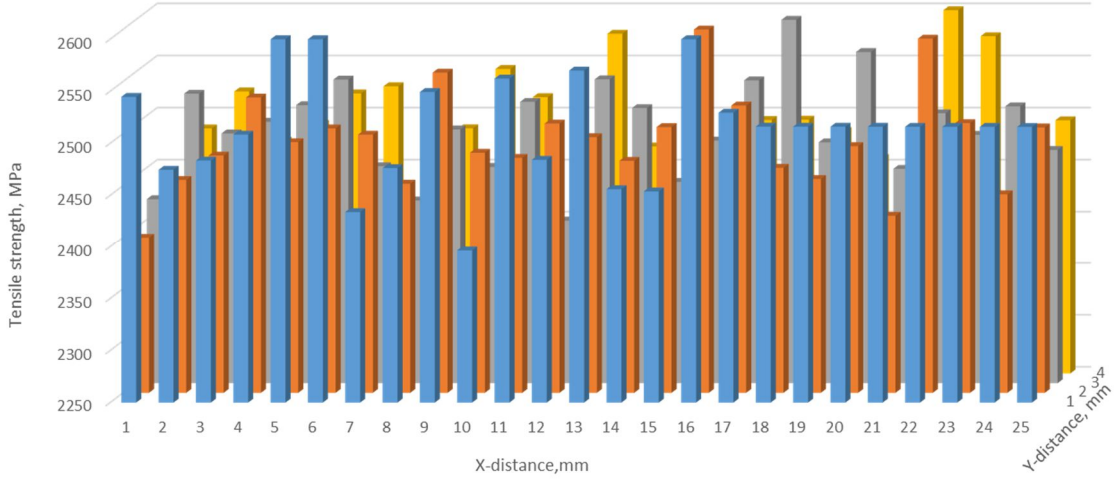

Figure 5-13: Variation of the longitudinal tensile strength in a small area in the model

It should be mentioned that for each time the model was solved, the distribution of the mechanical properties in all the plies in the model was different and consequently the number of cycles of failure obtained from the FPDM might be different. Figure 5-14, Figure 5-15 and Figure 5-16 show the damage evolution for different random distributions of properties for a cross-ply laminate (90/0/90*/0/0/0/90/0/90) with gap created in 90º layer. The attention was focused on the 0º layers in this type of laminates since they are the load carriers and they control the final failure of the laminate. The illustrated images are for the 0º layer adjacent to the defective 90º layer in the laminate, denoted by a bar in the stacking sequence, (90/0/90*/$\overline{0}$/0/0/90/0/90).

Damage initiates at random locations in which the strength values are less than the generated stresses. As a result of stress redistribution from the failed to intact elements, damage starts to propagate and the small damage areas aggregate with each other forming larger damage areas. When damage accumulates and some elements lose the support from the

surrounding elements due to damage mechanisms such as delamination and matrix cracks, the generated stresses in fiber direction become higher than the strength of fibers in those elements. Then, fiber failure (denoted by blue color) occurs and propagates aggressively up to final failure

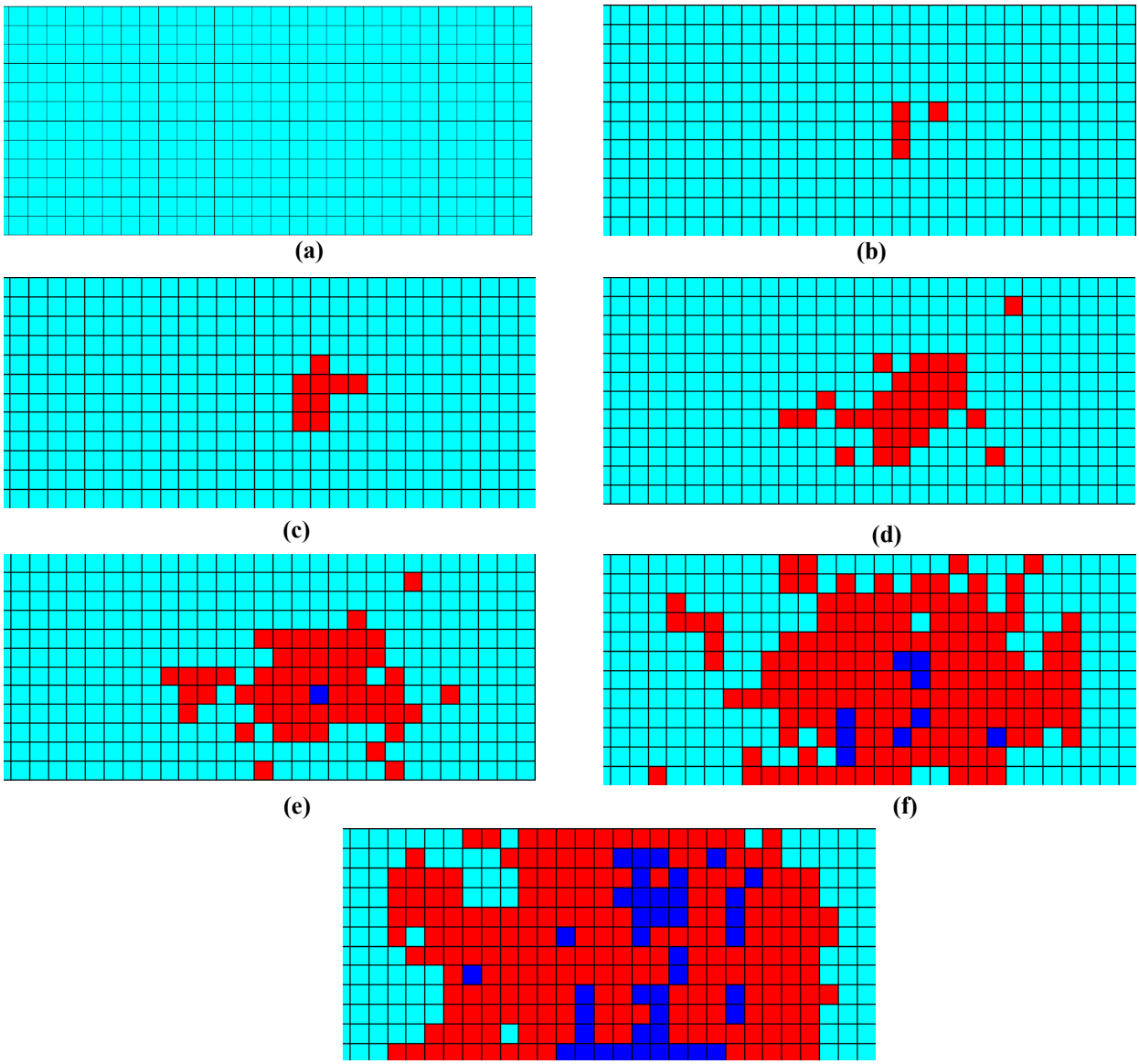

Figure 5-14: Damage evolution for cross-ply with gap in 90^{o} layer at 1200 MPa up to 140000 cycles

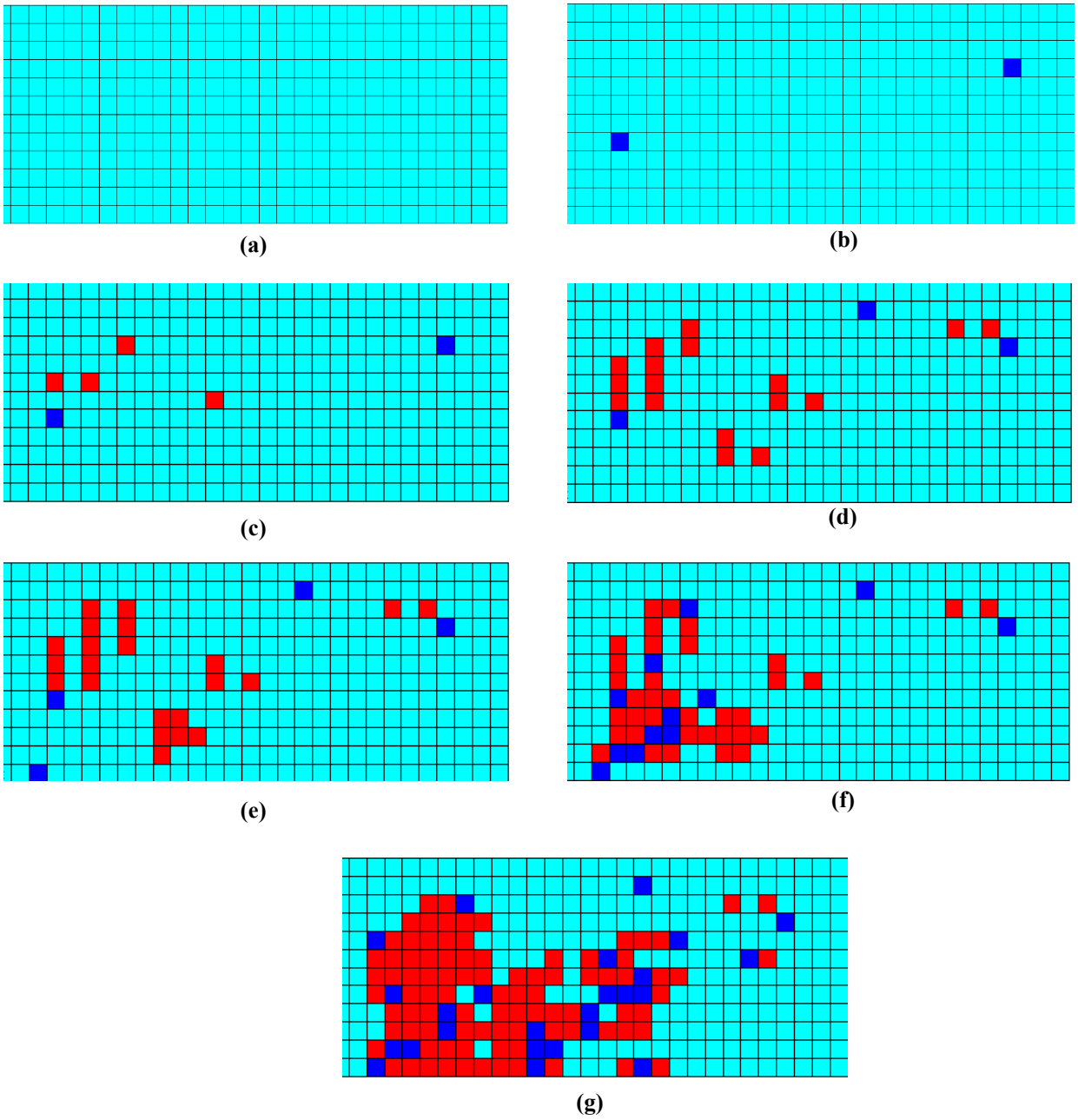

Figure 5-15: Damage evolution for cross-ply with gap in 90^{o} layer at 1200 MPa up to 43000 cycles

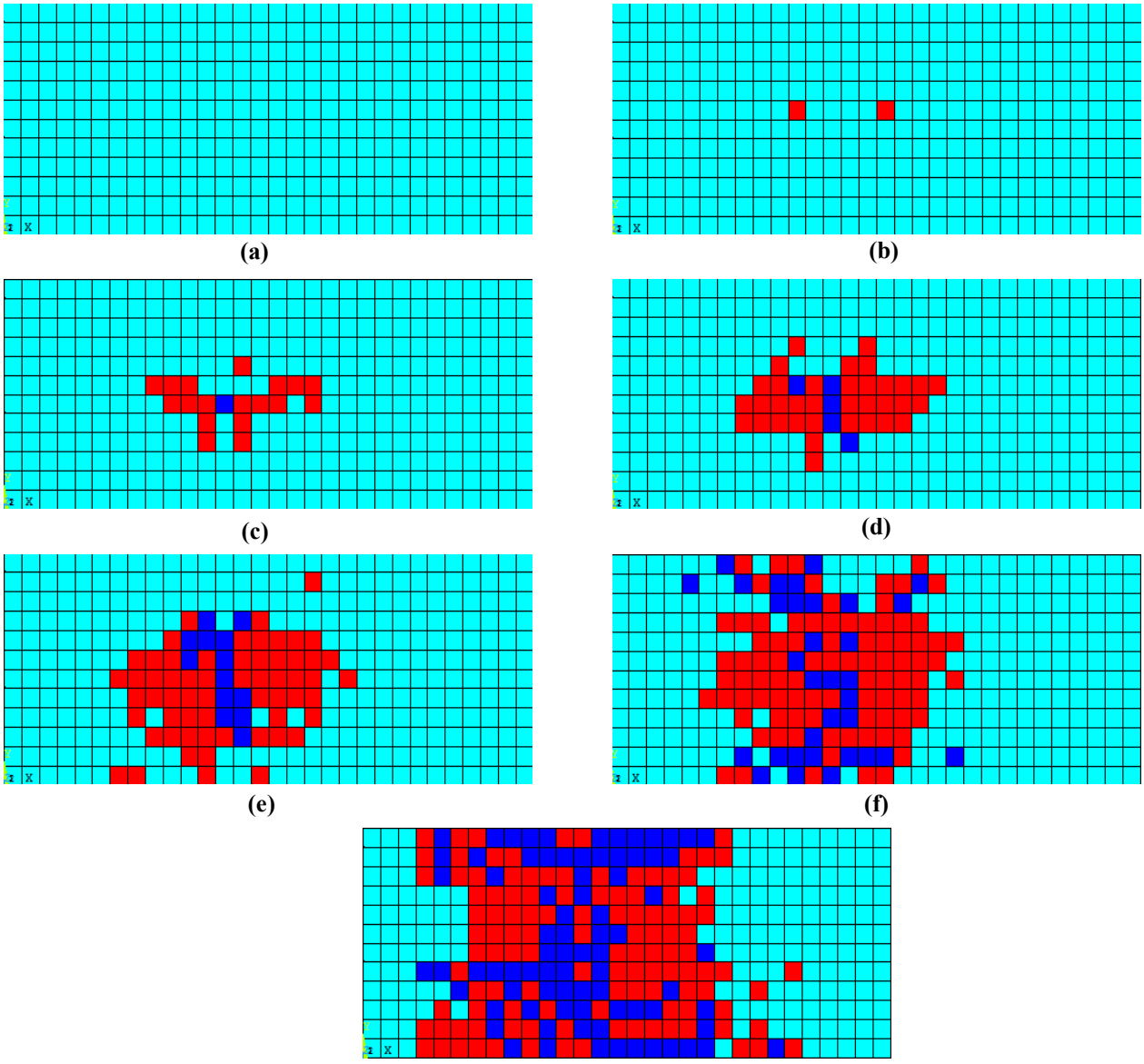

Figure 5-16: Damage evolution for cross-ply with gap in 90^{o} layer at 1200 MPa up to 140000 cycles

Figure 5-17 shows the variation in the number of cycles to failure as a result of considering the variation in mechanical properties for a cross-ply laminate containing a gap in 90^{o} layer. The illustrated results are for eight virtual samples at two applied stress levels. These results can show the effect of the non-uniformity in the material on the scattering in the fatigue life of tested

specimen. Figure 5-18 shows a comparison between the experimental and the predicted life of FPDM for carbon/epoxy cross-ply laminate with gap in 90º layer at different applied stress level.

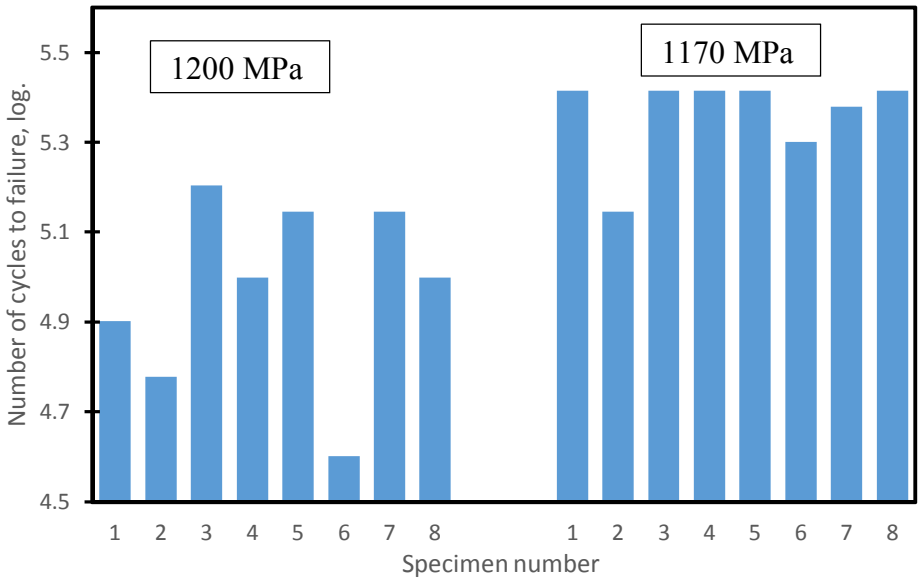

Figure 5-17: Effect of properties variation on fatigue life of cross-ply laminates with gaps in 90º at 1200 and 1170 MPa.

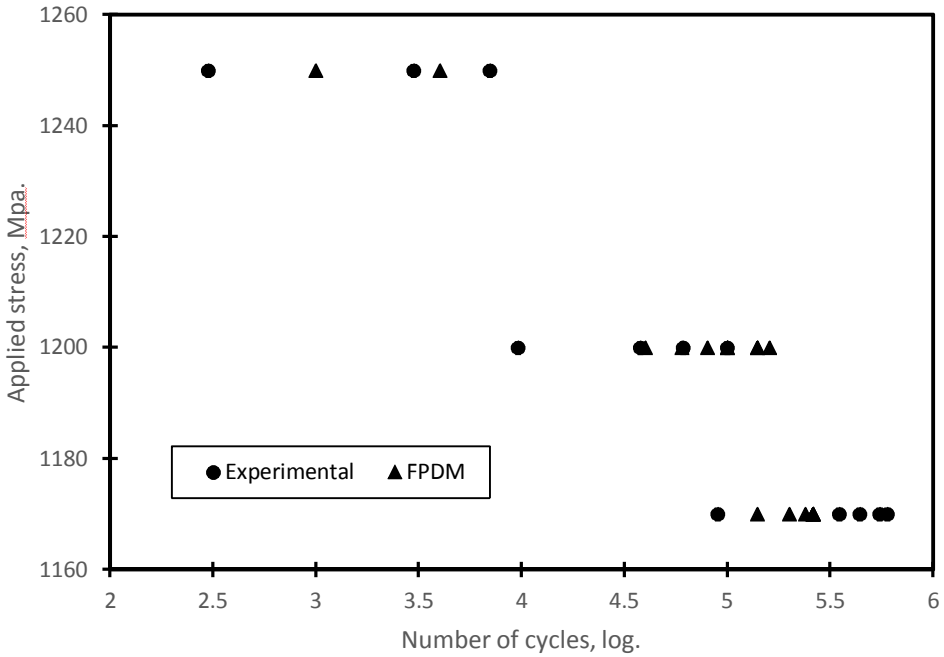

Figure 5-18: Comparison between the predicted FPDM and experimental results for cross-ply laminate with gap in 90º layer

The same procedures were performed for the FPDM of quasi-isotropic (90/45/-45*/0/0/0/-45/45/90) with gaps in 45° layer. Random values were generated for each mechanical property and then they were assigned to the elements of the FPDM to account for the scattering in the mechanical properties. Then, the model was solved several times to obtain the scattering in the fatigue life.

Figure 5-19, Figure 5-20 and Figure 5-21 show the damage evolution for different random distributions of properties for a quasi-isotropic laminate (90/45/-45*/0/0/0/-45/45/90) with gap created in -45° layer. The illustrated images are for the 0° layer adjacent to the defective -45° layer in the laminate, denoted by a bar in the stacking sequence (90/45/-45*/$\overline{0}$/0/0/-45/45/90). Damage starts randomly at the weak locations. Then, damage propagates due to stress redistribution from the failed to intact elements. Fiber failure occurs and propagates aggressively up to final failure of the laminate. Figure 5-22 shows the variation in the fatigue life for quasi-isotropic laminates with gaps in -45° layers. Figure 5-23 shows the comparison between the predicted results from the FPDM and the experimental results.

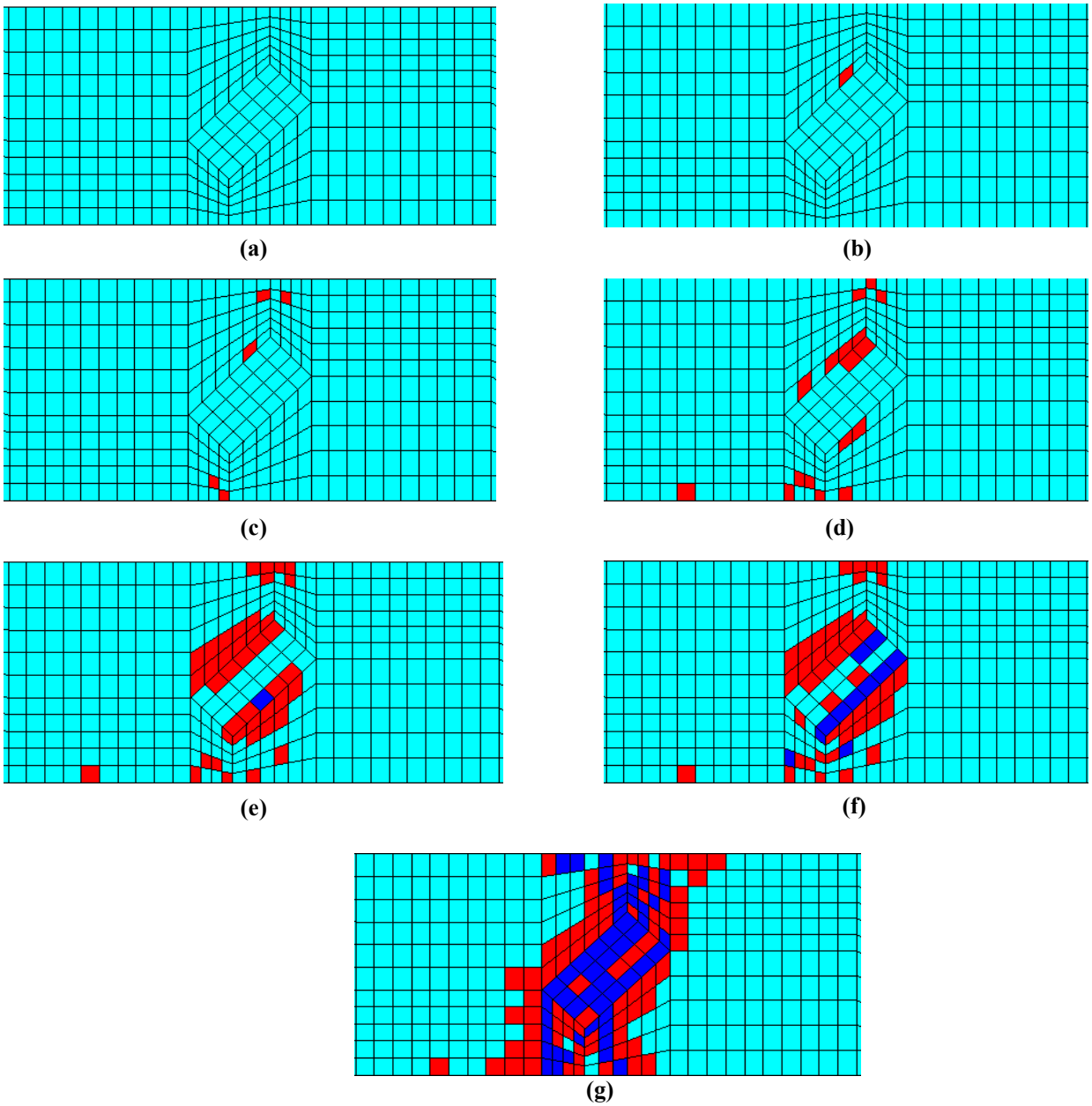

Figure 5-19: Damage evolution for quasi-isotropic laminate with gap in -45º layer at 750 MPa up to 17000 cycles

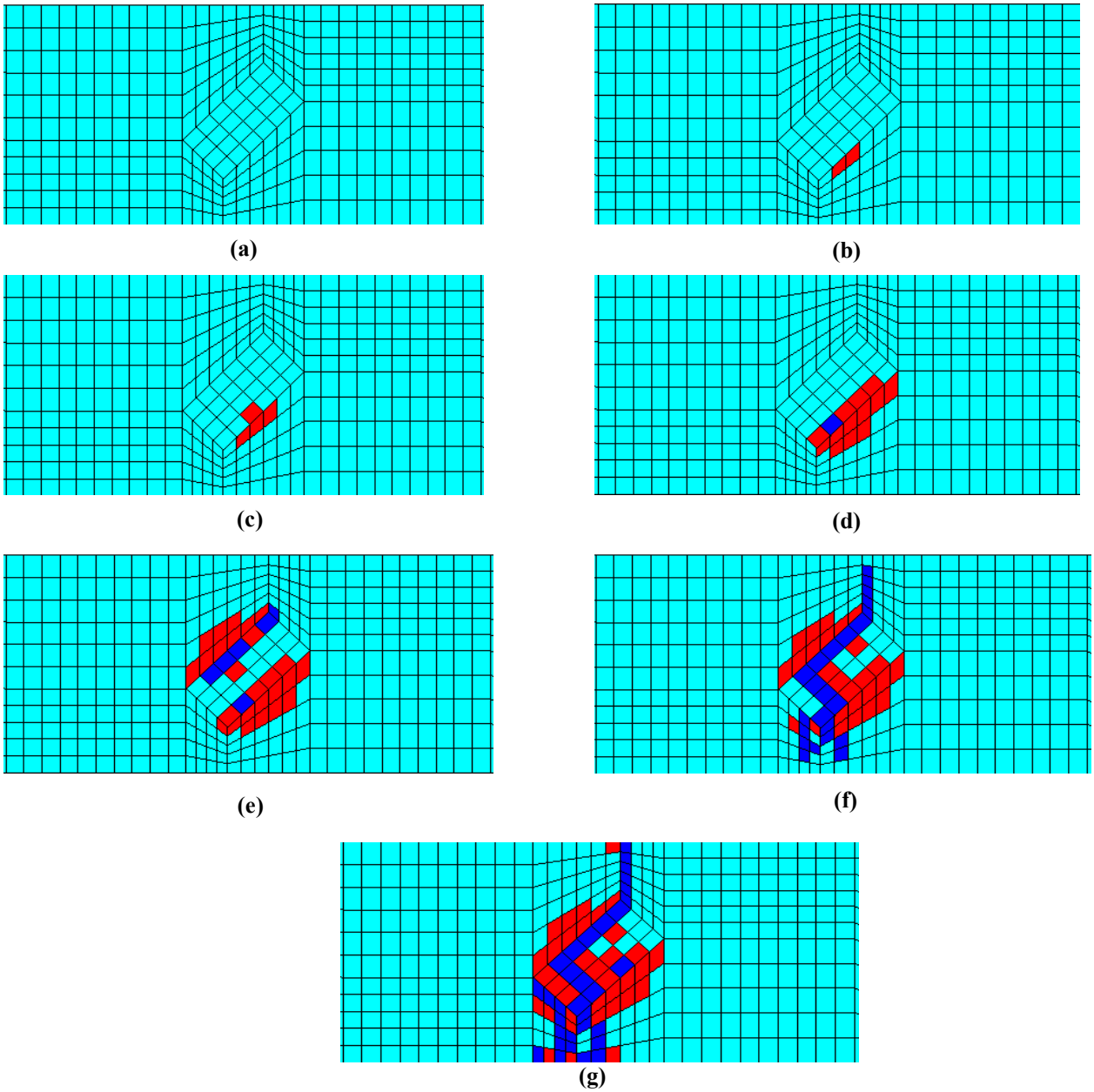

Figure 5-20: Damage evolution for quasi-isotropic laminate with gap in 45^{o} layer at 750 MPa up to 18000 cycles

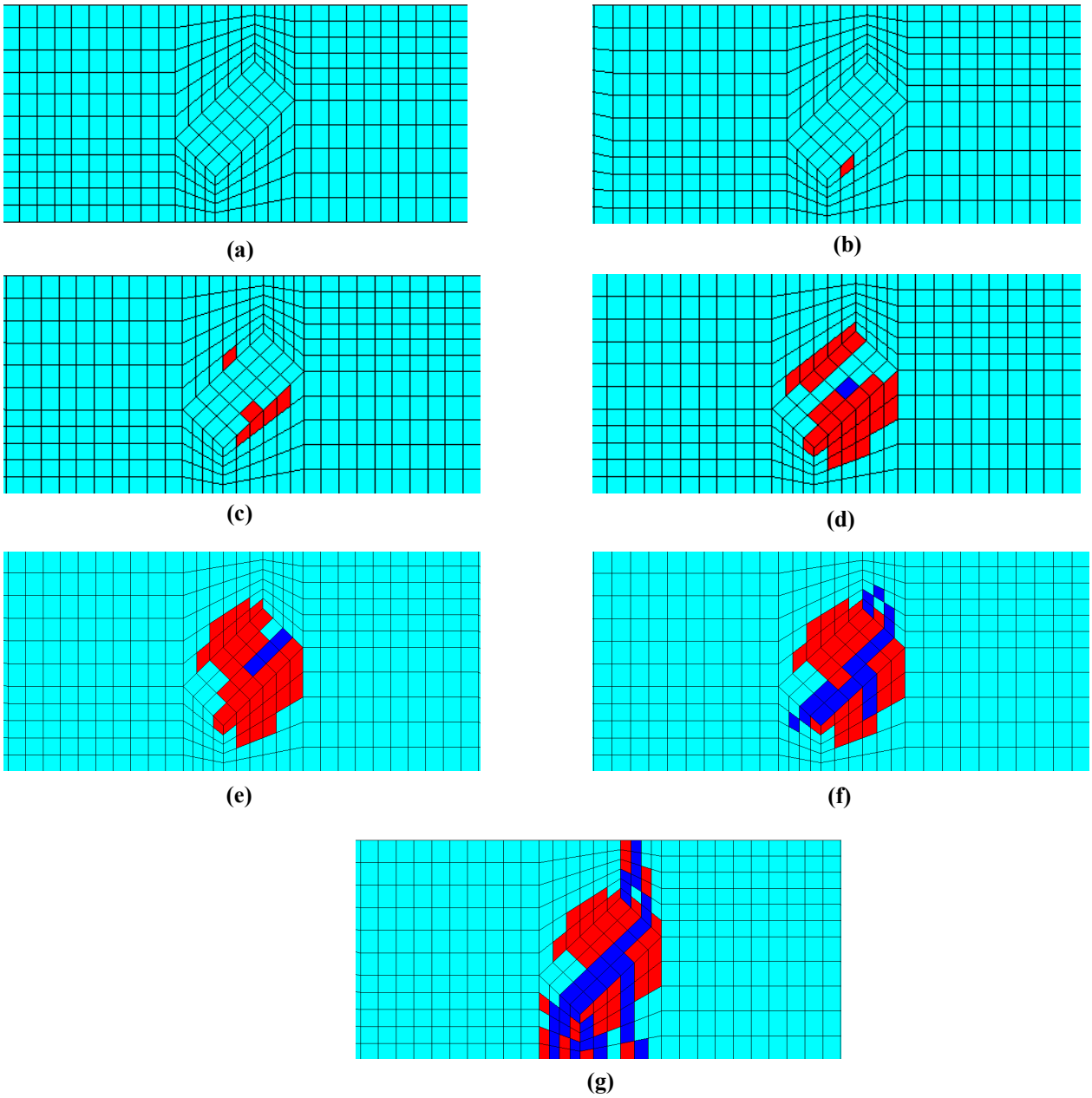

Figure 5-21: Damage evolution for quasi-isotropic laminate with gap in 45° layer at 750 MPa up to 28000 cycles

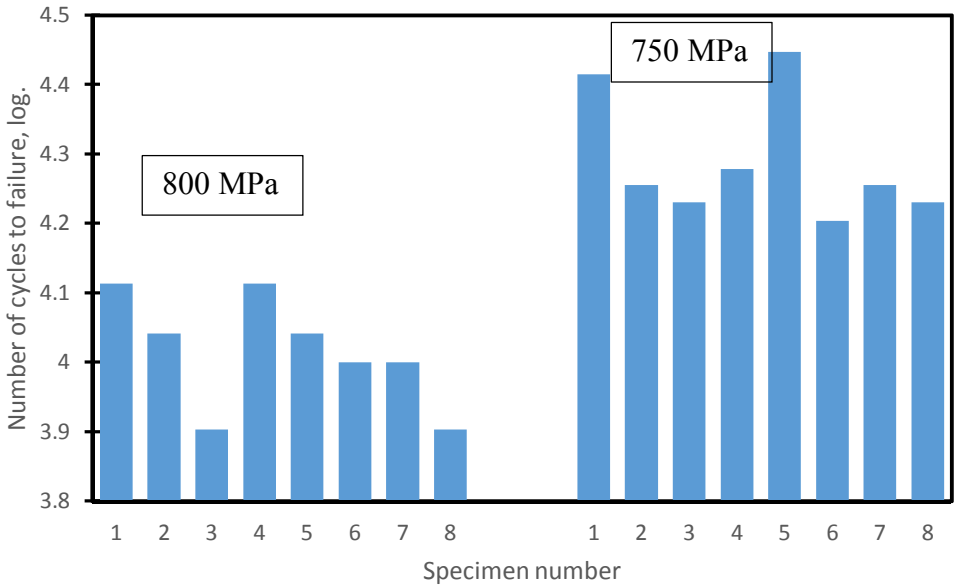

Figure 5-22: Effect of properties variation on fatigue life of quasi-isotropic laminates with gaps in 45^{o} at 750 and 800 MPa.

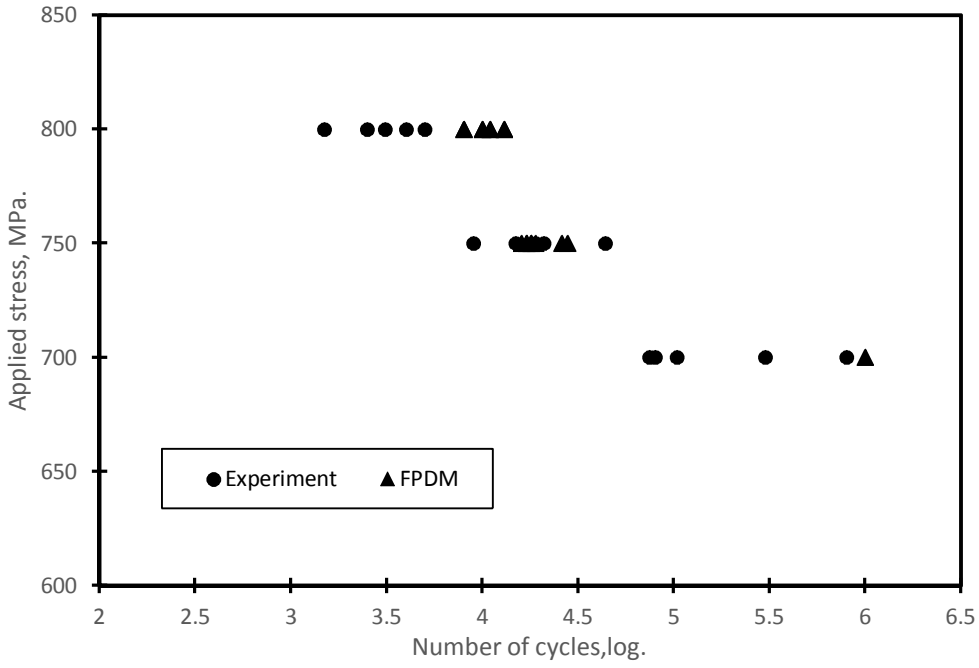

Figure 5-23: Comparison between the predicted FPDM and experimental results for cross-ply laminate with gap in 90^{o} layer

The observed variation in the results for the cross-ply and quasi-isotropic laminates confirms the complexity of the damage behavior in the case of off-axis laminates and the difficulty of modeling such laminates as a result of the non-uniformity and randomness of the mechanical properties which greatly affect the performance of this type of laminates.

5.2.3 **Gap with different shapes**

The FPDM was applied for the case of laminates containing triangular gaps to investigate its applicability for different gap shapes. A unidirectional laminate was modeled and a triangular volume was created in the middle layer to represent a triangular gap. Resin properties were assigned to the elements representing the triangular volume.

One of the interesting observations was that the generated interlaminar shear stress at the inclined edge (denoted as edge (1)) of the gap was less as compared to that generated at the other straight edge (denoted as edge (2)) as shown in Figure 5-24. This might be attributed to the gradual cutting of fibers at the inclined edge of the triangular gap which reduced the amount of load transferred between the cut fibers and the intact fibers in the adjacent layer. Consequently, the generated interlaminar stresses are less at the inclined side.

Figure 5-25 shows the damage evolution from the triangular gap in a unidirectional laminate. Damage process starts by delamination at the elements adjacent to the straight edge of the triangular gap. Then, by increasing the cycles, delamination initiated at the elements adjacent to the other inclined side of the gap. At the end of the fatigue life fiber failure occurs and aggressively propagates across the specimen width.

The FPDM was tested for triangular gaps with different aspect ratios to be compared with performed experiments. Figure 5-26 shows a comparison between the predicted fatigue life and the obtained from experiments at 1850 MPa and for three aspect ratios (1, 2 and 3). It can be observed that the predicted fatigue lives for different aspect ratios are close to each other which was confirmed from the performed experiments. The overestimation of the predicted results can be attributed to the used parameters in the FPDM or the real manufacturing defects as explained previously for the case of unidirectional laminates with gaps in 0^o layers.

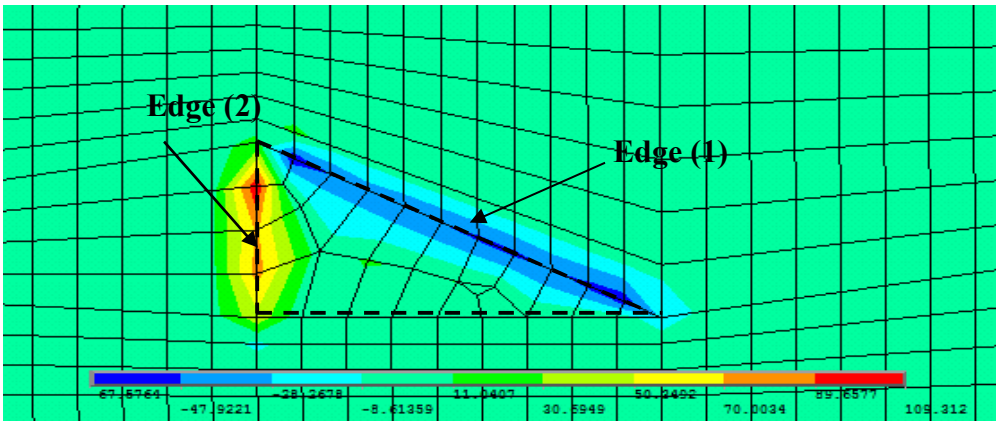

Figure 5-24 Interlaminar stress distribution at the boundaries of the triangular gap

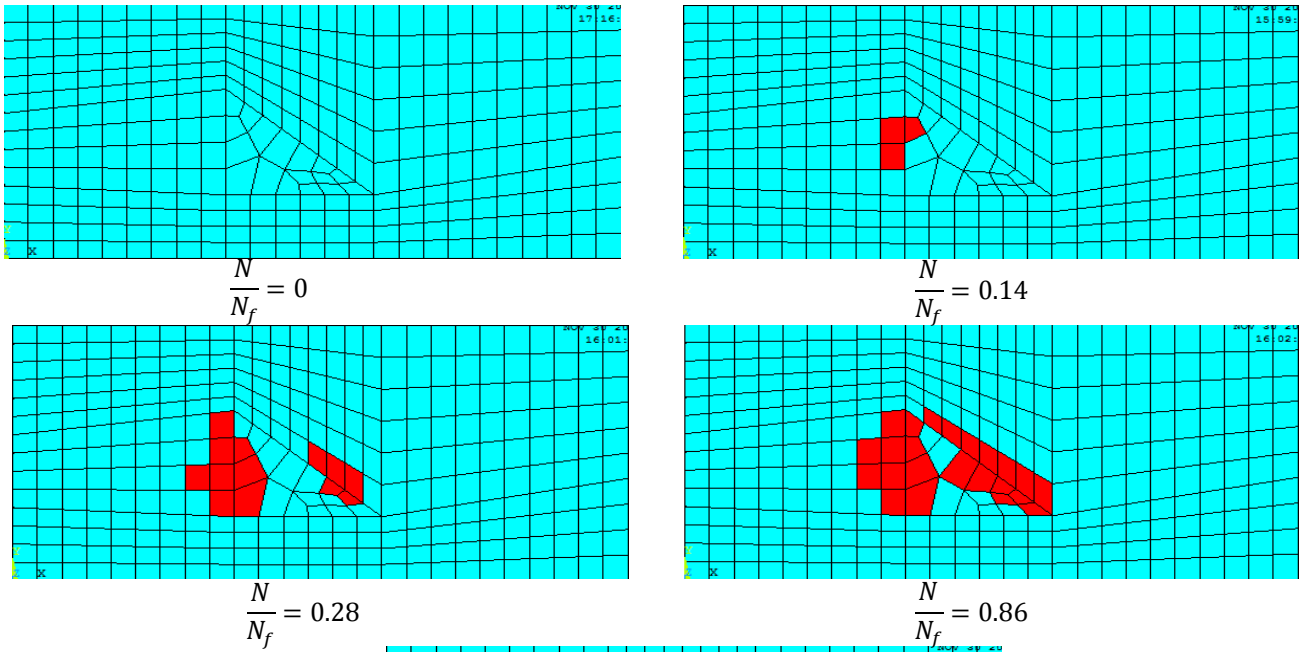

$\frac{N}{N_f} = 0$ $\frac{N}{N_f} = 0.14$

$\frac{N}{N_f} = 0.28$ $\frac{N}{N_f} = 0.86$

$\frac{N}{N_f} = 1$

Figure 5-25: Damage evolution for unidirectional laminate with triangular gap at 1850 MPa

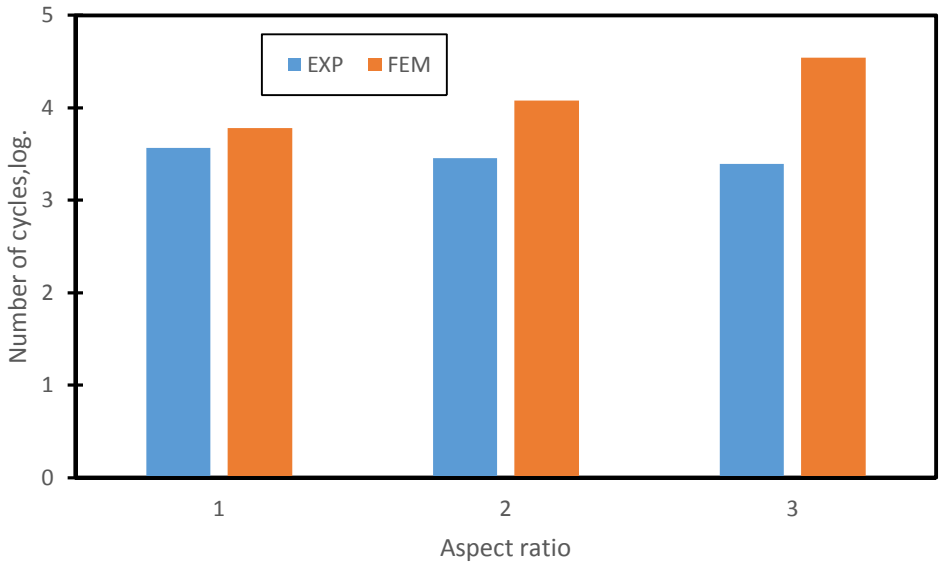

Figure 5-26: Comparison between the predicted FPDM and experimental results for unidirectional laminate with triangular gaps with different aspect ratios at 1850 MPa.

5.2.4 **Defective laminates with more than one gap**

Initially, it was required to investigate the effect of adding more gaps on fatigue performance experimentally by creating two gaps in unidirectional laminates and subjecting the specimens to fatigue loading. Since the two created gaps can be separated by any distance along the width or the length of the specimen, so it was decided to test the worst case scenario. This case can be determined by manufacturing and testing specimens with two gaps at variety of separating distances along both width and length direction. This was found to be impractical and very material and time consuming.

The FPDM was used to save time and material required to perform fatigue tests. Different models were developed containing two gaps with different separating distances along length and width to investigate the effect of the distance between gaps on fatigue life from which the critical case can be determined. The distance between the two created gaps was defined as (X, Y) which is the distance, in mm, between the centers of the two gaps along the length (X-) and width (Y-)

directions. Figure 5-27 shows the number of cycles to failure at applied stress of 1900 MPa for unidirectional specimens containing two gaps with 25 different separating distances between the gaps' centers along the width and length of specimens.

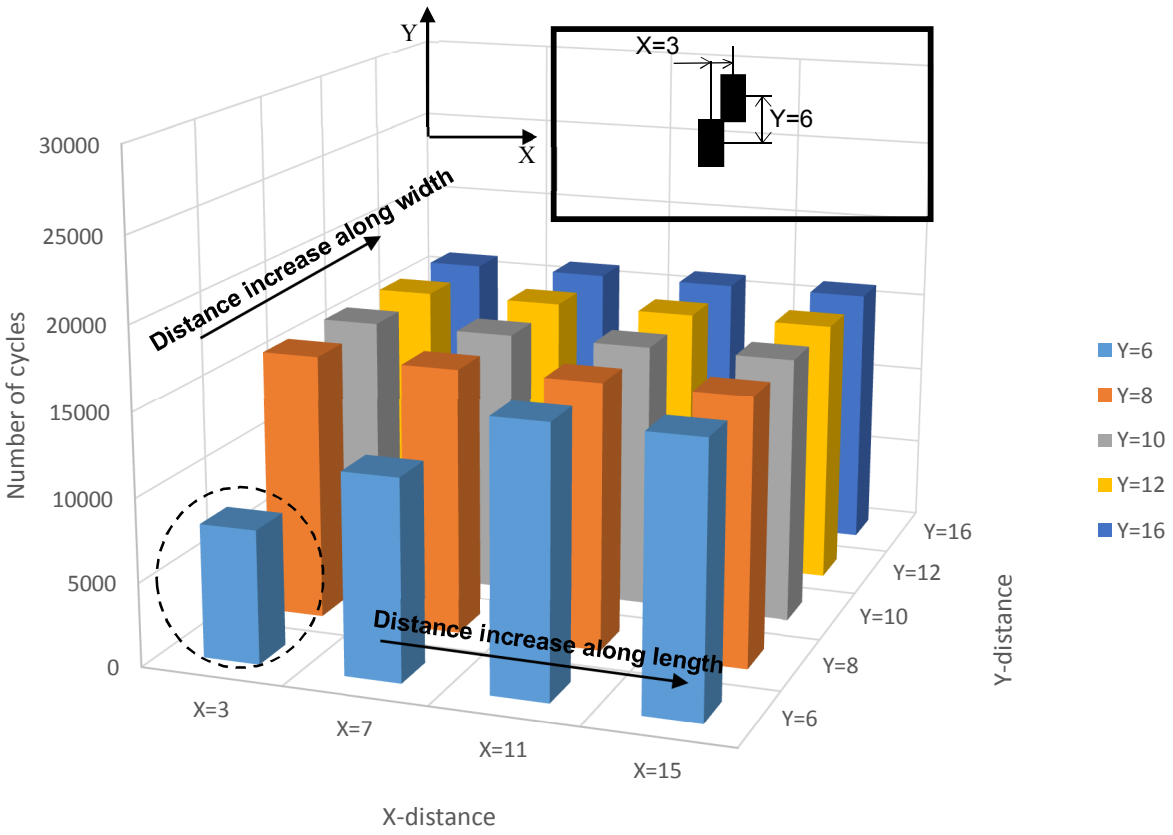

Figure 5-27: Effect of separating distance between 2 gaps on fatigue life for unidirectional laminate at 1900 MPa.

It can be observed that the critical situation, denoted by dashed circle in Figure 5-27,with the smallest fatigue life was found at (X,Y) = (3,6) which occurs when the two gaps are created as shown in the scheme of the gaps illustrated in Figure 5-27. As the distance between the centers of the gaps increases along the length and/or the width directions the fatigue life increases. This was confirmed later by performing fatigue tests for laminates containing two gaps with separating

distance between centers of (3,6) and (10,6) as shown in the experimental results of investigating the effect of adding more gaps.

Figure 5-28 shows the interlaminar shear stress distribution, responsible for the delamination occurrence in the defective specimen, for the case of laminate with two gaps at separating distances between centers (X,Y) of (3,6) and (10,6) mm. It can be observed that there is an increase in the maximum value of shear stress of about 12% for the case of two gaps of (3,6) separating distance compared to the case of (10,6) separating distance. So, it can be concluded that as the distance between the two gaps increases, their effect on each other decreases. This helps reducing the generated interlaminar shear stresses and eventually increases the fatigue life. This was confirmed from the experiments.

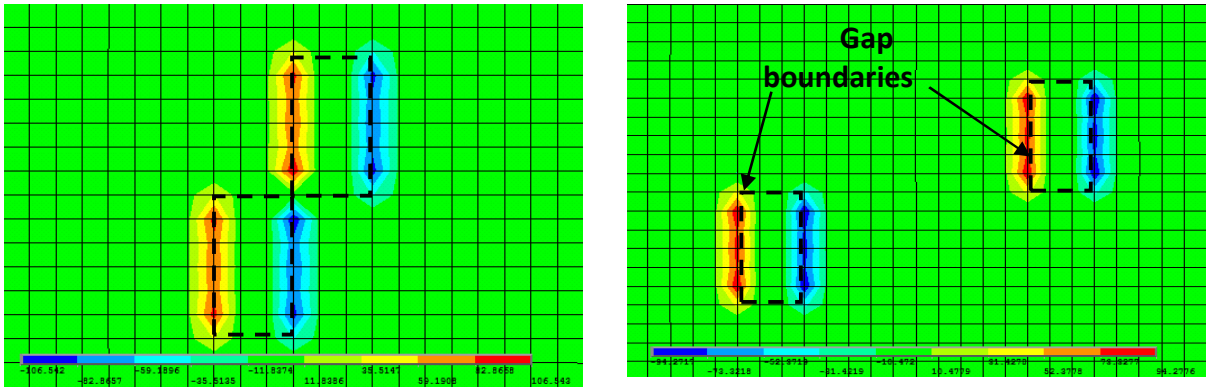

(a) (b)

Figure 5-28 Shear stress distribution for two gaps with separating distances of (a) (3,6) and (b) (10,6).

Figure 5-29 shows the damage evolution from the 2 created gaps in a unidirectional laminate with a separating distance between centers of (X,Y) = (3,6). Delamination initiated at the two gaps at the same time and by increasing the number of cycles it propagated as a result of redistribution of stress from the failed to intact elements. At the ends of the fatigue life, fiber failure occurred at the 2 gaps and it propagated aggressively across the width of the specimen up to final failure.

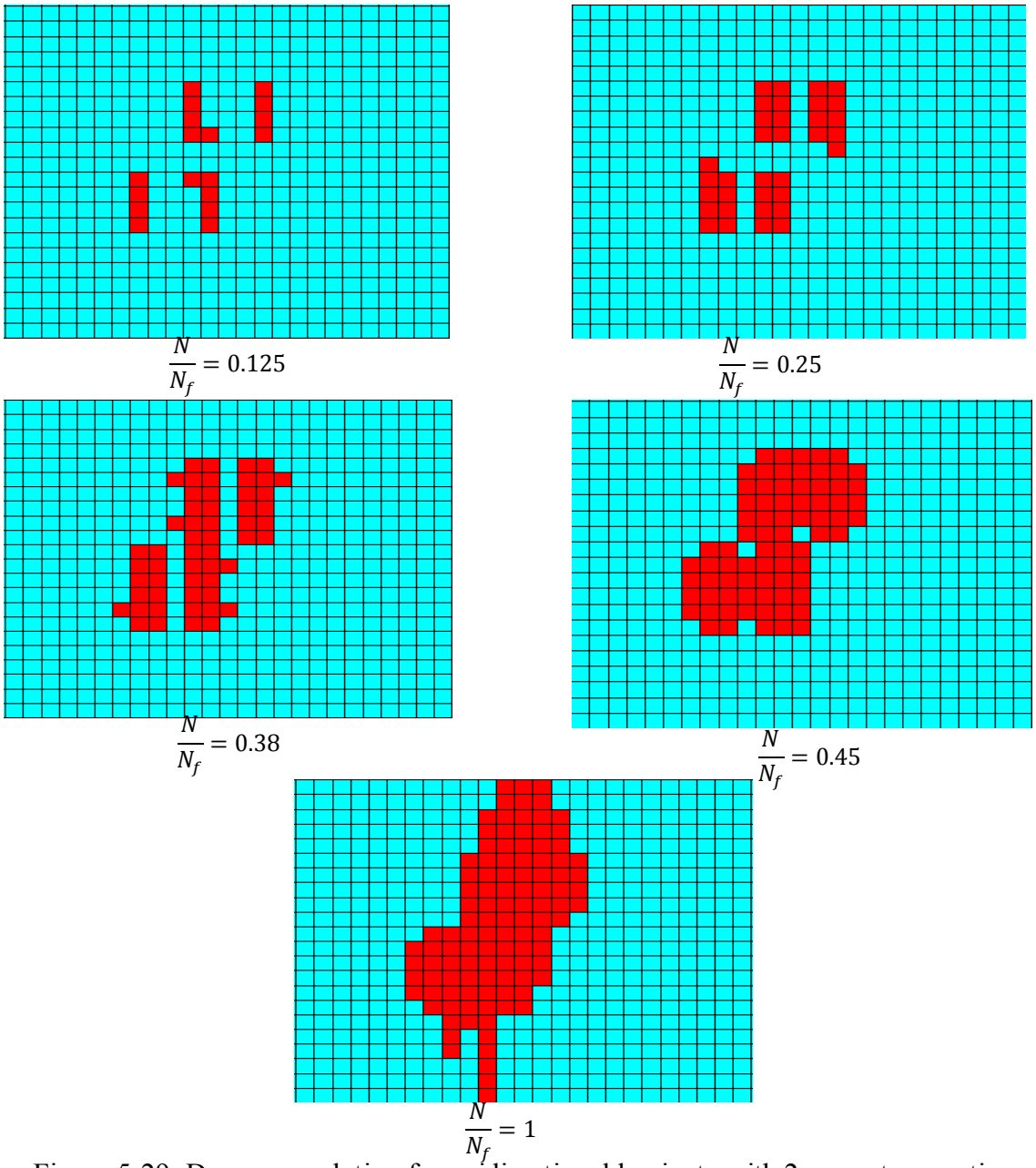

Figure 5-29: Damage evolution for unidirectional laminate with 2 gaps at separating distance of (3,6)

Figure 5-30 and Figure 5-31 show the comparison between the predicted fatigue life from the FPDM and the experimental results of the fatigue tests for the cases of unidirectional laminates containing two in-plane gaps and two out-of-plane gaps, respectively. It can also be observed that the FPDM over predicts the fatigue life which might be attributed to the reasons mentioned previously for the case of unidirectional laminates.

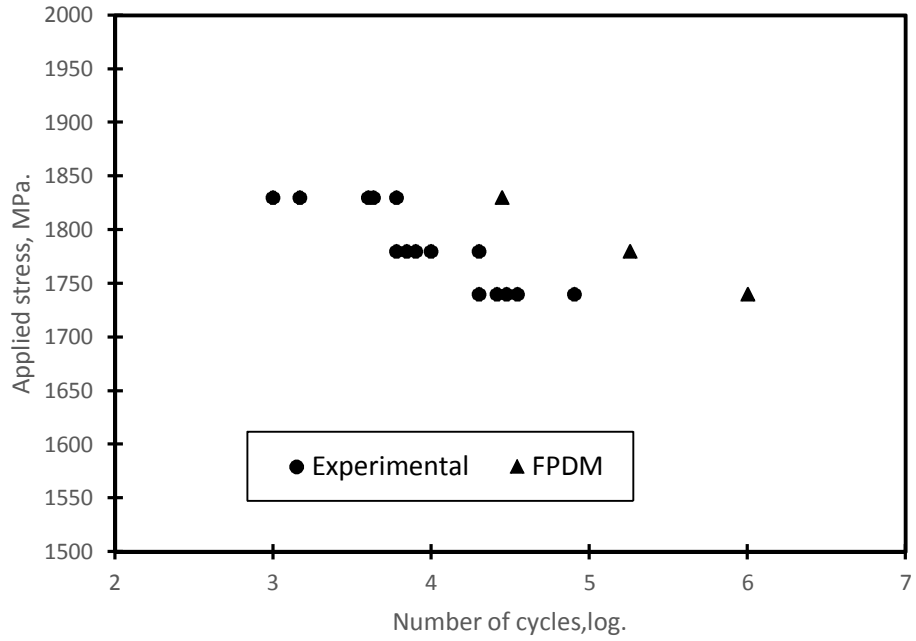

Figure 5-30: Comparison between the predicted FPDM and experimental results for unidirectional laminates with 2 in-plane gaps

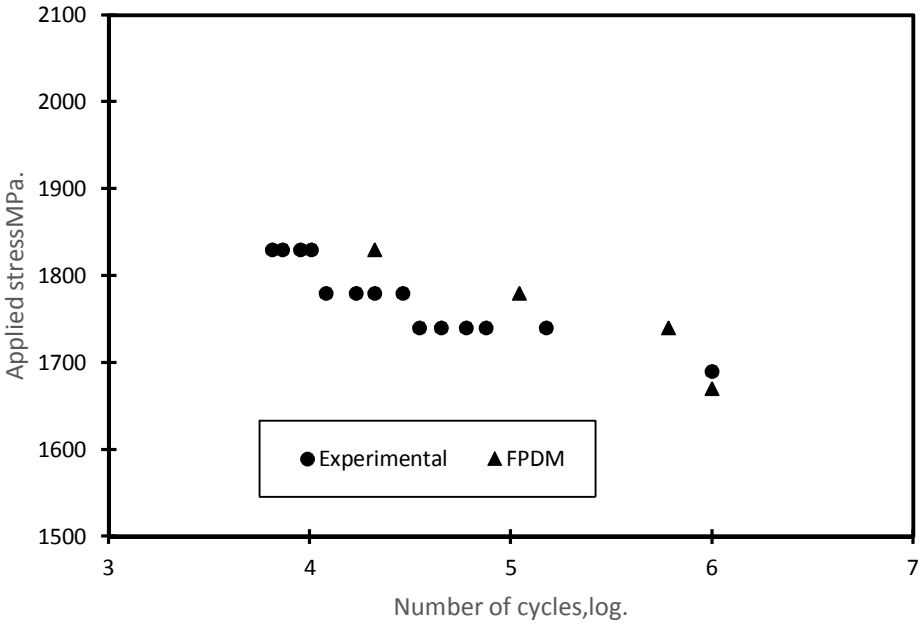

Figure 5-31: Comparison between the predicted FPDM and experimental results for unidirectional laminates with 2 out-of-plane gaps

5.3 **Summary**

A fatigue progressive damage model (FPDM) was developed using Ansys Parametric Design Language (APDL) to simulate the laminates containing gaps as a representation of induced defects during composite manufacturing using AFP. The model is an integration of stress analysis, failure analysis, fatigue life model, gradual and sudden degradation of mechanical properties.

The predicted results from the FPDM were compared with results obtained from the performed fatigue experiments while considering different parameters such as gap orientation, gap shape and number of gaps. The damage mechanisms predicted from the FPDM for the case of unidirectional laminates agreed well with the observed ones from experiments. For the case of cross-ply and quasi-isotropic laminates, the model predicted the occurrence of different damage mechanisms except for the occurrence of the transverse cracks, which were observed in the experimentally tested specimens, propagating through 0^o layers from delamination due to the gap to the interface of $0^o/90^o$ or $0^o/45^o$ layers. Using interface elements at the interface between layers might help in better simulation of damage mechanisms.

Non-uniformity and variation of mechanical properties of composite material are the main reasons for the scattering of the results especially for the case of off-axis laminates as shown in Figure 5-17 and Figure 5-22. The effect of non-uniformity was incorporated in the model to address this problem. This was done by assigning random values of the material properties to the different elements in the model. The obtained results showed the large variation in the predicted fatigue life as a result of the variation in mechanical properties.

To sum, in spite of the observed deviation in the predicted fatigue life from the experimental results, this model can be useful in the preliminary design steps to have an idea about the damage behavior and the performance of the designed part. For more accurate results, some further steps might be performed as it will be mentioned in the future work.

Chapter 6 Conclusions, contributions and recommendations for future work

6.1 Conclusions

According to the thesis work, presented in previous chapters, the following points are concluded:

- Existence of the induced gaps during AFP manufacturing affects the fatigue performance of laminates with different stacking sequences. The reduction in the fatigue life due to gaps depends on the applied stress level. At high stresses, the reduction in fatigue life is high and it decreases by reducing the maximum stress in the fatigue cycles.
- The effect of induced gaps on fatigue life decreases till reaching a threshold stress below which there is no effect for the gaps on fatigue life. This value of stress can be defined as the intersection point of the stress/life curves of both reference, free from defects, and

defective laminates. The threshold stress values for the laminates tested in the study were found to range between 55 – 70% of the tensile strength of the laminate. So, in order to avoid the effect of the gap during fatigue loading, the applied stress should be less than the threshold values.

- The stress/life curves can be obtained by conducting long fatigue tests till final failure of the tested specimens. This method was found to be very material and time consuming.
- In defective laminates with gaps in 0^o layer, it was found that as a result of transferring the load from the defective 0^o layer to the adjacent intact 0^o layers, high interlaminar stresses generate at the interface. This facilitates the occurrence of delamination at the interface between the defective 0^o layer and the surrounding layers.
- For the case of cross-ply and quasi-isotropic laminates with gaps in 0^o layer, in addition to the delamination at the interface of the defective layer and the adjacent layers, there are transverse cracks that propagate from the delamination to the closest interface of $0^o/90^o$ or $0^o/45^o$ layers. The transverse propagation of these cracks through the intact 0^o layers affects their integrity which eventually influences the performance of the laminate.
- For cross-ply laminates with gaps in 0^o layers, the existence of 90^o layer at one layer away of the gap location helps blocking the transverse propagation of cracks which alleviates its effect in the cross-ply laminates.
- For quasi-isotropic laminates with gaps in 0^o layers, the existence of $\pm 45^o$ layers directly adjacent to the defective 0^o layers helps in gradual transition of load and controls the occurrence of the delamination especially at the interface of intact 0^o layers.
- Fatigue testing of laminates with triangular gaps of different sizes revealed that the effect of changing the shape and the size of the gap was small compared to the effect of inducing the gap in the laminate. Consequently, the gaps in 0^o layers have a severe effect on fatigue life regardless their shape or size.
- For unidirectional laminates with multiple gaps, it was found that the additional reduction in the threshold stress due to adding more gaps in the same layer or in different layers was small compared to the initial severe reduction of creating the first gap in the laminate. In

addition, it was concluded that increasing the staggering distance between the gaps in different layers helps improving the performance of the laminate.

- Existence of gaps in 90^o layers has no effect on the fatigue performance of the AFP laminates. However gaps in 45^o layers have a less effect on fatigue life compared to those in 0^o layers.

- Infrared (IR) thermography was found to be a highly effective method for in-situ detection of non-uniformity in the laminates such as the existence of gaps generated during AFP manufacturing. As a result of damage occurrence within the laminate due to gaps, heat is generated at the location of damage. This heat is transferred through the thickness of the laminates causing a surface temperature increase which can be captured using IR thermography.

- IR thermography and Risitano method were applied to the case of AFP laminate containing gaps for the purpose of rapid evaluation of the threshold stress value for the defective specimens. Thermal observations of gapped specimens with different stacking sequences showed a bilinear relation between the rate of the temperature increase during the first 1000 cycles in fatigue life and the applied stress from which the threshold stress could be obtained. The obtained results showed good agreement with the results obtained from the conventional method. This has a great potential in saving time and material needed while using the traditional method.

- A fatigue progressive damage model (FPDM) was developed and applied to the case of defective laminates containing gaps in order to predict the damage growth and final failure of laminates. The developed FPDM is helpful in saving material and time required for manufacturing specimens and performing long fatigue tests especially in the initial design steps.

6.2 **Contributions**

The main contributions of this study are:

1- Investigating the effect of the induced gaps on the fatigue performance of the laminate manufactured by Automated Fiber Placement process. To the best of our knowledge, no work has been performed in this field. Many parameters were considered during the study such as the stacking sequence, gap shape, gap orientation and number of gaps.
2- Based on understanding the performance of the defective laminates, a few design recommendations lines were proposed that can be helpful for design of laminates manufactured by AFP.
3- Infrared thermography and Risitano method was applied to the case of laminates containing gaps to rapidly evaluate the fatigue threshold stress values. This is a novel application of this technique into the field of AFP laminates containing gaps that can help saving time and material.
4- A FPDM was developed and applied to the case of laminates containing gaps. This is a new application of this type of models to the case of AFP laminates containing gaps that are representative to the induced defects during manufacturing.

6.3 **Recommendations for future work**

According to this study, some future work can be recommended as follows:

- Investigating the effect of gaps under different fatigue loading conditions such as compression-tension or compression-compression loading.
- Investigating the fatigue performance of laminates with gaps that emerge parallel to fibers at the boundaries of tows which might happen as a result of inaccuracy of the AFP machine.
- Investigating the effect of gaps at the end of tows, normal to fibers, for the case of variable stiffness laminates subjected to fatigue loading.
- Investigate the effect of gaps on fatigue performance of AFP laminates cured without using caul plates.

- Studying the effect of the changing the location of the gap across the width especially for the case of cross-ply and quasi-isotropic laminates to account for the interaction between the edge effect and the gap effect.
- Investigating the applicability of using IR thermography techniques in both evaluating the threshold stress and damage detection with different material having less thermal conductivity such as glass fiber composites.
- Fully fatigue characterizing the used material for better prediction of FPDM results.
- Applying and validating the used FPDM for different loading conditions.
- Using cohesive zone elements at the interfaces of the defective layers for better practical simulation of damage between interfaces.
- Considering the viscoelastic behavior of the laminates under fatigue loading in the used FPDM.

6.4 **Publications**

1- Y. M. Elsherbini and S. V. Hoa, "Experimental and numerical investigation of the effect of gaps on fatigue behavior of unidirectional carbon/epoxy automated fiber placement laminates," *Journal of Composite Materials,* 2017,vol. 51, pp. 759-772

2- Y. M. Elsherbini and S. V. Hoa, "Fatigue threshold-stress determination in AFP laminates containing gaps using IR thermography," *Composites Science and Technology,* 2017, vol. 146, pp. 49-58.

3- Y. ELsherbini and S. Hoa, "Fatigue Behavior of Unidirectional Carbon/Epoxy AFP Laminates Containing Gaps," in *Proceedings of the American Society for Composites: Thirty-First Technical Conference*, 2016.

6.5 **Messages to designer:**

1- The threshold of the material is determined using the traditional Wohler method or IR thermography.
2- If the applied stresses were lower than the threshold values, then the existence of gaps can be neglected.
3- If the applied stresses were higher than the threshold values, then putting ±45^{o} layers directly adjacent to the defective 0^{o} layers helps improving the behavior of the defective laminates.

References

[1] www.Boeing.com/commercial/787.

[2] A. K. Kaw, *Mechanics of composite materials*. Boca Raton, Florida: CRC press, 2010.

[3] M. N. Grimshaw, C. G. Grant, and J. M. L. Diaz, "Advanced technology tape laying for affordable manufacturing of large composite structures," in *International SAMPE Symposium and Exhibition*, 2001, pp. 2484-2494.

[4] http://www.mmsonline.com/.

[5] R. B. Deo, J. H. Starnes, and R. C. Holzwarth, "Low-cost composite materials and structures for aircraft applications," in *NATO RTO AVT Panel spring symposium and specialists' meeting Loen, NORWAY*, 2001.

[6] Z. Gürdal, B. F. Tatting, and C. Wu, "Variable stiffness composite panels: effects of stiffness variation on the in-plane and buckling response," *Composites Part A: Applied Science and Manufacturing,* vol. 39, pp. 911-922, 2008.

[7] C. S. Lopes, P. P. Camanho, Z. Gürdal, and B. F. Tatting, "Progressive failure analysis of tow-placed, variable-stiffness composite panels," *International Journal of Solids and Structures,* vol. 44, pp. 8493-8516, 2007.

[8] M. Rouhi, H. Ghayoor, S. V. Hoa, and M. Hojjati, "The effect of the percentage of steered plies on the bending-induced buckling performance of a variable stiffness composite cylinder," *Science and Engineering of Composite Materials,* vol. 22, pp. 149-156, 2015.

[9] Z. Gürdal, B. F. Tatting, and K. C. Wu, "Tow-placement technology and fabrication issues for laminated composite structures," in *Proceedings of the AIAA/ASME/ASCE/AHS/ASC structures, 46th structural dynamics & materials conference*, 2005.

[10] www.pasini.ca.

[11] A. W. Blom, "Structural performance of fiber-placed, variable-stiffness composite conical and cylindrical shells," PhD, department of aerospace engineering, TU Delft, Delft University of Technology, 2010.

[12] M. Dupuis, "DESIGN FOR MANUFACTURE FOR AIRFRAME STRUCTURE OPTIMIZATION," Coriolis Composites, France.

[13] W. A. T. Walker, L. Ilcewicz, C. Poe, "Tension fracture of tow-placed laminates for transport fuselage," in *Fibrous Composites in Structural Design*, United States, 1991, pp. 747-78.

[14] D. S. Cairns, L. B. Ilcewicz, and T. Walker, "Far-field and near-field strain response of Automated Tow-Placed laminates to stress concentrations," *Composites Engineering,* vol. 3, pp. 1087-1097, 1993.

[15] H. Hsiao and I. Daniel, "Effect of fiber waviness on stiffness and strength reduction of unidirectional composites under compressive loading," *Composites Science and Technology,* vol. 56, pp. 581-593, 1996.

[16] D. O. H. Adams and M. W. Hyer, "Effects of layer waviness on the compression fatigue performance of thermoplastic composite laminates," *International Journal of Fatigue,* vol. 16, pp. 385-391, 8// 1994.

[17] A. Sawicki and P. Minguet, "The effect of intraply overlaps and gaps upon the compression strength of composite laminates," in *39th AIAA structural, dynamics, & materials conference. Long Beach, CA*, 1998, pp. 744-54.

[18] K. Croft, L. Lessard, D. Pasini, M. Hojjati, J. Chen, and A. Yousefpour, "Experimental study of the effect of automated fiber placement induced defects on performance of composite laminates," *Composites Part A: Applied Science and Manufacturing,* vol. 42, pp. 484-491, 2011.

[19] N. C. Kimball, "Open hole compressive behavior of laminates with converging gap defects," Mechanical Engineering, The University of Utah, 2011.

[20] M. A. Nik, K. Fayazbakhsh, D. Pasini, and L. Lessard, "Optimization of variable stiffness composites with embedded defects induced by automated fiber placement," *Composite Structures,* vol. 107, pp. 160-166, 2014.

[21] A. W. Blom, C. S. Lopes, P. J. Kromwijk, Z. Gurdal, and P. P. Camanho, "A theoretical model to study the influence of tow-drop areas on the stiffness and strength of variable-stiffness laminates," *Journal of composite materials,* vol. 43, pp. 403-425, 2009.

[22] K. Fayazbakhsh, M. Arian Nik, D. Pasini, and L. Lessard, "The Effect of Gaps and Overlaps on the In-Plane Stiffness and Buckling Load of Variable Stiffness Laminates

Made by Automated Fiber Placement," in *Proceedings of 15th European Conference on Composite Materials, Venice, Italy*, 2012.

[23] K. Fayazbakhsh, M. A. Nik, D. Pasini, and L. Lessard, "Defect layer method to capture effect of gaps and overlaps in variable stiffness laminates made by automated fiber placement," *Composite Structures,* vol. 97, pp. 245-251, 2013.

[24] O. Falcó, J. Mayugo, C. Lopes, N. Gascons, and J. Costa, "Variable-stiffness composite panels: Defect tolerance under in-plane tensile loading," *Composites Part A: Applied Science and Manufacturing,* vol. 63, pp. 21-31, 2014.

[25] O. Falcó, C. Lopes, J. Mayugo, N. Gascons, and J. Renart, "Effect of tow-drop gaps on the damage resistance and tolerance of Variable-Stiffness Panels," *Composite Structures,* vol. 116, pp. 94-103, 2014.

[26] X. Li, S. R. Hallett, and M. R. Wisnom, "Modelling the effect of gaps and overlaps in automated fibre placement (AFP)-manufactured laminates," *Science and Engineering of Composite Materials,* vol. 22, pp. 115-129, 2015.

[27] M. Lan, D. Cartié, P. Davies, and C. Baley, "Microstructure and tensile properties of carbon–epoxy laminates produced by automated fibre placement: Influence of a caul plate on the effects of gap and overlap embedded defects," *Composites Part A: Applied Science and Manufacturing,* vol. 78, pp. 124-134, 2015.

[28] M. Lan, D. Cartié, P. Davies, and C. Baley, "Influence of embedded gap and overlap fiber placement defects on the microstructure and shear and compression properties of carbon–epoxy laminates," *Composites Part A: Applied Science and Manufacturing,* vol. 82, pp. 198-207, 2016.

[29] A. Brot, "Development of Fatigue Life Regulations based on Lessons Learned from Several Aircraft Accidents," in *46 th Israel Annual Conference on Aerospace Sciences*, Haifa, Israel, 2006.

[30] B. Harris, *Fatigue in composites: science and technology of the fatigue response of fibre-reinforced plastics*: Woodhead Publishing, 2003.

[31] A. Baker, "The fatigue of fibre-reinforced aluminium," *Journal of Materials Science,* vol. 3, pp. 412-423, 1968.

[32] M. Owen and R. Howe, "The accumulation of damage in a glass-reinforced plastic under tensile and fatigue loading," *Journal of Physics D: Applied Physics,* vol. 5, p. 1637, 1972.

[33] P. Curtis, "The fatigue behaviour of fibrous composite materials," *The Journal of Strain Analysis for Engineering Design,* vol. 24, pp. 235-244, 1989.

[34] R. Talreja, "Fatigue of composite materials: damage mechanisms and fatigue-life diagrams," *Proceedings of the Royal Society of London. A. Mathematical and Physical Sciences,* vol. 378, pp. 461-475, 1981.

[35] T. Myers, H. Kytömaa, and T. Smith, "Environmental stress-corrosion cracking of fiberglass: Lessons learned from failures in the chemical industry," *Journal of hazardous materials,* vol. 142, pp. 695-704, 2007.

[36] B. Harris, N. Gathercole, J. Lee, H. Reiter, and T. Adam, "Life–prediction for constant–stress fatigue in carbon–fibre composites," *Philosophical Transactions of the Royal Society of London. Series A: Mathematical, Physical and Engineering Sciences,* vol. 355, pp. 1259-1294, 1997.

[37] P. Soden, M. Hinton, and A. Kaddour, "Lamina properties, lay-up configurations and loading conditions for a range of fibre-reinforced composite laminates," *Composites Science and Technology,* vol. 58, pp. 1011-1022, 1998.

[38] P. Curtis and B. Moore, "A comparison of the fatigue performance of woven and non-woven CFRP laminates in reversed axial loading," *International journal of fatigue,* vol. 9, pp. 67-78, 1987.

[39] M. Bureau and J. Denault, "Fatigue behavior of continuous glass fiber composites: effect of the matrix nature," *Polymer composites,* vol. 21, pp. 636-644, 2000.

[40] C. Bathias, "Fracture and fatigue of high performance composite materials: mechanisms and prediction," *Engineering fracture mechanics,* vol. 40, pp. 757-783, 1991.

[41] R. Nagalingam, S. Sundaram, B. Stanly, and J. Retnam, "Effect of nanoparticles on tensile, impact and fatigue properties of fibre reinforced plastics," *Bulletin of Materials Science,* vol. 33, pp. 525-528, 2010.

[42] O. Konur and F. Matthews, "Effect of the properties of the constituents on the fatigue performance of composites: a review," *Composites,* vol. 20, pp. 317-328, 1989.

[43] S. V. Hoa, *Principles of the manufacturing of composite materials*: DEStech Publications, Inc, 2009.

[44] G. Shih and L. Ebert, "The effect of the fiber/matrix interface on the flexural fatigue performance of unidirectional fiberglass composites," *Composites science and technology,* vol. 28, pp. 137-161, 1987.

[45] J. F. Mandell and U. Meier, "Effects of stress ratio, frequency and loading time on the tensile fatigue of glass-reinforced epoxy," *Long-term behavior of composites, ASTM STP,* vol. 813, pp. 55-77, 1983.

[46] M. Kawai, S. Yajima, A. Hachinohe, and Y. Kawase, "High-temperature off-axis fatigue behaviour of unidirectional carbon-fibre-reinforced composites with different resin matrices," *Composites science and technology,* vol. 61, pp. 1285-1302, 2001.

[47] M.-H. R. Jen, Y.-C. Tseng, H.-K. Kung, and J. Huang, "Fatigue response of APC-2 composite laminates at elevated temperatures," *Composites Part B: Engineering,* vol. 39, pp. 1142-1146, 2008.

[48] J. Ferreira, J. Pires, J. Costa, O. Errajhi, and M. Richardson, "Fatigue damage and environment interaction of polyester aluminized glass fiber composites," *Composite structures,* vol. 78, pp. 397-401, 2007.

[49] Y.-M. Jen and C.-Y. Huang, "Combined Temperature and Moisture Effect on the Strength of Carbon Nanotube Reinforced Epoxy Materials," *Trans. of the Canadian Society for Mechanical Engineering,* 2013.

[50] R. L. Carlson, *Introduction to Fatigue in Metals and Composites*: Springer Science & Business Media, 1995.

[51] J. Tong, "Characteristics of fatigue crack growth in GFRP laminates," *International journal of fatigue,* vol. 24, pp. 291-297, 2002.

[52] A. G. Evans, M. Y. He, and J. W. Hutchinson, "Interface debonding and fiber cracking in brittle matrix composites," *Journal of the American Ceramic Society,* vol. 72, pp. 2300-2303, 1989.

[53] H. Thom, "A review of the biaxial strength of fibre-reinforced plastics," *Composites Part A: Applied Science and Manufacturing,* vol. 29, pp. 869-886, 1998.

[54] Y. Dzenis, "Cycle-based analysis of damage and failure in advanced composites under fatigue: 1. Experimental observation of damage development within loading cycles," *International journal of fatigue,* vol. 25, pp. 499-510, 2003.

[55] E. Gamstedt and R. Talreja, "Fatigue damage mechanisms in unidirectional carbon-fibre-reinforced plastics," *Journal of materials science,* vol. 34, pp. 2535-2546, 1999.

[56] S. Kobayashi and N. Takeda, "Experimental and analytical characterization of transverse cracking behavior in carbon/bismaleimide cross-ply laminates under mechanical fatigue loading," *Composites part B: Engineering,* vol. 33, pp. 471-478, 2002.

[57] A. Hosoi, H. Kawada, and H. Yoshino, "Fatigue characteristics of quasi-isotropic CFRP laminates subjected to variable amplitude cyclic two-stage loading," *International journal of fatigue,* vol. 28, pp. 1284-1289, 2006.

[58] A. Hosoi, K. Takamura, N. Sato, and H. Kawada, "Quantitative evaluation of fatigue damage growth in CFRP laminates that changes due to applied stress level," *International Journal of Fatigue,* vol. 33, pp. 781-787, 2011.

[59] A. Hosoi, Y. Arao, and H. Kawada, "Transverse crack growth behavior considering free-edge effect in quasi-isotropic CFRP laminates under high-cycle fatigue loading," *Composites Science and Technology,* vol. 69, pp. 1388-1393, 2009.

[60] C. Colombo and L. Vergani, "Influence of delamination on fatigue properties of a fibreglass composite," *Composite Structures,* vol. 107, pp. 325-333, 2014.

[61] M. Ibrahim, "Nondestructive evaluation of thick-section composites and sandwich structures: A review," *Composites Part A: Applied Science and Manufacturing,* vol. 64, pp. 36-48, 2014.

[62] A. Hosoi, N. Sato, Y. Kusumoto, K. Fujiwara, and H. Kawada, "High-cycle fatigue characteristics of quasi-isotropic CFRP laminates over 10 8 cycles (Initiation and propagation of delamination considering interaction with transverse cracks)," *International Journal of Fatigue,* vol. 32, pp. 29-36, 2010.

[63] T. Yokozeki, T. Aoki, and T. Ishikawa, "Fatigue growth of matrix cracks in the transverse direction of CFRP laminates," *Composites science and technology,* vol. 62, pp. 1223-1229, 2002.

[64] J. Montesano, Z. Fawaz, and H. Bougherara, "Use of infrared thermography to investigate the fatigue behavior of a carbon fiber reinforced polymer composite," *Composite structures,* vol. 97, pp. 76-83, 2013.

[65] L. Toubal, M. Karama, and B. Lorrain, "Damage evolution and infrared thermography in woven composite laminates under fatigue loading," *International journal of Fatigue,* vol. 28, pp. 1867-1872, 2006.

[66] L. Maio, V. Memmolo, S. Boccardi, C. Meola, F. Ricci, N. Boffa*, et al.*, "Ultrasonic and IR Thermographic Detection of a Defect in a Multilayered Composite Plate," *Procedia Engineering,* vol. 167, pp. 71-79, 2016.

[67] J. N. Zalameda, E. R. Burke, F. R. Parker, J. P. Seebo, C. W. Wright, and J. B. Bly, "Thermography inspection for early detection of composite damage in structures during fatigue loading," in *SPIE Defense, Security, and Sensing*, 2012, pp. 835403-835403-9.

[68] Y. P. Pan, R. A. Miller, T. P. Chu, and P. Filip, "Detection of defects in commercial C/C composites using infrared thermography," in *SEM Annual Conference and Exposition on Experimental and Applied Mechanics*, 2009.

[69] R. Montanini and F. Freni, "Non-destructive evaluation of thick glass fiber-reinforced composites by means of optically excited lock-in thermography," *Composites Part A: Applied Science and Manufacturing,* vol. 43, pp. 2075-2082, 2012.

[70] W. Bai and B. Wong, "Evaluation of defects in composite plates under convective environments using lock-in thermography," *Measurement science and technology,* vol. 12, p. 142, 2001.

[71] C. Meola, G. M. Carlomagno, and L. Giorleo, "Geometrical limitations to detection of defects in composites by means of infrared thermography," *Journal of Nondestructive Evaluation,* vol. 23, pp. 125-132, 2004.

[72] http://www.cytec.com/products/cycom-977-2.

[73] ASTM, "D3039, Standard test method for tensile properties of polymer matrix composite materials," in *American Society for Testing Materials*, ed, 2003.

[74] ASTM, "D3410,Standard tests method for compressive properties of polymer matrix composite materials," ed, 2003.

[75] ASTM, "D3518, Standard test method for in-plane shear response of polymer matrix composite materials by tensile test of a±45◦ laminate.," in *American Society of Testing Materials.*, ed, 2001.

[76] Z. Hashin, "Failure criteria for unidirectional fiber composites," *Journal of applied mechanics,* vol. 47, pp. 329-334, 1980.

[77] G. S. Patience, D. C. Boffito, and P. Patience, *Communicate Science Papers, Presentations, and Posters Effectively*: Academic Press, 2015.

[78] U. Makkar, M. Rana, and A. Singh, "ANALYSIS OF FATIGUE BEHAVIOR OF GLASS/CARBON FIBER EPOXY COMPOSITE," *International Journal of Research in Engineering and Technology,* vol. 4, pp. 211-216, 2015.

[79] A. M. Neville and J. B. Kennedy, "Basic statistical methods for engineers and scientists," in *Basic statistical methods for engineers and scientists*, ed: International Textbook, 1964.

[80] J. M. Ketterer, "Fatigue crack initiation in cross-ply carbon fiber laminates," MSC, George W. Woodruff School of Mechanical Engineering, Georgia Institute of Technology, 2009.

[81] R. Talreja and C. V. Singh, *Damage and failure of composite materials*: Cambridge University Press, 2012.

[82] I. DANIEL and A. CHAREWICZ, "Damage mechanisms and accumulation in graphite/epoxy laminates," *Composite materials: Fatigue and fracture,* 1986.

[83] G. La Rosa and A. Risitano, "Thermographic methodology for rapid determination of the fatigue limit of materials and mechanical components," *International journal of fatigue,* vol. 22, pp. 65-73, 2000.

[84] G. Curti, G. La Rosa, M. Orlando, and A. Risitano, "Analisi tramite infrarosso termico della temperatura limite in prove di fatica," in *14th AIAS Italian National Conference*, Catania, Italy, 1986, pp. 211–220.

[85] M. P. Luong, "Fatigue limit evaluation of metals using an infrared thermographic technique," *Mechanics of materials,* vol. 28, pp. 155-163, 1998.

[86] C. Colombo, L. Vergani, and M. Burman, "Static and fatigue characterisation of new basalt fibre reinforced composites," *Composite structures,* vol. 94, pp. 1165-1174, 2012.

[87] E. Kordatos, K. Dassios, D. Aggelis, and T. Matikas, "Rapid evaluation of the fatigue limit in composites using infrared lock-in thermography and acoustic emission," *Mechanics Research Communications,* vol. 54, pp. 14-20, 2013.

[88] F. Curà, G. Curti, and R. Sesana, "A new iteration method for the thermographic determination of fatigue limit in steels," *International Journal of Fatigue,* vol. 27, pp. 453-459, 2005.

[89] V. Crupi, E. Guglielmino, M. Maestro, and A. Marinò, "Fatigue analysis of butt welded AH36 steel joints: thermographic method and design S–N curve," *Marine Structures,* vol. 22, pp. 373-386, 2009.

[90] C. Colombo, F. Libonati, F. Pezzani, A. Salerno, and L. Vergani, "Fatigue behaviour of a GFRP laminate by thermographic measurements," *Procedia Engineering,* vol. 10, pp. 3518-3527, 2011.

[91] M. Guagliano, C. Colombo, F. Libonati, and L. Vergani, "Fatigue damage in GFRP," *International Journal of Structural Integrity,* vol. 3, pp. 424-440, 2012.

[92] X. Li, H. Zhang, D. Wu, X. Liu, and J. Liu, "Adopting lock-in infrared thermography technique for rapid determination of fatigue limit of aluminum alloy riveted component and affection to determined result caused by initial stress," *International Journal of Fatigue,* vol. 36, pp. 18-23, 2012.

[93] Ansys, "v15," *ANSYS Corporation Software, Pittsburgh, PA, USA,* 2014.

[94] M. M. Shokrieh, "Progressive fatigue damage modeling of composite materials," PhD, Mechanical Engineering, McGill University, Canada, 1996.

[95] N. Gathercole, H. Reiter, T. Adam, and B. Harris, "Life prediction for fatigue of T800/5245 carbon-fibre composites: I. Constant-amplitude loading," *international Journal of Fatigue,* vol. 16, pp. 523-532, 1994.

[96] T. Adam, R. Dickson, C. Jones, H. Reiter, and B. Harris, "A power law fatigue damage model for fibre-reinforced plastic laminates," *Journal of Mechanical Engineering Science,* vol. 200, pp. 155-166, 1986.

[97] P. Papanikos, K. I. Tserpes, and S. P. Pantelakis, "Modelling of fatigue damage progression and life of CFRP laminates," *Fatigue & Fracture of Engineering Materials & Structures,* vol. 26, pp. 37-47, 2003.

[98] K. I. Tserpes, G. Labeas, P. Papanikos, and T. Kermanidis, "Strength prediction of bolted joints in graphite/epoxy composite laminates," *Composites Part B: Engineering,* vol. 33, pp. 521-529, 10// 2002.

[99] T. Kermanidis, G. Labeas, K. Tserpes, and S. Pantelakis, "Finite element modeling of damage accumulation in bolted composite joints under incremental tensile loading," in *Proceedings of the Third ECCOMAS Congress*, Barcelona, Spain, 2000, pp. 11-14.

[100] W. Lian and W. Yao, "Fatigue life prediction of composite laminates by FEA simulation method," *International Journal of Fatigue,* vol. 32, pp. 123-133, 2010.